# BEHAVIOR OF SOILS UNDER IMPACT LOADING

By Paul A. Hustad and William R. Cox

The University of Texas at Austin
Department of Civil Engineering
Austin, Texas



Prepared for
NATIONAL AERONAUTICS AND SPACE ADMINISTRATION
Langley Research Center
Hampton, Virginia
Grant NsG-604

July 1969

**Page intentionally left blank**

# BEHAVIOR OF SOILS UNDER IMPACT LOADING

by

Paul A. Hustad
William R. Cox

Prepared for

NATIONAL AERONAUTICS AND SPACE ADMINISTRATION

Langley Research Center
Hampton, Virginia

Grant NsG-604

THE UNIVERSITY OF TEXAS AT AUSTIN

DEPARTMENT OF CIVIL ENGINEERING

Austin, Texas

July 1969

**Page intentionally left blank**

# PREFACE

The research work described herein was conducted at The University of Texas under sponsorship of Grant NsG-604, An Investigation of Soil Modeling Problems Related to Impact Studies, from the National Aeronautics and Space Administration, Langley Research Center, Hampton, Virginia. Mr. M. E. Hathaway of Langley Research Center was technical monitor of the Grant.

This is the final report in a series of reports which have been issued under sponsorship of Grant NsG-604.

The investigation was performed under the supervision of Dr. William R. Cox, Associate Professor of the Department of Civil Engineering.

Mr. Olen L. Hudson, Technical Staff Assistant, and Mr. Harold H. Dalrymple, Research Engineer Associate, provided much of the technical knowledge that was necessary during the investigation.

ABSTRACT

The space exploration program of the United States has created a need for a better understanding of how soils behave under impact loading. The purpose of this investigation is to present and analyze experimental impact data which were derived from the past five years of testing.

Prior to this investigation, over 15 investigators have been involved with a program on soil impact at The University of Texas. A brief review of each investigation is presented.

During the course of this study, approximately 175 impact tests were performed by the author. The rigid projectiles consisted of wedges, cylinders, spheres, and cones. The projectile weights varied from approximately 40 to 130 lbs. The angle of projectile impact varied between 10 and 90 degrees from the horizontal soil surface. Horizontal and vertical components of the impacting velocities ranged from 0 to 20 fps and 10 to 30 fps, respectively.

The author conducted approximately 50 impact tests for the purpose of evaluating projectile edge effect equations and soil pressure equations which were developed by D. R. Reichmuth in an earlier study at The University of Texas.

Approximately 125 vertical impact tests were conducted by the author for the purpose of obtaining information on the response characteristics of sands when subjected to impact loading with conical projectiles having 60 degree apex angles. The target materials were composed of a uniformly graded sand and a well-graded sand. The sands were prepared in two states of density and moisture content to encompass a wide range of naturally occurring soil conditions. It was found that the peak soil force, experienced during impact, could be represented by the product of the unit weight of soil, initial momentum of the cone, and a proportionality constant K. Values of K

are calculated for each of the two weights of cones and target materials. For similar states of soil density and moisture content the tests on uniformly- and well-graded sands yielded $K$ values of similar magnitude, which indicates that possibly these $K$ values are representative for sands other than those utilized in this investigation.

In addition to the analyses which are performed by the author on the 175 impact tests, the data from approximately 75 vertical impact tests from previous investigations at The University of Texas are analyzed. Values of $K$ are obtained for various types of projectile shapes and weights, and also a wide range of target materials. These values of $K$ along with those derived from the author's cone impact tests provide the information necessary for predicting peak soil forces under a broad range of impact conditions.

A comparison study is made of the peak soil forces developed during impact and the forces obtained from static load tests. The ratios of peak impact forces to static forces were found to be approximately 2.5 for tests on silt and clays. The force ratios for tests on sands were in most cases well over 100.

A review is made of the effect of the rate of load application upon the soil strength properties of cohesion and of angle of internal friction. A discussion of failure modes occurring beneath dynamically loaded footings is also presented.

TABLE OF CONTENTS

LIST OF TABLES

LIST OF FIGURES

Page

Page

## NOTATION

| | |
|---|---|
| $c$ | cohesive soil strength |
| $D_P$ | projectile width (5.5 in., 11 in. or 16.5 in.) |
| $D_t$ | vertical penetration of projectile tip beneath soil surface |
| $F_{peak}$ | peak soil force developed during vertical impact |
| $g$ | acceleration of gravity |
| $K$ | empirical coefficient which relates the peak soil force to $\gamma MV$ |
| $K_e$ | edge effect constant |
| $M$ | mass of projectile |
| $V$ | velocity when projectile is restricted to vertical motion |
| $V_H$ | horizontal velocity of projectile |
| $V_V$ | vertical velocity of projectile |
| $V_\theta$ | angular velocity of projectile |
| $Z_f$ | final penetration of cone tip beneath the soil surface |
| $\alpha$ | angle of projectile impact |
| $\beta$ | angle between leading face of wedge and horizontal soil surface |
| $\gamma$ | unit soil density (this term includes both the weight of water and solids) |
| $\phi$ | angle of internal friction |
| * | see Appendix A for test nomenclature and sign conventions |

# CHAPTER I

# INTRODUCTION

During the past forty years a vast amount of engineering knowledge has been obtained concerning the behavior of soil. Although the importance of the dynamic behavior of soil has been recognized for years, major concentrated efforts toward an understanding of soil dynamics have only been made within the past twenty years. This late development can principally be attributed to the complex nonlinear load-deformation characteristics exhibited by soil.

Since systems in which only static loading conditions exist are less complex than their counterparts with dynamic loads, these systems have been studied first and are a prerequisite for the understanding of dynamic soil behavior.

Strictly speaking it is not possible to separate the static and dynamic behavior of soil since all systems in reality involve some rate of load application. It is customary to delineate between static and dynamic soil behavior on the basis of their importance to the system. Richart[20] has stated the following: "A dynamically loaded foundation is one for which the effect of rate of loading introduces significant differences between the actual displacements and failure conditions and those which might be computed by conventional static procedures."

## OBJECTIVE

This investigation was undertaken to obtain information that would be utilized by the National Aeronautics and Space Administration for the purpose of designing prototype impact testing programs. The principal objective

was to determine the behavior of soils under impact loading conditions. An attempt has been made to attain this objective by performing field impact studies using a broad range of soil types and projectile configurations. In addition to this testing, the data obtained from the previous four years of field and laboratory testing have been analyzed and correlated with the results derived from this investigation.

## SCOPE OF INVESTIGATION

The scope of this investigation encompasses the behavior of soil-projectile systems which may be classified as "surface impact systems". All of the projectiles utilized in this and previous investigations at The University of Texas were essentially rigid and no attempt has been made to model the deformation characteristics of actual spacecraft. This investigation is composed of the following four phases.

(1) Phase 1 consists of a brief review of the previous investigations which were part of a program on soil impact at The University of Texas during the past four years. These investigations consisted of impacting projectiles having spherical, flat, cylindrical, and conical striking surfaces on sands, clays, and silt. The projectile weights ranged from approximately 1 to 150 lbs. The horizontal and vertical components of the impact velocities were varied from 0 to 30 fps and from 6 to 35 fps, respectively.

(2) During the second phase the author conducted approximately 175 impact tests. Approximately 50 of these tests were conducted for the purpose of evaluating the edge effect equations and soil force prediction equations which were empirically derived by Reichmuth et al[19].

Approximately 125 tests were performed to obtain data on the behavior of sands under vertical impact of two cones having 60 degree apex

angles. The initial impact velocities of the cones were varied between 10 and 25 fps. The cone weights were 43.0 and 129.5 lbs. The target materials consisted of two types of sand which were placed in a test pit at various densities and moisture contents. A method, based on results from the cone impact tests, is presented for predicting peak soil forces experienced during vertical impact. A method is also given for predicting final cone penetrations in sand.

(3) In phase 3 analyses are made of vertical impact data obtained from previous investigations at The University of Texas. A method is given for predicting peak soil forces developed during vertical impact of cones, cylinders, spheres, and flat plates on sands, clays, and silt.

(4) A brief review of the existing literature on the effect of rate of load application on soil cohesion and angle of internal friction is presented in phase 4 along with a discussion of current knowledge concerning failure modes beneath dynamically loaded footings.

# CHAPTER II

## REVIEW OF THE UNIVERSITY OF TEXAS IMPACT STUDIES

Space exploration by the United States has given rise to the need for information concerning the behavior of spacecraft when landing on soil.

The impact testing program at The University of Texas began in 1963 and has been oriented toward the collection of experimental data which would aid in defining the dynamic behavior of soils under various types of projectile impact conditions. Although the primary purpose of the program was to determine the dynamic behavior of soils, a number of static tests were also performed. The purpose of this chapter is to briefly describe and discuss the previous investigations which were part of the impact program.

No attempt was made to model the deformation characteristics of actual spacecraft. Rigid projectiles were selected for the investigation since the primary purpose was to define soil behavior under impact loading and not to define soil-structure interaction under impact conditions.

The program can conveniently be divided into the following three general categories:

(1) Vertical motion of foundation elements,

(2) Horizontal motion of foundation elements,

(3) Combined vertical and horizontal motion of foundation elements.

The foundation elements were spherical segments, cones, cylinders, and flat plates that were utilized to apply either static or impact loadings to the soil. Projectile accelerations were measured with accelerometers and the acceleration-time histories were recorded on oscilloscopes. The acceleration-time data were reduced by numerically integrating once to obtain the velocity-time history, and again to yield the penetration-time history.

## VERTICAL MOTION

The early impact studies at The University of Texas were restricted to vertical motion of the foundation elements. The investigations which involved predominately impact tests are listed under the impact test section and those which were composed mainly of static loadings are listed under the static test section.

### Impact Tests

The first series of impact tests were performed by Reese et al[18] for the purpose of developing some concepts which would be useful for predicting the behavior of the Apollo space capsule during impact on soil.

The problem was approached through the use of similitude. Three scale models (1/64, 1/32, 1/4 scale) of the Apollo capsule were dropped on prepared beds of compacted Montopolis Silt. No attempt was made to model the soil properties and, therefore, distortion of the model was introduced into the experimental design. To check the effect of distortion upon the dependent variable (soil force) the 1/64 and 1/32 scale models were utilized. The 1/32 scale model was assumed to be the prototype and the smaller projectile (1/64) the scale model. Tests were then performed at the impact velocities required for similarity. The measured response of the prototype and the predicted response from measurements on the model were in close agreement.

Although the distortion of the Pi terms, in the Theory of Similitude, that contain the chosen soil properties was not significant for a scale ratio of 1/2, the effect may be substantial as the scale ratio becomes smaller. It is unfortunate that tests were not conducted so that the 1/64 and 1/4 scale models could be used to check the distortion caused by using the same soil. This would have provided valuable information on whether one

is justified in not modeling the soil for larger ranges of scaling. However, the results do show that the use of dimensional analysis and modeling have promise as a method of predicting the behavior of spacecraft landing on soil.

Extrapolation of the observed behavior of the small-scale projectiles was suggested as another method for predicting the behavior of the prototype. Equations 1 and 2 were empirically derived by Reese from the experimental test results and were given as methods of predicting the slope of the rising portion of the soil force-penetration curve (I) and the maximum soil force ($F_c$), respectively.

$$I = 52.0 + 91.3\ R + [7.0 + (207 + 11.0\ R)\ M]\ V_i \tag{1}$$

$$F_c = 95.0\ M^{0.786}\ V_i \tag{2}$$

The variables appearing in the above equations are defined as follows:

$I$ = Initial modulus of force-penetration curve (lb/in.),

$R$ = Radius of striking surface (in.),

$M$ = Mass of projectile (lb-sec$^2$/in.),

$V_i$ = Initial impact velocity (in./sec),

$F_c$ = Maximum soil force (lb).

The values predicted by Eqs 1 and 2 were compared with experimental results and the agreement was within 15 percent for most cases.

Static load tests were conducted using the same test vehicles that were utilized in the impact phases. The static force-penetration characteristics were found to be considerably different from the dynamic characteristics. It was concluded that static load tests, or static strength parameters, such as cohesion (c) and angle of internal friction ($\phi$) could not be used to directly predict soil behavior during impact.

Poor et al[16] performed a series of vertical drop tests on a partially saturated sandy clay located in a terrace of the Colorado River. Unlike the earlier tests of Reese et al[18], the drop tests were conducted in the field on undisturbed soil. The projectile striking surface geometries included conical, spherical, and flat surfaces.

Two methods, similar to those proposed by Reese, were proposed for predicting the behavior of projectiles during impact. The first method was based on the Theory of Similitude for dynamic similarity. Two cases were chosen to illustrate the distortion caused by using the same soil for both the model and prototype tests. The first case involved the use of projectiles having weights of 8 and 64 lbs with spherical radii of 5 and 10 in., respectively. The larger projectile was assumed to be the prototype while the smaller projectile was considered to be the model. The comparison of predicted and observed maximum forces yielded errors of approximately 50 percent. A similar comparison was made using 16 and 128 lb projectiles with radii of 5 and 10 in., respectively. The maximum force values predicted by similitude were approximately twice the experimental values.

The results have shown that the use of the same soil for model and prototype tests introduces a significant amount of error.

The second method was based on the observed behavior of the projectiles. Equations 3 through 6 were developed from a least square analysis of the experimental data.

Cone

$$E_{dc} = 1{,}049 \tag{3}$$

Plate

$$E_{dp} = 4{,}787.6\ r + 230.24\ r^2 \tag{4}$$

Sphere

$$E_{ds} = 585.2\ R + 35.08\ R^2 \tag{5}$$

$$f_s = 530 + 114\ (MV_i) - 0.214\ (MV_i)^2 \tag{6}$$

The variables appearing in the above equations are defined as follows:

$E_{d(c,p,s)}$ = Modulus of deformation (lb/in.),

$r$ = Radius of plate (in.),

$R$ = Spherical radius (in.),

$f_s$ = Maximum soil force (lb),

$M$ = Projectile mass (lb-sec$^2$/ft),

$V_i$ = Initial impact velocity (fps).

The equations fit the experimental data reasonably well; however, it was suggested they not be used to predict the behavior of larger scale projectiles. The results from several larger scale tests would help to more clearly define the limitations of the equations.

Awoshika and Cox[1] applied similitude principles to a series of vertical drop tests on Ottawa and Colorado River Sand. The sands were placed in loose and dense states. The moisture content was also varied so that the sands were utilized in nearly dry and saturated states. The projectiles were right circular cones having 60 degree apex angles, with weights of 43.0 and 129.5 lbs. The 129.5 lb cone was assumed to be the prototype and the 43.0 lb model results were utilized to predict the behavior of the prototype. Even though the same

soil was used for the model and prototype tests, the agreement between peak accelerations and final penetrations was good for each of the three states of the two sands. It should be emphasized that the results indicate agreement for relatively small scale factors and for tests involving larger scale factors the distortion introduced by using the same soil may become prohibitive.

Womack and Cox[33] developed a soil penetrometer having a flat, circular foot approximately one square inch in area and a weight of 5.384 lbs. The initial impact velocity was held constant at approximately 15 fps. The target materials consisted of gravels, sands, and clay. The characteristic force-penetration curve generally exhibited a sharp rise in force which was followed by a rapid decrease to a force plateau. The spike portion of the curve was of extremely short duration and the major portion of the penetration occurred at a relatively constant force level. The spike force value was not considered to be important and the relatively constant force plateau was used as the significant force characteristic of the soil.

Womack and Cox concluded that the results of their investigation generally support the assumptions about mechanisms and failure conditions based primarily on the Prandtl-Terzaghi[26] system. This conclusion was based principally on visual observations of the final soil surface displacements.

The author tends to disagree with the above statement for the following reasons. First of all, in dry, dense sands a relatively large amount of sand is ejected away from the impact vicinity, leaving behind a funnel shaped crater surrounding the penetrometer. The soil surface surrounding the rim of the crater is generally slightly higher than the original level; however, it is not known whether this is due to a general upward movement of the sand mass, or if it is formed by material ejected from the crater. Failure plane

outcroppings, which are characteristic of Prandtl-Terzaghi systems, were also not visible. Impact on dry, loose sands produced some particle spray; however, the hole created by the penetrometer was immediately filled by the surrounding material. The impact loading also causes the sand to assume a denser state. Thus, the final position of the surrounding soil surface is not indicative of the true soil behavior during the impact event. The problems associated with trying to discern the type of failure mechanism present during the impact event are also common to tests on saturated sand. The tests on partially saturated clay exhibited a slight upward movement of the surrounding soil surface, although no failure plane outcroppings were noted. A slight rise in the soil surface is certainly not sufficient information to indicate that the soil behaves principally as a Prandtl-Terzaghi system.

Womack and Cox also concluded that the magnitude of the relatively constant penetrating force appeared to be largely dependent upon the static shearing strength of the soil. The author is also in disagreement with this statement. Chapters VI and VII contain discussions of soil shearing strength as related to the dynamic soil forces developed during impact.

Static Tests

Iliya and Reese[8] performed a series of laboratory load tests on the surface of a dry, medium dense Colorado River Sand. Circular plates, a cone, and spheres were utilized as the foundation elements. The circular plates had 2.22, 3.14, and 4.44 in. diameters. The cone had a 60 degree apex angle. Spherical segments having spherical diameters of 3.14 and 5.00 in. were also utilized. The force-penetration characteristics of each foundation element were studied and compared with one another. The circular plate results were in good agreement with the ultimate bearing values predicted by Terzaghi's[26]

equation for circular footings at the soil surface. Based on the load tests, equations were developed for the bearing capacity of conical and spherical foundation elements. The equations are as follows:

Cone

$$q = 0.24\ \gamma\ B\ N_{\gamma}\ , \tag{7}$$

Sphere

$$q = 0.165\ \gamma\ B\ N_{\gamma}\ . \tag{8}$$

The variables are defined as follows:

$q$ = Bearing capacity ($lb/ft^2$),

$\gamma$ = Soil density ($lb/ft^3$),

$B$ = Cross-sectional diameter at the level of embedment (ft),

$N_{\gamma}$ = Bearing capacity coefficient.

It should be noted that to calculate the static bearing forces on the foundation elements the $q$ values should be multiplied by the cross-sectional area at the level of embedment.

Ghazzaly and Cox[4] conducted a series of static load tests in sandy clay at the field site which was utilized by Poor et al[16]. The foundation elements consisted of spheres (3.14 and 5.00 in. spherical diameters), a cone (60 degree apex angle), and flat circular plates (2.22 and 3.14 in. diameters). The ultimate bearing capacities of the plates were approximately 1.75 times the values predicted by Terzaghi's equation[26] for circular footings at the ground surface. A detailed discussion of the force-penetration characteristics of the various foundation elements was presented along with some comparisons between the experimental plate data and values calculated using previously proposed methods[24,27].

Ghazzaly and Dawson[5] studied the laboratory stress-deformation characteristics of sands and clays. A comprehensive review of conventional methods and testing techniques for obtaining soil strength properties was presented. A limited study was conducted on the influence of rate of strain on the angle of internal friction of a dry Colorado River Sand. The times to failure ranged from 30 to 240 sec. The angle of internal friction increased by approximately one degree as the time to failure decreased from approximately 240 sec to 30 sec.

## HORIZONTAL MOTION

The horizontal loading phase of the testing program consisted of pushing vertical walls (1 ft high and 3 ft long; 1.5 ft high and 3 ft long) into loose or dense backfills of dry sand. The rate of wall penetration was not large enough to develop inertial effects, thus, the tests were considered to be static. Although all of the experimental test results were obtained from essentially static tests, a computer program was developed to simulate the dynamic behavior of sand under plane strain loading conditions.

### Dynamic Behavior

Oweis and Cox[15] developed a computer program for the analysis of earth pressure problems which closely approximate plane strain type of soil behavior under dynamic loading conditions. The program was based on a finite difference approach. The soil was assumed to exhibit nonlinear stress-strain characteristics and an iterative process using the point relaxation technique was utilized to solve the resulting nonlinear equations. The effect of dynamic loading was represented by soil inertia terms in the finite difference equations. Soil properties were input in the form of modulus of deformation versus axial

strain and lateral strain ratio versus axial strain. Modulus of deformation and lateral strain ratio are analogous to Young's modulus of elasticity and Poisson's ratio, respectively.

The computer program was utilized to solve for the stresses and strains induced in a dry sand which was horizontally penetrated by a rigid plate. The computed results were compared with experimental results obtained by Hustad and Cox[7] and the agreement was generally poor. The experimental results were obtained from tests in which the rate of movement of the plate was varied between 0.0067 and 2.67 ips. These tests may essentially be considered static in nature, therefore, even if the program had given good agreement this would not provide an indication of whether the program is accurate for problems involving soil dynamics. The program was also utilized to predict the horizontal soil forces on the wall as it moved at higher rates of penetration. The computed results indicate that for constant rates of penetration above 10 fps the ultimate horizontal load remains constant.

Static Tests

Vallabhan and Reese[29] conducted a limited series of passive earth-pressure tests on a dry Colorado River Sand. The experimental test setup simulated an infinitely long, vertical retaining wall one foot high. As the wall was pushed into the soil, the horizontal soil reaction and wall penetration were recorded. A computer program, based on the finite element method, was developed to predict force-deflection characteristics of soils under plane strain and axially symmetric cases. The program required the input of pseudo-elastic values of Young's modulus of elasticity and Poisson's ratio, which are strain dependent for soils. The necessary values were obtained from triaxial compression tests.

The computed soil force-deflection values agreed remarkably well with the measured values. Comparisons were also made between an experimental force-penetration curve for a circular footing resting on the surface of a saturated clay and the curve predicted by computer solutions. Once again, the agreement was good.

The test apparatus, developed by Vallabhan and Reese[29] was modified by Hustad and Cox[7] and a series of tests were performed using 12 and 18 in. high walls. The constant rate at which the walls penetrated into the sand backfill was varied between 0.00667 and 2.67 ips. Dry Colorado River Sand was utilized as backfill material. The rates of wall penetration utilized in this investigation did not have a measurable effect upon the force penetration characteristics of the soil. Coulomb's[26] theory for passive earth pressure was used to predict earth pressures. The predicted values were generally within 20 percent of the experimental values.

Cones and spherical segments were also penetrated horizontally into dry Colorado River Sand. In the retaining wall tests the sand backfill was supported by the wall itself; however, in the tests with cones and spheres the sand required support. A circular hole was cut in one end of the sand box and the opening was covered with a polyethylene membrane. The membrane laterally supported the sand prior to and during the penetration tests. The soil behavior was strongly influenced by the boundary conditions created by the membrane and it is difficult to visualize such conditions occurring in nature. Therefore, the results are of limited value.

## COMBINED VERTICAL AND HORIZONTAL MOTION

Reichmuth et al[19] developed a portable testing rig capable of launching projectiles at impact angles ranging between 30 and 90 degrees with

respect to the ground surface. Wedges, cylinders, and spheres were utilized as projectile shapes. The projectile sizes and weights were chosen so that the developed pressures and penetrations would roughly correspond to those observed for manned spacecraft. The vertical component of the impact velocity was varied between 10 and 35 fps, and the horizontal component from 0 to 30 fps. Target materials consisted of two types of sand and a clay. The sands were tested under dry and saturated conditions, and in loose and dense states. The clay soil was utilized in an undisturbed state.

A method for predicting prototype impact behavior was presented by Reichmuth. The method requires information concerning the dynamic response characteristics of the prototype and soil. It was beyond the scope of the investigation to determine the dynamic response characteristics of the prototype; however, equations were developed to predict soil forces during impact. The equations were developed for wedge, cylindrical, and spherical striking surfaces. These equations are listed on pp. 53 through 61 in Chapter 5. The procedure is as follows:

(1) Start with initial conditions of impact such as, projectile velocity and attitude,

(2) Determine soil forces for these conditions,

(3) Apply these forces to the projectile and determine the change in behavior,

(4) This will then give a new projectile velocity and attitude,

(5) Repeat steps 2 through 4.

This procedure involves a large number of calculations and it was recommended that a high-speed computer be utilized.

A method was also presented for predicting peak accelerations experienced during prototype impact. A three-phase earth materials diagram was

presented, in which values for ratios of the maximum target accelerations to the maximum water acceleration were plotted. The use of the method requires that the peak accelerations experienced during water impact be known.

## SUMMARY OF IMPACT STUDIES

The soil impact studies at The University of Texas have been concerned with defining the behavior of soils when subjected to the impact of rigid projectiles having motion both in vertical and horizontal directions. The primary purpose for the impact studies was to develop methods whereby the behavior of prototypes could be predicted from impact data obtained from model or small scale tests.

The problem of defining prototype behavior was approached from two directions. The first direction consisted of using the Theory of Dynamic Similitude. The second direction consisted of extrapolating the observed behavior of small scale projectiles to predict the behavior of larger projectiles.

### Vertical Motion

The early studies were limited to vertical impact of projectiles on basically cohesive soils. These studies were concerned mainly with determining if the application of the Theory of Dynamic Similitude to surface impact problems offers a means of predicting prototype behavior from model behavior. The projectiles were essentially rigid and no attempt was made to model the deformation characteristics of spacecraft. No attempts were made to model the target materials, thus, distortion was introduced into the model design.

The model impact tests of Reese et al[18] showed that for small ranges of scaling the distortion introduced by using the same soil for model and

prototype tests does not introduce a significant amount of error. The similitude analysis performed by Poor et al[16] showed that even for small ranges of scaling a significant amount of error was introduced by not modeling the soil.

Awoshika and Cox[1] in later vertical impact studies on sands obtained good prediction accuracy for a small range of scaling even though the same soils were utilized for the model and prototype tests.

Horizontal Motion

The experimental studies that pertained purely to the horizontal motion of the soil loading element (vertical plate) essentially involved only the static behavior of soil. A theoretical analysis, however, was performed by Oweis and Cox[15] in which a computer program was developed to predict the behavior of sands when subjected to dynamic horizontal loadings.

Combined Vertical and Horizontal Motion

Inclined impact of projectiles on various types of soils was studied by Reichmuth[19]. Reichmuth empirically developed equations which account for projectile edge effects. These equations permit the extrapolation of the observed projectile behavior to that of larger projectiles.

Reichmuth also proposed a method for predicting peak soil forces experienced by prototype space capsules when impacting on soil.

NEED FOR FURTHER RESEARCH

Although a concentrated effort has been made over the past four years to obtain an understanding of how soil behaves under impact loading conditions, much research was still needed to extend and fill the gaps in our knowledge. The purpose of this section is to list possible avenues of research which will

further our knowledge of soil behavior under impact conditions and to acknowledge topics of research undertaken by the author.

## Modeling

The previous studies have shown that the application of modeling techniques shows promise; however, it is not known whether it is necessary to model the soil or, if it is necessary, which soil properties should be modeled. Research in this direction seems to offer the most general approach to the problem of surface impact.

## Prototype Behavior

Prototype impact tests on soil are needed for evaluating the problems involved in extrapolating the behavior of small scale projectiles to predict the behavior of larger projectiles.

## Soil Behavior Under Impact Loading

The application of model techniques and performance of prototype impact tests were beyond the scope of this investigation. However, impact tests were conducted by the author to evaluate the edge effect constants that were empirically derived by Reichmuth[19]. The edge effect constants are of prime importance since they permit extrapolation to larger projectiles.

Reichmuth also derived regression equations to predict soil forces during impact. These equations were derived from inclined impact data taken from tests where the angle of impact was varied between 30 and 90 degrees to the horizontal soil surface. The author conducted tests to evaluate the prediction accuracy of these equations for impact angles less than 30 degrees.

The previous vertical impact studies at The University of Texas have been concerned mainly with cohesive soils. To add additional information on

the behavior of sands under vertical impact the author has conducted a series of tests with conical projectiles.

Until the present time, no attempt has been made to correlate the data from each of the previous impact investigations. The author has attempted to correlate only the previous vertical impact data. Special emphasis has been given to the prediction of peak soil forces.

# CHAPTER III

# TEST APPARATUS

The test apparatus utilized during this investigation was designed and built by Reichmuth[19]. It was necessary to make several minor modifications to the apparatus so it could be used for tests in which the projectile impact angles were less than 30 degrees to the horizontal ground surface. To be consistent with the previous work of Reichmuth the same test nomenclature was adopted. Appendix A contains a listing of this nomenclature.

A general view of the test apparatus is shown in Fig. 1. The apparatus essentially consisted of a pair of guide rails mounted on the bed of a half-ton truck, a thrust assembly for accelerating the projectile, a wagon and table assembly which carried the projectile along the guide rails, and a braking assembly which decelerated the wagon and table assembly once the projectile was released.

The accelerometer and velocity detector data were recorded on two oscilloscopes.

## LAUNCHING SYSTEM

The major portion of the launching system was constructed of aluminum so two men could easily adjust the angle of impact. Although the inclination of the guide rails could be set at angles ranging from 5 to 90 degrees with the horizontal, the angle of impact of the projectile ranged from 10 to 90 degrees. The projectile was released from the table when its tip was approximately 8 in. above the soil surface; however, at low angles of release the acceleration of gravity significantly increases the projectiles' vertical velocity, thus increasing the angle of impact which is determined by the ratio of the vertical to horizontal impact velocity.

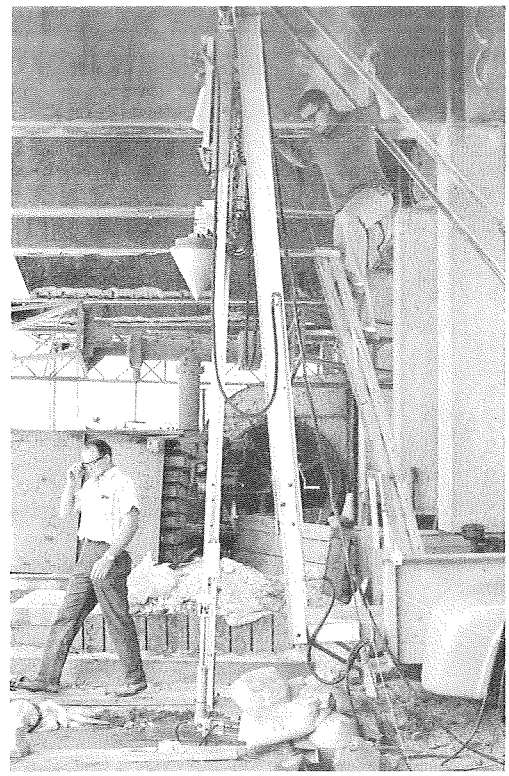

Fig. 1 General View of Test Setup During Vertical Impact Tests at Balcones Research Center

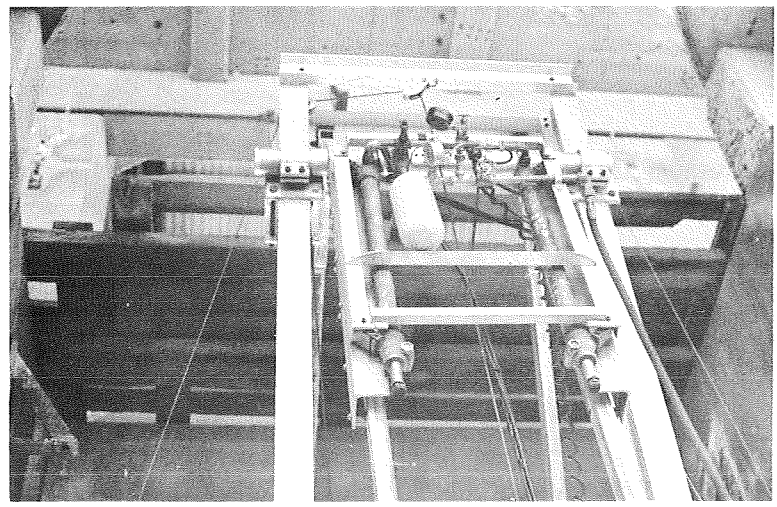

Fig. 2 Details of Thrust System Assembly

Thrust Assembly

Details of the thrust system are shown in Fig. 2. Prior to each test the cylindrical bottle was pressurized with nitrogen. A solenoid operated a valve which allowed the gas to pressurize the thrust cylinders and thereby accelerate the wagon along the guide rails.

Wagon Assembly

The purpose of the wagon assembly was to carry the projectile down the guide rails. The friction between the guide rails and the wagon was reduced by rollers which are shown in Fig. 3. The wagon also housed the table assembly and the wire leads from the accelerometers.

Table Assembly

The table assembly contained jaws which held the projectile as it traveled along the guide rails. A cam operated microswitch actuated the jaws for the release of the projectile. The pitch of the projectile, which is defined as the angle between the longitudinal axis of the projectile and a line perpendicular to the ground surface, could be varied by rotating the table assembly (see Appendix A). However, during this investigation the pitch angle was maintained at zero degrees. The details of the table assembly are shown in Fig. 4.

Braking Assembly

The braking system provided a means of bringing the wagon to rest once the projectile was released. The assembly is also shown in Fig. 3 and consists of two pistons which travel in pressurized cylinders.

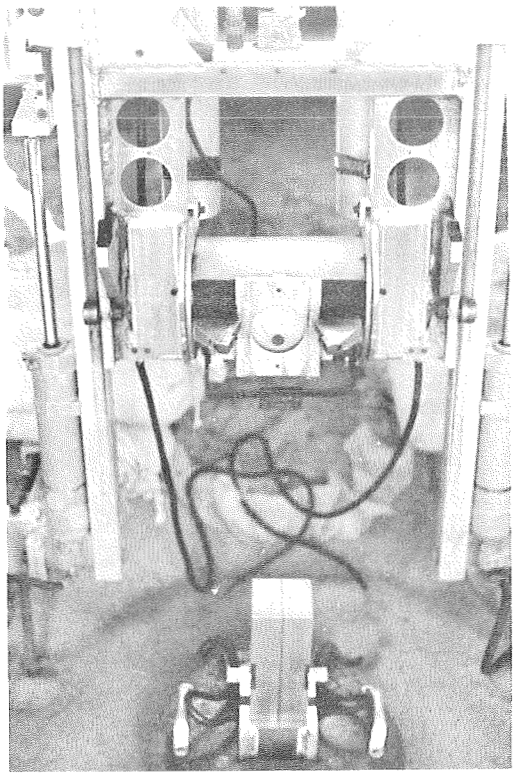

Fig. 3 Wagon Assembly Details

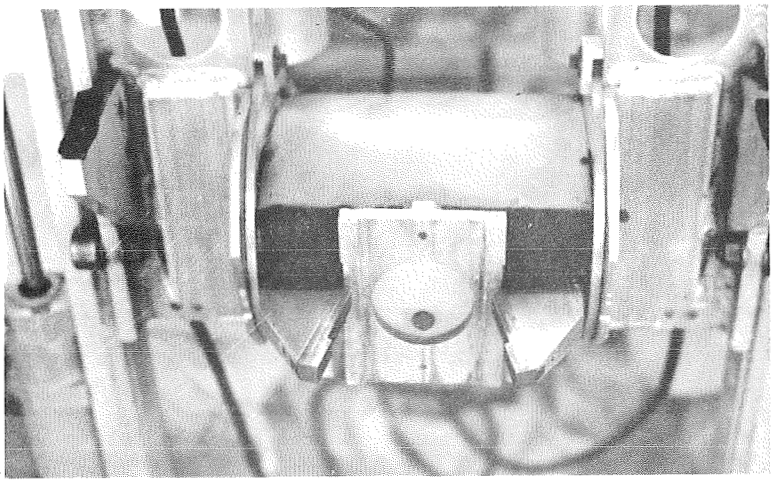

Fig. 4 Table Assembly Details

## INSTRUMENTATION

The measuring and recording devices utilized during this investigation are identical to those used by Reichmuth[19]. The projectile acceleration, during the impact event, was measured with accelerometers and recorded on an oscilloscope. A second oscilloscope was used to record information necessary for calculation of the initial impact velocity.

### Velocity Detector

The velocity detector was composed of an oscilloscope triggering circuit and a set of 4 piano-wire pins connected in a series parallel circuit. The pins were mounted on the edge of a guide rail and as the wagon moved down the rails an outrigger from the wagon made successive contact with each pin. These contacts produced voltage steps on the oscilloscope screen which were recorded on Polaroid film. This record permitted calculation of the velocity of the wagon. The projectile was released from the jaws of the table during this time and for angles of impact greater than 30 degrees the wagon velocity closely approximates the projectile impact velocity.

### Accelerometers

Two type 4-204, Consolidated Electrodynamics Corporation, triaxial accelerometers were utilized to measure projectile accelerations. The accelerometers were mounted in a mast which was interchangeable between projectiles. Each accelerometer consisted of a four-active-arm, spring-type unbonded strain gage element and a seismic mass damped by the shear action of fluid. The axial and rotational axis for each accelerometer had a maximum range of plus or minus 250 g's. The transverse axis range, which was not needed because of the planar motion of the projectiles, was plus or minus 100 g's. Each axis

had a full range output of approximately 40 millivolts, at a rated excitation voltage of 5 volts DC. The natural frequencies ranged from 1300 to 1600 cps.

## AUXILIARY EQUIPMENT

The auxiliary equipment consisted of a balancing unit, filter networks, two oscilloscopes, a gasoline driven generator, and a regulated DC power supply. The balancing unit was used for the positioning of each accelerometer trace on the oscilloscope. Symmetrical "parallel T" filter networks were used to attenuate high frequency signals which were approximately 30 times greater than the acceleration frequencies encountered during testing.

The impact velocity measurements were recorded on a type 502A dual beam Tektronix oscilloscope. The accelerometer measurements were recorded on a type 565 dual beam Tektronix oscilloscope having two type 3A3 dual trace differential vertical amplifiers.

Power for the system was furnished by a one and one-half KVA generator. A Harrison Labs Model 6204A electronically regulated DC power supply furnished power for the accelerometers. Since the accelerometer voltage is critical, it was continuously monitored with a large scale meter by the operator. Power for the velocity and oscilloscope trigger circuits was furnished by 6 volt lantern batteries.

## PROJECTILE CONFIGURATIONS

As stated earlier, no attempt was made to model the deformation characteristics of spacecraft. Rigid projectiles were used in all tests. The projectile geometries utilized during the course of the testing program consisted of:

(1) Spherical segment having a 10 in. spherical radius,

(2) Cylindrical segments having a 10 in. radius,

(3) Wedges with 60 degree and 120 degree included angles,

(4) Cones with 60 degree apex angles.

Three basic reasons existed for the selection of these projectile configurations. First of all, these geometries closely approximate the shapes of the impacting surfaces of the United States space exploration vehicles. The spherical segment resembles the Apollo heat shield and the 120 degree wedge approximates the impacting edge of the Gemini spacecraft.

These projectiles also represented a wide range of surface geometries which provided data concerning the effect of the striking surface shape on the soil behavior.

This investigation had a twofold purpose, in that it was intended to extend the work of Reichmuth[19] and also to correlate with the previous impact studies that have been conducted at The University of Texas. The correlation with previous work and the extension of Reichmuth's work necessitated the use of similar projectiles and therefore the shapes listed above were utilized. Reichmuth constructed wedge and cylindrical projectiles in three separate 5.5 in. wide sections. These sections could be bolted together so that they formed 11 in. and 16.5 in. wide projectiles. Reichmuth tested with projectiles 5.5 in. and 16.5 in. wide and from the test data he derived equations to express the edge effects. To supplement the data obtained by Reichmuth, projectiles 11 in. wide were tested.

Approximately 125 vertical impact tests were also conducted with two conical projectiles. The cone weights were 43.0 and 129.5 lbs.

Figure 5 illustrates the projectile shapes that were utilized in this investigation. Appendix B lists the significant projectile properties.

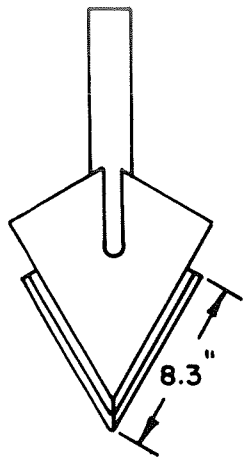


60° WEDGE

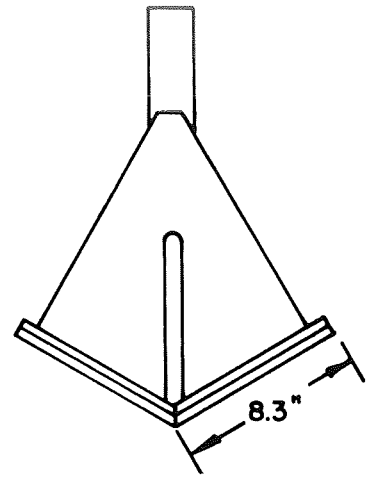


120° WEDGE

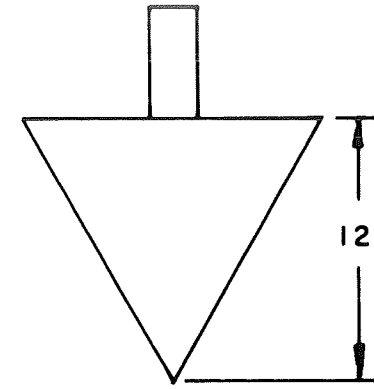


60° CONE

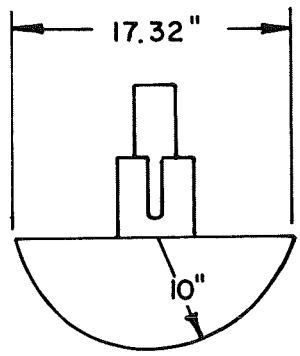


SPHERICAL SEGMENT

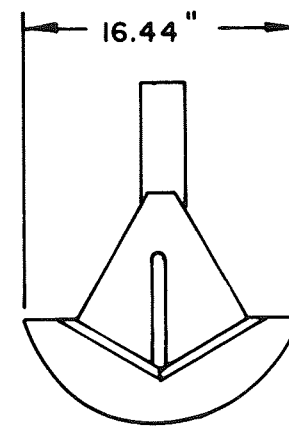


10" RADIUS CYLINDERICAL SEGMENT

FIG. 5 PROJECTILE CONFIGURATIONS

# CHAPTER IV

# TEST PROCEDURES AND DATA REDUCTION

The testing program was conducted at the following field sites which were located within the city limits of Austin:

(1) Capitol Aggregates property,

(2) Artificially constructed soil bed at Balcones Research Center,

(3) Clayey flat at Balcones Research Center.

The test equipment was transported to the site with the pickup truck and it required approximately one hour to set up the test apparatus. Due to the large number of tests all procedures for testing and data reduction were standardized to save time and minimize human errors.

## TEST PROCEDURES

After arriving at the test site the truck was leveled and the guide rails were placed at a predetermined launch angle. The oscilloscope traces were then balanced to zero and the test bed made ready. The measurements for velocity determination and oscilloscope settings were recorded. When necessary, the thrust system was pressurized and the projectile was then launched. Following impact, soil measurements were made. Appendix C contains descriptions of soils utilized in this and previous investigations.

### Soil Bed Preparation

Studies in the field of soil mechanics have shown that the type and condition of soil strongly influence the behavior of foundation elements subjected to both static and dynamic loading. Therefore, it is advantageous to perform tests on a wide range of soils. In this investigation, three types of sands were used for target materials. In addition, the sands were each

prepared at densities which corresponded to loose and dense states. Tests were also performed on a clay in an in-situ condition.

Sands

The Capitol Aggregates test site was located near the shore of a small lake that had formed in a borrow pit area. The sand is known as Colorado River Sand and classified as well-graded according to the Unified System. The loose state of density was formed by removing the sand from the immediate impact area and then carefully replacing it with shovels. The reworked area was 2 ft by 3 ft by 1.5 ft in depth. The dense state was obtained by replacing the sand in approximately 4 in. thick layers which were successively tamped. These procedures produced densities of approximately 90 and 100 pcf. Several tests were also performed on the soil in a saturated state. This state was obtained by setting up the rig near the water's edge and then excavating the soil above the existing water table.

Ottawa Sand and a Colorado River Sand were used as target materials at Balcones Research Center. The sand was placed in a 3 ft wide, 6 ft long, and 4 ft deep pit which was lined with plastic. The performace of tests on saturated sand necessitated the use of a pit lining. Figures 6 and 7 illustrate the procedures for preparing the test bed. The previously described procedures were employed to obtain loose and dense states.

Clay

A series of tests were conducted on Del Rio Clay at Balcones Research Center. Since the soil was tested in place it was necessary to remove the existing top 4 in. of overburden. Each time a test was completed the apparatus would be moved several feet to a new target area for the next test. Extensive manicuring was required to obtain a level impact area.

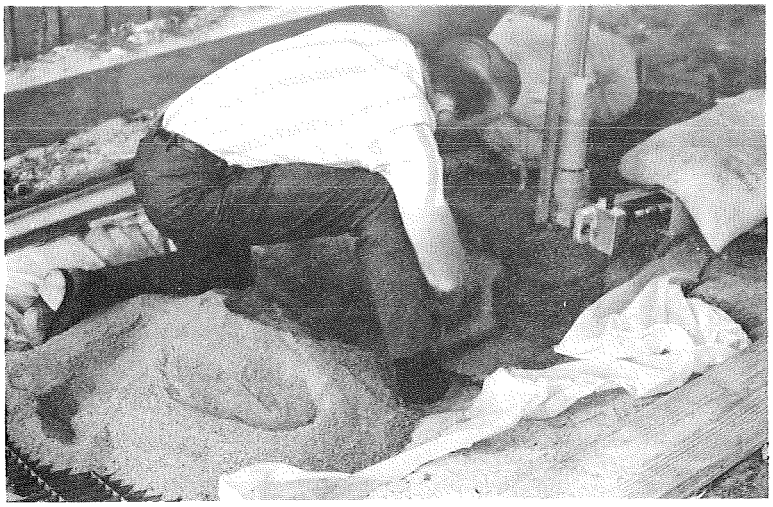

Fig.6 Preparing Soil Bed in Dense State at Balcones Research Center

Fig. 7 Leveling Soil Surface While Conducting Field Tests on Saturated Colorado River Sand

Measurements Prior to Impact

The impact velocity of the projectile was predetermined by setting the pressure level in the thrust system. In some situations the thrust system was not required and the desired velocity was obtained by varying the drop distance of the wagon and projectile.

The impact velocity was calculated by two independent methods. The first method used the information obtained from the velocity detector record and the second method required the measurement of the vertical distance between the trigger pin on the velocity detector and the ground surface. The final step was to record the sensitivity and initial position for each accelerometer trace along with the sweep time for each oscilloscope.

Measurements After Impact

Following impact, the vertical projectile penetration was measured as shown in Fig. 8. Density samples were also taken with brass rings that were approximately 2 in. in diameter and 1.3 in. wide. Ring wall thicknesses were approximately 0.03 inches. Figure 9 shows the sampling method.

DATA REDUCTION

Data reduction was carried out concurrently with field testing so modifications in testing procedures could be made if necessary. The data from the velocity records, acceleration records, and soil logs were punched on computer cards and reduced to a usable form with two computer programs. The soil data were reduced by Program SOIL and the remaining data were reduced using Program IMPACT. Program SOIL performed standard moisture content and density calculations. A discussion and FORTRAN listing of Program IMPACT has been given by Reichmuth[19].

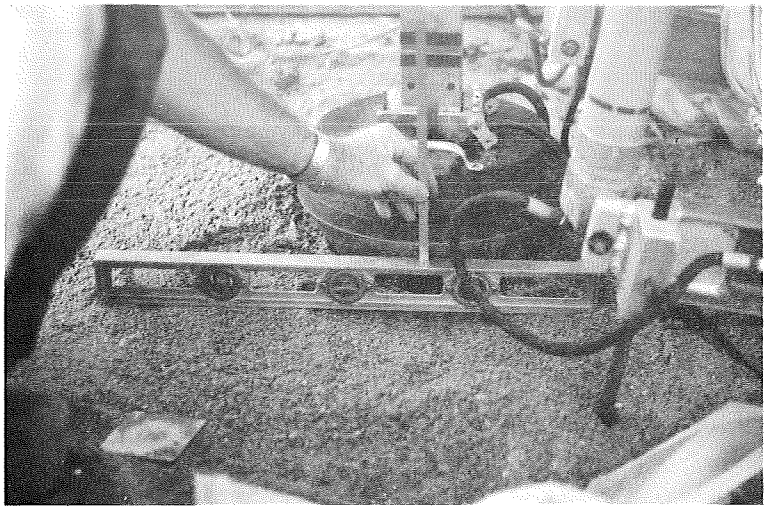

Fig. 8 Measurement of Final Cone Penetration Following Vertical Impact Test

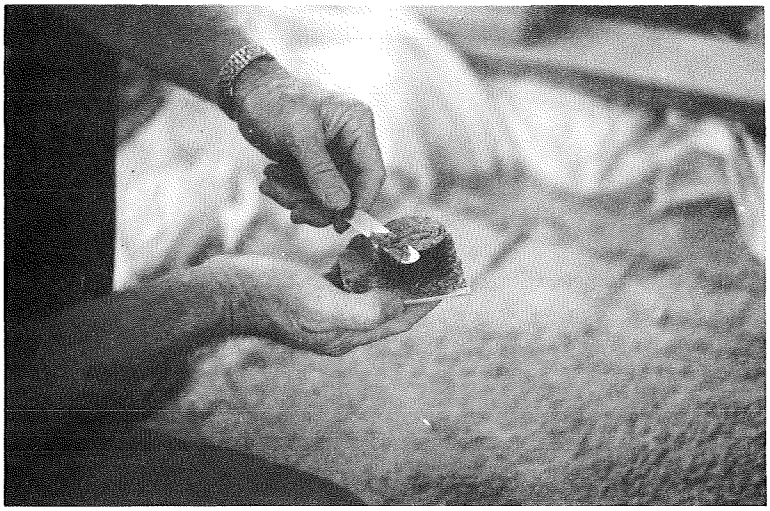

Fig. 9 Trimming a Ring Density Sample

Manual Reduction

The acceleration and velocity records came from the field in the form of 3 by 4 in. Polaroid photos. A Model 70 dry photo copier made by the 3M Company was used to make positive image transparencies of the field records. An overhead projector was then used to enlarge the image and project it onto graph paper where it was traced. Points were taken off the traced acceleration record at equal time increments. Generally 20 to 30 points were required for an accurate simulation of the acceleration-time curve in Program IMPACT.

Computer Calculations

Program IMPACT performed the manipulations that were necessary to describe the acceleration, velocity, and displacement of the projectile at the chosen time increments. The program also contained a subroutine which plotted the vertical displacement versus horizontal displacement of the projectile center of gravity and tip.

Impact Velocity Determination

The initial velocity of the projectile at the instant of impact was calculated by several methods. The method of calculation depended upon the angle of impact and the type of projectile.

Figures 10 and 11 show typical velocity data taken in the field. The first method of velocity calculation is represented by

$$Vel_1 = \frac{P_d}{T_{1-4}} \tag{9}$$

where,

$P_d$ = Distance between pins 1 and 4,

$T_{1-4}$ = Travel time between pins 1 and 4.

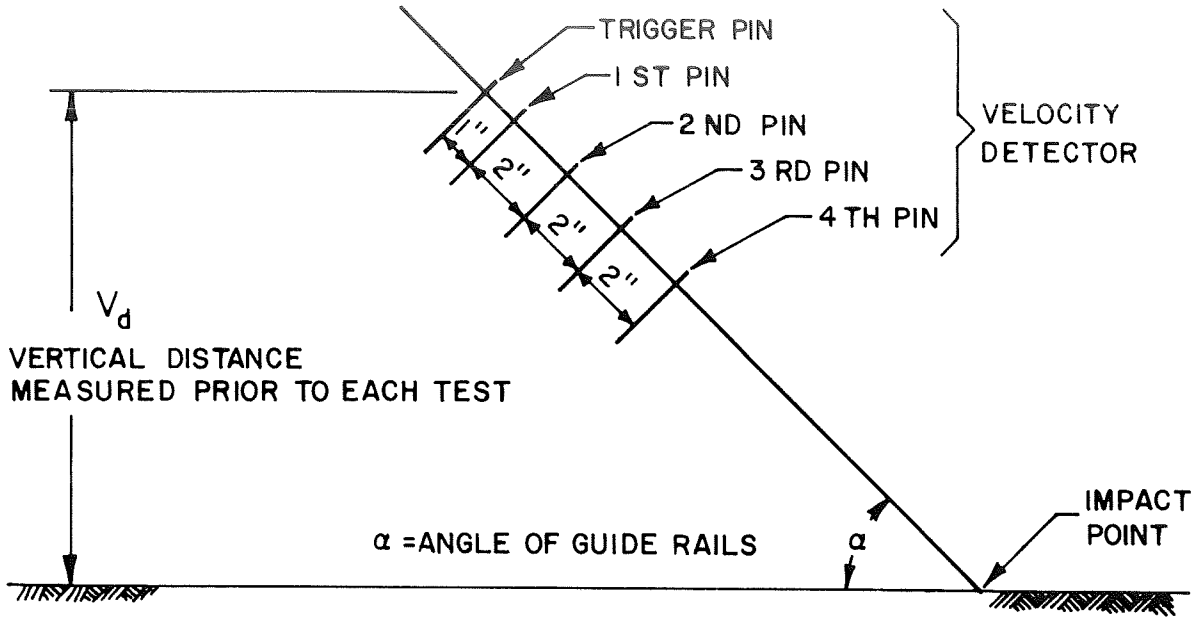


FIG. 10 SKETCH OF THE VELOCITY DETECTOR SYSTEM

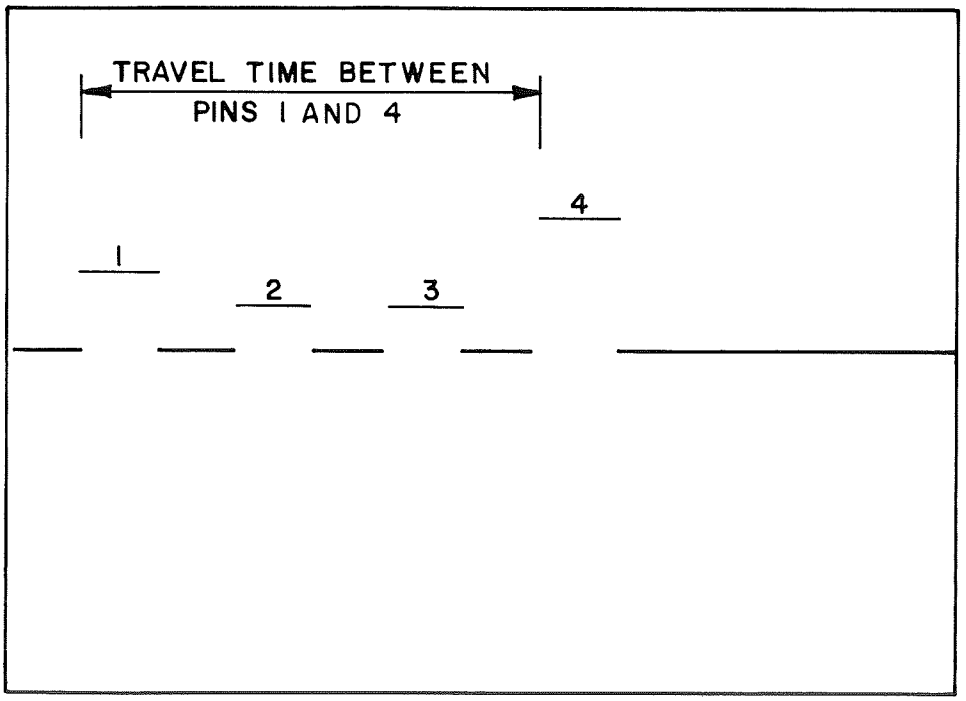


FIG. 11 TYPICAL VELOCITY RECORD

Equation 9 gives an average velocity over a 6 in. track distance; however, this approximation generally involves less than 5 percent error for angles of impact greater than 30 degrees.

The second method of calculation is given by

$$Vel_2 = \frac{V_d}{(T_d + T_p) \sin \alpha} \tag{10}$$

where,

$V_d$ = Vertical distance in Fig. 10,

$T_d$ = Oscilloscope delay time,

$T_p$ = Photo time in Fig. 12,

$\alpha$ = Impact angle.

The delay time is a setting on the oscilloscope which determines the time between the trigger and the start of the sweep. It should be noted that this is also an average velocity. Generally, the agreement between $Vel_1$ and $Vel_2$ was within ±5 percent for angles of impact greater than 30 degrees and for cylindrical, spherical, and wedge shaped projectiles. This agreement was considered acceptable and the impact velocity was calculated by

$$V_i = \frac{Vel_1 + Vel_2}{2} \tag{11}$$

where,

$Vel_1$ = Velocity calculated by method 1,

$Vel_2$ = Velocity calculated by method 2.

The angle of impact ($\alpha$) was assumed to be the same as the angle at which the guide rails were set. High speed photographs have shown that this assumption involves negligible error.

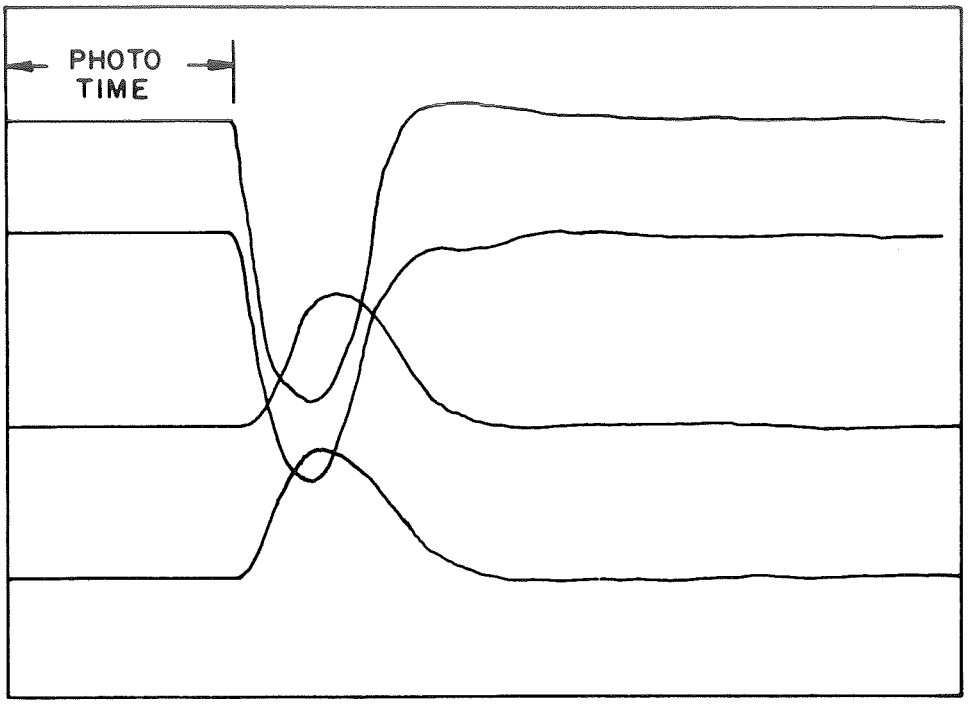


FIG. 12 ACCELERATION RECORD

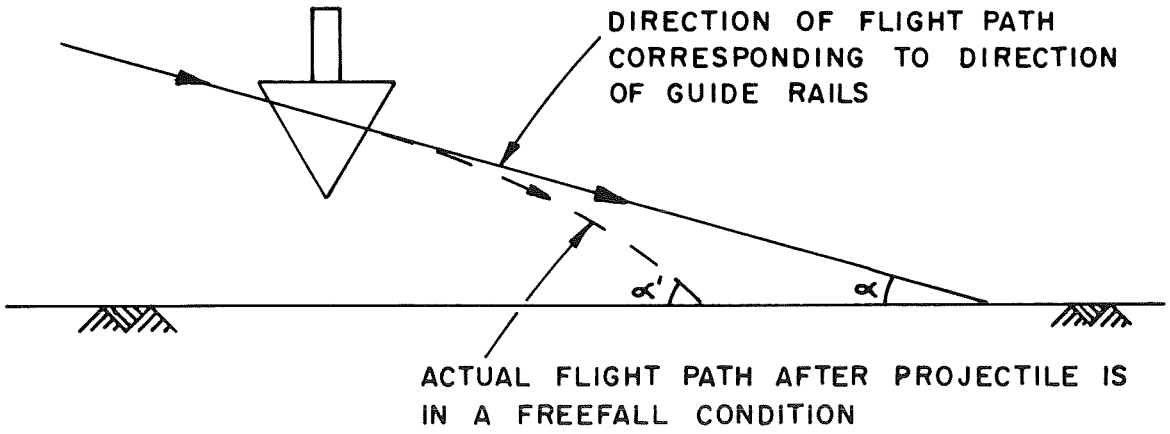


FIG. 13 EFFECT OF GRAVITY ON THE PROJECTILE FLIGHT PATH

When projectiles were launched at angles below 30 degrees the acceleration of gravity significantly changed both the magnitude and direction of the velocity between release and the instant of impact. Figure 13 illustrates the effect of gravity on the flight path of the projectile. The vertical velocity at impact was calculated by

$$V_v = [Vel_1 + 2.0\ (Vel_2 - Vel_1)\ ] \sin \alpha\ . \qquad (12)$$

This method assumes that the vertical velocity of the projectile increases linearly from the time of release to the instant of impact. $Vel_2$ is an average velocity which reflects the effect of gravity. $Vel_1$ is approximately the velocity of the projectile at the time of release. The horizontal velocity was calculated by

$$V_H = (Vel_1) \cos \alpha\ . \qquad (13)$$

The impact angle is

$$\alpha' = \tan^{-1} V_v/V_H\ . \qquad (14)$$

When the conical projectiles were tested, velocity $Vel_1$ and $Vel_2$ did not agree because $Vel_2$ was calculated using the photo time ($T_p$) which assumes the acceleration record begins at the instant the projectile contacts the soil. However, for the first few inches of cone penetration the soil reaction was not large enough to produce measurable deflections on the acceleration record. This caused the photo time (Fig. 12) to be greater than it actually was, thus producing an error in the calculation of $Vel_2$. Therefore, $Vel_1$ was used as the initial impact velocity.

Projectile History Calculations

The acceleration curves were input to Program IMPACT in the form of points at equal time intervals. It was found by Reichmuth[19] that the best approximation of the area under the curve was obtained by using the trapezoidal rule for the first increment of area, Simpson's rule for the sum of the first two increments of area, and the three-eighths rule for the following increments of area. The first integration of the acceleration curve yielded the velocity-time history of the projectile. The velocity-time relationship was then integrated to yield the displacement-time history. The acceleration of gravity was neglected for all projectiles except the cones. In many of the cone tests the accelerations were not large enough to permit gravity to be neglected.

# CHAPTER V

## TEST RESULTS AND ANALYSES

The author's testing program was divided into three phases. The first phase consisted of obtaining additional data for the evaluation of edge effects produced by projectiles which have finite dimensions in a direction perpendicular to the plane of motion. The second phase involved the impacting of projectiles at angles of impact less than 30 degrees. These tests were performed to check the accuracy of Reichmuth's[19] regression equations in predicting soil pressures developed during low angle impact. The third and final phase yielded data concerning the behavior of vertical impact of cones on sands.

### EDGE EFFECTS

The test apparatus and projectiles were constructed so that the projectiles, upon impact, traveled in a plane. This planar motion was verified by high speed film data and also by examination of soil imprints. Since the projectiles had finite dimensions in a plane perpendicular to the plane of motion, the accelerations were affected by this width. It should be noted that the width of the projectile is defined as the linear dimension in a direction perpendicular to the plane of motion. If small scale projectile test results are to be used to predict the behavior of similar, but larger projectiles it is advantageous to know the magnitude of the edge effects.

Reichmuth[19] used wedges and cylindrical projectiles, having widths of 5.5 in. and 16.5 in., to study edge effects. He developed the empirical equation

$$\frac{F_m}{F_p} = \frac{K_e}{D_p} + 1.00 \qquad (15)$$

where,

$F_m$ = Measured force per inch width,

$F_p$ = Plane strain force per inch width,

$K_e$ = Edge effect constant,

$D_p$ = Width of impact surface.

The edge effect constant was solved for by substituting each value of $D_p$ into Eq. 15, which yielded

$$\frac{F_{m(5.5)}}{F_p} = \frac{K_e}{5.5} + 1.00 \tag{16}$$

and

$$\frac{F_{m(16.5)}}{F_p} = \frac{K_e}{16.5} + 1.00 \quad . \tag{17}$$

Division of Eq. 16 by Eq. 17 yields

$$\frac{F_{m(5.5)}}{F_{m(16.5)}} = \frac{K_{e/5.5} + 1.00}{K_{e/16.5} + 1.00} \quad . \tag{18}$$

The ratio of $F_{m(5.5)}$ to $F_{m(16.5)}$ is equal to the peak acceleration ratio of the 5.5 in. wide projectile to the 16.5 in. wide projectile. This ratio was determined from field tests and thereby a measure of $K_e$ was obtained. This method of solving for $K_e$ involves the assumption that the edge effects are constant for projectiles having widths equal to, or greater than 5.5 inches. Figure 14 shows the effect of the projectile width on measured impact forces as determined by Reichmuth[19]. This figure indicates that the edge effect constant is highly dependent upon whether the target material is clay or sand. Impact on clay produced pressures larger than the plane strain pressure, while impact on sands produced the opposite effect.

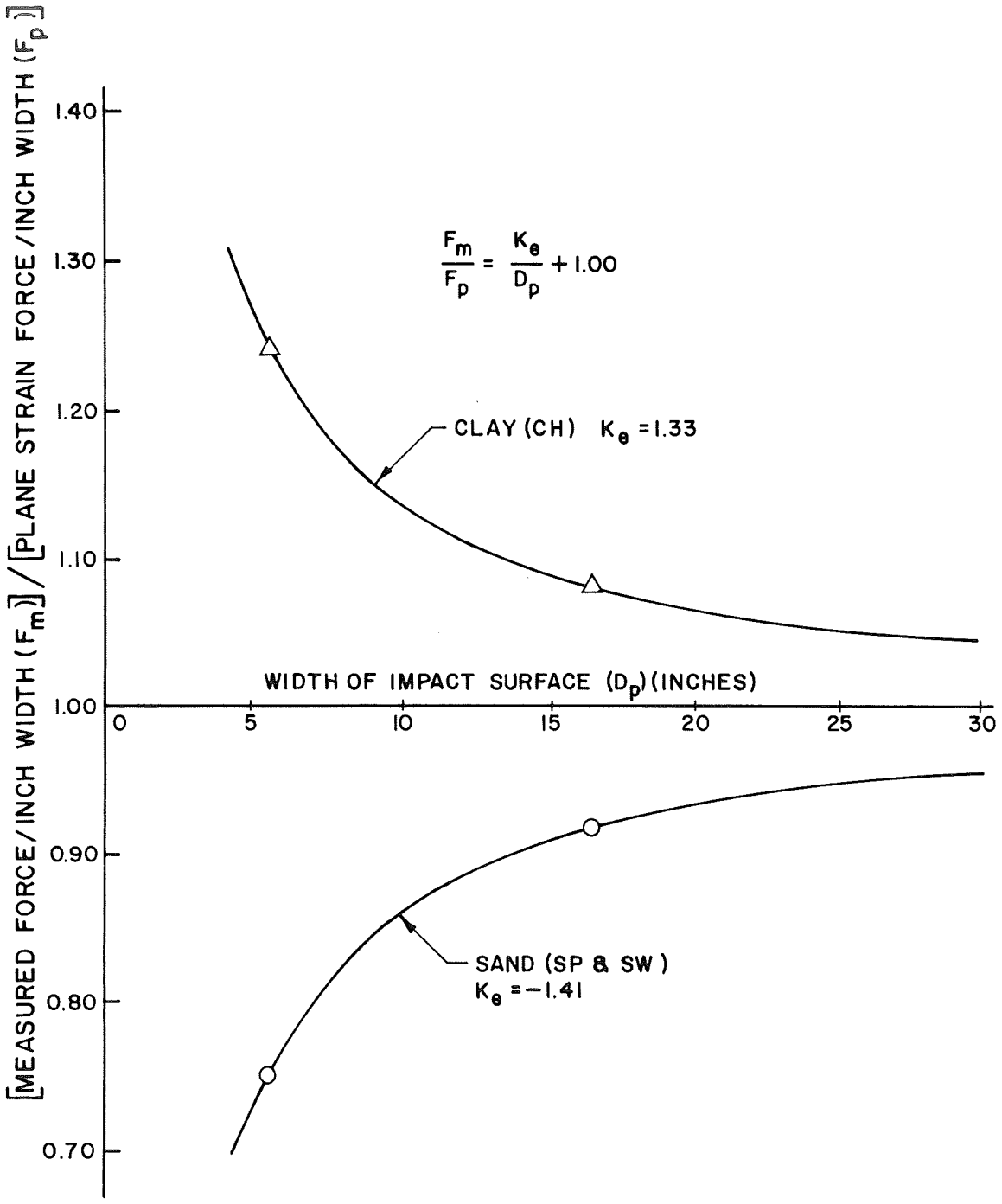


FIG. 14 EFFECT OF PROJECTILE WIDTH ON MEASURED IMPACT FORCES (AFTER REICHMUTH)

Double Width Projectile Results

In the derivation of Reichmuth's equations, which account for edge effects, it was necessary to assume that the edge effects were constant for widths equal to, or greater than 5.5 inches. At the present time, there are no theoretical methods for determining the minimum width above which the edge effects remain constant. Tests with double width projectiles (11.0 in. wide) were conducted to determine the validity of this assumption.

A series of tests were run using double width wedges and cylinders. Since these tests were to be compared to the previous single and triple width projectile tests of Reichmuth, extreme care was taken to reproduce similar testing conditions. Table No. 1 shows a tabulation of the results obtained for the single, double, and triple width tests on Del Rio Clay (CH) and Ottawa Sand (SP). The code used for identifying the tests is explained in Appendix A. Figure 15 illustrates the results from the single, double, and triple width tests on saturated Capitol Aggregates Sand (SW). The results are presented in the form of peak accelerations. If deviations in peak acceleration values due to experimental error are neglected, the variation of peak accelerations within a comparison test series is due to the change in projectile widths. Table No. 2 lists peak acceleration ratios for single and double width projectiles. These ratio values were then averaged and the resulting numerical values presented in Table No. 3.

The values from Table No. 3 were substituted into Eq. 19.

$$\frac{F_{m(5.5)}}{F_{m(11.0)}} = \frac{K_{e/5.5} + 1.00}{K_{e/11.0} + 1.00} \qquad (19)$$

TABLE NO. 1

COMPARISONS OF RESULTS FOR TESTS USING SINGLE (5½" WIDE), DOUBLE (11" WIDE) AND TRIPLE (16½" WIDE) WIDTH PROJECTILES

| TEST IDENTIFICATION | SOIL | | | TRACK VEL. (fps) | VALUES AT PEAK VERT. ACCELERATION | | | |
|---|---|---|---|---|---|---|---|---|
| | TYPE | γ (pcf) | w % | | Horiz. (g's) | Vert. (g's) | Angular (g's/ft) | Time (msec) |
| 8-19-7-WHO3-30-0 | CH | 121 | 28.4 | 20.86 | -17.5 | 26.4 | -29.2 | 12.58 |
| 5-18-4-WHO2-30-0 | CH | 115 | 32.0 | 20.85 | -24.8 | 39.8 | -46.2 | 8.94 |
| 8-19-4-WHO1-30-0 | CH | 113 | 33.7 | 20.99 | -14.5 | 22.4 | -27.4 | 13.64 |
| 8-19-6-WHO3-30-0 | CH | 113 | 32.8 | 27.26 | -22.8 | 32.2 | -33.5 | 12.58 |
| 5-18-5-WHO2-30-0 | CH | 115 | 35.5 | 28.06 | -28.9 | 48.5 | -43.6 | 11.17 |
| 8-19-5-WHO1-30-0 | CH | 113 | 33.7 | 29.39 | -28.4 | 41.3 | -42.3 | 11.72 |
| 8-16-5-WLA3-45-0 | CH | 112 | 32.4 | 14.93 | - 3.5 | 22.5 | -12.5 | 16.00 |
| 6- 5-1-WLA2-45-0 | CH | 115 | 33.1 | 15.08 | - 4.0 | 23.2 | -15.1 | 15.48 |
| 8-16-3-WLA1-45-0 | CH | 112 | 31.9 | 15.42 | - 2.8 | 29.2 | -11.5 | 14.00 |
| 8-16-6-WLA3-45-0 | CH | 114 | 32.4 | 28.70 | - 7.8 | 46.3 | -23.0 | 15.00 |
| 6- 5-2-WLA2-45-0 | CH | 113 | 36.1 | 30.24 | - 9.2 | 48.5 | -29.5 | 14.04 |
| 8-16-2-WLA1-45-0 | CH | 110 | 35.5 | 27.50 | - 8.7 | 41.9 | -30.0 | 13.91 |
| 8-18-3-CYL3-45-0 | CH | 112 | 33.9 | 16.33 | -13.6 | 36.1 | -23.8 | 11.69 |
| 5-25-4-CYL2-45-0 | CH | 116 | 34.5 | 16.09 | -15.2 | 45.8 | -32.4 | 7.14 |
| 8-19-3-CYL1-45-0 | CH | 115 | 33.6 | 15.79 | -16.1 | 35.3 | -26.2 | 8.71 |
| 8-18-4-CYL3-45-0 | CH | 114 | 31.6 | 27.30 | -20.0 | 48.1 | -33.7 | 7.55 |
| 6- 5-5-CYL2-45-0 | CH | 116 | 33.3 | 27.46 | -24.5 | 73.2 | -37.5 | 5.95 |
| 8-19-2-CYL1-45-0 | CH | 115 | 30.9 | 28.64 | -26.1 | 57.5 | -43.1 | 6.77 |
| 8-18-8-CYL3-45-0 | CH | 115 | 32.0 | 14.82 | -13.9 | 34.3 | -18.5 | 12.66 |
| 5-25-3-CYL2-45-0 | CH | 116 | 35.0 | 15.29 | -15.0 | 46.8 | -31.2 | 7.19 |
| 8-18-6-CYL1-45-0 | CH | 116 | 32.6 | 15.24 | -18.1 | 41.6 | -22.1 | 11.32 |

TABLE NO. 1 (CONT'D)

| TEST IDENTIFICATION | SOIL TYPE | SOIL γ (pcf) | SOIL w % | TRACK VEL. (fps) | VALUES AT PEAK VERT. ACCELERATION Horiz. (g's) | Vert. (g's) | Angular (g's/ft) | Time (msec) |
|---|---|---|---|---|---|---|---|---|
| 8-18-9-CYL3-45-0 | CH | 111 | 35.3 | 28.89 | -22.8 | 44.6 | -29.1 | 11.61 |
| 5-25-2-CYL2-45-0 | CH | 117 | 34.9 | 29.05 | -22.2 | 72.9 | -40.5 | 4.79 |
| 8-18-5-CYL1-45-0 | CH | 115 | 35.4 | 28.60 | -29.8 | 61.3 | -26.5 | -- |
| 8-17-1-WLA3-75-0 | CH | 113 | 32.9 | 11.62 | - 0.8 | 29.4 | - 3.0 | 14.71 |
| 6- 4-4-WLA2-75-0 | CH | 116 | 33.1 | 11.22 | - 2.3 | 31.2 | - 6.1 | 10.41 |
| 8-17-7-WLA1-75-0 | CH | 113 | 31.7 | 11.46 | - 1.5 | 30.0 | - 4.4 | 14.42 |
| 8-17-4-WLA3-75-0 | CH | 113 | 33.0 | 32.50 | - 3.4 | 68.2 | - 7.9 | 12.66 |
| 6- 4-2-WLA2-75-0 | CH | 117 | 34.4 | 32.79 | - 6.1 | 73.4 | -12.7 | 12.05 |
| 8-17-5-WLA1-75-0 | CH | 112 | 34.7 | 33.27 | - 3.7 | 77.6 | - 7.8 | 12.50 |
| 8-18-1-CYL3-75-0 | CH | 116 | 30.9 | 21.95 | - 9.3 | 55.6 | -10.4 | 5.84 |
| 5-25-6-CYL2-75-0 | CH | 117 | 33.0 | 21.03 | - 8.3 | 68.5 | -10.2 | 5.95 |
| 8-17-15-CYL1-75-0 | CH | 115 | 28.4 | 21.73 | -10.3 | 67.9 | - 9.4 | 6.04 |
| 8-18-2-CYL3-75-0 | CH | 115 | 32.3 | 11.34 | -11.4 | 42.2 | + 2.5 | 7.74 |
| - - - - - - - - | -- | -- | -- | -- | -- | -- | -- | -- |
| 8-17-14-CYL1-75-0 | CH | 112 | 32.1 | 11.27 | -10.3 | 44.0 | + 1.1 | 8.60 |
| 8-17-11-WHO3-75-0 | CH | 113 | 31.2 | 29.57 | - 7.0 | 76.4 | -14.9 | 8.65 |
| 5-16-3-WHO2-75-0 | CH | 116 | 30.8 | 29.53 | -15.7 | 95.6 | -13.7 | 8.00 |
| 8-17-10-WHO1-75-0 | CH | 110 | 32.9 | 30.19 | -12.9 | 90.5 | -10.0 | 9.12 |
| 8-17-12-WHO3-75-0 | CH | 114 | 29.2 | 21.76 | - 5.6 | 46.9 | - 6.4 | 10.58 |
| 5-18-1-WHO2-75-0 | CH | 113 | 34.3 | 21.18 | - 7.2 | 55.5 | -13.8 | 8.94 |
| 8-17-9-WHO1-75-0 | CH | 116 | 32.2 | 21.45 | - 8.9 | 59.0 | - 7.7 | 11.07 |
| 8-17-13-WHO3-75-0 | CH | 115 | 32.0 | 11.53 | - 5.9 | 33.8 | - 3.3 | 13.46 |
| 5-18-3-WHO2-75-0 | CH | 117 | 31.9 | 11.66 | - 4.6 | 36.7 | - 8.6 | 10.11 |
| 8-17-9-WHO1-75-0 | CH | 111 | 30.0 | 11.40 | - 6.9 | 41.0 | -10.5 | 12.16 |

TABLE NO. 1 (CONT'D)

| TEST IDENTIFICATION | SOIL TYPE | SOIL γ (pcf) | SOIL w % | TRACK VEL. (fps) | VALUES AT PEAK VERT. ACCELERATION Horiz. (g's) | Vert. (g's) | Angular (g's/ft) | Time (msec) |
|---|---|---|---|---|---|---|---|---|
| 8- 1-4-WLA3-30-0 | SP | 105 | 0 | 18.95 | - 6.5 | 7.3 | -15.8 | 17.20 |
| - - - - - - - | -- | -- | -- | -- | -- | -- | -- | -- |
| 8- 4-4-WLA1-30-0 | SP | 105 | 0 | 19.33 | - 5.8 | 9.3 | -16.1 | 22.64 |
| 8- 4-18-WHO3-45-0 | SP | 105 | 0 | 16.20 | - 6.6 | 17.0 | - 6.2 | 14.91 |
| 5- 4-4-WHO2-45-0 | SP | 105 | 0 | 14.72 | - 2.5 | 21.1 | - 4.7 | 10.06 |
| 8- 4-16-WHO1-45-0 | SP | 105 | 0 | 15.47 | - 3.1 | 13.2 | - 1.5 | 18.00 |
| 7-9-4-WHA3-75-0 | SP | 105 | 0 | 30.19 | - 8.1 | 32.8 | -13.8 | 14.09 |
| 5-2-6-WHA2-75-0 | SP | 104 | 0 | 30.30 | - 6.5 | 32.2 | -15.3 | 11.07 |
| 7-9-3-WHA1-75-0 | SP | 105 | 0 | 29.91 | - 7.1 | 31.7 | -13.7 | 13.73 |
| 7-13-10-WHO3-75-0 | SP | 103 | 0 | 10.88 | - 2.4 | 23.4 | - 0.2 | 12.08 |
| 4-27-9-WHO2-75-0 | SP | 103 | 0 | 10.80 | - 3.0 | 25.2 | - 2.5 | 8.24 |
| 7-13-8-WHO1-75-0 | SP | 103 | 0 | 11.11 | - 3.1 | 24.8 | + 1.9 | 10.91 |
| 7-13-11-WHO3-75-0 | SP | 103 | 0 | 21.32 | - 1.8 | 46.7 | - 0.5 | 6.08 |
| 4-27-6-WHO2-75-0 | SP | 103 | 0 | 21.51 | - 3.8 | 39.4 | - 3.7 | 4.40 |
| 7-13-7-WHO1-75-0 | SP | 103 | 0 | 21.29 | - 3.4 | 41.0 | + 3.2 | 8.00 |
| 7-13-12-WHO3-75-0 | SP | 103 | 0 | 29.54 | - 4.3 | 45.8 | - 2.5 | 6.08 |
| 4-27-3-WHO2-75-0 | SP | 99 | 0 | 30.15 | - 7.5 | 72.3 | - 7.5 | 4.40 |
| 7-13-6-WHO1-75-0 | SP | 103 | 0 | 29.75 | - 2.7 | 68.0 | - 6.8 | 7.36 |
| 9-2-11-WHO3-90-0 | SP | 102 | 4.7 | 21.17 | - 0.5 | 39.4 | + 0.1 | 7.14 |
| - - - - - - - - - | -- | -- | -- | -- | -- | -- | -- | -- |
| 9-9-2-WHO1-90-0 | SP | 101 | 5.0 | 20.05 | - 0.2 | 38.8 | + 0.1 | 6.15 |
| 9-2-12-WHO3-90-0 | SP | 104 | 4.2 | 11.28 | - 0.9 | 31.0 | + 0.0 | 8.52 |
| - - - - - - - - - | -- | -- | -- | -- | -- | -- | -- | -- |
| 9-9-1-WHO1-90-0 | SP | 103 | 6.2 | 9.29 | - 0.3 | 18.7 | + 1.3 | 12.30 |

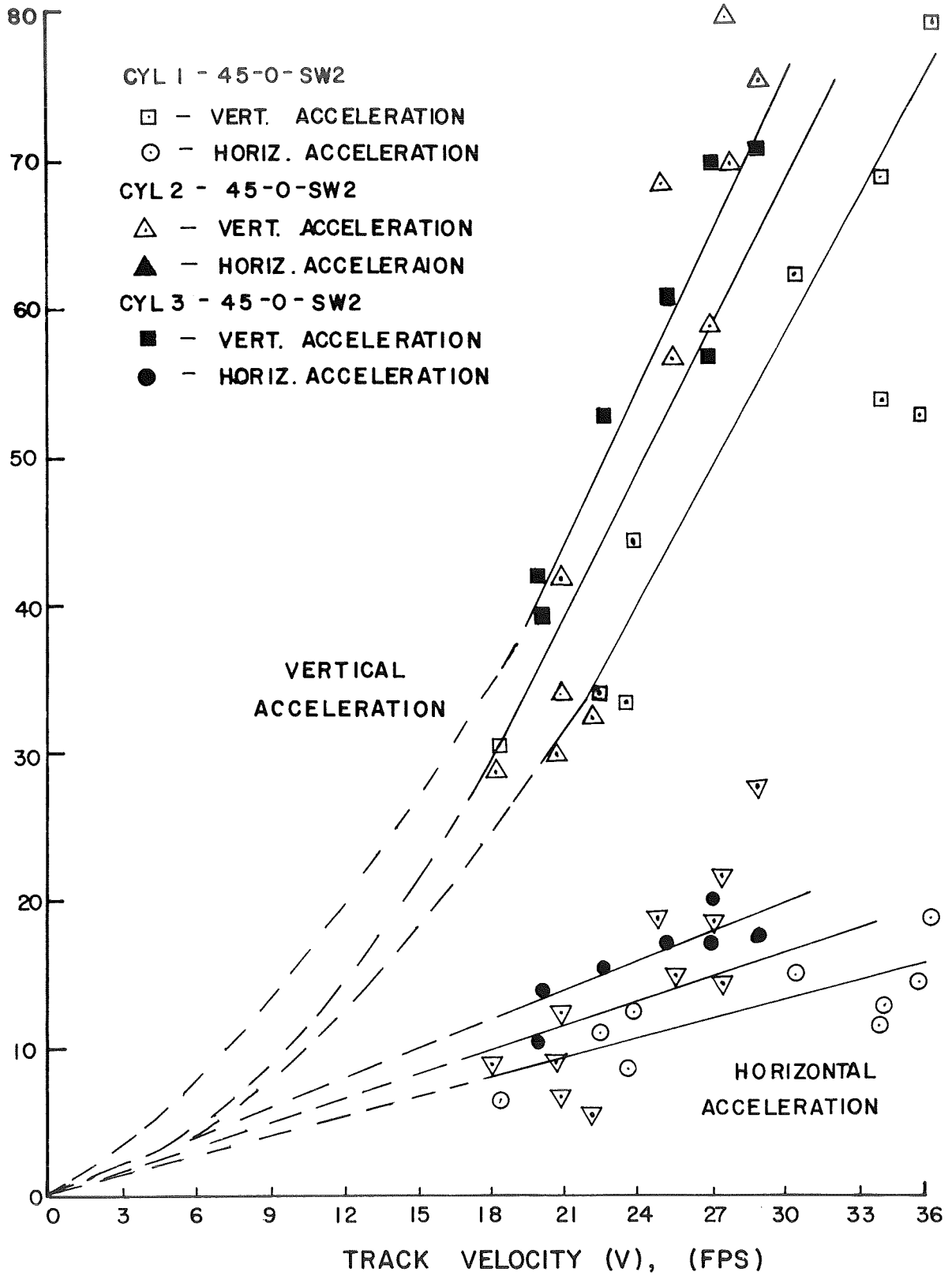


FIG. 15 EFFECT OF PROJECTILE WIDTH ON ACCELERATION – CYLINDER TESTS ON SATURATED COLORADO RIVER SAND

TABLE NO. 2

RELATIVE ACCELERATION OF SINGLE AND DOUBLE WIDTH PROJECTILES

| Soil | Peak Acceleration Ratio (Single Width/Double Width) | | | No. of Comparisons |
|---|---|---|---|---|
| | Vert. | Horiz. | Angular | |
| Del Rio Clay[1] (CH) | 0.93 | 1.00 | 0.82 | 14 |
| Ottawa Sand[1] (SP) | 0.91 | 0.93 | [3] | 5 |
| Capitol Aggregates Sand[2] (SW) | 0.85 | 0.80 | | |

NOTE: 1 Values taken from Table No. 1
2 Values taken from Fig. 15
3 Accelerations too small for valid comparison

TABLE NO. 3

AVERAGE RATIOS OF PEAK ACCELERATIONS
FOR SINGLE AND DOUBLE WIDTH PROJECTILES

| Type Soil | Single Width/Double Width |
|---|---|
| Clay | 0.92 |
| Sand | 0.87 |

This substitution yielded edge effect constant values ($K_e$) of -1.26 for sand and -0.82 for clay. As shown in Fig. 14, the values obtained by Reichmuth were -1.41 for sand and 1.33 for clay.

There is some deviation in the constants for sand; however, the ratio of $F_m$ to $F_p$ is relatively insensitive to changes in $K_e$ and from this viewpoint the agreement is extremely good. The good agreement indicates that the assumption of constant edge effects for projectiles having widths equal to, or greater than 5.5 in. is valid.

The agreement for tests on clay was unsatisfactory. Reichmuth's results, for clay, indicate that as the width of the projectile increases the force per inch of width decreases, while the results from this investigation indicate the opposite effect. Two factors which may have contributed to the disparity in results will now be discussed. Examination of Table No. 2 shows that the peak angular acceleration values for the double width projectiles are on the average approximately 20 percent greater than single width values. Since the projectile penetrations in clay were relatively small compared to the tests in sand, in all cases less than 1.0 in., the angular acceleration is extremely sensitive to angle of impact. As stated previously, the angle of impact was predetermined by setting the inclination of the guide rails. The rails were composed of 2 by 2 in. box aluminum members which were fairly flexible, thus causing the measured impact angle to be a function of where it was measured along the rails. The point of measurement of the rail inclination, which was approximately two feet above the lower end of the rail, may not have been the same as that used by Reichmuth[19].

The soil conditions may have been slightly different since the tests were conducted with a 9 month interval; however, the collected soil data gave no indication of this nature.

Edge Effects for Static Loading

The dynamic test data indicates a large difference between the edge effects for tests on sand and clay. This large difference has also been noted in static tests.

Figure 16 illustrates pressure distributions beneath statically loaded rigid footings on cohesionless and cohesive soils. Figure 16a depicts a case in which the footing has undergone a uniform displacement and the pressure distribution across the width of the footing is approximately parabolic. Taylor[25] has stated that if the average pressure is relatively small, or if the footing width is large, the pressure distribution is flatter over the central portion of the footing and is nearer ellipsoidal than parabolic, as shown in Fig. 16b. The stresses at the edges of a footing resting on cohesionless soil are zero because the soil just outside the footing edges is not under pressure and therefore has no strength. If the footing has an infinite length (plane strain case), the ultimate average contact pressure that can be developed is approximately 20 percent greater than the ultimate average pressure for a square footing having the same width as the infinitely long footing. It should be noted that the width of the footing is always the least plan dimension according to conventional nomenclature. This nomenclature has not been adopted for the dynamic tests. The width of the projectile is referred to as the linear dimension in a direction perpendicular to the plane of motion.

Figure 17 shows the failure pattern for a strip footing (footing of infinite length). Bearing failure of a strip footing involves movement of the soil in two directions, with the displacement of the soil in the Z direction being zero. Figure 18 illustrates a three dimensional failure mode in sand, upon impact of a 5.5 in. wide projectile. Although the sand is

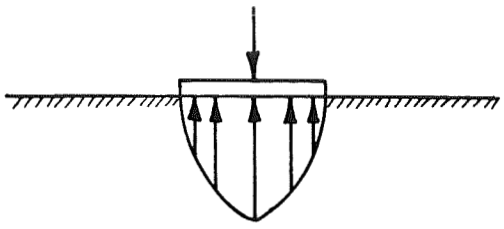

(a)

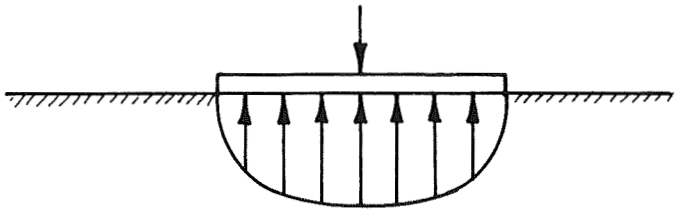

(b)

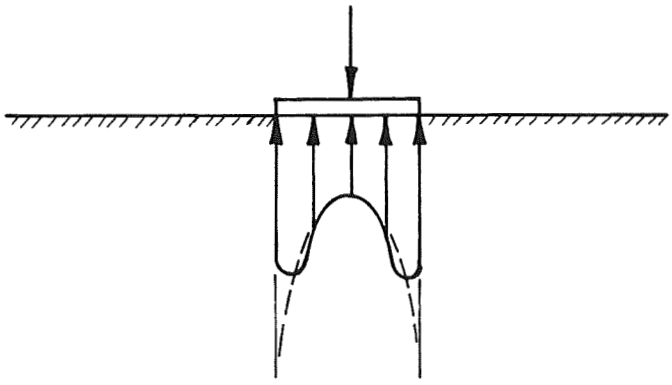

(c)

FIG. 16 PRESSURE DISTRIBUTION BENEATH STATICALLY LOADED RIGID FOOTINGS. (a) COHESIONLESS SOIL; NARROW FOOTING, (b) COHESIONLESS SOIL; WIDE FOOTING, (c) COHESIVE SOIL

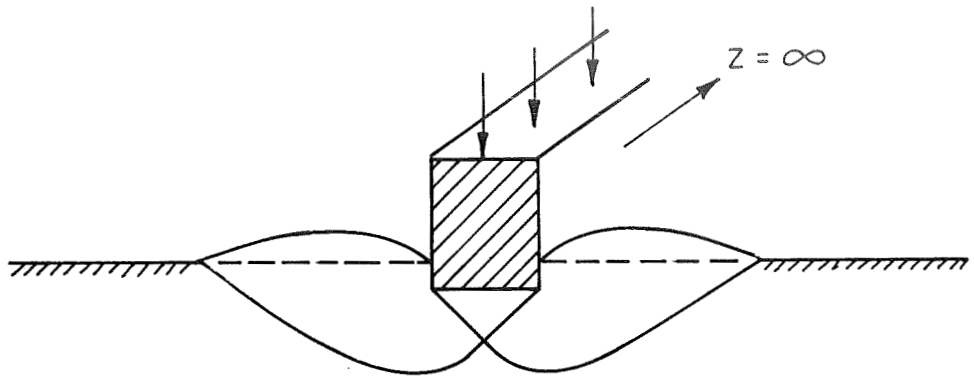


FIG. 17 FAILURE PATTERN BENEATH AN INFINITELY LONG, STATICALLY LOADED STRIP FOOTING

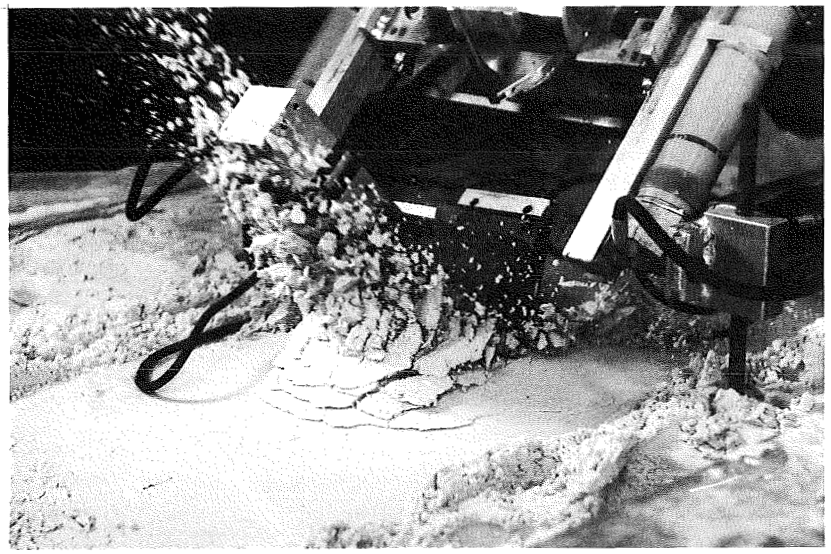

FIG. 18 EXAMPLE OF THREE DIMENSIONAL FAILURE MODE IN PARTIALLY SATURATED OTTAWA SAND. IMPACT OF A 120 DEGREE WEDGE AT 45 DEGREES (PHOTO AFTER REICHMUTH)

partially saturated, a large amount of soil is ejected away from the impact area. A series of failure plane outcroppings are visible; indicating that possibly the soil which remains in the impact area behaves in a manner similar to that in static systems.

The stress distribution beneath a rigid footing on a cohesive soil is shown in Fig. 16c. The dashed line indicates the pressure distribution, shown by theory of elasticity, for an elastic material of infinite strength. Since it is not possible to have a material of infinite strength the actual distribution is indicated by the heavy line. The high stresses at the edge of the footing are caused by the large shearing force which is developed by relative movement between the soil under the edge of the footing and the soil just outside the edge. Along the perimeter of a rigid footing on sand these same shearing strains exist but due to the lack of rigidity in sand stresses are not developed. The ultimate average stress developed beneath a square footing on clay is approximately 30 percent greater than the ultimate average stress beneath a strip footing on clay.

Summary of Edge Effects

It has been shown that the edge effects, under static loading conditions, are of an opposite nature for sands and clays. For a constant width footing resting on sand, an increase in footing length will produce an increase in the ultimate average contact pressure beneath the footing. For footings on clay the contact pressure decreases with an increase in length. Thus, the edge effect constant for static loading conditions would be positive for clays and negative for sands. Reichmuth's[19] impact test results (single and triple width projectiles) indicated a similar type of behavior. However, the double width projectile tests of the author indicated negative edge effect values for both sands and clays. It is believed that the author may not have

been able to reproduce the testing techniques of Reichmuth, which were especially critical for tests on clay. Since Reichmuth's single and triple width tests were performed under similar test conditions, it was assumed that the single and triple width clay test results indicate the true soil behavior.

As previously stated on p. 48, the agreement for tests on sand was good. This agreement tends to substantiate Reichmuth's assumption that the edge effects are approximately constant for projectile widths equal to, or greater than 5.5 inches.

## LOW ANGLE IMPACT

A series of tests were conducted to determine how well the equations generated by Reichmuth[19] predict soil pressures for impact angles less than 30 degrees. These equations were generated by applying regression type analyses to experimental data that were obtained from the impact of wedges, cylinders, and spheres, at angles of impact ranging between 90 and 30 degrees.

### Wedge

Reichmuth assumed that the soil pressures generated during impact could be represented by equations which involved the product of test variables raised to exponential powers. He developed the following equations; which represent best fits, by the least squares method, of the experimental wedge data.

$$(F_p)_N = 3.54(-V_\theta)^{0.44}(-V_V)^{0.28}V_H^{0.43}\gamma^{0.70}(-D_t)^{-0.04}\beta^{-1.19} \qquad (20)$$

$$(F_p)_T = 3.10\ \beta^{0.89}\ (F_p)_N^{0.04} - 100 \qquad (21)$$

The variables appearing in these equations are defined as follows:

$(F_p)_N$ = Plane strain normal pressure on the loading face of wedge (lb/in.),

$(F_p)_T$ = Plane strain tangential pressure on the leading face of wedge (lb/in.),

$V_\theta$ = Rotational velocity (radians/sec),

$V_V$ = Vertical velocity of wedge tip (fps),

$V_H$ = Horizontal velocity of wedge tip (fps),

$\gamma$ = Soil density (pcf),

$D_t$ = Vertical penetration (in.),

$\beta$ = Face angle (angle between leading face of wedge and horizontal soil surface), (degrees).

The sign conventions used in this investigation are given in Appendix A.

Equations 20 and 21 were derived from data that were taken solely from the rising and peak portions of the acceleration-time curves. Another limitation is that data were used from tests in which only one face of the wedge was in contact with the soil. It was assumed that for angles of impact below 60 degrees the back face of the wedge was not in contact with the soil. In deriving the equations it was necessary to use data from tests which had a single face in contact with the soil since a maximum of three unknowns can be uniquely solved for using the three equations of equilibrium. The three unknowns were the resultant normal force $(F_N)$, resultant tangential force $(F_T)$, and the distance $F_N$ acts from the wedge tip (D). Figure 19 shows the nomenclature for wedges loaded on the leading face. The plane strain pressures were then calculated using

$$\frac{F_N}{(F_p)_N} = \frac{K_e}{D_p} + 1.00 \tag{22}$$

and

$$\frac{F_T}{(F_p)_T} = \frac{K_e}{D_p} + 1.00 \quad . \tag{23}$$

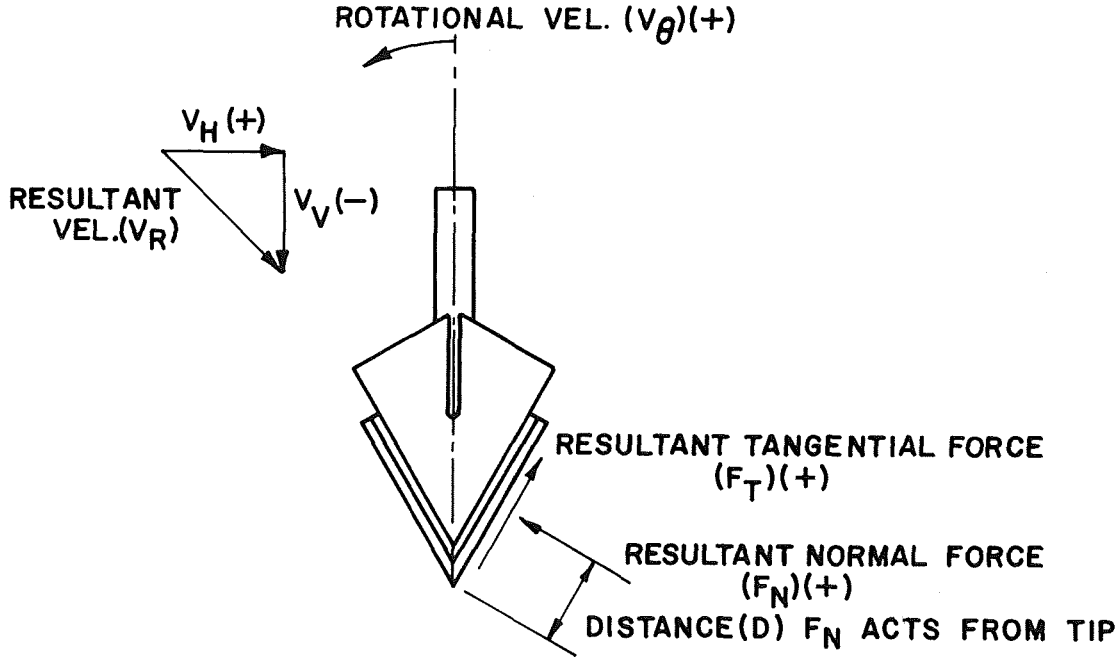


FIG. 19 NOMENCLATURE FOR WEDGE LOADED ON LEADING FACE (AFTER REICHMUTH)

Values of -1.41 and 1.33 were used for the edge effect constant ($K_e$) for sand and clay, respectively.

The reliability at which Eqs. 20 and 21 predict the soil pressures on the leading face of the wedges, at angles of impact below 30 degrees, was determined by substitution of the low angle impact test data. This substitution yielded calculated soil pressures which were compared with the measured values. Mean and standard deviation values for the impact tests performed during this investigation and from Reichmuth's work are listed in Table No. 4. Examination of this table shows that the mean normal and tangential pressures for the wedge tests, at impact angles below 30 degrees, are much lower than the higher angle tests. The standard deviation values for the low angle tests are approximately 60 percent of the high angle tests; however, standard deviation values by themselves do not indicate how well the regression equations fit the data. A relative indication of how well the equations fit the data can be obtained by comparing the mean and standard deviation values of the low and high angle tests. The table indicates that the regression equations do not fit the low angle wedge data nearly as well as they do the high angle tests.

Another measure of the applicability of these equations to low angle impact is the percent deviation between the predicted and measured pressures. Percent deviations for all of the low angle wedge results are given in Appendix D on pp.166 through 167. In only 8 out of the 81 cases listed for tangential pressures are the deviations less than 100 percent and in over half the comparisons the deviations are greater than 300 percent. In every instance the regression equations over-estimated the tangential pressures. Reichmuth has listed 108 cases in which only 3 cases have deviations exceeding 100 percent. It is interesting to note that the majority of the low angle tests with wedges

TABLE NO. 4

SOIL PRESSURE PREDICTION FOR LOW ANGLE IMPACT TESTS

| MODEL TYPE | DEPENDENT VARIABLE | STANDARD DEVIATION $\alpha \geq 30$ Degrees* | STANDARD DEVIATION $\alpha < 30$ Degrees | MEAN $\alpha \geq 30$ Degrees | MEAN $\alpha < 30$ Degrees |
|---|---|---|---|---|---|
| Wedge | $(F_p)_N$ | 71.6 lb/in. | 40.4 lb/in. | 135.3 lb/in. | 40.5 lb/in. |
| | $(F_p)_T$ | 41.3 lb/in. | 24.5 lb/in. | 122.1 lb/in. | 5.7 lb/in. |
| Cylinder | $(F_p)_H$ | 70.1 lb/in. | 26.4 lb/in. | 129.0 lb/in. | 35.6 lb/in. |
| | $(F_p)_V$ | 234.7 lb/in. | 65.1 lb/in. | 518.1 lb/in. | 73.8 lb/in. |
| Sphere | $F_H$ | 264.7 lb | 394.0 lb | 468.8 lb | 141.9 lb |
| | $F_V$ | 1066.8 lb | 525.9 lb | 2129.8 lb | 271.7 lb |

* $\alpha$ = Impact Angle

$$\text{Mean} = \frac{\text{Summation of Measured Values}}{\text{Number of Values}}$$

$$\text{Standard Deviation} = \sqrt{\frac{\Sigma(\text{Measured Value} - \text{Calculated Value})^2}{\text{No. of Values}}}$$

having 120 degree included angles (WL01 and WH02) develop tangential pressures which are negative. Thus, indicating that the major portion of soil in contact with the leading face is flowing in a downward direction. Figure 20 illustrates the difference in the soil flow for high and low impact angles. Reichmuth has postulated that in every case there is soil flow in both an upward and downward direction, with a stagnation region separating the flow directions. This phenomenon has been described by Wagner[30] and Korvin-Kroukovsky[10] in connection with hydroplane impact.

Unlike the tangential pressure predictions, Eq. 20 yields normal pressures which are much less than the measured values. The average deviation was approximately 85 percent. Out of the 108 cases listed by Reichmuth approximately two-thirds of these cases had deviations less than 50 percent.

The preceding presentation of wedge results has shown that the regression equations do not predict tangential and normal pressures for impact angles below 30 degrees nearly as well as for impact angles ranging between 30 and 60 degrees. A possible reason for the disagreement may be obtained by examining Eqs. 20 and 21. The magnitude of the exponent on each independent variable indicates the relative importance of each variable. In each equation, the face angle ($\beta$) is the more important variable. As previously discussed, the lower the angle of impact the larger the tendency is for the soil to flow in a downward direction. This downward flow not only affects the magnitude of the tangential pressure, but also the normal pressure. The normal pressures are inversely proportional to the face angle, while the tangential pressures are directly proportional to the face angle. The regression equations yield an over-estimate of the tangential pressures and an under-estimate of the normal pressures, which seems to indicate that the equations do not fully account for the soil flow pattern at angles of impact below 30 degrees.

HIGH ANGLE CONTACT

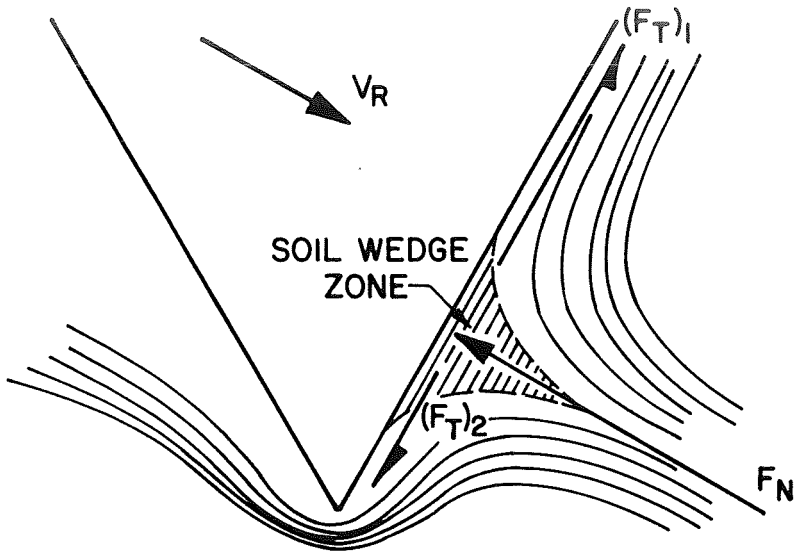


$(F_T)_1 > (F_T)_2$

LOW ANGLE CONTACT

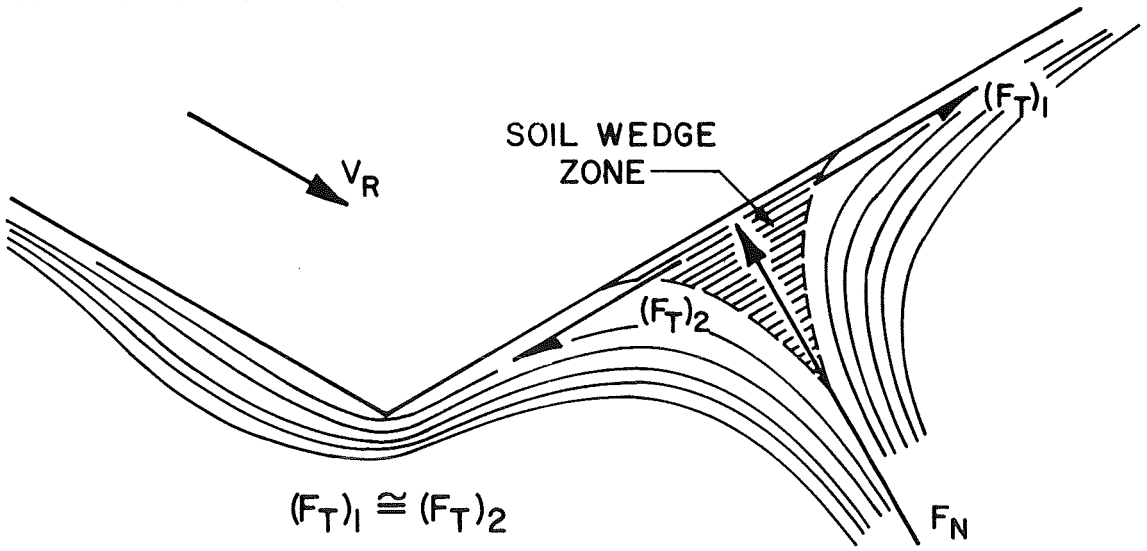


$(F_T)_1 \cong (F_T)_2$

FIG. 20 REICHMUTH'S POSTULATED FLOW PHENOMENA FOR WEDGE IMPACT (AFTER REICHMUTH)

Cylinder

Regression equations were also developed to predict the resultant horizontal and vertical plane strain pressures at the mass center of the projectiles having cylindrical impacting surfaces[19]. The angle of impact ranged between 30 and 90 degrees. The equations are:

$$(F_p)_H = 0.0859\ (-D_t)^{0.36}\ V_H^{0.27}\ (-V_V)^{0.58}\ (-V_\theta)^{0.39}\ \gamma^{1.09} \tag{24}$$

and

$$(F_p)_V = 0.131(-D_t)^{0.37}\ V_H^{-0.13}(-V_V)^{1.01}(-V_\theta)^{0.24}\gamma^{1.25} \tag{25}$$

The variables are defined as follows:

$(F_p)_H$ = Plane strain horizontal pressure at the projectile center of gravity (lb/in.),

$(F_p)_V$ = Plane strain vertical pressure at the projectile center of gravity (lb/in.),

$D_t$ = Vertical penetration (in.),

$V_H$ = Horizontal velocity at the center of gravity (fps),

$V_V$ = Vertical velocity at the center of gravity (fps),

$V_\theta$ = Rotational velocity (rps),

$\gamma$ = Soil density (pcf).

A comparison between the reliability of Eqs. 24 and 25 to predict horizontal and vertical pressures for low and high angle impact tests of cylindrical projectiles is given in Table No. 4. Standard deviations for the high angle ($\alpha > 30$ degrees) impact tests were approximately 55 and 45 percent of the mean values for the horizontal and vertical pressures, respectfully. The low angle ($\alpha < 30$ degrees) test data yielded standard deviations of approximately 75 and 90 percent of the horizontal and vertical mean pressure values. This comparison shows that the equations predict pressures for the high angle tests with a greater degree of accuracy.

Percent deviation values for the low angle test results are listed in Appendix D on pp. 175 and 176. Over 40 percent of the cases have deviations less than 50 percent. An interesting correlation was obtained by comparing the soil densities, listed on pp. 172 through 174, with the deviation values. It was found that for impact tests on soil in a dense state (for the sands utilized in this investigation densities of 99 pcf or greater may be considered dense) the deviation values were in nearly all cases much less than similar tests on the sands in looser states. After discovering this correlation, Reichmuth's experimental data were studied in more detail and it was found that in over 90 percent of the sets of data, utilized in developing the prediction equations, the densities were greater than 100 pcf.

Although the deviations are quite large in many instances for low angle impact tests on sands in a loose state, the equations do predict horizontal and vertical soil pressures with a reasonable degree of accuracy for tests on sands in dense states. The equations tend to over-estimate the pressures by approximately 300 percent for low angle impact tests on loose sand.

Sphere

A regression analysis was performed on the data which were derived from high angle ($\alpha \geq 30$ degrees) impact tests[19]. The equations obtained are

$$F_H = 0.683(-D_t)^{0.70} V_H^{0.52} (-V_V)^{-0.21} (-V_\theta)^{0.28} \gamma^{1.23} \qquad (26)$$

and

$$F_V = 1.89(-D_t)^{0.87} V_H^{-0.11} (-V_V)^{0.26} (-V_\theta)^{0.21} \gamma^{1.38} \qquad (27)$$

where,

$F_H$ = Horizontal force at the center of gravity (lb),

$F_V$ = Vertical force at the center of gravity (lb).

Definitions of the remaining variables have been given on p. 60. It should be noted that no attempt was made to account for edge effects.

Examination of Table No. 4 shows that the horizontal and vertical forces are predicted much better for the high angle sphere tests. The percent deviation values, listed on pp. 181 and 182, were found to be much lower for the tests on sand in a dense state. Once again, the data from which the equations were developed were examined and it was found that over 90 percent of the data sets were taken from tests on soils having densities greater than 100 pcf. In every instance with the exception of one, the equations overestimated the measured forces. Based on the deviation values, it is possible to state that the equations predict with a reasonable degree of accuracy the forces produced by low angle impact of the spherical projectile on sand in a dense state.

General Discussion of Regression Equations

The previous results have provided a comparison of how well the regression equations predict soil pressures and forces on wedges, cylinders, and spheres, when launched at angles below 30 degrees, as opposed to the prediction accuracy for the same projectiles when launched at angles above 30 degrees. The results clearly show that in many cases the prediction accuracy of the equations for the low angle tests is not consistent with that obtained for the high angle tests. However, in cases where the cylinders and spheres were dropped on dense sands the agreement was fair.

The previous analyses demonstrate the need for caution to be exercised in applying the equations to situations which differ from those utilized in developing the equations. Perhaps, the most significant information obtained from the equations is an indication of the relative importance of each independent variable.

## CONE IMPACT

The third and final phase of the field testing program consisted of obtaining data from the vertical impact of cones on sand. The scope of field testing is illustrated by the organizational chart in Fig. 21. The chart shows that two types of sands were utilized as target materials. These sands were placed in a test pit at three different states of density and moisture content, which represent limiting conditions for naturally occurring sands. Although two weights of cones were utilized, their soil-contact geometric properties were similar. Details concerning the cone properties and target material preparation are given in Chapters 3 and 4, respectively.

The purpose for the cone tests was twofold. These tests provided the data necessary for establishing a model law for the impact of rigid bodies on sands. The similitude analysis of the data was performed by Awoshika and Cox[1] and a brief summary of their findings has been presented in Chapter 2. In addition, data concerning the behavior of sands at limiting states of density under vertical impact loading have been obtained. The presentation and implications of this data are the primary purposes of this section.

### Peak Accelerations

In designing space exploration equipment, a primary factor to be considered is the peak acceleration developed during impact. A series of tests were performed, varying the impact velocity, on each soil at three states of density. It was found that if the peak acceleration for a given density state is plotted against the initial impact velocity, the points plot approximately as a straight line. This indicates that the peak acceleration experienced during impact is a linear function of the initial impact velocity. Graphs of

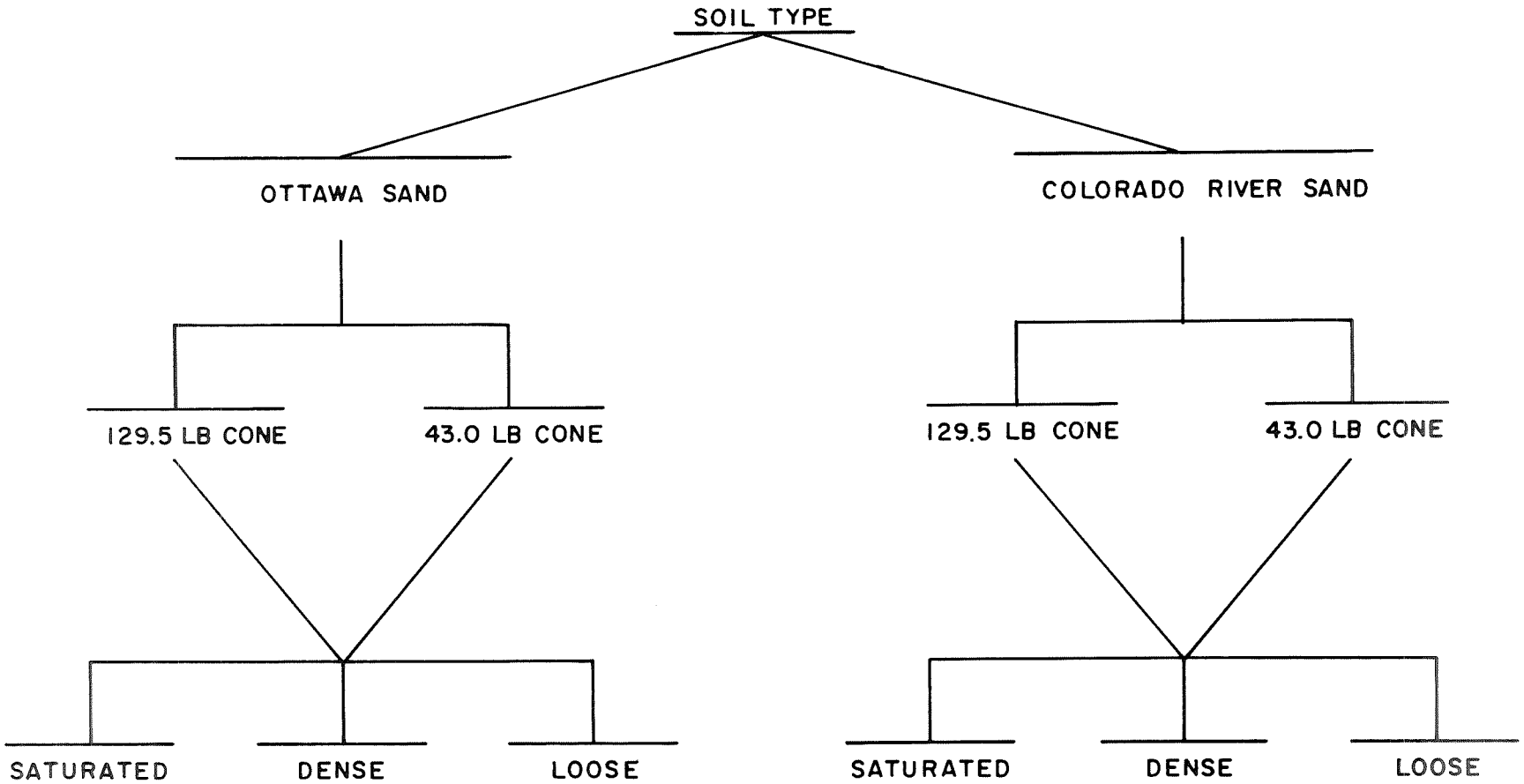


NOMINAL IMPACT VELOCITIES RANGED FROM 10 TO 25 FPS

FIG. 21 ORGANIZATIONAL CHART FOR VERTICAL IMPACT OF CONES

peak acceleration versus impact velocity for the cone tests on Ottawa Sand are shown in Figs. 22 through 24. These plots also show that the accelerations are somewhat higher for the light cone (43.0 lb) tests.

Scatter in the data may mainly be attributed to variations in soil conditions, drift of the accelerometer traces, and nonlinearity in the accelerometers. It was not possible to reproduce the same initial soil conditions for each tests. It should be noted that the values listed for soil density ($\gamma$) and moisture content ($w$) in Figs. 22 through 24 are average values. The individual values along with other pertinent information are listed in Appendix E. Drift of the accelerometer traces during the time of impact proved to be quite significant in many cases. The physical conditions of the impact system require the cone to be decelerated until it comes to rest. However, it was found upon complete integration of the acceleration-time curve the velocity of the cone was not zero as the laws of motion require. In every test the area under the acceleration curve was not large enough to reduce the downward cone velocity to zero. A detailed discussion of the sources and magnitudes of error in the accelerometer data is given in Appendix F.

In an attempt to determine the source, or sources of error, each step in the testing program and data reduction scheme was examined and carefully checked. Two main sources of error were found to exist. The most serious error was due to an upward shifting of the base line for the accelerometer trace during the impact event. This error became less significant as the magnitude of the accelerations increased and the test duration shortened. Thus, the tests affected most by drift of the base line were those on target materials in a loose state. The tests on saturated sands did not exhibit signs of drift; however, the area under the acceleration curve was still not large

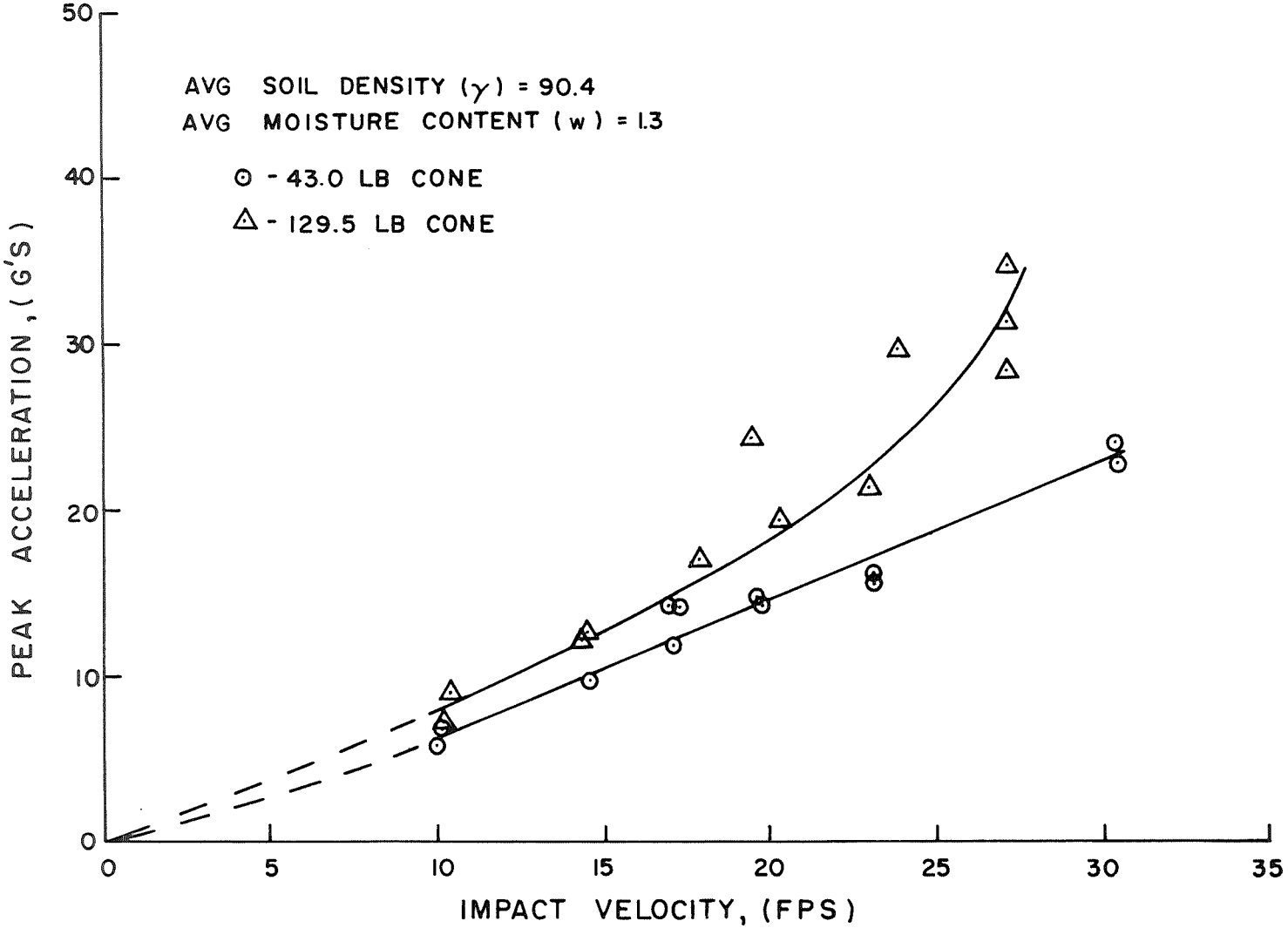


FIG. 22 PEAK ACCELERATION VERSUS IMPACT VELOCITY FOR LIGHT AND HEAVY CONES ON LOOSE, DRY OTTAWA SAND

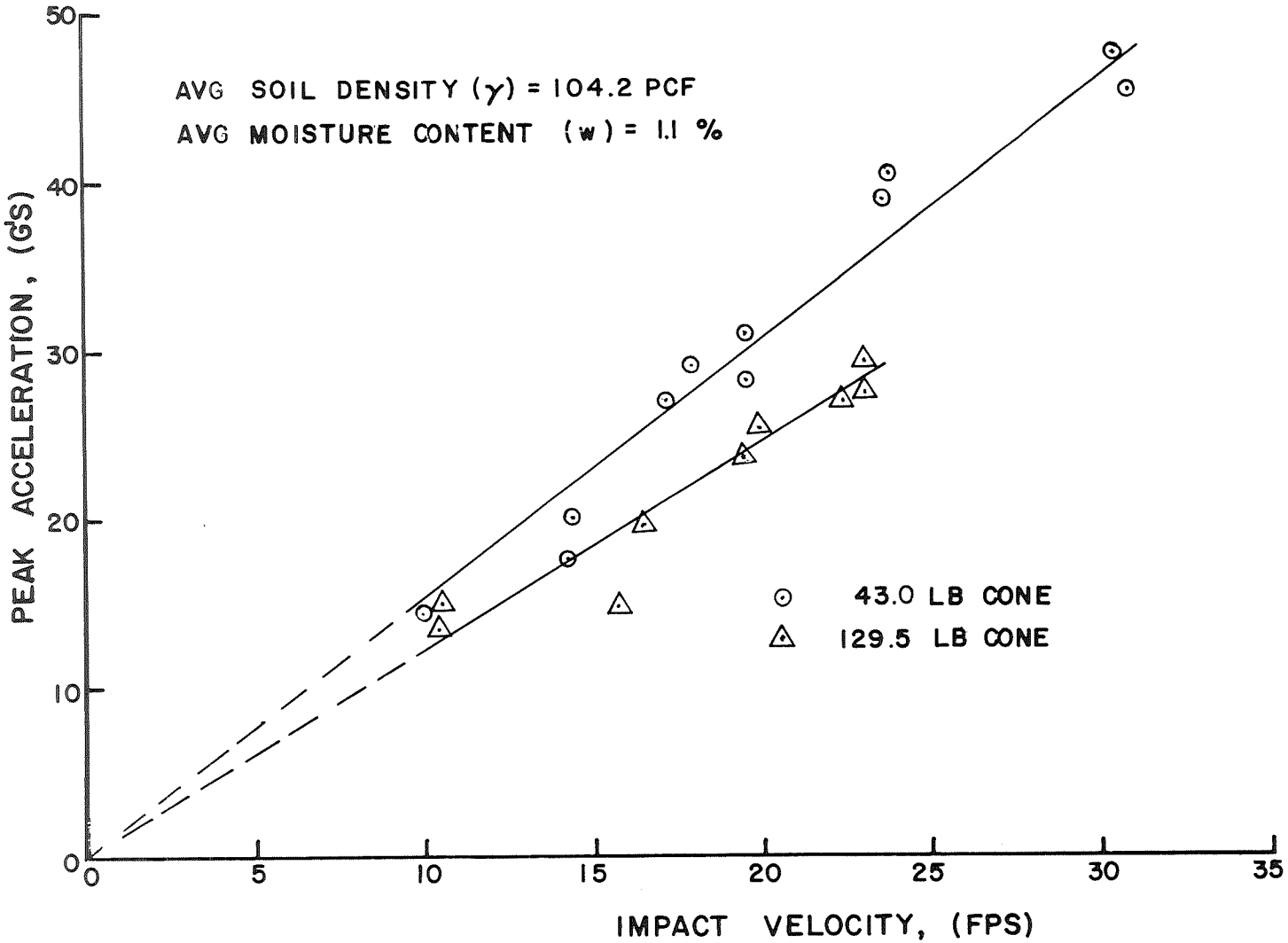


FIG. 23 PEAK ACCELERATION VERSUS IMPACT VELOCITY FOR LIGHT AND HEAVY CONES ON DENSE, DRY OTTAWA SAND

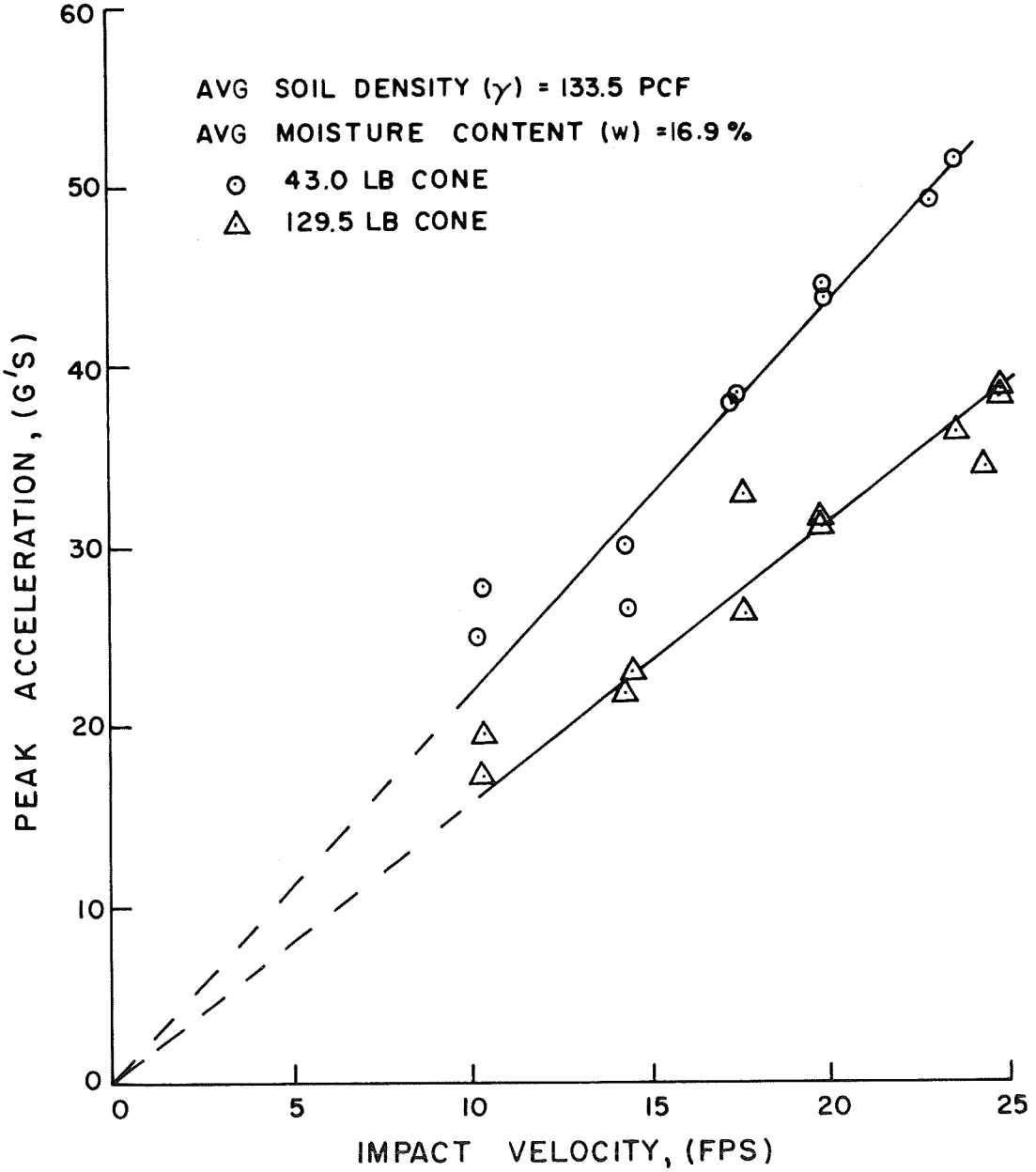


FIG. 24 PEAK ACCELERATION VERSUS IMPACT VELOCITY FOR LIGHT AND HEAVY CONES ON SATURATED OTTAWA SAND

enough to bring the calculated velocity of the cone to zero. Impact tests were performed under controlled conditions in the laboratory to determine the second source of error. It was concluded from these tests that the accelerometers consistently yielded accelerations which were on the average 15 percent below the true values.

Correction factors were applied to the measured acceleration data for the purpose of forcing the final calculated velocity to zero. Average correction factor values (CORFA) for each series of tests are listed in Table No. 5. Individual test values of CORFA are listed in Appendix E. A detailed discussion of the application of correction factors to the measured acceleration data is given in Appendix F.

Graphs of peak acceleration versus impact velocity for tests on Colorado River Sand are given in Figs. 25 through 27. Once again the heavy cone accelerations are somewhat less than the light cone values. The accelerations from the test on loose, dry Colorado River Sand are approximately the same for each cone; however, the sand was in a denser state for the heavy cone tests and this caused higher accelerations. When the differences in density are considered it is evident that the heavy cone accelerations are lower than the light cone values. It also should be noted that it was possible to pass a straight line through the light cone results, with a reasonable degree of accuracy, which intersected the origin. As can be seen from the graphs, it was not possible to represent the heavy cone results with a single straight line which passed through the origin and, therefore, a dashed curved section has been drawn for the early portion of the curve.

Force-Penetration Characteristics

Some of the most significant pieces of information that can be obtained from impact tests are the force-penetration characteristics of the target

TABLE NO. 5

LISTING OF AVERAGE SOIL DENSITIES AND CORRECTION FACTORS

| Soil Type | Cone Type | Soil $\gamma$ (pcf) | Soil w (%) | Correction Factor (CORFA) |
|---|---|---|---|---|
| Dry, Loose Ottawa Sand | Light | 91.2 | 1.6 | 1.94 |
| | Heavy | 89.5 | 1.0 | 1.89 |
| Dry, Dense Ottawa Sand | Light | 104.2 | 1.4 | 1.38 |
| | Heavy | 104.0 | 0.8 | 1.47 |
| Saturated Ottawa Sand | Light | 133.0 | 17.0 | 1.25 |
| | Heavy | 133.7 | 16.9 | 1.33 |
| Dry, Loose Colorado River Sand | Light | 94.4 | 2.1 | 1.86 |
| | Heavy | 97.6 | 1.3 | 1.80 |
| Dry, Dense Colorado River Sand | Light | 105.0 | 1.2 | 1.46 |
| | Heavy | 106.3 | 1.9 | 1.61 |
| Saturated Colorado River Sand | Light | 133.3 | 17.5 | 1.25 |
| | Heavy | 132.6 | 17.6 | 1.30 |

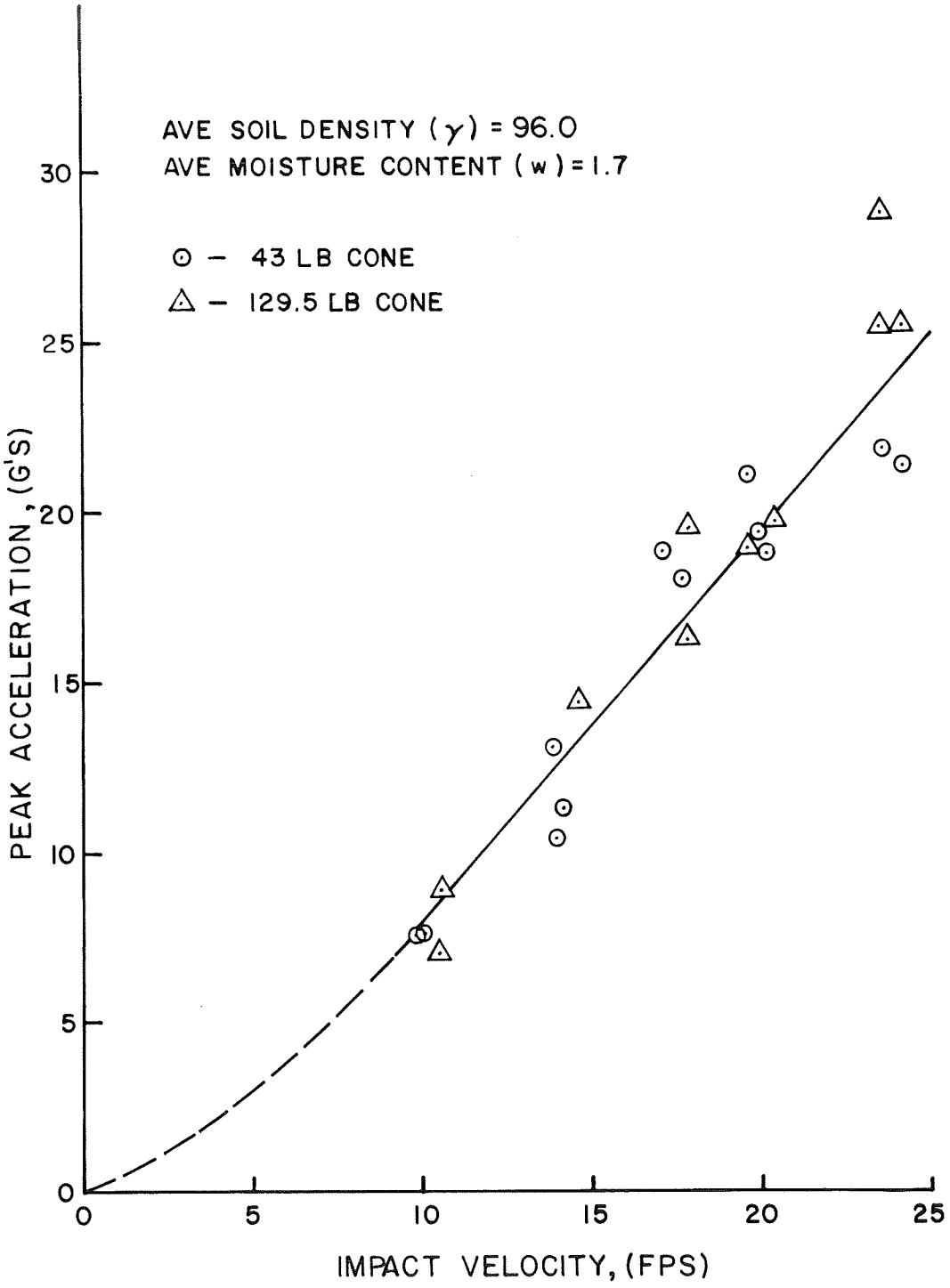


FIG. 25 PEAK ACCELERATION VERSUS IMPACT VELOCITY FOR LIGHT AND HEAVY CONES ON LOOSE, DRY COLORADO RIVER SAND

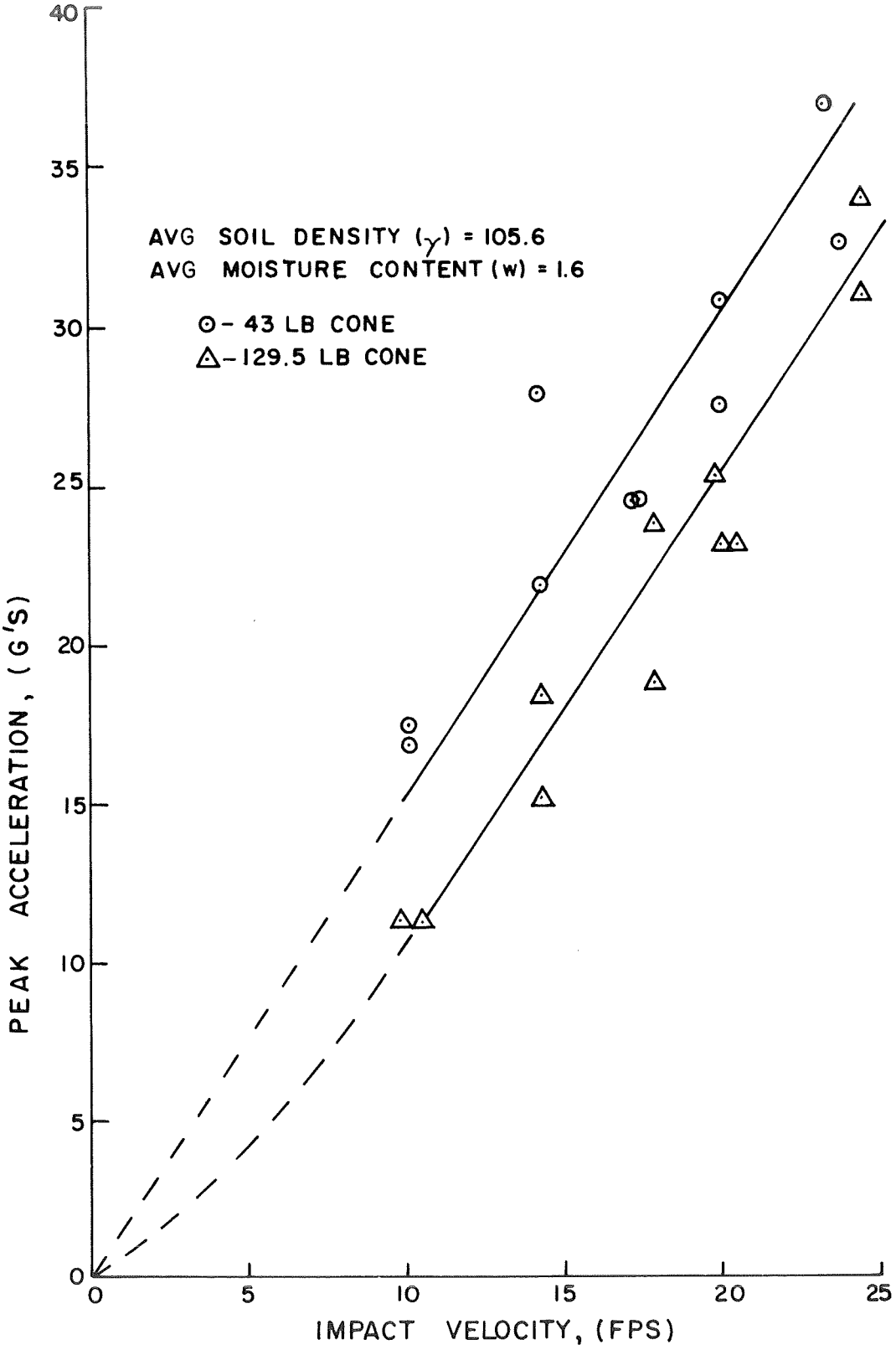


FIG. 26 PEAK ACCELERATION VERSUS IMPACT VELOCITY FOR LIGHT AND HEAVY CONES ON DENSE, DRY COLORADO RIVER SAND

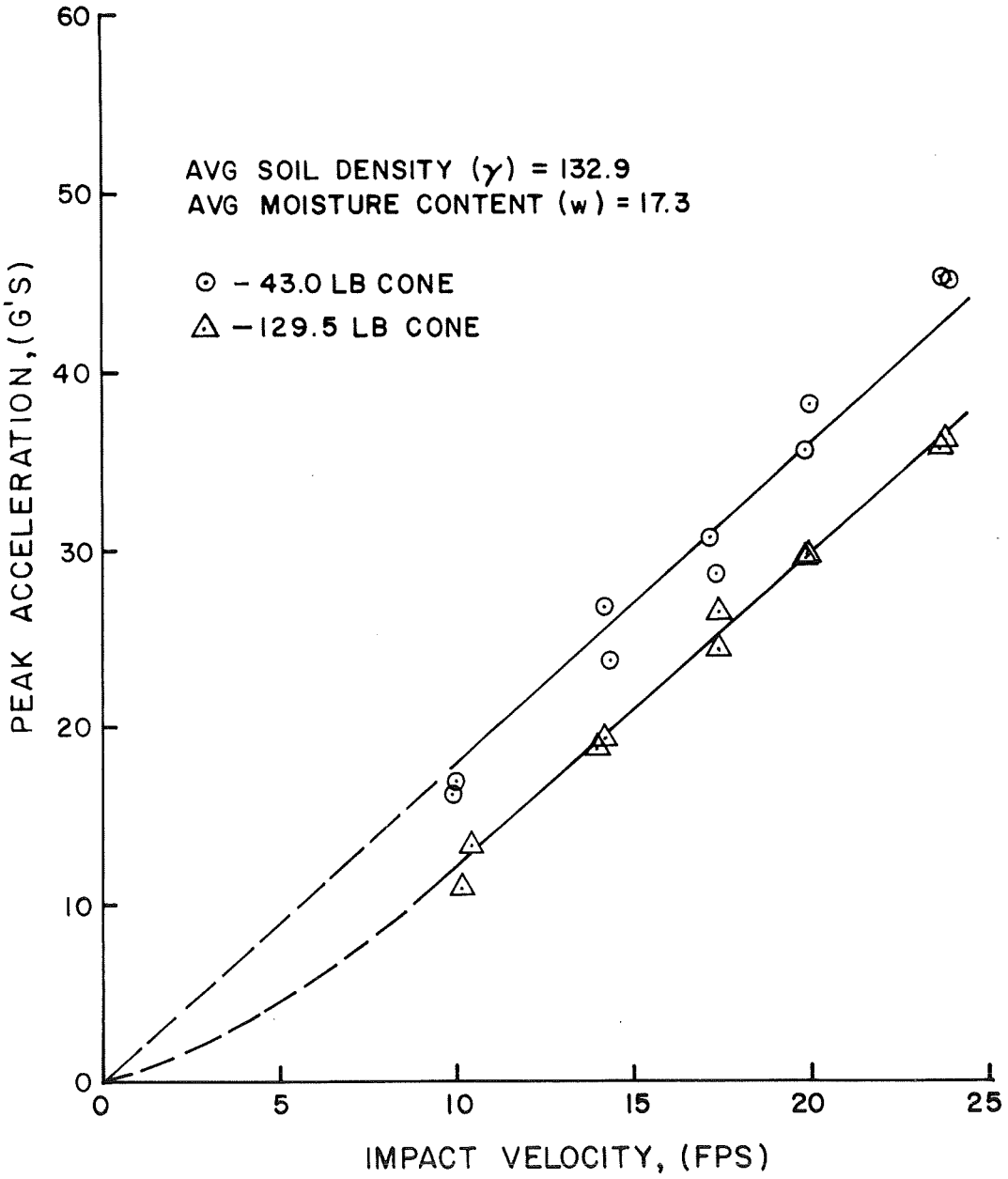


FIG. 27 PEAK ACCELERATION VERSUS IMPACT VELOCITY FOR LIGHT AND HEAVY CONES ON SATURATED COLORADO RIVER SAND

material. Once this information is known, it is possible through the use of numerical techniques to determine the dynamic behavior of the projectile during impact. Field tests have the disadvantage of being costly and the results cannot generally be directly applied to systems which involve different conditions. Static solutions for many problems in soil mechanics have been obtained by developing theories for failure mechanisms. The application of these theories involves the laboratory determination of basic soil properties. One of the major limitations is that these theories predict only the conditions at failure.

A great deal of effort has been put forth in attempting to apply static failure mechanisms to dynamic problems. Static laboratory equipment has been modified to permit the determination of basic soil properties under dynamic loading conditions. In connection with impact problems, this approach has met with little success. The present state of knowledge does not permit the prediction of peak forces developed during impact, let alone the prediction of developed soil forces for specified amounts of penetration.

Although the prediction of force-penetration curves for soil under impact loading is not possible at the present time, a great deal of qualitative information can be obtained from the examination of experimental curves. Figures 28 through 31 illustrate typical shapes of the force-penetration curves derived from the cone tests on sands at various states of density and water content. The graphs illustrate the large influence the state of sand has upon the dynamic force-penetration characteristics.

For ease of discussion Fig. 28 will be used to exemplify the dynamic force-penetration characteristics. The early portion of the curves are concave upward and as the cone penetration increases the curvature tends to reverse; however, a major portion of the rise section of the curve is nearly linear. The curves also illustrate the small amount of elastic rebound which took place.

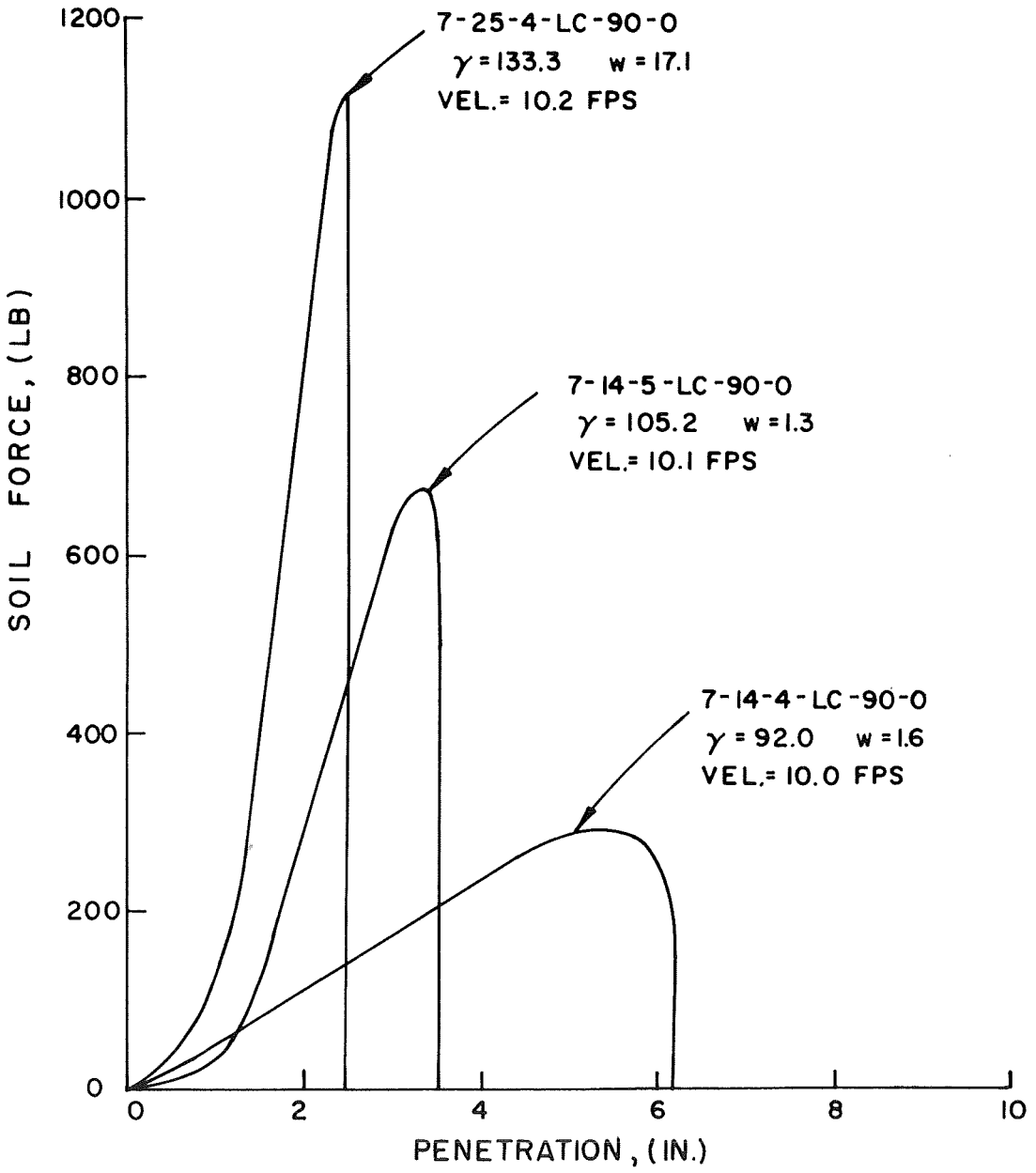


FIG. 28 SOIL FORCE VERSUS PENETRATION FOR LIGHT CONE TESTS ON OTTAWA SAND - NOMINAL IMPACT VELOCITY 10 FPS

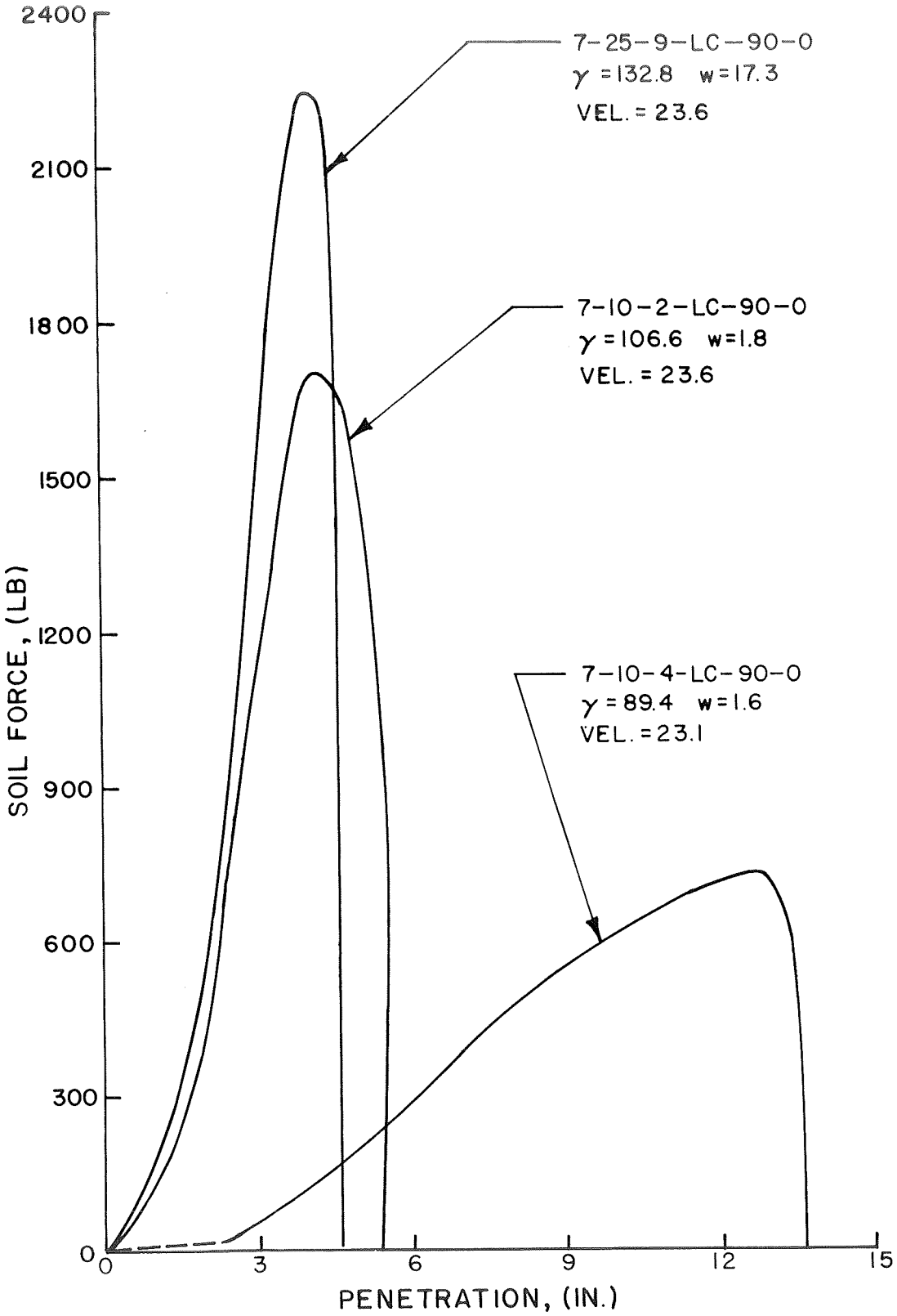


FIG. 29 SOIL FORCE VERSUS PENETRATION FOR LIGHT CONE TESTS ON OTTAWA SAND – NOMINAL IMPACT VELOCITY 23.5 FPS

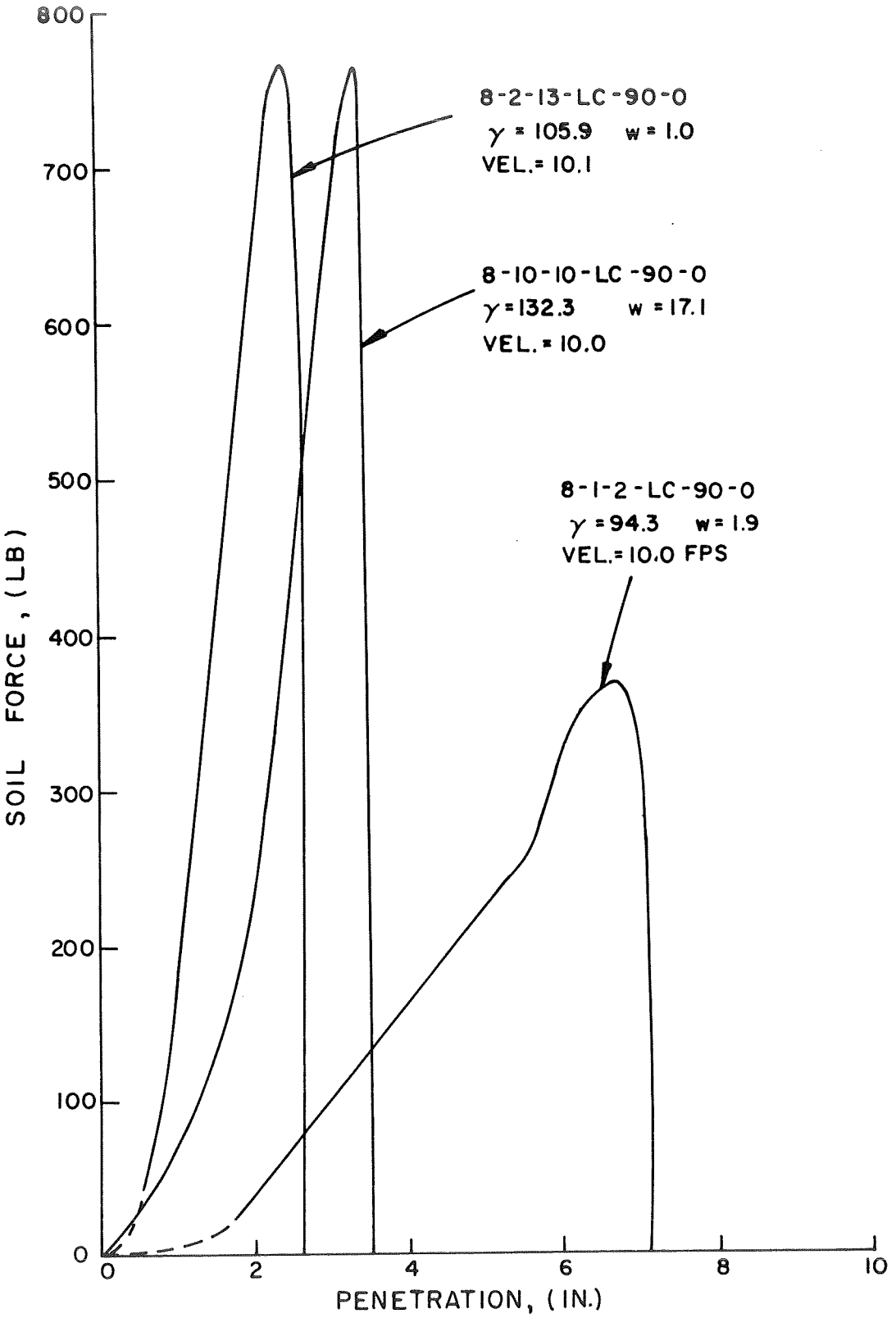


FIG. 30 SOIL FORCE VERSUS PENETRATION FOR LIGHT CONE TESTS ON COLORADO RIVER SAND - NOMINAL IMPACT VELOCITY 10 FPS

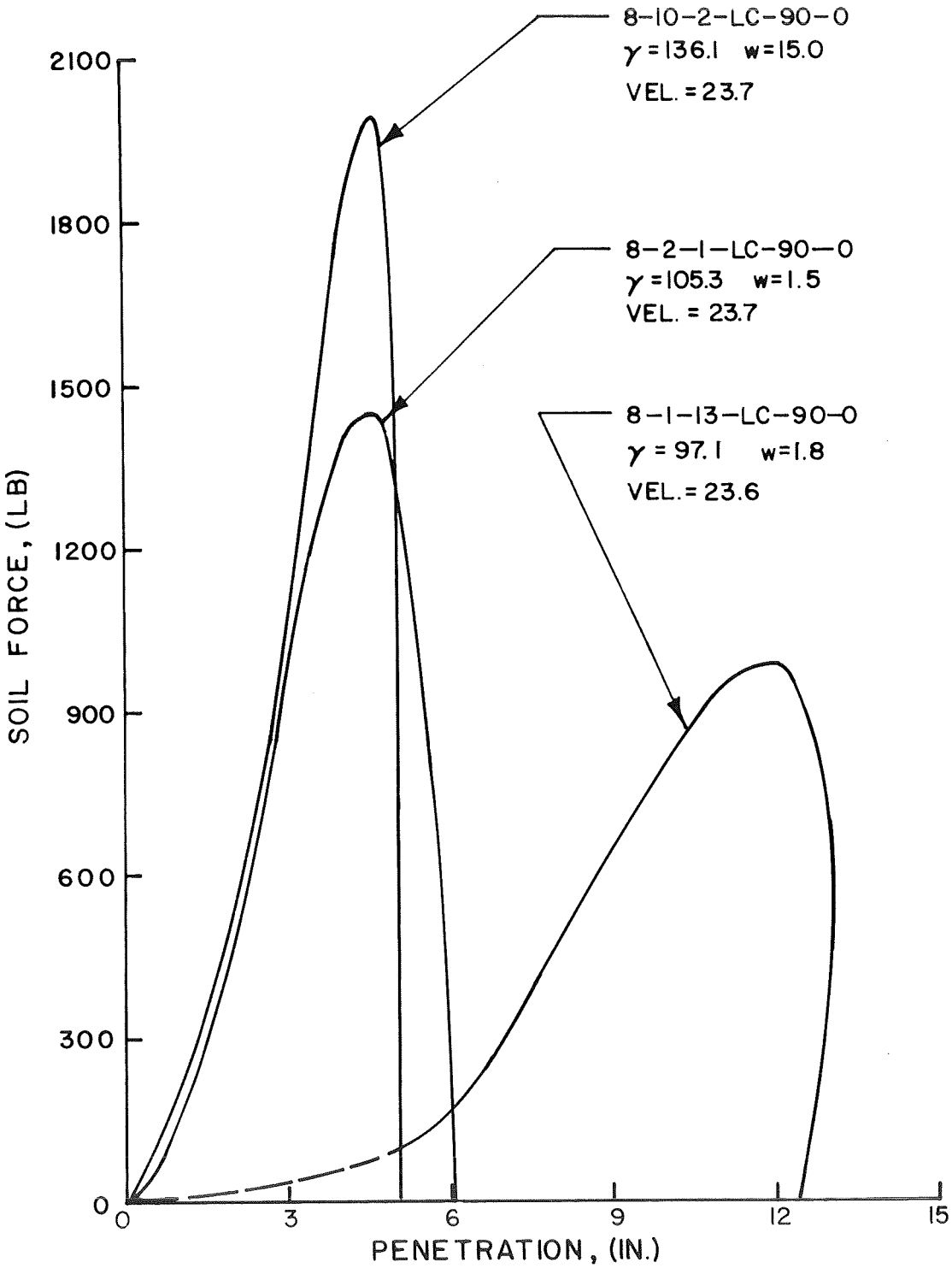


FIG. 31 SOIL FORCE VERSUS PENETRATION FOR LIGHT CONE TESTS ON COLORADO RIVER SAND - NOMINAL IMPACT VELOCITY 23.5 FPS

As the density of the soil increases the slope of the rise portion of the curves increases rapidly and the curves become more spiked. The curves could be approximated quite closely by a right triangle.

It can be noted from Figs. 28 and 29 that for a given state of density, the peak soil forces are approximately doubled when the impact velocity is approximately doubled. The curves show that dense sand in a saturated state offers the greatest resistance to penetration.

Figures 32 and 33 show the flooded test pit prior to and during impact. Figure 33 illustrates the ejection of a water spray from the immediate impact area. Sand was ejected in a similar manner when tested in a dry state. Immediately following impact a radial movement of water was noted by an apparent change in color of the sand mass. This movement clearly showed that a significant amount of pore water pressure had developed during the impact event. Figure 34 illustrates the lighter colored area which surrounded the cone after all excess pore water pressures had been dissipated.

The state of density has large influence on how saturated sands behave under rapid loadings. If the sand is in a loose, saturated state a shock type of loading will reduce the developed soil forces to almost zero. This phenomenon is referred to as spontaneous liquefaction[28]. It is caused by a collapse of the soil structure that is associated with a sudden increase in pore water pressure. The soil grains and pore water behave as a concentrated suspension. As soon as the pore pressures have dissipated the sand passes back to a state of sediment. This behavior does not occur in dense saturated sands because the sand structure does not collapse.

As stated previously in Chapter 4, the final cone penetration was recorded following each impact test. These measured values were then compared with the calculated values, which were obtained by double integration

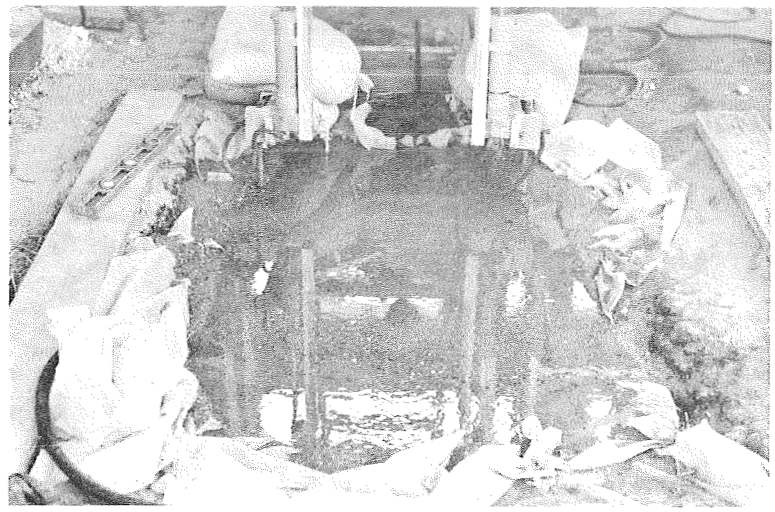

Fig. 32 View of Test Bed Area at Time of Cone Tests on Saturated Colorado River Sand

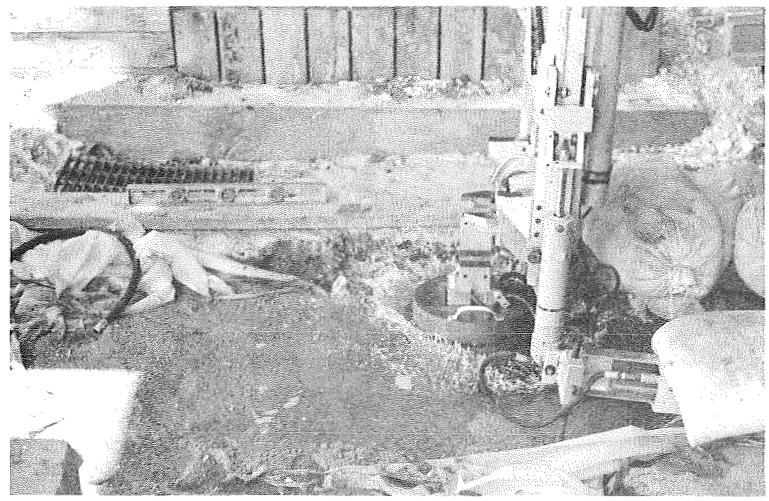

Fig. 33 Impact of Heavy Cone on Saturated Colorado River Sand

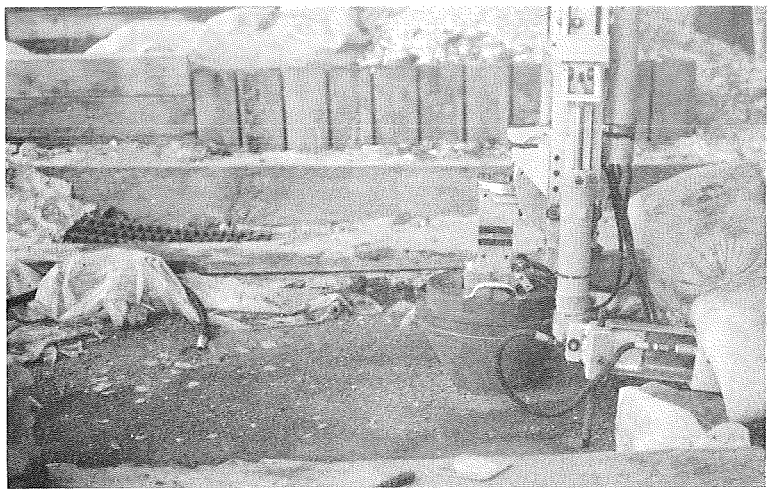

Fig.34 View of Final Resting Position of Heavy Cone - Saturated Colorado River Sand

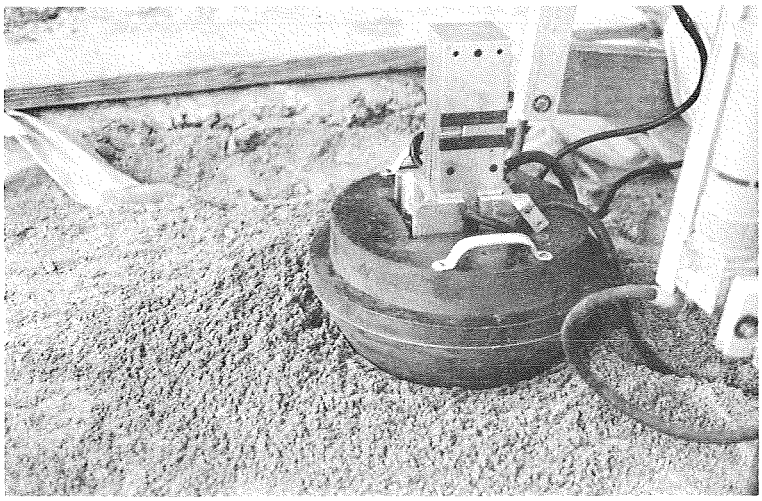

Fig. 35 View of Final Resting Position of Heavy Cone - Dry, Dense Colorado River Sand

of the corrected acceleration-time curves. Table Nos. 24 through 35, in Appendix E, list these values for each test. The comparisons show that generally the calculated values are less than the measured values. These discrepancies are believed to have resulted from the difficulty associated with the determination of the beginning point on the acceleration-time trace. The shape of the cone was such that extremely small amounts of soil resistance were developed during the first few inches of penetration, causing the acceleration-time trace to deviated gradually from the base line. Figure 35 shows the final resting position of a heavy cone on dense, dry Colorado River Sand.

When the final measured penetration was plotted against the initial impact velocity it was found that for the tests on dense, saturated sand the penetration linearly increased with impact velocity. The data from the tests on loose, dry sands and dense, dry sands show that the variation of penetration is also approximately linear for impact velocities ranging between 10 and 25 fps, as shown in Fig. 36 through 38. However, when these straight lines were extended back toward the origin the indicated penetrations were vastly different from those measured at zero impact velocity. Therefore, dashed curves have been inserted between the zero and 10 fps velocity range to indicate the probable relationships.

Comparison of the curves (Figs. 36 and 37) obtained from the tests on Ottawa and Colorado River Sand, in both dense and saturated states, readily shows that the curves have surprisingly similar shapes and magnitudes. Figure 38 shows that the penetration values are somewhat less for the tests on loose, dry Colorado River Sand. However, the average loose density of the Colorado River Sand was significantly higher than the average Ottawa Sand

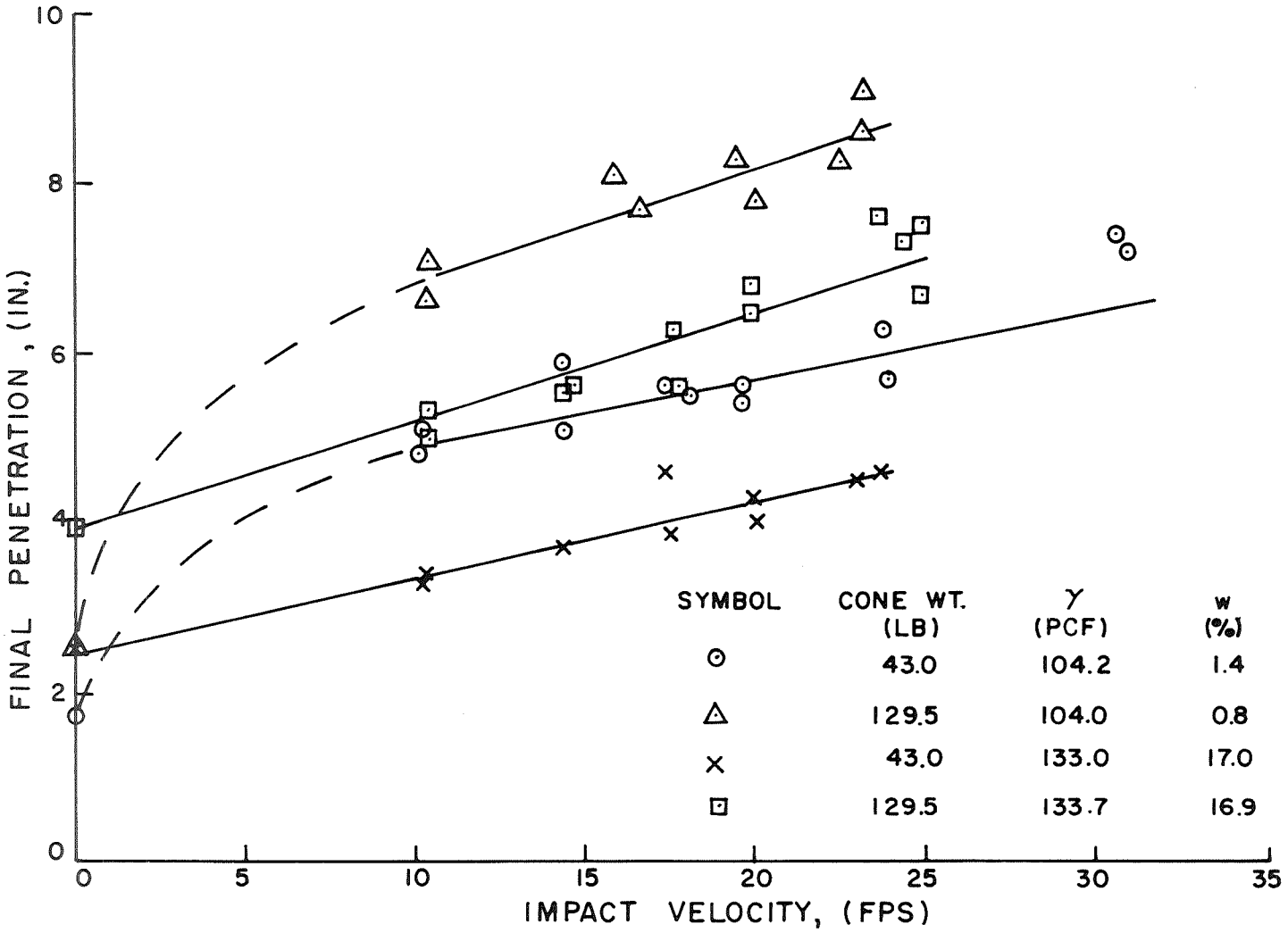


FIG. 36 FINAL PENETRATION VERSUS IMPACT VELOCITY - OTTAWA SAND IN DENSE AND SATURATED STATES

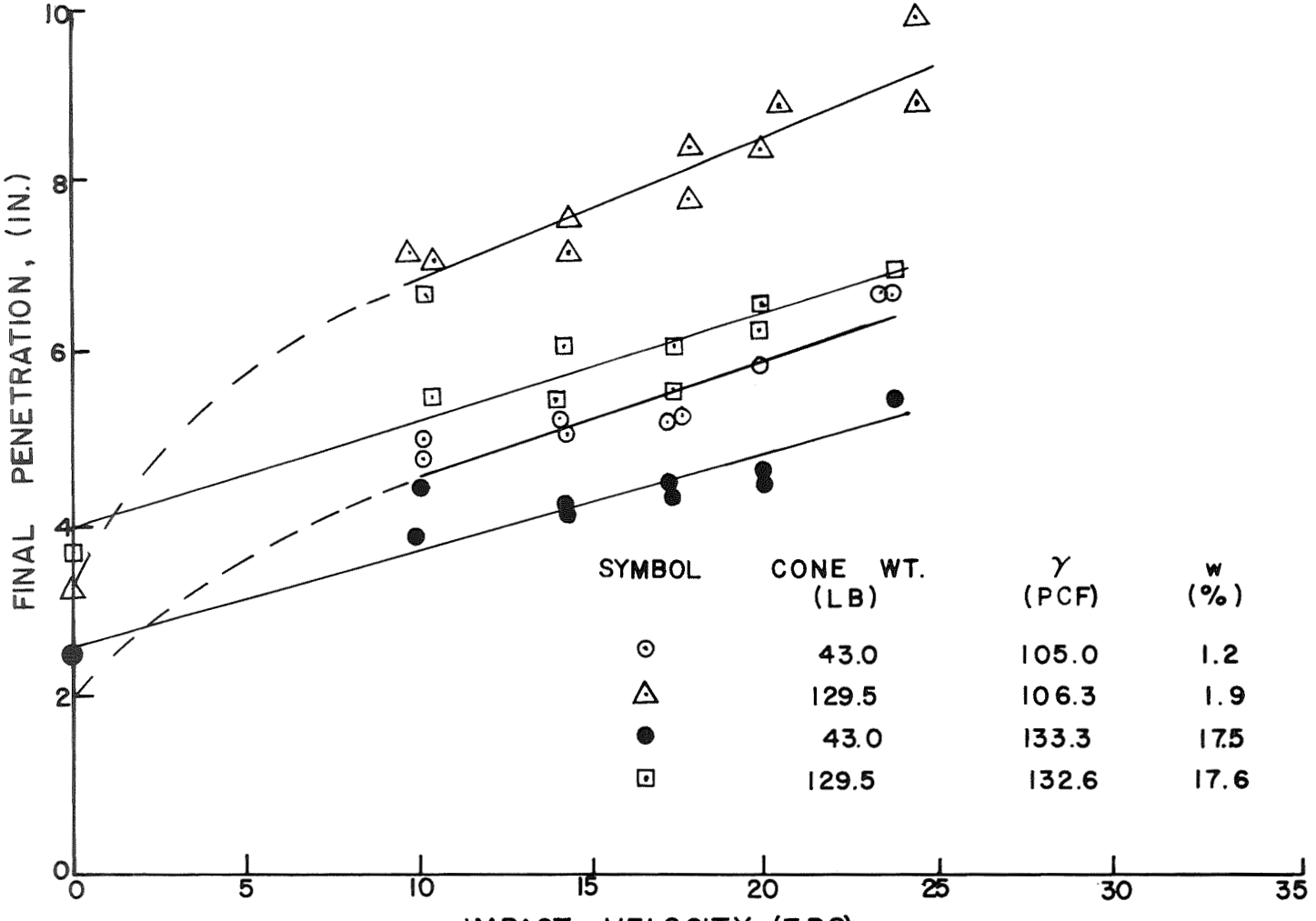


FIG. 37 FINAL PENETRATION VERSUS IMPACT VELOCITY – COLORADO RIVER SAND IN DENSE AND SATURATED STATES

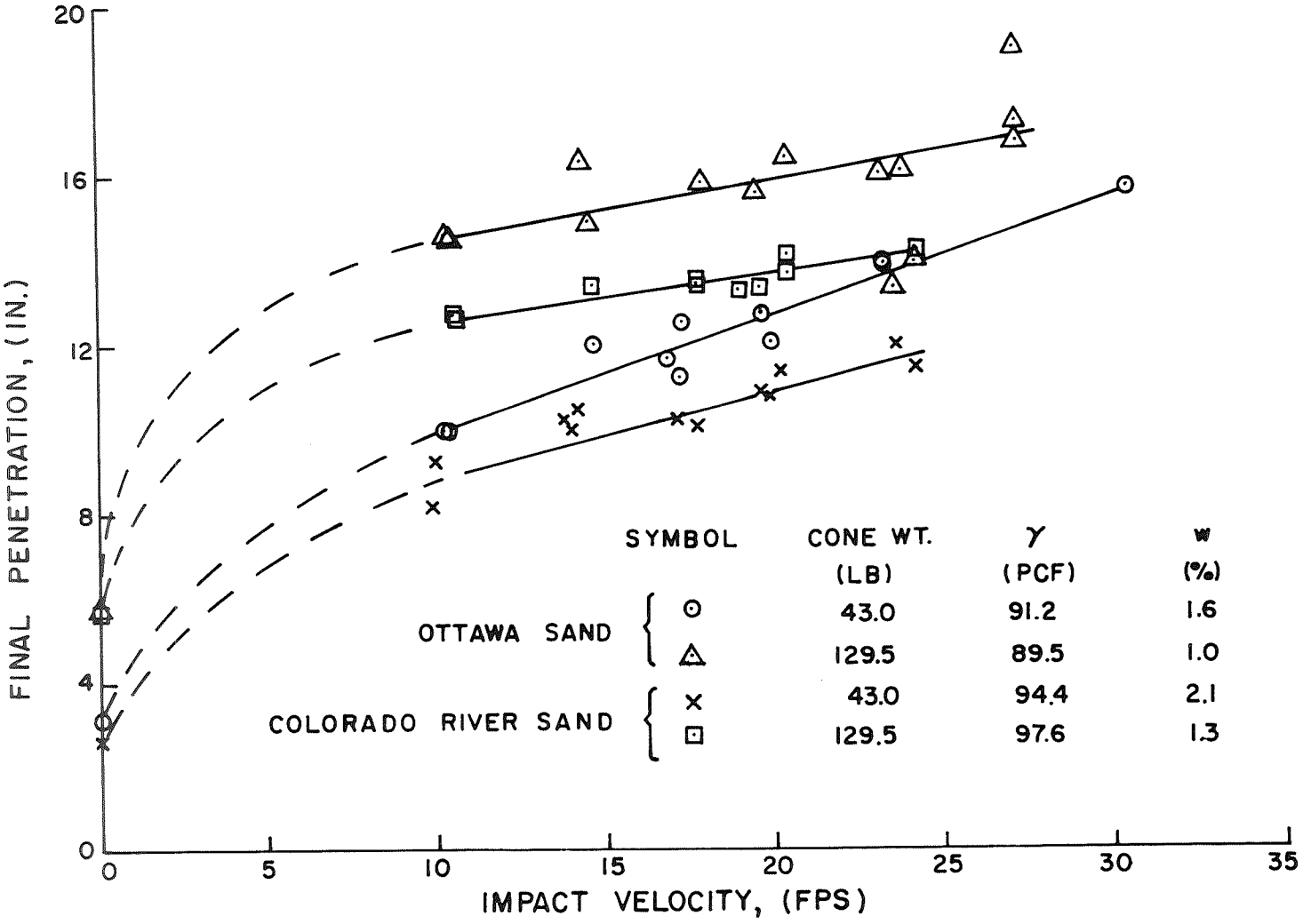


FIG.38 FINAL PENETRATION VERSUS IMPACT VELOCITY - OTTAWA AND COLORADO RIVER SAND IN LOOSE STATES

density. It also should be noted that in each of the heavy cone impact tests the penetrations were larger than the 12 in. height of the cone.

Peak Force Prediction

The acceleration plots shown in Figs. 22 through 27, illustrate an approximate linear relationship between peak acceleration and impact velocity. This relationship suggests that a relatively simple equation may be developed for the prediction of peak soil forces. Plots of peak force versus initial momentum for each of the soil states and cone types are shown in Figs. 39 and 40. Each test series has been represented by a straight line, which in most cases passed through the origin. If the peak acceleration values for the light and heavy cones had matched, one straight line could have been used to represent each state of soil density.

The light cone accelerations from the tests on dense and saturated sands are somewhat higher than the heavy cone accelerations under similar soil conditions. The opposite case is true for the tests on loose sand. The work of Poor et al[16] indicates that as the ratio of projectile weight to projectile surface area increases, the peak acceleration decreases. This is easily visualized if one imagines the dropping of two projectiles from a constant height. The projectile weights are equal and the surface areas are in the ratio of 10 to 1. It is obvious that the projectile with the larger area will penetrate less and, therefore, the time required to reduce its velocity to zero is also less. Since each projectile has the same impact velocity the acceleration experienced by the projectile with larger area must be greater if the impact event is of shorter duration. The cone tests on loose sand seem to contradict this argument; however, it was noted during these tests that the soil density increased with depth. The heavy cones which penetrated deeper

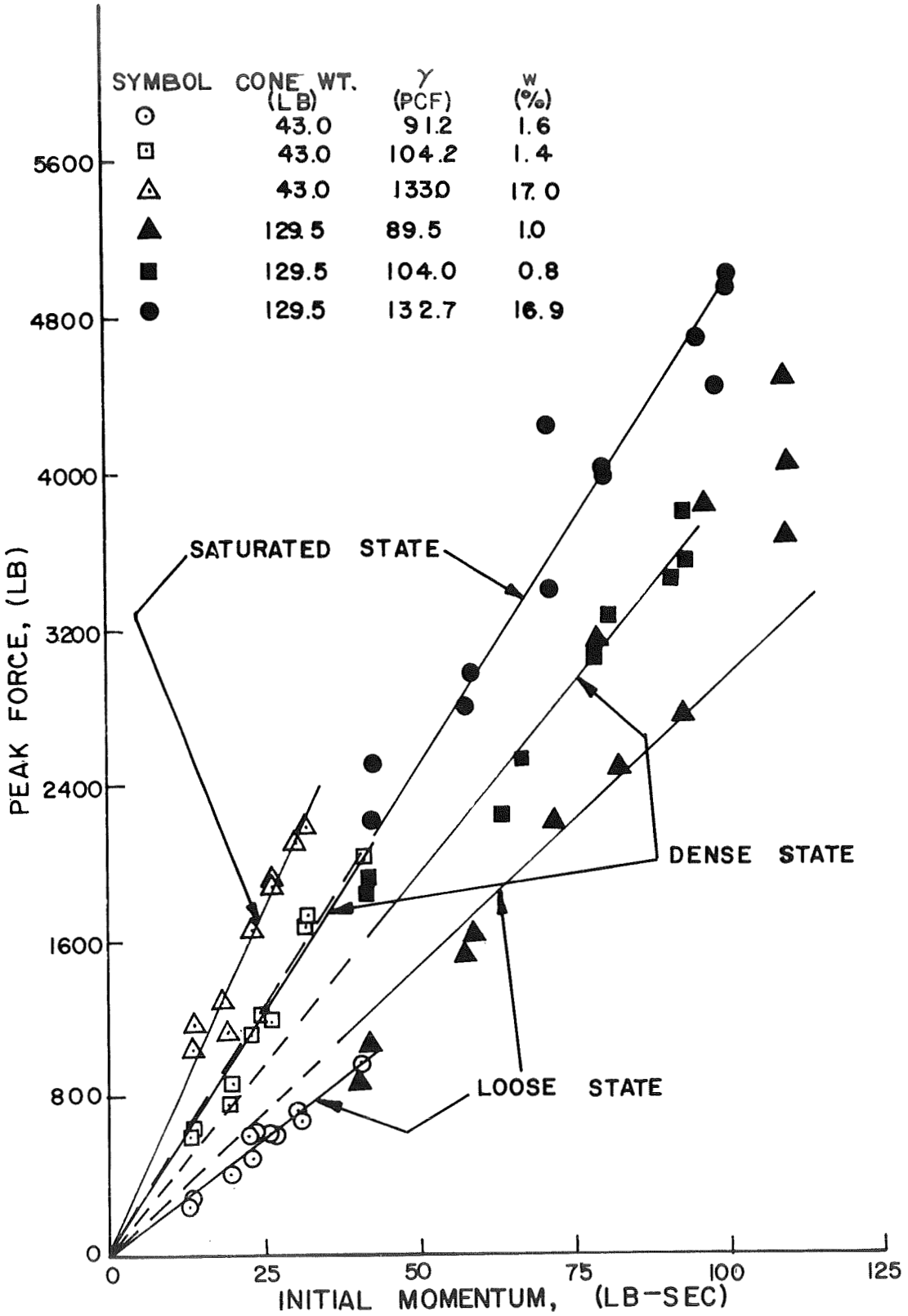


FIG. 39 PEAK FORCE VERSUS INITIAL MOMENTUM FOR CONE TESTS ON OTTAWA SAND

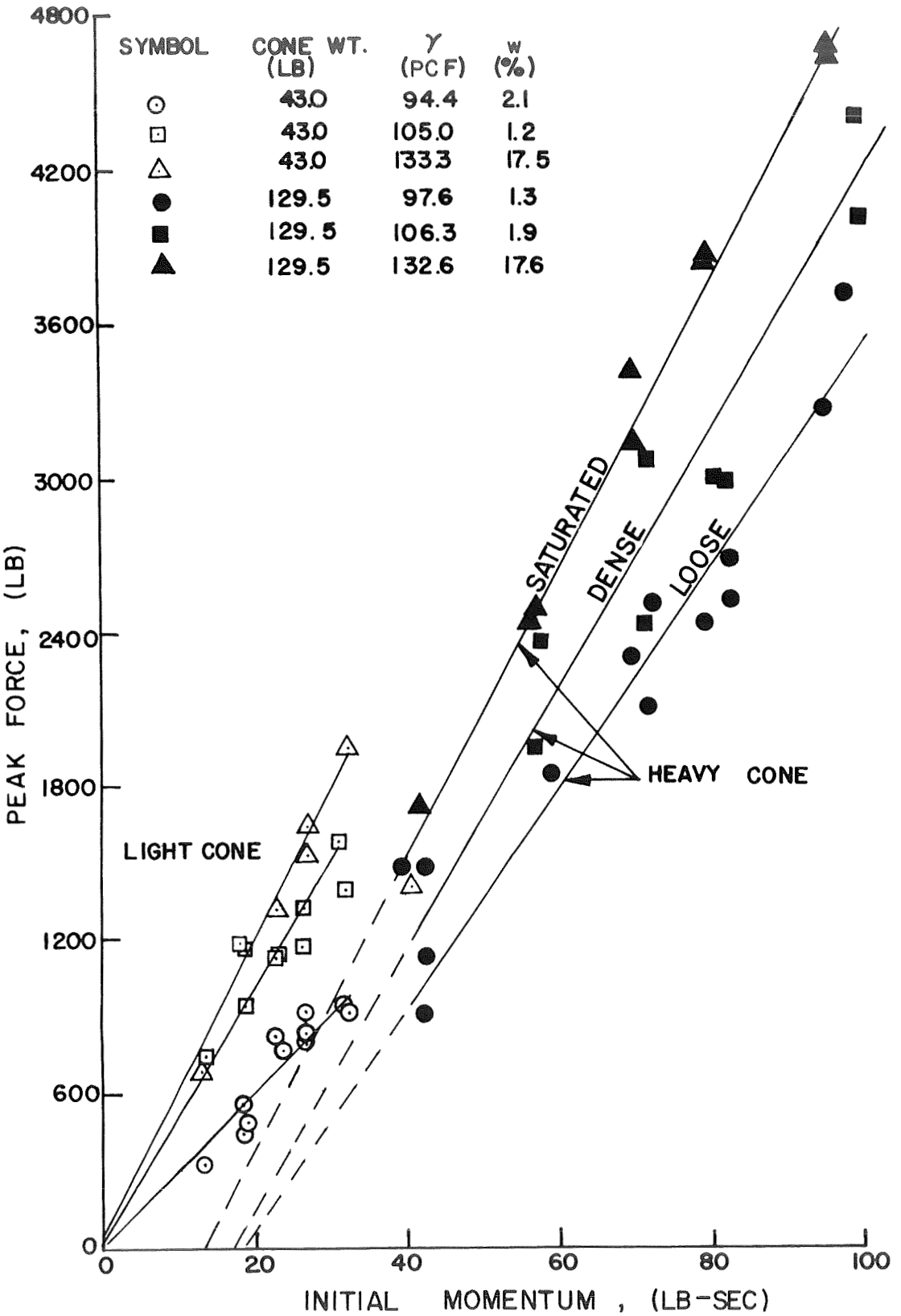


FIG. 40 PEAK FORCE VERSUS INITIAL MOMENTUM FOR CONE TESTS ON COLORADO RIVER SAND

into the sand bed were actually penetrating into a denser material which offered more resistance. It should be noted that the recorded density measurements listed in this chapter only reflect the soil density near the soil bed surface, although, density measurements with depth were recorded from time to time. It was observed that a significant variation in density only occurred during testing on loose sands. The density of the soil was found to be approximately 5 pcf greater at a depth of one foot below the surface of the undisturbed soil.

The following equation is proposed for predicting the peak soil forces produced by the vertical impact of a right circular cone:

$$F_{peak} = K_{cone} \gamma MV \tag{28}$$

where

$F_{peak}$ = Peak soil force (lb),

$K_{cone}$ = Empirical coefficient which relates the peak soil force to the product of soil density and initial momentum, $\gamma$ MV ($ft^3$/lb-sec),

$\gamma$ = Soil density (pcf),

M = Mass of cone (lb-$sec^2$/ft),

V = Initial impact velocity (fps).

Values for $K_{cone}$ were obtained by dividing the slopes of the straight lines in Figs. 39 and 40 by the appropriate soil densities. $K_{cone}$ values are listed in Table No. 6. The comparison of $K_{cone}$ values shows that a value of approximately 0.30 applies for the tests on loose sand and a value of approximately 0.45 is appropriate for the tests on dense and saturated sands. These values only apply for vertical impact of cones with 60 degree apex angles. It also should be emphasized that $K_{cone}$ is not only a function of the cone geometry, but also the mass. The values of $K_{cone}$ will increase as the cone apex angle

TABLE NO. 6

COMPARISON OF COEFFICIENTS ($K_{cone}$) WHICH RELATE PEAK SOIL FORCE TO PRODUCT OF SOIL DENSITY AND INITIAL MOMENTUM

| Soil Type | Soil Density $\gamma$ (pcf) | Moisture Content w (%) | Cone Type | $K_{cone}$ ($ft^3$/Lb-sec) |
|---|---|---|---|---|
| Loose Ottawa Sand | 91.2 | 1.6 | Light (43.0 lb) | 0.26 |
| Dense Ottawa Sand | 104.2 | 1.4 | | 0.47 |
| Saturated Ottawa Sand | 133.0 | 17.0 | | 0.53 |
| Loose Ottawa Sand | 89.5 | 1.0 | Heavy (129.5 lb) | 0.33 |
| Dense Ottawa Sand | 104.0 | 0.8 | | 0.38 |
| Saturated Ottawa Sand | 133.7 | 16.9 | | 0.37 |
| Loose Colorado River Sand | 94.4 | 2.1 | Light (43.0 lb) | 0.32 |
| Dense Colorado River Sand | 105.0 | 1.2 | | 0.48 |
| Saturated Colorado River Sand | 133.3 | 17.5 | | 0.45 |
| Loose Colorado River Sand | 97.6 | 1.3 | Heavy (129.5 lb) | 0.44* |
| Dense Colorado River Sand | 106.3 | 1.9 | | 0.52* |
| Saturated Colorado River Sand | 132.6 | 17.6 | | 0.43* |

$$F_{peak} = K_{cone} \gamma MV$$

*In every instance, except for these three, the $K_{cone}$ values represent slopes of straight lines which pass through the origin. In these cases the lines did not pass through the origin. (See Fig. 40)

increases. An increase in cone mass will tend to cause a decrease in $K_{cone}$ values.

Final Penetration Prediction

The purpose of this section is to present a rational method for predicting final cone penetrations. An expression for final penetration is derived from work-energy principles. This type of approach required the use of a soil force-penetration curve. The soil response was characterized by a right triangle, having an altitude equal to the value predicted by Eq. 28.

It may be stated from work-energy principles that the work done on a body is equivalent to the change in kinetic and potential energy of the body. Equation 29 represents the application of this principle.

$$\text{Work Done} = \Delta\text{Kinetic Energy} + \Delta\text{Potential Energy}$$

$$0.5\, F_{peak} Z_f = 0.5\, MV^2 + MgZ_f \tag{29}$$

The variables appearing in Eq. 29 are defined as follows:

$Z_f$ = Final penetration,

M = Mass of cone,

V = Initial impact velocity,

g = Acceleration of gravity,

$F_{peak}$ = Peak soil force which is assumed to occur at $Z_f$.

Substitution of Eq. 28 into Eq. 29 and solving for $Z_f$ yields

$$Z_f = \frac{V^2}{(K_{cone}\, \gamma\, V - 2g)} \quad . \tag{30}$$

A comparison of the penetrations calculated using Eq. 30 and those measured is shown in Table No. 7. As can be seen from the table, penetrations

TABLE NO. 7

COMPARISON OF MEASURED AND CALCULATED CONE PENETRATIONS

| Soil Type | Soil Density $\gamma$ (pcf) | Moisture Content w (%) | Cone Type | Impact Velocity (fps) | Measured Penetration (in.) | Calculated Penetration (in.) | Percent Error (%)* |
|---|---|---|---|---|---|---|---|
| Loose Ottawa Sand | 91.2 | 1.6 | Light Cone (43.0 lb) | 10 | 9.9 | 6.9 | 30.4 |
| | | | | 20 | 12.7 | 11.7 | 7.9 |
| | | | | 30 | 15.5 | 16.7 | -7.7 |
| Dense Ottawa Sand | 104.2 | 1.4 | | 10 | 4.9 | 2.8 | 42.9 |
| | | | | 20 | 5.7 | 5.3 | 7.0 |
| | | | | 30 | 6.5 | 7.7 | -18.5 |
| Saturated Ottawa Sand | 133.0 | 17.0 | | 10 | 3.3 | 1.9 | 42.5 |
| | | | | 20 | 4.3 | 3.6 | 16.3 |
| | | | | 30 | 5.4 | 5.4 | 0.0 |
| Loose Ottawa Sand | 89.5 | 1.0 | Heavy Cone (129.5 lb) | 10 | 14.5 | 5.2 | 64.0 |
| | | | | 20 | 15.9 | 9.1 | 42.7 |
| | | | | 30 | 17.2 | 13.2 | 23.2 |
| Dense Ottawa Sand | 104.0 | 0.8 | | 10 | 6.8 | 3.6 | 47.0 |
| | | | | 20 | 8.2 | 6.6 | 19.5 |
| | | | | 30 | 9.5 | 9.6 | -1.1 |
| Saturated Ottawa Sand | 133.7 | 16.9 | | 10 | 5.2 | 2.8 | 46.1 |
| | | | | 20 | 6.5 | 5.2 | 20.0 |
| | | | | 30 | 7.1 | 7.6 | 7.0 |

* Percent ERROR = $\left( \frac{\text{Measured - Calculated}}{\text{Measured}} \right) 100$

TABLE NO. 7 (CONT'D)

| Soil Type | Soil Density $\gamma$ (pcf) | Moisture Content w (%) | Cone Type | Impact Velocity (fps) | Measured Penetration (in.) | Calculated Penetration (in.) | Percent Error (%) |
|---|---|---|---|---|---|---|---|
| | | | | 10 | 4.6 | 2.7 | 41.4 |
| Loose Colorado River Sand | 94.4 | 2.1 | | 20 | 6.0 | 5.1 | 15.0 |
| | | | | 30 | 7.3 | 7.4 | -1.4 |
| | | | Light | 10 | 4.6 | 2.7 | 41.3 |
| Dense Colorado River Sand | 105.0 | 1.2 | Cone (43.0 lb) | 20 | 6.0 | 5.1 | 15.0 |
| | | | | 30 | 7.3 | 7.4 | -1.4 |
| | | | | 10 | 3.8 | 2.2 | 42.0 |
| Saturated Colorado River Sand | 133.3 | 17.5 | | 20 | 4.9 | 4.2 | 1.4 |
| | | | | 30 | 6.0 | 6.2 | -3.3 |

were calculated for impact velocities of 10, 20 and 30 fps. The measured penetrations corresponding to these impact velocities were taken from the curves shown in Figs. 36 through 38. The percent error column reflects the accuracy of prediction. The approximate average errors for 10, 20, and 30 fps impact velocities are 45, 15, and 5 percent, respectively. Undoubtedly, the idealization of the soil force-penetration curve has introduced error; however, for impact velocities above 20 fps the error is more acceptable.

Examination of Eq. 30 shows that as the impact velocity increases the 2g term becomes less significant. For situations in which this term may be neglected, the final penetration becomes a linear function of the impact velocity. The final penetration versus impact velocity graphs in Figs. 36 through 38 substantiate linear tendencies for impact velocities between 10 and 30 fps.

Young[34] has found that for deep penetrating projectiles, which have impact velocities greater than 200 fps, the penetration depth varies linearly with the impact velocity. For velocities between 100 and 200 fps, he has stated that the penetration depth varies as the natural logarithm of the square of the impact velocity. Although Young has proposed a logarithmic relationship between penetration and velocity, he has presented some data which indicate a linear variation for velocities below 200 fps.

Water Impact

A limited number of water impact tests were performed in order to provide a comparison between peak accelerations experienced during water and soil impact. Information of this nature is extremely useful since a number of prototype tests on water have been conducted by NASA[12], McDonnell Aircraft Corporation[11], and North American Aviation, Inc.[13]. The prototypes tested were full

scale boiler plate models of Mercury and Gemini capsules. A number of prototype tests on soil have also been performed by these same organizations. Reichmuth[19] has discussed these tests and concluded that the ratios of peak accelerations on soil to those on water generally range between 3 and 10. Unfortunately, detailed information concerning the target material and geometry of the penetrating portion of the prototypes is not available. Therefore, a large degree of uncertainty is involved with the use of these results for correlation purposes.

The basic purpose for the cone impact tests on water was to provide information that could be correlated with the previously discussed impact tests on sand. Table No. 8 lists the peak accelerations developed during water impact. Table No. 9 lists the ratio values for the soil to water peak accelerations. The ratios range from 4.3 to 12.5. It should be noted that a ratio value has also been given for sandy clay. These data were obtained from the work of Poor[16], in which cones were utilized having the same geometry as the cones used in this investigation. However, it was necessary to interpolate between the curves given in Fig. 42 on p.100, since the peak acceleration is a function of the impact velocity.

The close agreement between the range of cone ratio values in Table No. 9 and the prototype values, as discussed by Reichmuth[19], suggests that it may be possible to grossly approximate the peak forces experienced by prototype capsules when impacting on soil. This could be done by either performing water impact tests with the prototype or by using existing data and then multiply these results by the appropriate ratio values listed in Table No. 9.

TABLE NO. 8

TABULATION OF PEAK ACCELERATIONS FOR
LIGHT CONE IMPACT TESTS ON WATER

| Test No. | Impact Velocity (fps) | Peak Acceleration (g's) |
|---|---|---|
| 1 | 23.5 | 4.3 |
| 2 | 23.6 | 3.8 |
| 3 | 23.8 | 3.7 |
| 4 | 23.3 | 4.4 |

Avg Impact Velocity = 23.6 fps
Avg Peak Acceleration = 4.1 g's

TABLE NO. 9

SUMMARY OF THE RATIOS OF THE PEAK ACCELERATION VALUES
FOR IMPACT ON SOIL TO THE VALUES FOR WATER IMPACT

| Type of Soil | Impact Velocity (fps) | Peak Accel for Impact on Soil (g's) | Ratio of Peak Accel for Soil to Avg Peak Accel for Water |
|---|---|---|---|
| Saturated Ottawa Sand | 23.6 | 51.4 | 12.5 |
| Dense, Dry Ottawa Sand | 23.6 | 36.0 | 8.8 |
| Loose, Dry Ottawa Sand | 23.6 | 17.6 | 4.3 |
| Saturated Colorado River Sand | 23.6 | 42.5 | 10.4 |
| Dense, Dry Colorado River Sand | 23.6 | 36.0 | 8.8 |
| Loose, Dry Colorado River Sand | 23.6 | 23.6 | 5.8 |
| Sandy Clay | 23.6 | 50.0 | 12.2 |

# CHAPTER VI

## ANALYSES OF PREVIOUS VERTICAL IMPACT DATA

In Chapter V it was shown that the peak accelerations experienced by a cone upon vertical impact varied linearly with the initial impact velocity. Using this information the peak soil force was represented by

$$F_{peak} = K \gamma M V \quad . \tag{31}$$

The values of soil density ($\gamma$), mass of the projectile (M), and impact velocity (V), can easily be estimated or measured. However, the value of K depends upon the type soil, the geometry of the impacting surface, and also the weight-area ratio of the projectile. Values of K for two weights of cone and two types of sands, at various states of density and moisture content, are listed in Table No. 6 on p. 90.

The use of these K values is limited, in that they only apply for projectiles which impact on cohesionless soils and have the same geometry and weight range as the cones utilized in this investigation. Fortunately, well documented impact data are available from the work of Poor[16], Reichmuth et al[19], Womack and Cox[33], and Reese et al[18]. The data encompass a wide range of soil conditions, and projectile shapes and sizes. The primary purpose of this chapter is to present values of K, which were derived from the aforementioned impact data. It should be noted that this chapter deals only with vertical impact cases. Each of the soils listed in this chapter is described in Appendix C.

### PROJECTILE TESTS ON SANDY CLAY BY POOR

Poor et al[16] performed a series of drop tests in which they utilized projectiles having conical, spherical, and flat impacting surfaces. Each

projectile shape was tested at four impact velocities, in a 20 to 30 fps range, and having weights of 8, 16, 64, and 128 lbs.

## Soil Conditions

The soil was an overconsolidated sandy clay of low plasticity which exists in a terrace of the Colorado River at the Austin Country Club. The test area was flooded prior to testing, in an attempt to obtain a uniform moisture content to a depth of 3 ft. Poor lists moisture content values, which tend to be fairly uniform; however, it is not known whether the soil was saturated at the time of testing. Since no soil densities were listed, it was necessary to make an assumption concerning the degree of saturation. Based on discussions with a technician who was present during the field tests the soil was assumed to be 90 percent saturated. Based on this assumption, the average soil density was 129.3 pcf. The average moisture content was 16.7 percent.

## K Values

A plot of peak acceleration versus impact velocity for each weight of cone is shown in Fig. 41. It should be noted that the cones used by Poor all had 60 degree apex angles. The accelerations are approximately linear functions of the impact velocity, which is similar to the cone test results on sands reported in Chapter V. For a given projectile geometry, impact velocity, and soil condition, the peak acceleration is strongly influenced by the weight of the projectile. Figure 42 shows that for large increases of projectile weight (16 to 1 ratio), the peak acceleration is decreased by approximately 80 percent.

Figures 43 through 45 show plots of peak soil force versus initial momentum for cone, spherical segment, and flat, circular plate tests. Soil

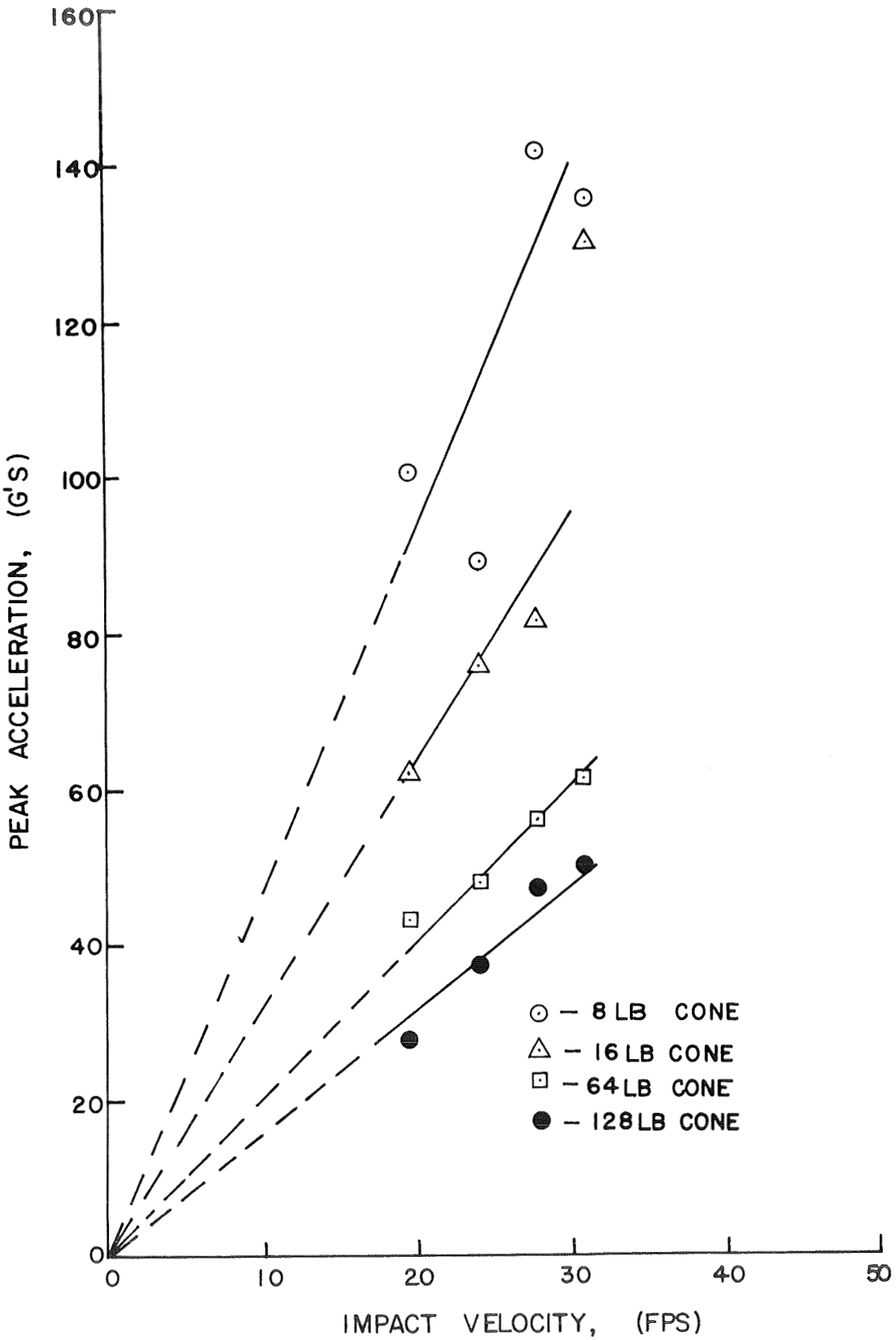


FIG. 41 PEAK ACCELERATION VERSUS IMPACT VELOCITY FOR CONE TESTS ON SANDY CLAY

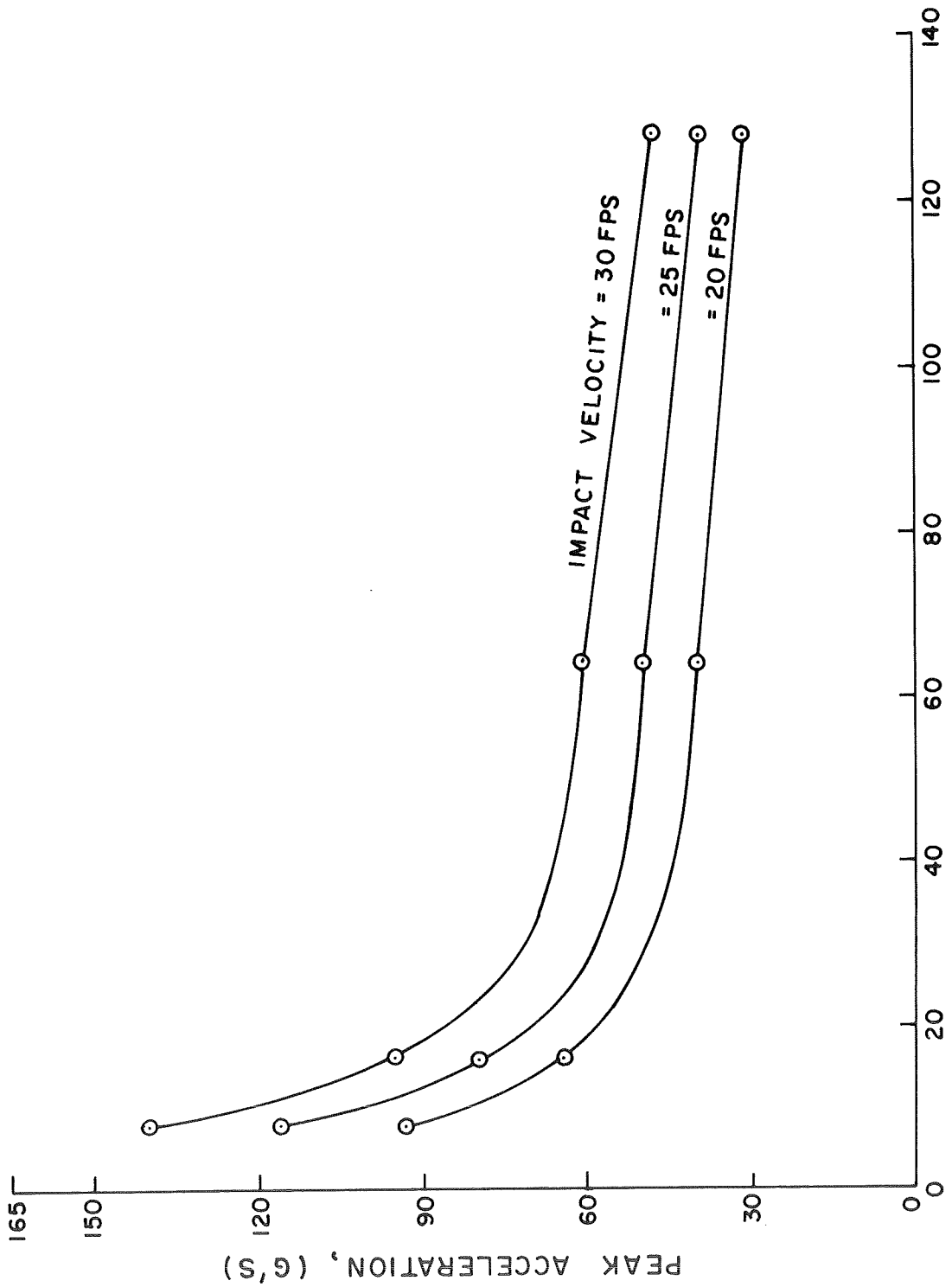


FIG. 42 PEAK ACCELERATION VERSUS CONE WEIGHT FOR IMPACT TESTS ON SANDY CLAY

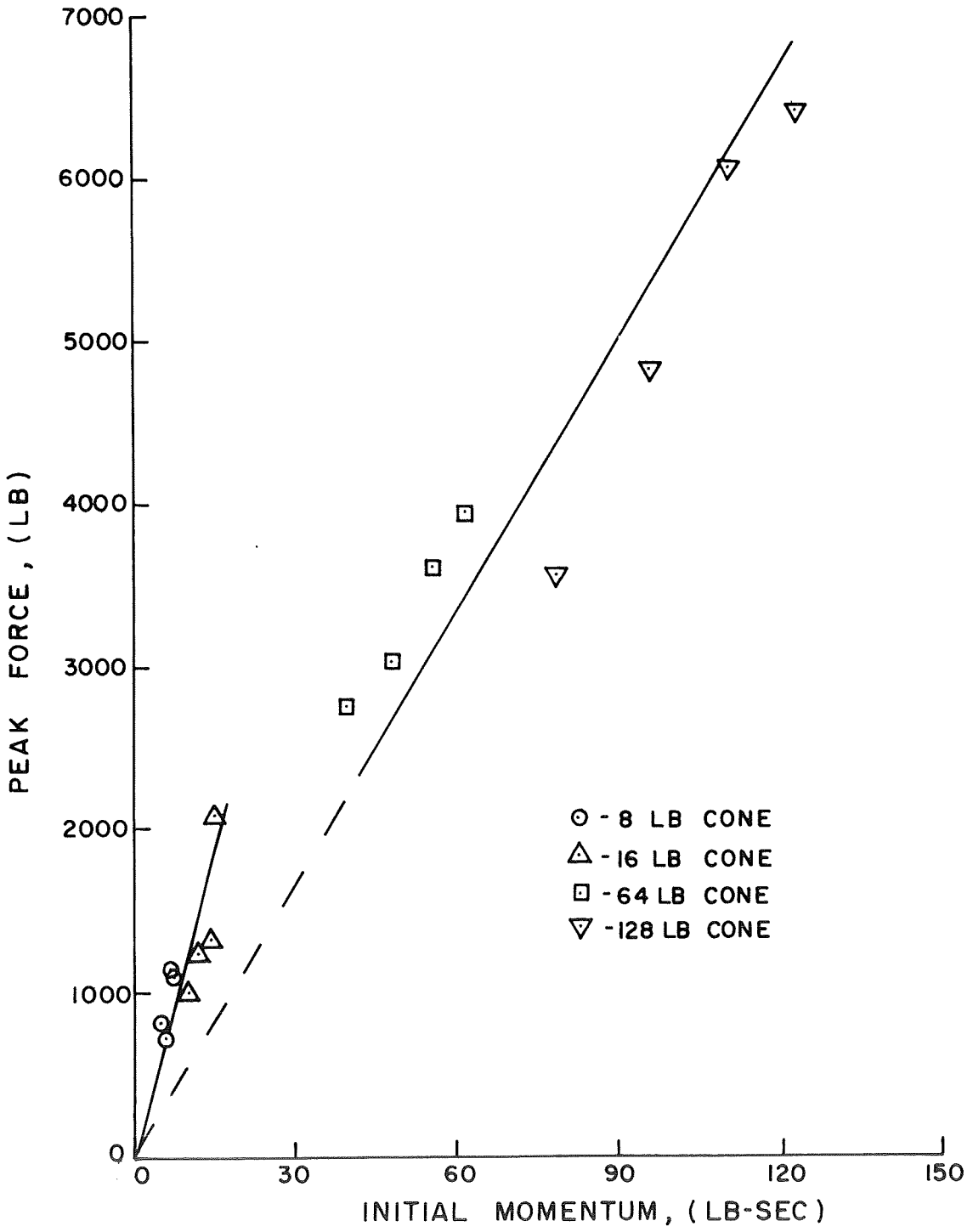


FIG. 43 PEAK FORCE VERSUS INITIAL MOMENTUM FOR CONE TESTS ON SANDY CLAY

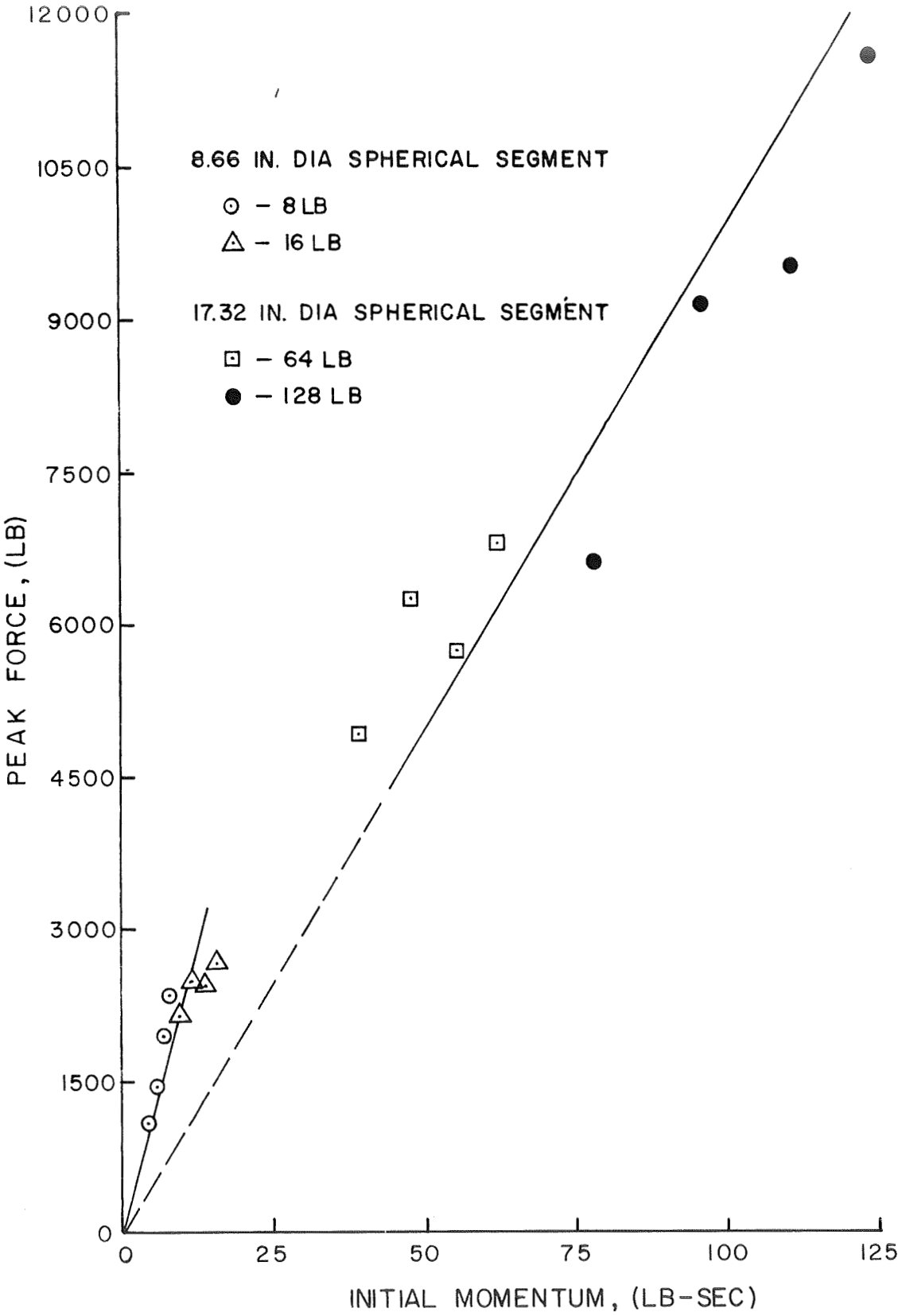


FIG. 44 PEAK FORCE VERSUS INITIAL MOMENTUM FOR SPHERICAL SEGMENT TESTS ON SANDY CLAY

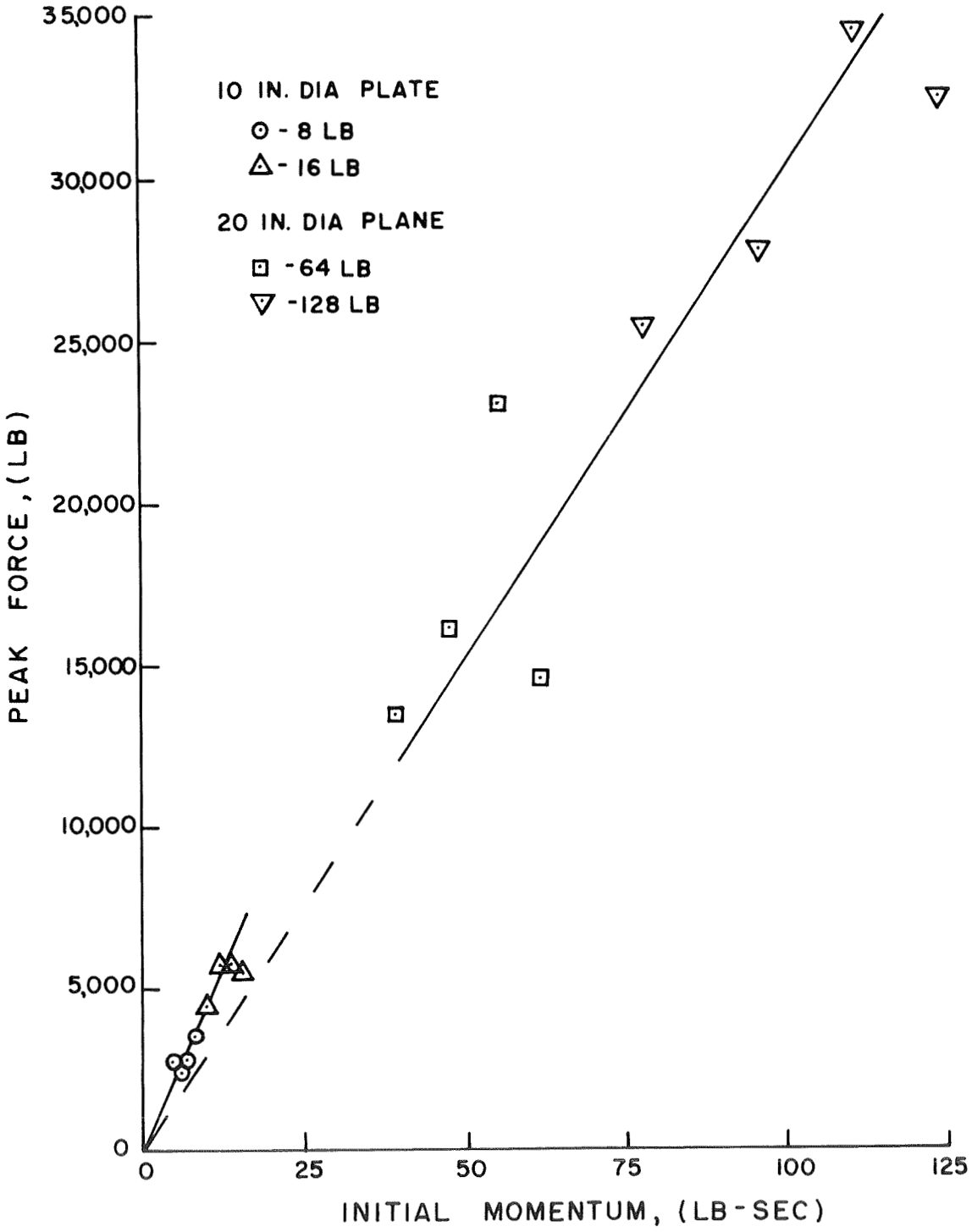


FIG. 45 PEAK FORCE VERSUS INITIAL MOMENTUM FOR FLAT, CIRCULAR PLATE TESTS ON SANDY CLAY

densities and moisture contents for each of the cone tests are presented in Table No. 10. Poor's test data indicate that the values listed in this Table are also representative of the soil conditions for the sphere and plate tests. Using the average soil density listed in Table No. 10 and the soil force-momentum plots in Figs. 43 through 45, K values were calculated for each projectile. These K values are listed in Table No. 11. Poor also performed a limited number of drop tests on dry, dense Colorado River Sand. Values of K for these tests are also listed in Table No. 11. Examination of the table shows that the 8 and 16 lb projectiles and the 64 and 128 lb projectiles have each been represented by a single K value. The K values for equal weight projectile tend to increase as the projectile surfaces become more blunt. The $K/K_{cone}$ column provides a comparison of how the geometry of the projectile effects the K values. The K values for dry sand are much more sensitive to geometry changes, than are the values for nearly saturated clay. This occurrence is to be expected since cohesionless materials derive strength from confinement. The cone allows the soil to flow freely along its surface; whereas, the flat plate confines the sand and consequently much higher impact forces are produced. It should be noted that the 8.66 and 17.32 in. dia. spherical segments had spherical diameters of 10 and 20 in., respectively. The segment diameters have been listed in Table No. 11 to remain consistent with Poor's nomenclature.

## Measured Soil Penetrations

Final measured soil penetrations for each type of projectile are shown in Figs. 46 through 48. The cone test results (Fig. 46) show a marked degree of linearity between impact velocity and final penetration. The cone penetrations at zero impact velocity were taken from the load-penetration

TABLE NO. 10

SOIL PROPERTIES FOR CONE TESTS ON SANDY CLAY

| Test No. | Soil Density $\gamma$ (pcf) | Moisture Content w (%) |
|---|---|---|
| 18 | 125.0 | 19.6 |
| 19 | 126.9 | 18.6 |
| 20 | 127.1 | 17.9 |
| 21 | 126.5 | 18.5 |
| 22 | 129.2 | 16.5 |
| 23 | 128.0 | 17.5 |
| 24 | 126.7 | 18.5 |
| 25 | 128.9 | 17.0 |
| 1 | 130.8 | 15.7 |
| 2 | 131.9 | 15.2 |
| 3 | 133.2 | 14.1 |
| 4 | 132.0 | 14.8 |
| 6 | 133.0 | 14.1 |
| 7* | 146.0 | 7.3 |
| 8 | 133.0 | 14.3 |
| 9 | 127.0 | 18.2 |

Average Moisture Content = 16.7%

Average Soil Density = 129.3 pcf

*Test No. 7 values were not used in calculating the average values, since it is believed they are in error.

TABLE NO. 11

COMPARISON OF K VALUES FOR CONES, SPHERICAL SEGMENTS AND FLAT, CIRCULAR PLATES

| Soil Type | Soil Density $\gamma$ (pcf) | Moisture Content w (%) | Projectile Type | Projectile Weight (Lb) | K Value ($Ft^3$/Lb-Sec) | $K/K_{cone}$ |
|---|---|---|---|---|---|---|
| Sandy Clay | 129.3 | 16.7 | Cone | 8 & 16 | 0.97 | 1.00 |
| | 129.3 | 16.7 | Cone | 64 & 128 | 0.43 | 1.00 |
| | 129.3 | 16.7 | 8.66 in. Dia Spherical Seg | 8 & 16 | 1.76 | 1.81 |
| | 129.3 | 16.7 | 17.32 in. Dia Spherical Seg | 64 & 128 | 0.77 | 1.79 |
| | 129.3 | 16.7 | 10 in. Dia. Plate | 8 & 16 | 3.48 | 3.59 |
| | 129.3 | 16.7 | 20 in. Dia. Plate | 64 & 128 | 2.34 | 5.45 |
| Colorado River Sand | 101.0 | 0.0 (Air Dry) | Cone | 8 | 0.33 | 1.00 |
| | 101.0 | 0.0 | 8.66 in. Dia Spherical Seg | 8 | 1.45 | 4.60 |
| | 101.0 | 0.0 | 10 in. Dia. Plate | 8 | 5.20 | 15.80 |

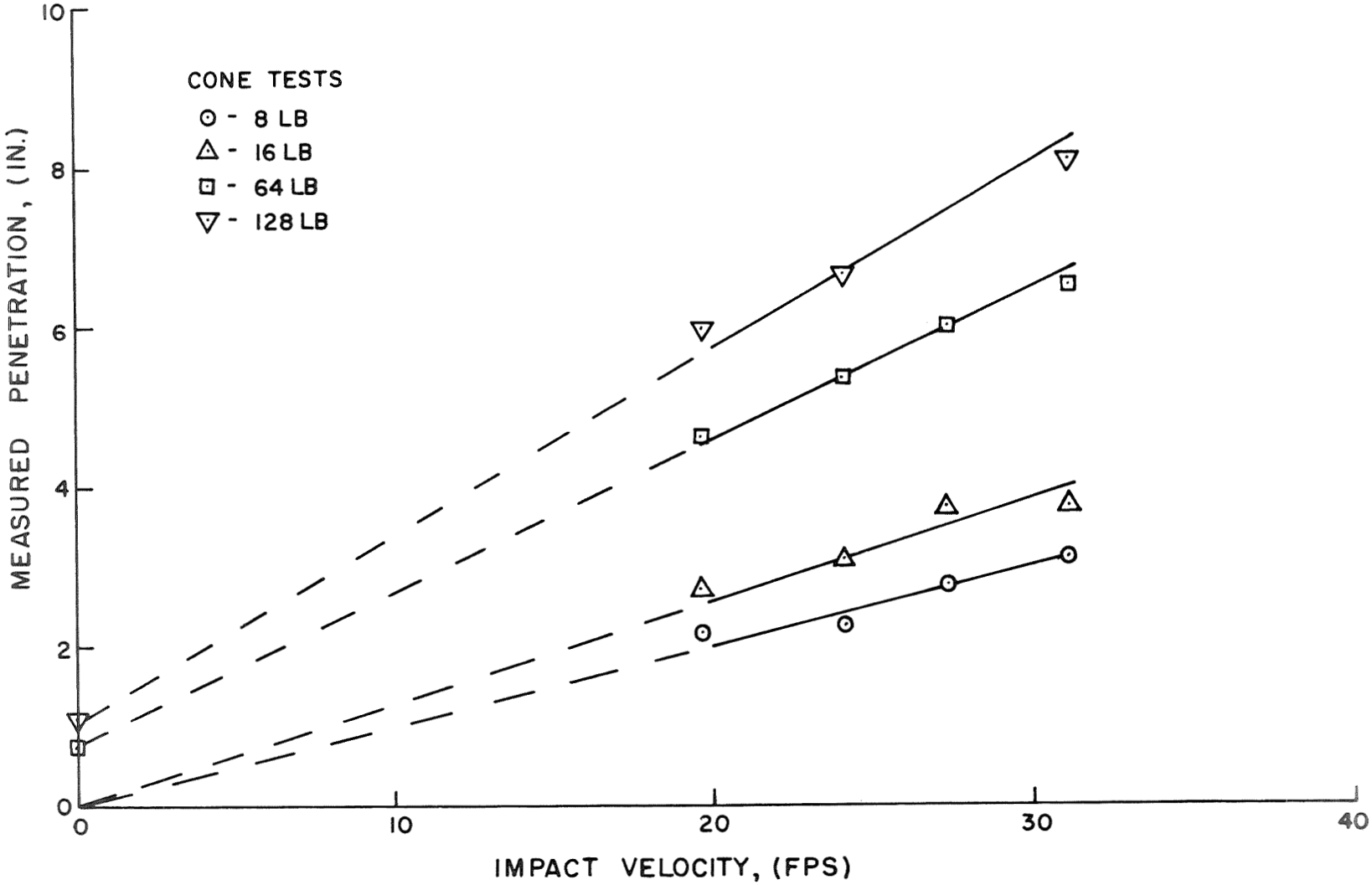


FIG. 46 MEASURED PENETRATION VERSUS IMPACT VELOCITY FOR CONE TESTS ON SANDY CLAY

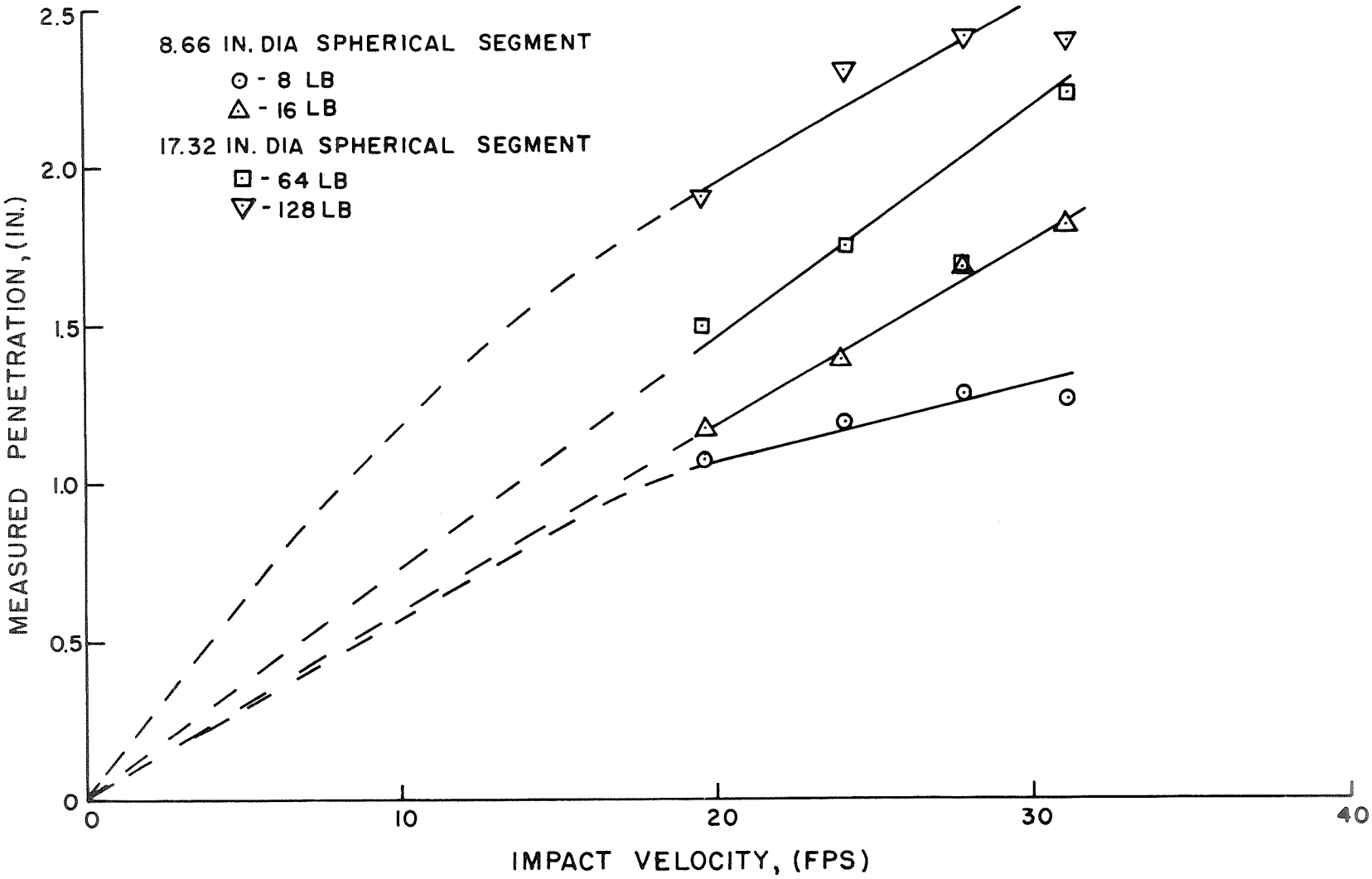


FIG. 47 MEASURED PENETRATION VERSUS IMPACT VELOCITY FOR SPHERICAL SEGMENT TESTS ON SANDY CLAY

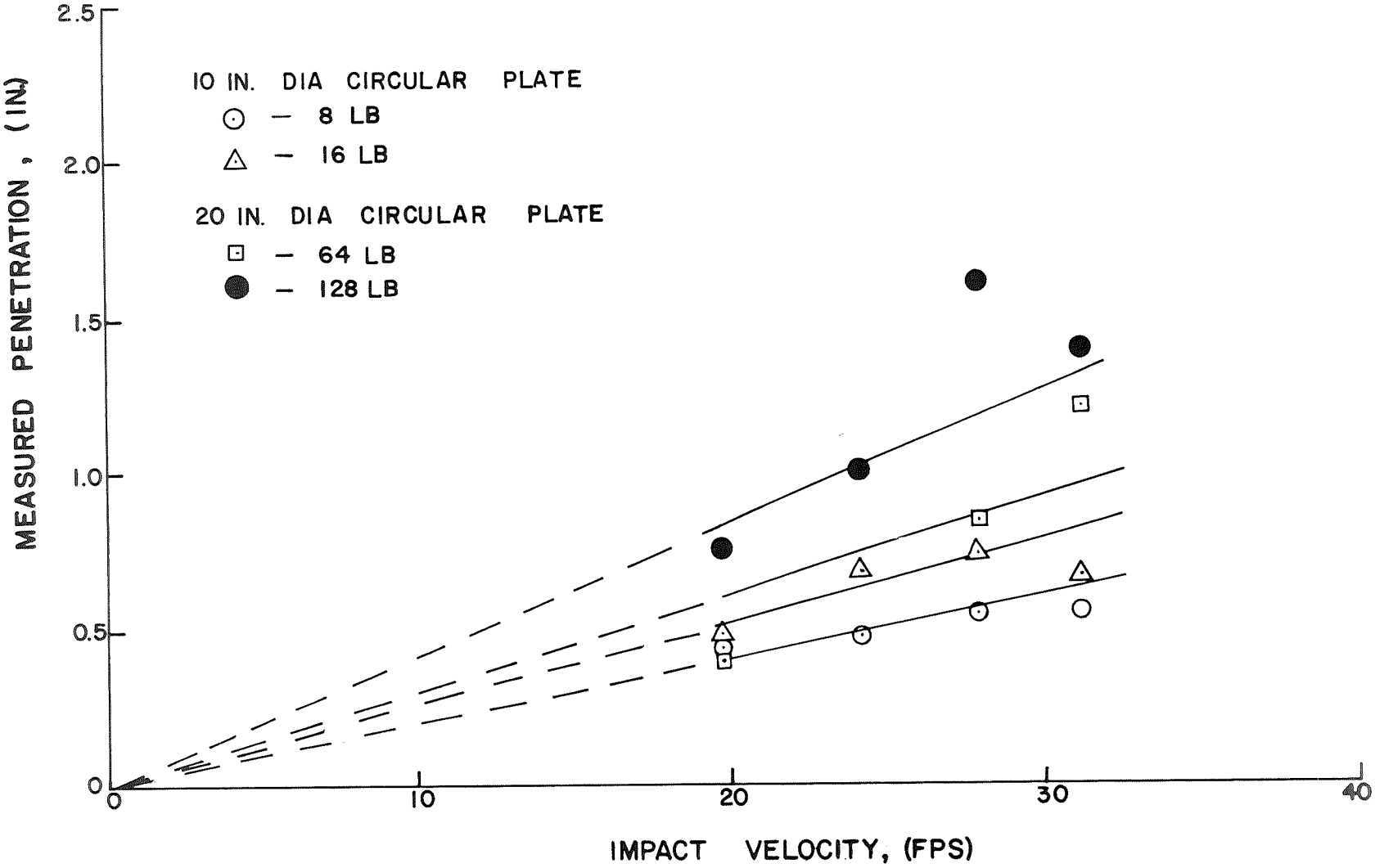


FIG. 48 MEASURED PENETRATION VERSUS IMPACT VELOCITY FOR FLAT, CIRCULAR PLATE TESTS ON SANDY CLAY

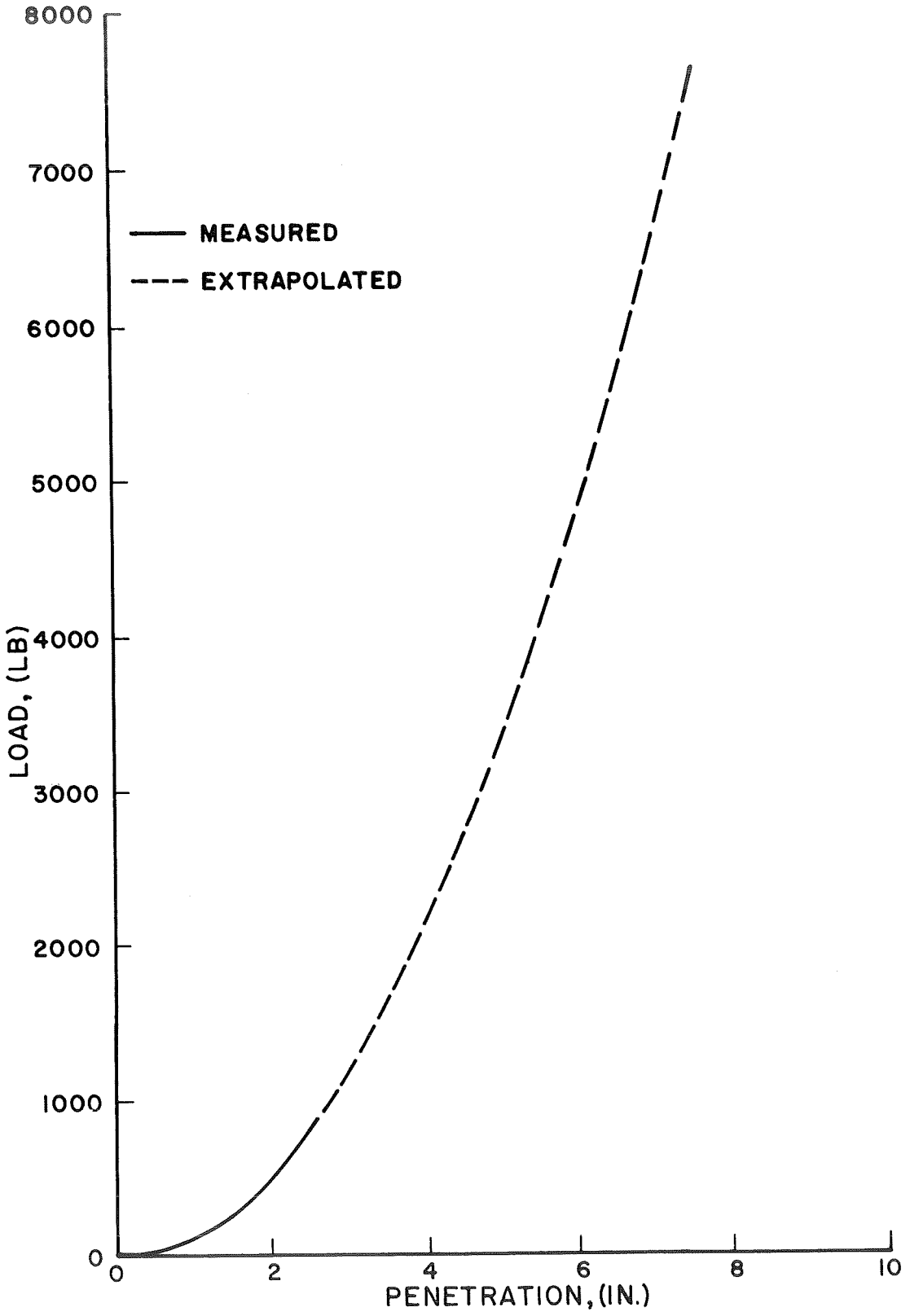


FIG. 49 STATIC LOAD - PENETRATION CURVE FOR 60 DEGREE, RIGHT CIRCULAR CONE TEST ON SANDY CLAY

curve in Fig. 49. The solid portion of the curve was obtained from a field load-test performed by Ghazzaly and Cox[4]. The test was performed at the impact site utilized by Poor using a cone with a 60 degree apex angle.

It is of interest to note the close agreement between the magnitudes of the penetrations obtained from the cone tests on sandy clay and the cone tests on dense, saturated sands (pp. 83-84). The $K_{cone}$ values for sandy clay and dense, saturated sand are also similar in magnitude. Examination of the general shape of the soil force-penetration curves shows that they are similar. These similarities suggest that possibly the behavior of dense, saturated sand under impact loading may not be significantly different from that of nearly saturated clay.

Dynamic-Static Force Ratios

Data were available that permitted a comparison study of soil forces developed during dynamic and static loading of sandy clay. Table No. 12 lists 16 tests in which the peak soil forces, developed upon impact of various weight cones, are compared with measured static soil forces. The static values were taken from the curve in Fig. 49, at penetrations which were equal to the penetrations that corresponded to the peak dynamic soil forces. Column 8 shows that the ratio of the peak dynamic force to the static force ranges from approximately 1.6 for the 8 lb cone, to 0.75 for the 128 lb cone. It seems highly improbable that the dynamic forces are ever less than the static forces since the strength of clay increases as the rate of loading increases.

Several factors may be responsible for ratio values less than one. First of all, the static force-penetration curve was obtained from a single field test which may not be representative of the soil over the entire impact site. Also, it was necessary to extrapolate a large portion of the force-

TABLE NO. 12

COMPARISON OF DYNAMIC AND STATIC CONE TEST RESULTS FOR SANDY CLAY

| 1<br>Test No. | 2<br>Cone Wt.<br>(lb) | 3<br>Impact Vel.<br>(fps) | 4<br>Vel. at Peak Accel.<br>(fps) | 5<br>Col 4/ Col 3<br>(%) | 6<br>Dynamic Force<br>(lb) | 7<br>Static Force<br>(lb) | 8<br>Col 6/ Col 7<br>(%) | 9<br>Penetration at Peak Accel.<br>(in.) | 10<br>Maximum Penetration<br>(in.) | 11<br>Col 9/ Col 10<br>(%) |
|---|---|---|---|---|---|---|---|---|---|---|
| 18 | 8 | 19.66 | 8.28 | 42.1 | 806 | 515 | 157 | 2.02 | 2.16 | 93.5 |
| 19 | 8 | 24.07 | 11.80 | 49.0 | 714 | 685 | 104 | 2.30 | 2.61 | 88.0 |
| 20 | 8 | 27.80 | 13.71 | 49.4 | 1136 | 900 | 126 | 2.63 | 2.80 | 94.0 |
| 21 | 8 | 31.08 | 11.60 | 37.4 | 1086 | 1150 | 95 | 2.92 | 3.12 | 93.5 |
| 22 | 16 | 19.66 | 7.36 | 37.4 | 992 | 925 | 107 | 2.65 | 2.83 | 93.5 |
| 23 | 16 | 24.07 | 9.41 | 39.1 | 1213 | 1250 | 97 | 3.04 | 3.30 | 92.0 |
| 24 | 16 | 27.80 | 11.43 | 41.1 | 1309 | 1420 | 109 | 3.43 | 3.75 | 91.5 |
| 25 | 16 | 31.08 | 13.12 | 42.2 | 2080 | 1600 | 130 | 3.45 | 3.73 | 92.5 |
| 1 | 64 | 19.66 | 6.58 | 33.4 | 2758 | 2800 | 99 | 4.57 | 4.77 | 95.8 |
| 2 | 64 | 24.07 | 10.17 | 42.2 | 3030 | 3160 | 96 | 4.85 | 5.37 | 90.4 |
| 3 | 64 | 27.80 | 11.43 | 41.1 | 3603 | 4200 | 86 | 5.60 | 6.05 | 92.5 |
| 4 | 64 | 30.82 | 12.54 | 40.7 | 3927 | 5000 | 79 | 6.10 | 6.61 | 92.2 |
| 6 | 128 | 19.66 | 3.70 | 18.8 | 3551 | 4800 | 74 | 5.98 | 6.08 | 98.5 |
| 7 | 128 | 24.07 | 7.93 | 32.9 | 4839 | 5800 | 83 | 6.58 | 6.90 | 95.4 |
| 8 | 128 | 27.80 | 15.17 | 54.5 | 6086 | 5500 | 111 | 6.40 | 7.34 | 87.3 |
| 9 | 128 | 30.82 | 14.51 | 47.0 | 6410 | 7150 | 90 | 7.29 | 8.11 | 89.7 |

penetration curve in order to provide strength comparisons at penetrations greater than 2.7 inches. Ordinarily, such a large extrapolation is not justified; however, for cone penetrations above 1.8 in. the soil stress based on the cross-sectional area of the cone at the ground surface remained essentially constant. Therefore, the assumption was made that a constant soil stress was developed for penetrations greater than 2.7 inches.

Table No. 12 also shows that the peak soil forces occurred when the cone had a downward velocity of approximately 40 percent of the initial impact velocity (column No. 5).

The penetration corresponding to peak dynamic force was, on the average, approximately 90 percent of the maximum penetration.

PROJECTILE TESTS ON SAND AND CLAY BY REICHMUTH

Reichmuth et al[19] performed several vertical impact tests using a 10 in. radius cylindrical segment and two 10 in. radius spherical segments. The cylindrical segment was 5.5 in. wide and weighed 50.2 lbs. The spherical segments had weights of 41.3 and 94.0 lbs. The impact velocities ranged from 10 to 30 fps. The target materials were; dry and saturated Ottawa Sand, dry Colorado River Sand, and Del Rio Clay.

The K values obtained from these tests are listed in Table No. 13. A comparison of measured and calculated penetrations has also been presented. The calculated values were obtained from the double integration of the acceleration-time trace. In general, the calculated and measured values agree quite well. Average K values for each type of soil are given in Table No. 14.

It was previously noted on p. 89 that the $K_{cone}$ values for tests on dry, dense sand and saturated, dense sand were approximately the same. The $K_{cone}$ values for similar states of Ottawa and Colorado River Sand were also

TABLE NO. 13

COMPARISON OF $K_{cylinder}$ AND $K_{sphere}$ VALUES FROM TESTS ON OTTAWA SAND, COLORADO RIVER SAND, AND DEL RIO CLAY

| Test Identification | Impact Velocity (fps) | Soil Density $\gamma$ (pcf) | Moisture Content w (%) | Peak Force (Lb) | Projectile Weight (Lb) | Measured Penet. (in.) | Calc. Penet. (in.) | K Value ($Ft^3$/Lb-Sec) |
|---|---|---|---|---|---|---|---|---|
| 9-9-10-CYL1-90-0-OS | 10.8 | 98.8 | 3.5 | 1,545 | 50.2 | 1.9 | 1.1 | 0.93 |
| 9-9-9-CYL1-90-0-OS | 20.9 | 101.6 | 3.6 | 2,429 | 50.2 | 2.9 | 2.7 | 0.73 |
| 9-9-7-CYL1-90-0-OS | 29.8 | 94.7 | 3.6 | 4,453 | 50.2 | 2.8 | 2.9 | 1.01 |
| 6-29-22-SL-90-0-CA | 21.8 | 99.2 | 1.7 | 3,847 | 41.3 | 1.4 | 1.4 | 1.39 |
| 6-29-23-SL-90-0-CA | 28.7 | 97.4 | 2.8 | 5,069 | 41.3 | 1.7 | 2.3 | 1.42 |
| 9-9-12-SL-90-0-OS | 10.9 | 125.6 | 17.0 | 2,138 | 41.3 | 0.8 | 0.8 | 1.22 |
| 9-9-14-SL-90-0-OS | 27.9 | 127.9 | 19.0 | 7,126 | 41.3 | 1.4 | 1.6 | 1.56 |
| 9-10-3-SH-90-0-OS | 30.7 | 124.0 | 18.3 | 12,450 | 94.0 | 1.8 | 2.1 | 1.12 |
| 6-29-17-SH-90-0-CA | 23.7 | 101.0 | 2.3 | 6,352 | 94.0 | 2.4 | 2.7 | 0.91 |
| 8-19-20-SL-90-0-BS | 20.2 | 116.0 | 33.4 | 3,238 | 41.3 | 1.6 | 1.5 | 1.08 |
| 8-19-21-SL-90-0-BS | 28.8 | 114.6 | 32.5 | 5,143 | 41.3 | -- | 1.8 | 1.22 |
| 8-19-16-SH-90-0-BS | 18.2 | 114.6 | 32.5 | 4,425 | 94.0 | 2.1 | 1.3 | 0.73 |
| 8-19-17-SH-90-0-BS | 19.1 | 114.6 | 32.5 | 5,237 | 94.0 | 1.7 | 2.0 | 0.82 |

OS = Ottawa Sand; CA = Capitol Aggregates; BS = Del Rio Clay

TABLE NO. 14

COMPARISON OF AVERAGE $K_{cylinder}$ and $K_{sphere}$ VALUES FROM TESTS ON OTTAWA SAND, COLORADO RIVER SAND, AND DEL RIO CLAY

| Soil Type | Avg Soil Den. $\gamma$ (pcf) | Avg Moist. Content w (%) | Projectile Type | Projectile Weight (Lb) | K Value ($Ft^3$/Lb-Sec) |
|---|---|---|---|---|---|
| Ottawa Sand | 98.4 | 3.6 | Cylinder 10 in. Radius (CYL1) | 50.2 | 0.89 |
| Saturated Ottawa Sand | 125.6 | 17.0 | | 41.3 | 1.39 |
| | 125.9 | 18.7 | | 94.0 | 1.12 |
| Colorado River Sand | 98.3 | 2.3 | Sphere 10 in. Radius (SL) & (SH) | 41.3 | 1.41 |
| | 101.0 | 2.3 | | 94.0 | 0.91 |
| Del Rio Clay | 115.3 | 33.0 | | 41.3 | 1.15 |
| | 114.6 | 32.5 | | 94.0 | 0.78 |

found to be of similar magnitude. Examination of Table No. 14 shows the same trend holds true for spherically shaped projectiles.

The $K_{sphere}$ values (Table No. 14) for the light sphere tests on saturated Ottawa Sand and dense Colorado River Sand are approximately three times greater than the $K_{cone}$ values (Table No. 6, p. 90) obtained from tests on similar states of Ottawa and Colorado River Sand. It should be noted that the influence of the projectile shape can only be determined for cases where the soil conditions are similar and the projectile weights are approximately the same.

It is interesting to note that a $K_{sphere}$ value of 0.78 was obtained for the heavy sphere (94 lb) tests on Del Rio Clay and a $K_{sphere}$ value of 0.77 (Table No. 11) was obtained from the 64 and 128 lb sphere tests on sandy clay. The comparison is valid since the projectiles have approximately the same weight. However, the target materials are significantly different in composition. The cohesion values for each of the soils are approximately the same, but the angle of internal friction for the sandy clay is significantly higher. From a static strength point of view, the sandy clay is the stronger of two and therefore should offer more resistance to penetration.

## PENETROMETER TESTS ON SAND AND CLAY BY WOMACK

Womack[33] developed a penetrometer for the purpose of evaluating the impact characteristics of soils. The penetrometer weighed 5.38 lbs and had a flat, circular foot approximately one square inch in area. Ottawa Sand and Del Rio Clay are among some of the soils tested by Womack. The impact velocity was maintained approximately constant at 15 fps.

The force-penetration curves from the penetrometer tests exhibited a rapid rise in force as the penetrometer foot contacted the soil surface. The rapid rise was followed by a sudden decrease to a relatively constant force level. Womack considered the spike portion of the curve as not being significant to the force-penetration characteristics of the target material. His primary reason for arriving at this conclusion was that after examining comparison test data he found that the spike force levels were not consistent with one another. He considered the average penetration force which was present during more than 90 percent of the penetration depth to be the significant force level.

The vital characteristics of the force-penetration curves produced by impact of the penetrometer on various states of soil are shown in Table No. 15. It will be noted that a peak force and average penetration force column have been included within the table.

The table shows that there are significant differences in both the peak and average force penetration values which were recorded for similar impact conditions on separate days of testing. This disparity becomes readily evident when the force levels from the tests on the dates 10-9, 11-10, and 11-11 are compared.

The characteristic spike portion of the curve was not present in the tests on Del Rio Clay nor in several of the tests on saturated Ottawa Sand. In general, there was a tendency for the ratio of the peak force to average penetrating force to decrease as the moisture content of the sand increased. $K_{plate}$ values were calculated using both the peak force and the average penetration force. These values are listed in Table No. 16. Average $K_{plate}$ values for each soil condition are listed in Table No. 17. The peak $K_{plate}$ values for dense, saturated Ottawa Sand are approximately 50 percent

TABLE NO. 15

TABULATION OF FORCE-PENETRATION CHARACTERISTICS
FROM PENETROMETER TESTS

| Test Ident. | Impact Velocity (fps) | Soil Density $\gamma$ (pcf) | Moist. Content w (%) | Peak Force (Lb) | Avg. Penet. Force (Lb) | Penet. at Peak Force (in.) | Penet. at Avg. Force (in.) | Total Penet. (in.) | Rise Time (msec) |
|---|---|---|---|---|---|---|---|---|---|
| 11-15-1-OS | 14.90 | 105.8 | 0 | 255.3 | 45 | 0.13 | 0.26 | 3.59 | 0.77 |
| 11-15-2-OS | 15.66 | 104.0 | 0 | 251.0 | 56 | 0.21 | 0.41 | 3.85 | 1.16 |
| 11-15-3-OS | 15.40 | 108.0 | 0 | 262.2 | 60 | 0.14 | 0.27 | 3.55 | 0.77 |
| 11-9-3-OS | 15.63 | 107.0 | 11.4 | 284.0 | 80 | 0.08 | 0.23 | 3.22 | 0.43 |
| 11-9-4-OS | 15.58 | 111.7 | 11.3 | 247.3 | 118 | 0.16 | 0.45 | 2.02 | 0.86 |
| 10-9-4-OS | 15.47 | 124.9 | 24.5 | 177.4 | --* | 1.59 | -- | 1.79 | 11.66 |
| 10-9-5-OS | 14.80 | 123.9 | 25.6 | 174.4 | 135 | 0.07 | 0.15 | 1.68 | 0.43 |
| 11-10-1-OS | 14.34 | 124.7 | 24.6 | 116.8 | 100 | 0.15 | 0.29 | 2.35 | 0.86 |
| 11-10-2-OS | 14.56 | 124.3 | 25.2 | 126.4 | -- | 1.91 | -- | 2.51 | 12.88 |
| 11-11-1-OS | 15.86 | 123.7 | 25.8 | 165.7 | 70 | 0.14 | 0.28 | 3.49 | 0.77 |
| 11-11-2-OS | 15.38 | 128.4 | 21.4 | 183.6 | 80 | 0.14 | 0.28 | 2.66 | 0.77 |
| 11-11-3-OS | 15.38 | 128.8 | 21.0 | 207.0 | 110 | 0.14 | 0.27 | 2.15 | 0.77 |
| 11-11-4-OS | 14.99 | 130.4 | 19.3 | 176.8 | 130 | 0.21 | 0.40 | 1.84 | 1.16 |
| 10-10-9-BS | 15.69 | 112.0 | 32.0 | 310.7 | -- | 0.67 | -- | 0.96 | 4.30 |
| 10-10-10-BS | 15.46 | 117.0 | 31.0 | 286.7 | -- | 0.63 | -- | 1.06 | 3.90 |

*These tests did not have a spike portion; OS = Ottawa Sand; BS = Del Rio Clay

TABLE NO. 16

LISTING OF $K_{plate}$ VALUES FOR PENETROMETER TESTS

| Soil Type | Impact Velocity (fps) | Soil Density $\gamma$ (pcf) | Moisture Content w (%) | Peak $K_{plate}$ ($Ft^3$/lb-sec) | Residual $K_{plate}$ ($Ft^3$/lb-sec) |
|---|---|---|---|---|---|
| Dry Ottawa Sand | 14.90 | 105.8 | 0 | 0.97 | 0.17 |
| | 15.66 | 104.0 | 0 | 0.93 | 0.21 |
| | 15.40 | 108.0 | 0 | 0.94 | 0.22 |
| Partially Saturated Ottawa Sand | 15.63 | 107.0 | 11.4 | 1.01 | 0.29 |
| | 15.58 | 111.7 | 11.3 | 0.85 | 0.41 |
| Saturated Ottawa Sand | 15.47 | 124.9 | 24.5 | 0.55 | -- |
| | 14.80 | 123.9 | 25.6 | 0.57 | 0.44 |
| | 14.34 | 124.7 | 24.6 | 0.39 | 0.34 |
| | 14.56 | 124.3 | 25.2 | 0.42 | -- |
| | 15.86 | 123.7 | 25.8 | 0.51 | 0.21 |
| | 15.38 | 128.4 | 21.4 | 0.56 | 0.24 |
| | 15.38 | 128.8 | 21.0 | 0.63 | 0.33 |
| | 14.99 | 130.4 | 19.3 | 0.54 | 0.40 |
| Del Rio Clay | 15.69 | 112.0 | 32.0 | 1.06 | -- |
| | 15.46 | 117.0 | 31.0 | 0.95 | -- |

TABLE NO. 17

LISTING OF AVERAGE $K_{plate}$ VALUES FOR PENETROMETER TESTS

| Soil Type | Average Soil Density $\gamma$ (pcf) | Average Moisture Content w (%) | Average Peak $K_{plate}$ ($Ft^3$/Lb-Sec) | Average Residual $K_{plate}$ ($Ft^3$/Lb-Sec) |
|---|---|---|---|---|
| Dry Ottawa Sand | 105.9 | 0 | 0.95 | 0.20 |
| Partially Saturated Ottawa Sand | 109.4 | 11.4 | 0.93 | 0.35 |
| Saturated Ottawa Sand | 126.1 | 23.4 | 0.52 | 0.33 |
| Del Rio Clay | 114.5 | 31.5 | 1.00 | -- |

the values obtained from the tests on dense, dry Ottawa Sand, while examination of the residual $K_{plate}$ values shows that the dense, saturated sand values are approximately 50 percent greater than the dense, dry sand values. The previous tests with larger projectiles have shown that the K values for sands in dry and saturated dense states are approximately the same.

The above comparison shows that the trends in the penetrometer data are significantly different from those observed during impact of larger projectiles. Possibly a better design for a penetrometer would be to decrease the weight-contact area ratio to a value which would correspond more closely to those of projectiles which undergo relatively small penetrations. This decreased weight-area ratio would cause the penetrometer to behave mainly as a body impacting on the soil surface, rather than a body which impacts and then penetrates a relatively large distance beneath the soil surface.

Womack also utilized a Proctor[17] type penetrometer for measuring the static soil resistance. His results show that the dynamic-static force ratio is approximately 2.25 for Del Rio Clay. This ratio was obtained by dividing the dynamic force by the static force that corresponded to the penetration value at the time of peak dynamic force development. When the same type of ratio calculation method was applied to the sand test results, it was found that the ratio values were in many cases over 100. However, the ratio values varied widely from test to test and no consistent trends were noted.

## PROJECTILE TEST ON SILT BY REESE

Reese et al[18] performed a series of laboratory impact tests in which he utilized spherical segments. The segments had spherical radii of 3 and 6 in. and weights which ranged from 0.895 to 11.32 lbs. The impact velocities were varied between 6 and 17 fps. A series of 8 drop tests were also conducted using a one-quarter scale Apollo model.

## Soil Conditions

The target material was composed of a sandy silt containing a small percentage of clay. The soil was compacted in layers to an approximate density of 125 pcf. The moisture content was maintained essentially at 10 percent. The soil containers were approximately 2 ft in diameter and 1 ft deep. The quarter-scale model tests were performed in a test bed located outside the laboratory. A 6 ft square by 2 ft deep test bed was utilized for the target area. Target area preparation methods were closely controlled to insure that the soil density and moisture content corresponded closely to that of the laboratory test beds.

## $K_{sphere}$ Values

Plots of peak acceleration versus impact velocity for each of the spherical segment drop tests are shown in Figs. 50 and 51. These plots show that for a given projectile type, the peak acceleration is linearly related to the impact velocity. The figures also illustrate the effect of projectile weight upon peak accelerations. Figures 52 and 53 illustrate the relative range of peak soil forces developed during impact. Using these figures and the average soil properties listed in Table No. 18, $K_{sphere}$ values were calculated and listed in Table No. 19. It is interesting to note the close agreement between the K values obtained from the 2.83 and 4.96 lb projectile tests. This close agreement is accompanied by nearly equal weight-spherical radius ratios, which indicates that this type of ratio might be useful in estimating appropriate $K_{sphere}$ values. Figure 54 shows the variation in $K_{sphere}$ values as the weight-radius ratio changes.

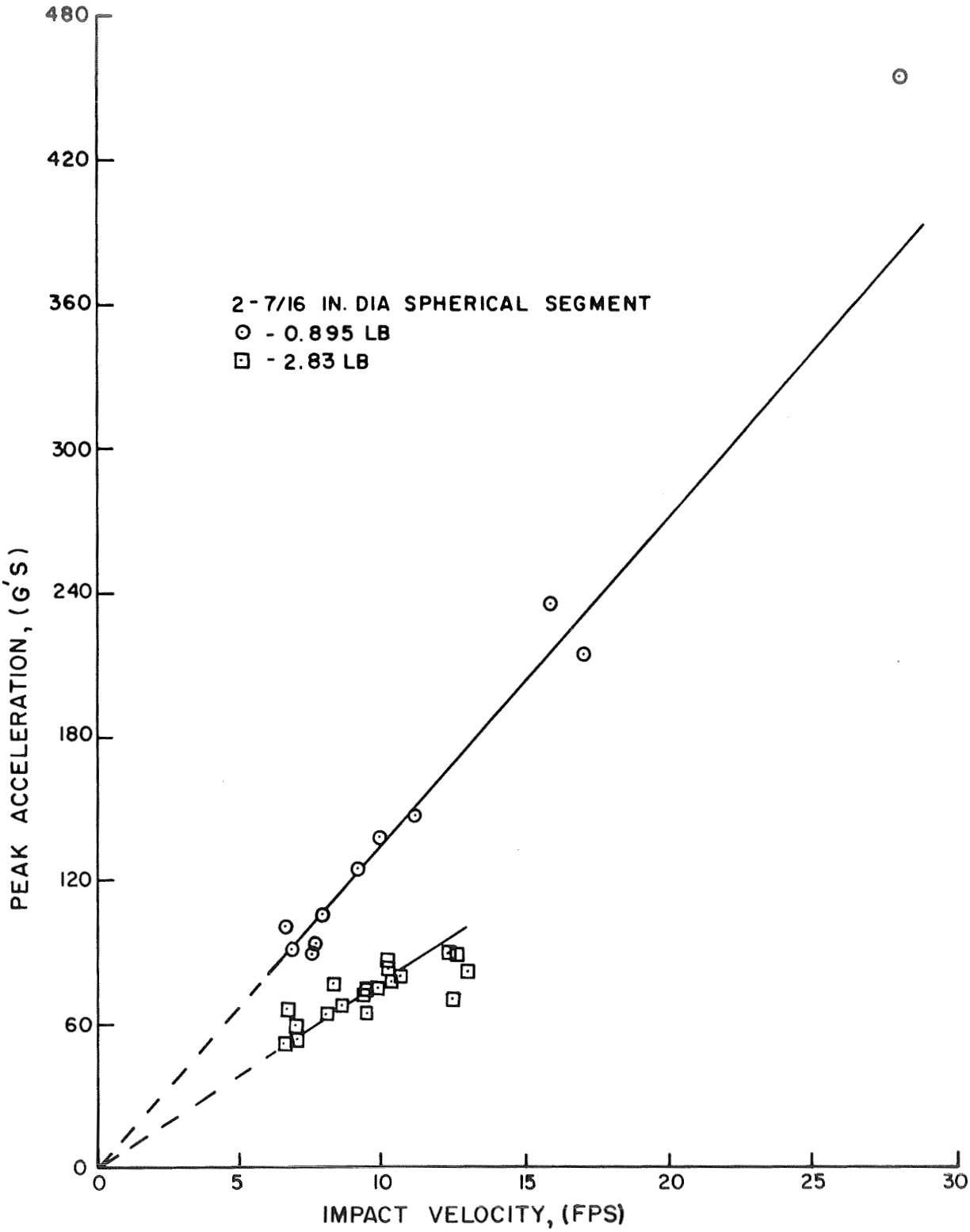


FIG. 50 PEAK ACCELERATION VERSUS IMPACT VELOCITY FOR TESTS ON MONTOPOLIS SILT

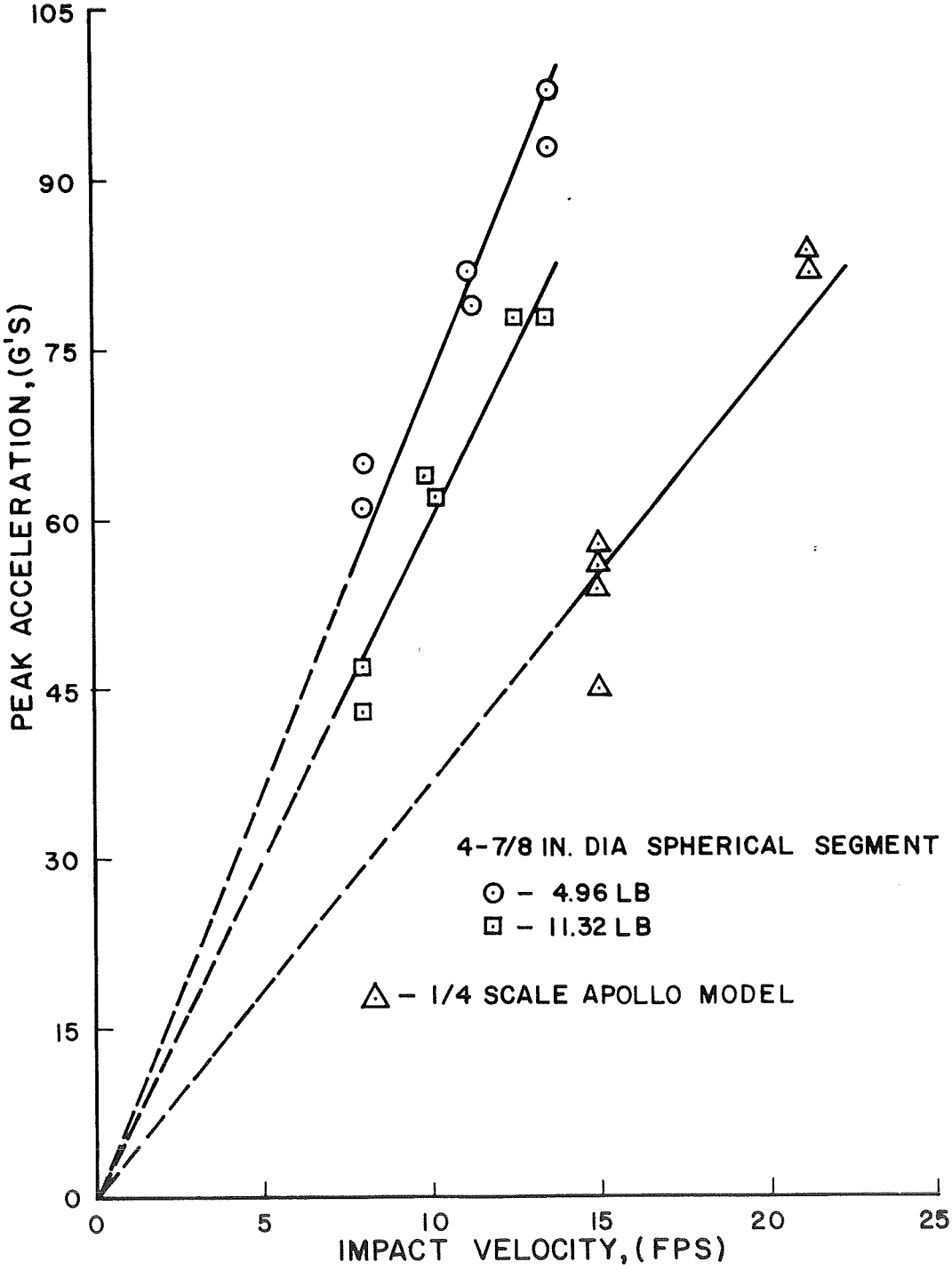


FIG. 51 PEAK ACCELERATION VERSUS IMPACT VELOCITY FOR TESTS ON MONTOPOLIS SILT

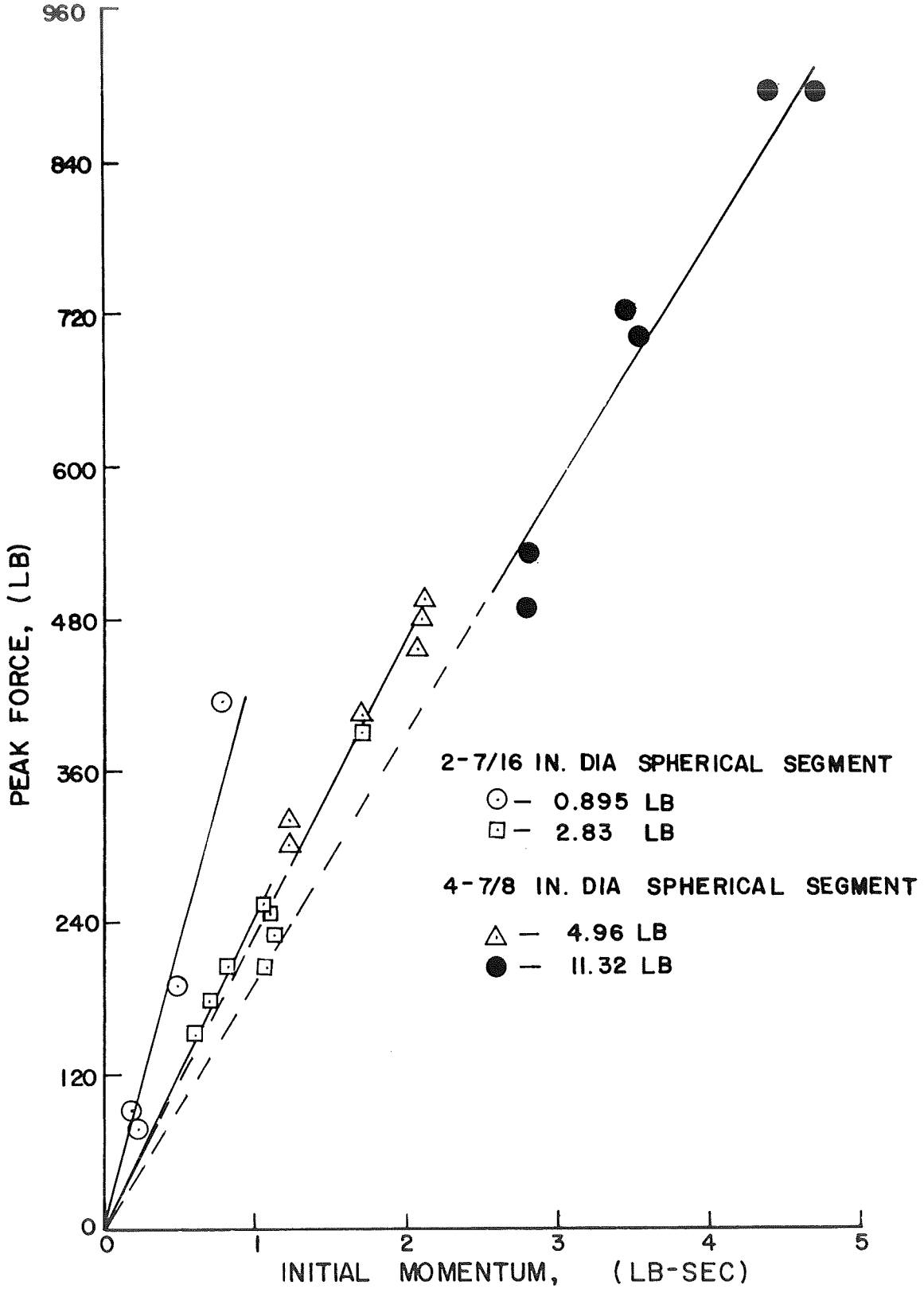


FIG. 52 PEAK FORCE VERSUS INITIAL MOMENTUM FOR TESTS ON MONTOPOLIS SILT

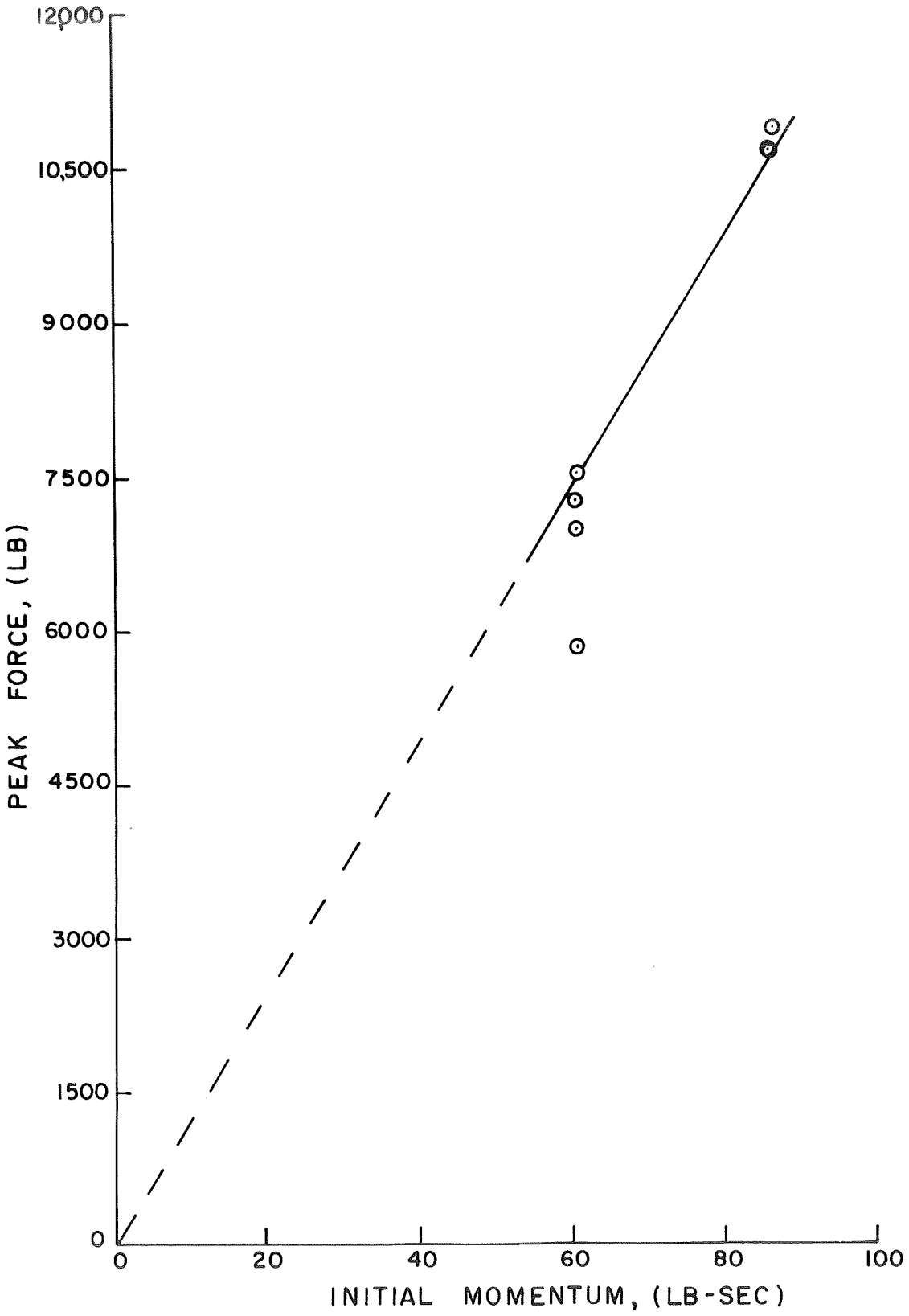


FIG. 53 PEAK FORCE VERSUS INITIAL MOMENTUM FOR ONE-QUARTER-SCALE APOLLO MODEL TESTS ON MONTOPOLIS SILT

TABLE NO. 18

AVERAGE SOIL PROPERTIES FOR TESTS ON MONTOPOLIS SILT

| Spherical Radius (in.) | Weight (lb) | Soil Density $\gamma$ (pcf) | Moisture Content w (%) |
|---|---|---|---|
| 3 | 0.895 | 125.6 | 8.6 |
| 3 | 2.83 | 127.3 | 10.1 |
| 6 | 4.96 | 125.6 | 8.6 |
| 6 | 11.32 | 125.6 | 8.6 |
| 44.2 | 130.00 | 126.5 | 9.4 |

TABLE NO. 19

LISTING OF $K_{sphere}$ VALUES FOR TESTS ON MONTOPOLIS SILT

| Spherical Radius (in.) | Weight (lb) | Weight/ Spherical Radius (lb/in.) | K ($Ft^3$/lb-sec) |
|---|---|---|---|
| 3 | 0.895 | 0.30 | 3.54 |
| 3 | 2.83 | 0.94 | 1.93 |
| 6 | 4.96 | 0.82 | 1.86 |
| 6 | 11.32 | 1.89 | 1.54 |
| 44.2 | 130.00 | 2.94 | 0.98 |

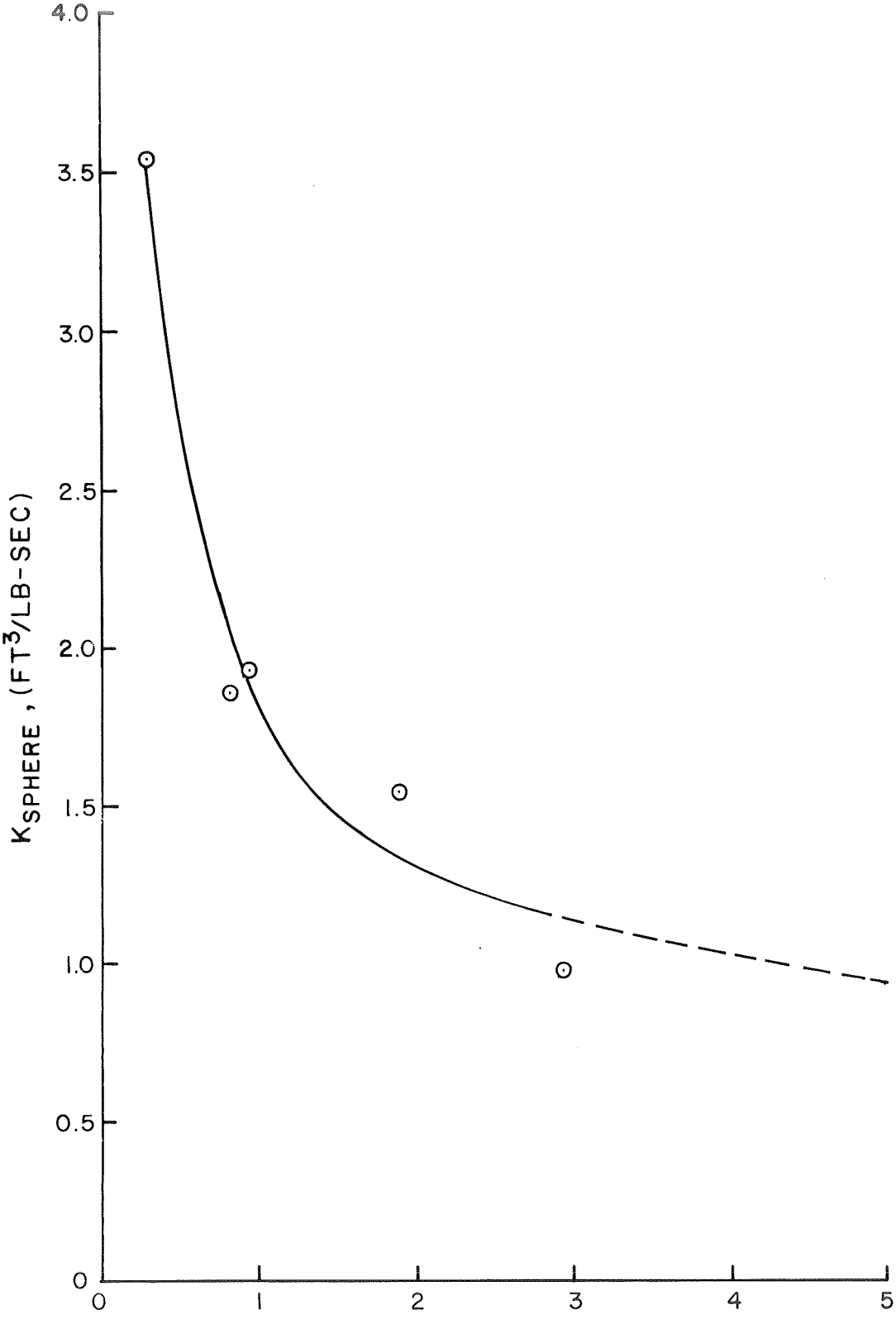


FIG. 54 $K_{SPHERE}$ VERSUS WEIGHT-RADIUS RATIO FOR TESTS ON MONTOPOLIS SILT

Dynamic-Static Force Ratios

Static force-penetration curves were given for each of the projectiles. This data permitted the calculation of dynamic-static force ratios. Table No. 20 shows that the ratio values range from approximately 150 to 600 percent, with the average being 275 percent. It should be noted that the static force values correspond to penetrations that were equal to the penetrations at which the peak dynamic soil forces occurred.

SUMMARY OF K VALUES

This chapter has basically been concerned with the presentation and comparison of K values that were developed from a wide range of projectile and soil conditions. It has previously been noted that the K values are mainly a function of the target material, projectile geometry, and the projectile weight. This dependence of K necessitates the use of extreme care in estimating K values for projectile and soil conditions differing from those listed in this chapter. However, it is felt that enough data are available to permit the estimation of K values with a reasonable degree of accuracy.

The test results have shown that the most unfavorable projectile shape, from a maximum force viewpoint, is one which has a flat striking surface. Conical projectiles were found to be the most favorable. The ratio of $K_{plate}$ to $K_{cone}$ was 3.59 for tests on sandy clay and 15.80 for tests on dry Colorado River Sand (Table No. 11, p. 106). The projectile geometry has a much larger influence on the forces developed in sand, because sands derive their rigidity from confinement; whereas, the resistance of clay to penetration is derived from cohesion between water and soil particles. When sands are contacted by a flat striking surface the particles are confined by the projectile itself and are forced to move mainly downward and in a transverse direction to the projectile path.

TABLE NO. 20

COMPARISONS OF RATIO OF PEAK DYNAMIC FORCE
TO STATIC FORCE FOR TESTS ON MONTOPOLIS SILT

| Spherical Radius (in.) | Weight (lb) | Impact Velocity (fps) | Penetration (in.) | Dynamic Force (lb) | Static Force (lb) | Col 5/Col 6 (%) |
|---|---|---|---|---|---|---|
| 3 | 0.895 | 6.6 | 0.10 | 90 | 28 | 322 |
| 3 | 0.895 | 7.8 | 0.12 | 105 | 32 | 328 |
| 3 | 0.895 | 9.2 | 0.16 | 110 | 50 | 220 |
| 3 | 0.895 | 9.9 | 0.16 | 120 | 50 | 240 |
| 3 | 0.895 | 11.1 | 0.17 | 131 | 55 | 238 |
| 3 | 0.895 | 15.8 | 0.18 | 210 | 61 | 344 |
| 3 | 0.895 | 17.0 | 0.18 | 190 | 61 | 312 |
| 3 | 2.83 | 6.6 | 0.23 | 145 | 78 | 186 |
| 3 | 2.83 | 8.1 | 0.25 | 177 | 84 | 210 |
| 3 | 2.83 | 9.4 | 0.23 | 220 | 78 | 282 |
| 3 | 2.83 | 10.1 | 0.22 | 240 | 72 | 333 |
| 3 | 2.83 | 10.6 | 0.28 | 225 | 97 | 232 |
| 3 | 2.83 | 12.3 | 0.28 | 252 | 97 | 260 |
| 6 | 4.96 | 8.0 | 0.26 | 318 | 164 | 194 |
| 6 | 4.96 | 11.2 | 0.33 | 390 | 231 | 169 |
| 6 | 4.96 | 13.8 | 0.37 | 492 | 274 | 180 |
| 6 | 11.32 | 8.0 | 0.39 | 490 | 297 | 165 |
| 6 | 11.32 | 10.1 | 0.39 | 700 | 297 | 236 |
| 6 | 11.32 | 12.5 | 0.43 | 880 | 333 | 264 |
| 6 | 11.32 | 13.4 | 0.46 | 900 | 370 | 243 |
| 44.2 | 130.00 | 15.0 | 0.36 | 5900 | 2875 | 206 |
| 44.2 | 130.00 | 15.0 | 0.36 | 6400 | 2875 | 223 |
| 44.2 | 130.00 | 15.0 | 0.27 | 6850 | 2225 | 308 |
| 44.2 | 130.00 | 15.0 | 0.27 | 6850 | 2225 | 308 |
| 44.2 | 130.00 | 15.0 | 0.36 | 5600 | 2875 | 195 |
| 44.2 | 130.00 | 21.3 | 0.17 | 9350 | 1575 | 594 |
| 44.2 | 130.00 | 21.3 | 0.20 | 10650 | 1775 | 600 |
| 44.2 | 130.00 | 21.3 | 0.45 | 10900 | 3500 | 312 |

The impact tests on sand have shown that the maximum soil forces are developed when the sand is in a relatively dense saturated state. However, a single $K_{cone}$ value of approximately 0.45 applies for both the dense, dry and saturated states (Table No. 6, p. 90). It is interesting to note that for the 64 lb cone the K value was 0.43 for the tests on sandy clay. This K value would be somewhat greater if it were adjusted to correspond to a 43 lb cone; however, the $K_{cone}$ values would still closely agree. This suggests that a single $K_{cone}$ value can be used for the two states of sand and for clays having approximately the same properties as the sandy clay utilized in Poor's[16] investigation.

The projectile tests with the 94 lb, 10 in. radius sphere yielded $K_{sphere}$ values of approximately 1.0 for dry and saturated sands in dense states (Table No. 14, p. 110). Whereas, $K_{sphere}$ values for the 64 and 128 lb (average of 96 lbs), 10 in. radius spheres in sandy clay were approximately 0.8 (Table No. 11, p. 101). The higher $K_{sphere}$ value for the sand tests may possibly have been caused by the confining effect of the projectile shape.

# CHAPTER VII

## DYNAMIC AND STATIC SOIL BEHAVIOR

During the past 20 years a large amount of research has been oriented toward the determination of strain rate effects upon soil shear strength parameters. The behavior of footings subjected to impulse loadings has also received a considerable amount of attention. The purpose of this chapter is to discuss both of these topics as they relate to projectile impact.

This chapter also contains a method for predicting peak forces developed during impact on clay soils.

### RATE OF STRAIN EFFECTS ON COHESION AND ANGLE OF INTERNAL FRICTION

A number of investigators have performed laboratory studies in which they investigated the effect of rate of loading upon the basic soil strength parameters of cohesion and angle of internal friction.

Casagrande and Shannon[2] were among the first to perform a comprehensive investigation on the dynamic strength properties of clay and sand. Compression tests were conducted on both unconfined and confined samples of clay in which the time to failure ranged from 10 min. to 0.02 seconds. Five clay soils having widely varying engineering properties were utilized in the testing program. The results indicated that the fast tests (time to failure $\approx$ 0.02 sec) exhibited strengths from 1.5 to 2 times the corresponding static strengths (time to failure $\approx$ 10 min). Vacuum triaxial compression tests were performed on a dry, dense sand. The dynamic strength (0.02 sec) was approximately 10 percent greater than the 10 min static tests.

Whitman[31] has reported dynamic-static strength ratios of approximately 1.5 to 2 for various types of clay. These ratios are in agreement with those of Casagrande and Shannon, even though some of Whitman's tests were performed

at higher rates of loading (time to failure ≈ 0.002 sec). Tests were also performed on samples of uniform Ottawa Sand and a well-graded sand. The sands were tested in dry, moist, and saturated states. The dry and moist sands exhibited increases in strength of 10 to 15 percent. The results of tests on saturated samples were inconclusive.

Schimming and Saxe[21] tested clays and sands in a direct shear type of apparatus. Generally, the dynamic clay strength ratios ranged between 1.5 and 2.0; however, values as high as 4 were noted. The time to failure was in the 0-5 millisecond range. Failure envelopes (shear stress versus normal stress) were determined from dynamic and static shear tests on soils possessing cohesion and internal friction. These plots indicated that the primary difference between the dynamic and static envelopes was the value of the cohesion. The dynamic cohesion values were approximately twice the static values, while the internal friction values remained essentially the same.

Olson and Parola[14] have studied the influence of the time to failure on the compressive strength of clay. The clay was compacted at various moisture contents ranging from 6.5 percent, relatively dry, to 18 percent which represents complete saturation. The samples were tested at confining pressures of 100 and 1000 psi. The dynamic strengths (time to failure of 0.006 sec) ranged from 1.2 to 1.6 times the corresponding strengths at times to failure of 60 seconds. It should be noted that the use of tests having times to failure of 60 sec as a reference for strength increases was arbitrary. Higher strength ratios would have been obtained, if tests having greater time to failure values had been utilized. The variation of moisture content and confining pressure did not yield any clear effect upon the strength increase as the time to failure decreased.

Summary of Rate of Strain Effects

The investigations discussed above have shown the dynamic compressive strengths of clay to generally be 1.5 to 2 times the corresponding static strengths. The dynamic compressive strength of sands as discussed above was found to be approximately 10 percent greater than the corresponding static strength. It should be noted that the dynamic results on sand and clay were obtained from tests in which the time to failure was in the range of 0.002 to 1 sec. While the static values resulted from test durations of 40 sec and greater.

LATERAL INERTIA EFFECT

Research at Massachusetts Institute of Technology[31] has shown that as the time to failure decreases below 0.002 sec two factors significantly influence the results. The first is a wave propogation phenomena, which produce non-uniform stresses. The second factor is referred to as "lateral inertia effect". As a soil sample is compressed, lateral strains must take place before failure can occur. In rapid tests inertia delays the development of lateral strains which permits the soil to develop, for an extremely short period of time, stresses which greatly exceed the true peak resistance.

Some impact tests were performed at Massachusetts Institute of Technology[31] in which short-duration loads were applied to a 2 in. dia, 32 in. long horizontal column of sand. The loads were applied by a 50 lb ram which was capable of being given a striking velocity of approximately 8 fps. The stress-time history at the impact end of the sample was characterized by a steep rise in stress and then a rapid decrease to a constant stress level. Pressure transducers at the reaction end indicated a maximum stress which was approximately equal to the constant stress level at the impact end. The

development of the spike portion of the stress-time curve is attributed to lateral inertial effects and the actual stress which is propogated through the sample is measured at the reaction end. A detailed discussion and explanation of the lateral inertia effect has been given by Whitman[32].

Penetrometer tests on sands by Womack and Cox[33] were characterized by a curve similar to that obtained at the impact end of the sand column. It seems highly possible that the lateral inertia effect concept explains the spike portion of the penetrometer curves. Womack's tests also showed that the ratio of spike force to the ensuing average force in the plateau was much less for saturated sands and non-existent for clay. The absence of the spike force for impact on clay may be due to the viscous nature of clay as opposed to the discrete particle behavior of dry sands. Saturated sands, under rapid loading, also tend to behave somewhat like a dense viscous fluid and this may explain the decrease in the spike force value (Table No. 15 p. 118).

## METHOD FOR PREDICTING PEAK IMPACT FORCES ON CLAY

The cone tests on sandy clay, yielded dynamic-static force ratios ranging between 0.75 and 1.6; whereas, an average ratio of 2.75 was obtained for the spherical segment tests on Montopolis Silt[18]. The limited number of penetrometer tests[33] yielded an average value of 2.25. The sandy clay and Montopolis Silt have approximately the same static strength properties ($c \approx 700$ psf, $\phi \approx 30$ degrees), while Del Rio Clay[33] has a cohesion value of approximately 700 psf and an average angle of internal friction of 4 degrees.

The magnitude of the dynamic-static force ratios correspond closely to the cohesion ratio values obtained from dynamic and static laboratory shear tests. The close agreement suggests that impact forces may possibly be estimated by applying the conventional Terzaghi[26] theory of bearing capacity.

Equation 32 expresses the static ultimate bearing capacity of a circular footing on the surface of a purely cohesive soil ($\phi = 0$).

$$F_{ult} = 7.4 \pi R^2 c \tag{32}$$

Where,

$F_{ult}$ = Ultimate bearing capacity,

R = Radius of footing,

c = Cohesion.

An estimate of the peak dynamic force experienced during impact can be obtained by using Eq. 32 in which the cohesion parameter (c) has been determined from dynamic compression tests.

Since apparatus necessary for the determination of dynamic cohesive strengths of soils is not readily available, a more practical approach would be to determine the static value of the cohesion parameter. This value could then be multiplied by a factor of 2, or so, to yield an approximation of the dynamic value. It should be noted that Eq. 32 is valid only for purely cohesive soils and therefore cannot be applied to soils which exhibit an angle of internal friction. However, equations for the prediction of the ultimate bearing capacity of soils exhibiting both c and $\phi$ have been derived by Terzaghi[26].

Summary of Peak Impact Force Prediction Method

The above method is very approximate and a great deal of judgment should be exercised in the interpretation of the values. It should be recognized that Eq. 32 is valid only for a circular footing where the contact area does not vary during penetration. It should also be kept in mind that the dynamic-static force ratios for the impact tests were developed on the basis of comparison of forces at equal penetrations. The use of Eq. 32 assumes that the penetration

necessary for the development of the ultimate bearing capacity has been achieved, which may or may not be the case.

Projectiles such as cones and spherical segments have increasing contact areas as the depth of penetration increases. When cones and segments of spheres are loaded statically the force-penetration curve does not have an ultimate force value, rather the force continues to increase as the contact area increases. Therefore, it is necessary to be able to predict the penetration of these projectiles under impact conditions before an appropriate static force can be estimated. Iliya and Reese[8] and Ghazzaly and Cox[4] have presented methods whereby static force-penetration curves for cones and spherical segments may be predicted. The prediction of projectile penetrations; however, is much more difficult and a high degree of judgment is necessary.

Once again, it should be emphasized that this method is very approximate and extreme caution and judgment should be exercised in interpreting the values. A better estimate of the peak force value experienced during impact could be obtained by performing a static load test with the projectile and then impacting the projectile on the same soil. The static load test would yield a static force-penetration curve and the impact test would yield the projectile penetration under impact conditions. The static force corresponding to the projectile penetration under impact conditions could then be multiplied by 2 to yield an estimate of the peak impact force. Although this approach is more accurate than the previously given method, it is more costly and time consuming.

## FAILURE MODES BENEATH DYNAMICALLY LOADED FOOTINGS

The solution to static bearing capacity problems involves the assumption of a failure mode. The strength parameters ($\phi$, c) are then assumed to be developed along the failure surfaces. These assumptions permit the

calculation of the ultimate bearing capacity. The solution to dynamic bearing capacity problems also requires that the type of failure mode be known. The purpose of this section is to review the types of failure modes various investigators observed beneath dynamically loaded footings.

Failure Modes in Sand

During the progress of this investigation dynamic-static force ratios were determined for tests on cohesionless material. The ratio values were extremely high and in many cases exceeded 100. It is evident from the high ratio values that the angle of internal friction ($\phi$) has a relatively minor influence upon the forces developed during impact. The high ratio values indicate that possibly the failure modes for static and impact loadings on sand are different.

In reference to small scale footing tests on sand, a number of investigations have been conducted to determine if the failure mode resulting from dynamic loading is similar to that resulting from static loading. The footings were placed at or near the sand surface and the dynamic loads were usually applied by a pneumatic-hydraulic apparatus or by dropping weights from various heights.

Selig and McKee[22] found that the failure modes differed. The dynamic tests resulted in a punching type of shear failure, rather than the classical general shear type failure. The punching shear failure is confined to an area which is primarily located beneath the footing. Whereas, the general shear failure involves a much larger volume of soil which extends both downward and horizontally from the perimeter of the footing. A general shear failure for a strip footing is shown in Fig. 17 on p. 51.

Cunny and Sloan[3] observed punching shear modes of failure for dynamically loaded footings, while Shenkman and McKee[23] observed general shear failures for footings under dynamic loads.

The results are somewhat confusing, in that Shenkman and McKee have observed general shear failures and the others have found punching shear types of failures for dynamically loaded footings. Heller[6] has examined the data obtained by many investigators, including those cited above, and has concluded that a general shear failure results when the footing accelerations are less than 13 g's. If footing accelerations above 13 g's are experienced, the inertial restraint of the soil surrounding the footing is so great that the soil is forced to fail in a punching mode.

Failure Modes in Clay

Jackson and Hadala[9] performed some static and dynamic load tests on small-scale footings resting on clay. Visual observations indicated the static and dynamic failure modes were significantly different. In the dynamic tests there appeared to be a slight heave of the soil surface around the footing. However, the soil surface around the statically loaded footing experienced large upward movements and cracks developed from the four corners of the footing and extended outward. The slight heave around the dynamically loaded footing is characteristic of punching modes of failure.

Summary of Failure Modes

The experimental evidence referred to in this section clearly indicates a significant difference between the failure modes developed during static and dynamic loading of surface footings on both sand and clay. Heller[6] has suggested that general shear failure modes may be assumed for

surface footings on dense sand which have accelerations below the 13 g level. It should be noted that in almost every impact test performed in this investigation, the accelerations were significantly above the 13 g level. The impact program at The University of Texas has shown that the peak accelerations experienced during surface impact of projectiles generally will be at least 2 or 3 times greater than the 13 g level. Therefore, it is reasonable to assume that static failure mechanisms are not applicable for projectile impact.

# CHAPTER VIII

# CONCLUSIONS AND RECOMMENDATIONS

The purpose of this chapter is to present a brief summary of the pertinent information obtained during the past five years from the soil dynamics research program at The University of Texas.

The program has been oriented toward the collection of experimental data which have aided in developing concepts concerning the behavior of soil under impact loading conditions. Approximately 700 impact tests were conducted on sand, clay, and silt. In addition to the impact tests, over 200 tests were performed to define soil behavior under static loading conditions.

The projectile shapes consisted of wedges, cones, cylinders, spheres, and plates. The weights of projectiles varied from approximately 1 to 150 lbs. The use of wide ranges of soil conditions and of projectile shapes and weights has provided a wealth of information which covers a broad range of test conditions.

## CONCLUSIONS

### Modeling

1. The use of modeling techniques shows promise as a method of predicting prototype behavior of projectiles impacting on soil. Reese et al[18] and Awoshika and Cox[1] obtained good agreement with modeling techniques for relatively small ranges of scaling; however, the agreement obtained by Poor et al[16] was not nearly as good. Each investigator made no attempt at modeling the soil. Thus, it must be emphasized that distortion due to the use of the same soil for model and prototype tests may become excessive for larger ranges of scaling.

Edge Effects

2. The author's results from inclined impact tests on sand using double width projectiles yielded an edge effect constant which was in good agreement with Reichmuth's[19] value. The author's results from tests on clay indicated that the edge effect constant was negative; whereas, Reichmuth's data yielded a positive value. It was concluded that Reichmuth's results indicated the true soil behavior. The edge effect constants indicate that for impact on clay the average peak soil pressure decreases as the width of the projectile increases and for impact on sand the average peak soil pressure increases as the projectile width increases. (See p. 41).

Regression Analyses

3. The method used by Reichmuth[19] to generate regression equations to describe the soil forces acting on projectiles during inclined impact shows promise. Generally, the regression equations developed by Reichmuth (pp. 53 through 61) do not predict soil forces developed during low angle impact ($\alpha < 30$ degrees) as well as for high angle tests ($\alpha \geq 30$ degrees).

Peak Impact Force Prediction

4. For a given projectile type and soil type the peak vertical acceleration was approximately a linear function of the initial vertical impact velocity. It should be noted that this statement applies only to systems restricted to vertical motion.

5. The peak vertical impact force may be represented with a reasonable degree of accuracy by the following equation:

$$F_{peak} = K \gamma M V \tag{31}$$

where,

$F_{peak}$ = Peak vertical soil force (lb),

$\gamma$ = Soil density (pcf)

M = Projectile mass (lb-sec$^2$/ft),

V = Initial impact velocity (fps),

K = Empirical coefficient (ft$^3$/(lb-sec)).

The value of K depends upon the physical properties of the projectile(mass, striking surface configuration) and the soil conditions.

6. Values of the empirical coefficient K for cones, spheres, cylinders, and plates have been determined for tests on the following sands, silt, and clays:

(1) Ottawa Sand,

(2) Colorado River Sand,

(3) Montopolis Silt,

(4) Del Rio Clay,

(5) Sandy Clay in a terrace of the Colorado River.

The sands had widely varying engineering properties (grain size, angularity, angle of internal friction). However, the K values are approximately the same for similar states of sand density, and for a given type of projectile. The close agreement indicates that possibly the most important impact property of sand is the state of density.

The tests on cohesive soils also show that the K values are of similar magnitude for tests with projectiles having similar shapes and weights. A summary of K values for particular soil and projectile conditions is given on pp. 129.

7. The shape of the projectile striking surface has a distinct influence on the peak soil forces developed during impact. The effect is much more pronounced in sands than in clays. The peak soil forces developed with cones were used as a base of reference and the $K/K_{cone}$ column in Table No. 11 on p. 106 illustrates the influence of the surface shape of the projectile upon the value of K. As can be seen from the table, the $K/K_{cone}$ values for the 10 in. dia plate tests on nearly saturated sandy clay and dry Colorado River Sand were 3.59 and 15.80, respectively.

8. The ratio of peak cone accelerations experienced during impact on soil to those developed during impact on water ranged between 4 and 13. This is in good agreement with the values Reichmuth obtained from the analysis of prototype impact data. Ratio values for peak accelerations experienced during soil and water impact are given in Table No. 9 on p. 96.

Final Penetration Prediction

9. Final penetrations of conical and flat plate projectiles were approximately linear functions of the initial impact velocities for tests on clay and saturated sand. It should also be noted that this statement applies only to systems restricted to vertical motion.

10. The soil response (force-penetration curve) to impact of conical projectiles was idealized to a triangular force-penetration relationship. Work-energy principles were utilized to develop the following equation for final cone penetration:

$$Z_f = \frac{V^2}{(K_{cone} \gamma V - 2g)} \qquad (30)$$

where,

$Z_f$ = Final cone penetration (in.),

$K_{cone}$ = Empirical coefficient ($ft^3/(lb\text{-}sec)$),

$\gamma$ = Soil density (pcf),

$V$ = Initial impact velocity (fps),

$g$ = Acceleration of gravity ($fps^2$).

The predicted penetrations agreed well with the measured values for tests in the 20 and 30 fps velocity range. The agreement was not nearly as good for tests in the 10 fps velocity range (see Table No. 7 on p. 92.

Static and Dynamic Forces

11. For cohesionless soils, there seems to be no direct relationship between the forces developed during static loading of foundation elements and the forces experienced during impact of these elements. The peak dynamic forces were in many cases several hundred times the static forces for corresponding penetrations. The largest forces were developed for impact on saturated sands. Dry sand in a dense state offered less resistance than saturated sands. Dry sand in a dense state had resistances which were generally more than twice that of dry sands in loose states (See Figs. 28 through 31).

12. For cohesive soils, the peak forces experienced during vertical impact are on the average 2 to 3 times the static strengths for corresponding penetrations.

RECOMMENDATIONS

1. It is recommended that a series of large scale tests be conducted to determine the validity of the conclusions drawn from the small scale tests.
2. If large scale impact tests are conducted, the following target material properties should be determined:
   (A) Atterburg limits,
   (B) Grain size distribution,
   (C) Specific gravity of soil particles,
   (D) Water content,
   (E) In situ density,
   (F) Stress-strain properties,
   (G) Cohesion and angle of internal friction,
   (H) Maximum and minimum void ratio (sands only),
   (I) Color and local or regional name.

   The small scale impact tests indicate that some of the above properties are not important to impact behavior; however, these properties fully describe the target material and are believed necessary since the phenomena associated with projectile impact are not clearly understood.

# APPENDIX A

## TEST NOMENCLATURE

This appendix contains a description of the test numbering and coding system, nomenclature, and sign conventions. To illustrate the coding and numbering system the following example is presented:

8-19-7-WHO3-30-0 (Taken from Table No. 1 on p. 43).

The test was performed in the 8th month on the 19th day. This was the 7th test of the day. The projectile type (WHO3) was a wedge (W), heavy (H), obtuse angle (0), of triple width (3). The angle of impact was 30 degrees and the pitch angle was 0 degrees.

# TEST NUMBERING AND CODING SYSTEM

## IDENTIFICATION SEQUENCE

DATE - TEST NO. - Projectile-Launch Angle-Pitch

## PROJECTILE CODES

### Spheres

SL - Light Sphere

SH - Heavy Sphere

### Cylinders

CYL1 - Single width (5.5 in. wide)

CYL2 - Double width (11.0 in. wide)

CYL3 - Triple width (16.5 in. wide)

### Wedges

Wxyz

W - Wedge

x = L - Light

H - Heavy

y = A - Acute (60 degree included angle)

O - Obtuse (120 degree included angle)

z = 1 - Single width (5.5 in. wide)

2 - Double width (11.0 in. wide)

3 - Triple width (16.5 in. wide)

### Cones

LC - Light Cone

HC - Heavy Cone

LAUNCH ANGLE ($\alpha$)

5 - 5 degrees

10 - 10 degrees

20 - 20 degrees

30 - 30 degrees

45 - 45 degrees

75 - 75 degrees

90 - 90 degrees

PITCH ($\theta$)

0 - Zero degrees (all of the tests in this investigation were performed at a zero degree pitch angle)

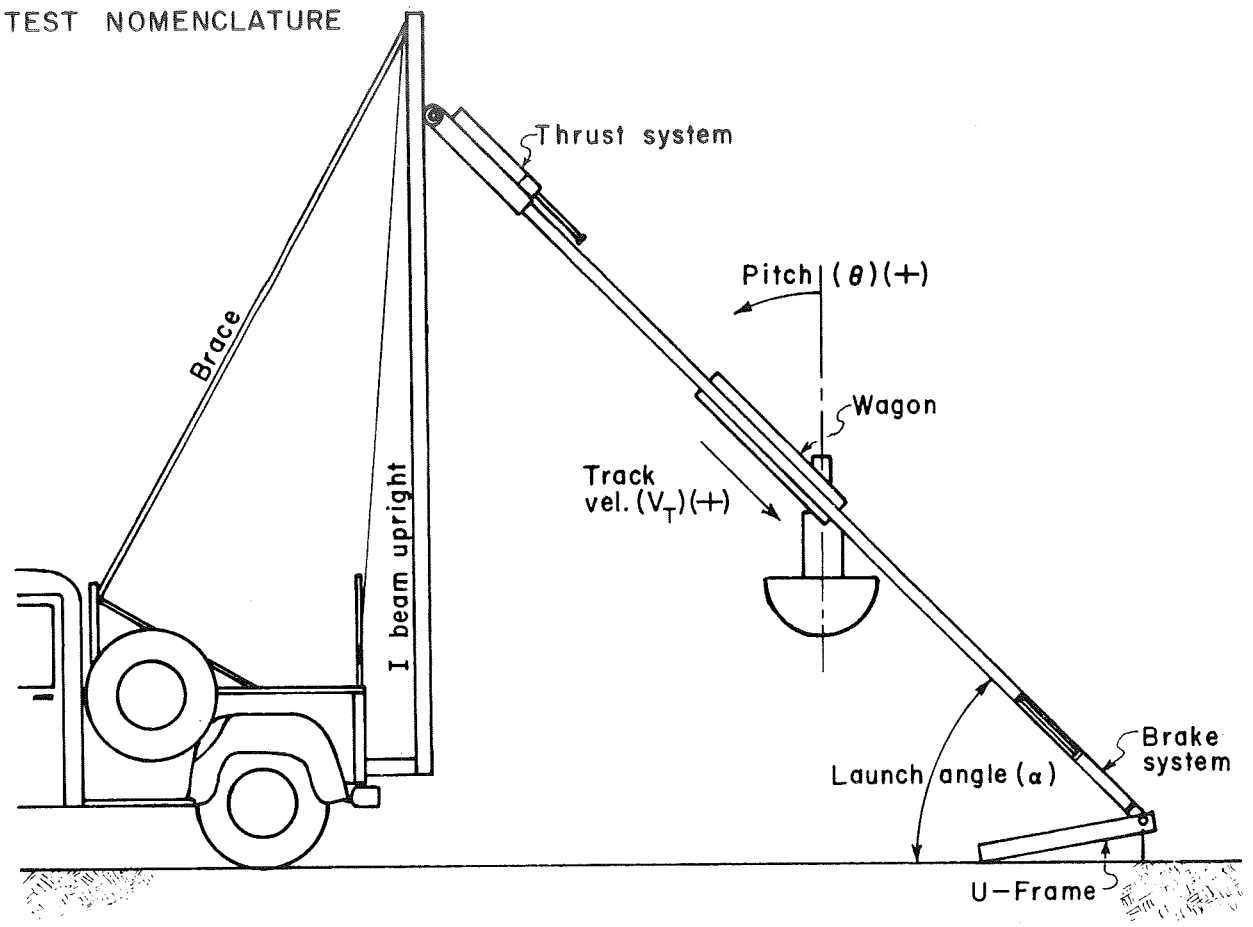


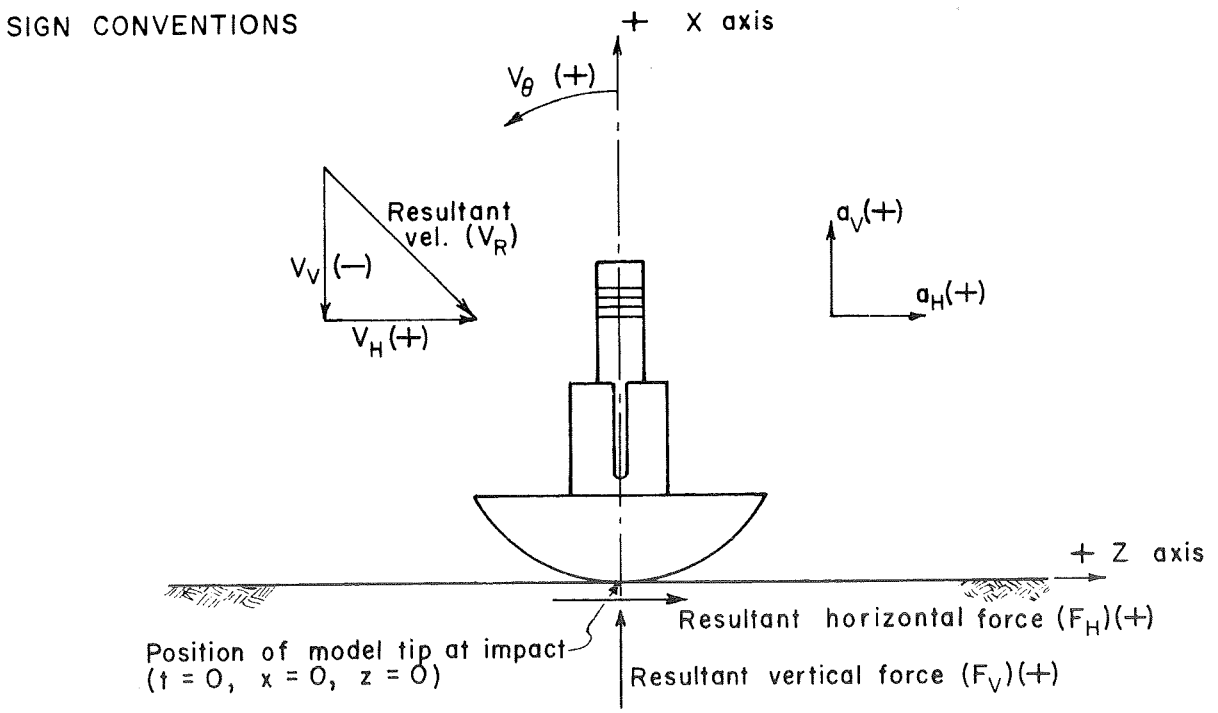


FIG. 55 TEST NOMENCLATURE AND SIGN CONVENTIONS
(AFTER REICHMUTH)

## APPENDIX B

## PROJECTILE PROPERTIES

The mass moments of inertia of the irregularly shaped projectiles were determined using the torisonal pendulum developed by Reichmuth[19]. The positions of the centers of gravity were obtained from a knife edge device, which was also developed by Reichmuth. The projectile properties are listed in Table No. 21. It should be noted that it was only necessary to determine the projectile properties for the double width projectiles (WLA2, WHA2, WHO2, and CYL2) and the conical projectiles, since the properties for the remaining projectiles listed in Table No. 21 were previously determined by Reichmuth.

TABLE NO. 21

PHYSICAL PROPERTIES OF PROJECTILES

| Projectile | C. G. to Top Accel. (ft) | C. G. to Bottom Accel. (ft) | C. G. to Axial Tip (ft) | Included Angle (degree) | Radius (ft) | Weight (Lb) | Mass (Slug) | Mass Moment of Inertia ($ft\text{-}Lb\text{-}Sec^2$) |
|---|---|---|---|---|---|---|---|---|
| WLA1 | 0.8208 | -0.1792 | 0.7117 | 60 | | 34.05 | 1.058 | 0.2163 |
| WLA2 | 0.8132 | -0.1850 | 0.7175 | 60 | | 68.59 | 2.132 | 0.4537 |
| WLA3 | 0.8142 | -0.1858 | 0.7183 | 60 | | 102.41 | 3.182 | 0.6615 |
| WHA1 | 0.9433 | -0.0567 | 0.6726 | 60 | | 44.05 | 1.369 | 0.2943 |
| WHA2 | 0.9424 | -0.0607 | 0.6758 | 60 | | 86.28 | 2.680 | 0.6007 |
| WHA3 | 0.9417 | -0.0683 | 0.6842 | 60 | | 132.28 | 4.112 | 0.8823 |
| WHO1 | 0.8950 | -0.1050 | 0.4810 | 120 | | 44.56 | 1.385 | 0.2797 |
| WHO2 | 0.8900 | -0.1101 | 0.4858 | 120 | | 87.56 | 2.721 | 0.5792 |
| WHO3 | 0.8850 | -0.1150 | 0.4910 | 120 | | 133.50 | 4.149 | 0.8602 |
| CYL1 | 0.9592 | -0.0408 | 0.4074 | | 0.833 | 50.21 | 1.562 | 0.3750 |
| CYL2 | 0.9483 | -0.0517 | 0.4183 | | 0.833 | 98.90 | 3.074 | 0.7531 |
| CYL3 | 0.9433 | -0.0567 | 0.4233 | | 0.833 | 151.66 | 4.714 | 1.0960 |
| SL | 0.8567 | -0.1433 | 0.5133 | | 0.833 | 41.31 | 1.284 | 0.2764 |
| SH | 0.8742 | -0.1258 | 0.4958 | | 0.833 | 94.04 | 2.923 | 0.4399 |
| LC* | | | | 60 | | 43.00 | 1.336 | |
| HC* | | | | 60 | | 129.50 | 4.024 | |

*The conical shaped projectiles were utilized only in vertical impact tests and it was, therefore, not necessary to determine mass moments and centers of gravity.

# APPENDIX C

## SOIL DATA

This appendix contains a description of the soils utilized in this and previous investigations at The University of Texas. Physical properties of the soils were determined using standard laboratory testing procedures. No attempt was made to determine the dynamic strength properties. The soils were classified according to the Unified System.

### Sands

Three types of sands were utilized in this investigation. Two of the sands (Colorado River Sand (1) and Colorado River Sand (2)) were obtained locally and the third sand (Ottawa Sand) was obtained from Ottawa, Illinois.

Colorado River Sand (1) was used by Reichmuth[19] in a previous investigation. This sand was also used by the author in his impact tests at low angles. Colorado River Sand (2) was used by the author in the cone impact testing phase.

#### Colorado River Sand (1)

This sand was located at the Capitol Aggregates test site. As mentioned above Reichmuth also utilized this sand; however, he chose to call the sand Capitol Aggregates (CA). It is a light brown color and has subangular particles composed basically of quartz. The sand is well-graded and classified as (SW). Figure 56 contains grain size distribution curves of the sands discussed in this Appendix. Table No. 22 contains engineering properties for each sand. The laboratory tests were conducted on the sands in an air-dry state.

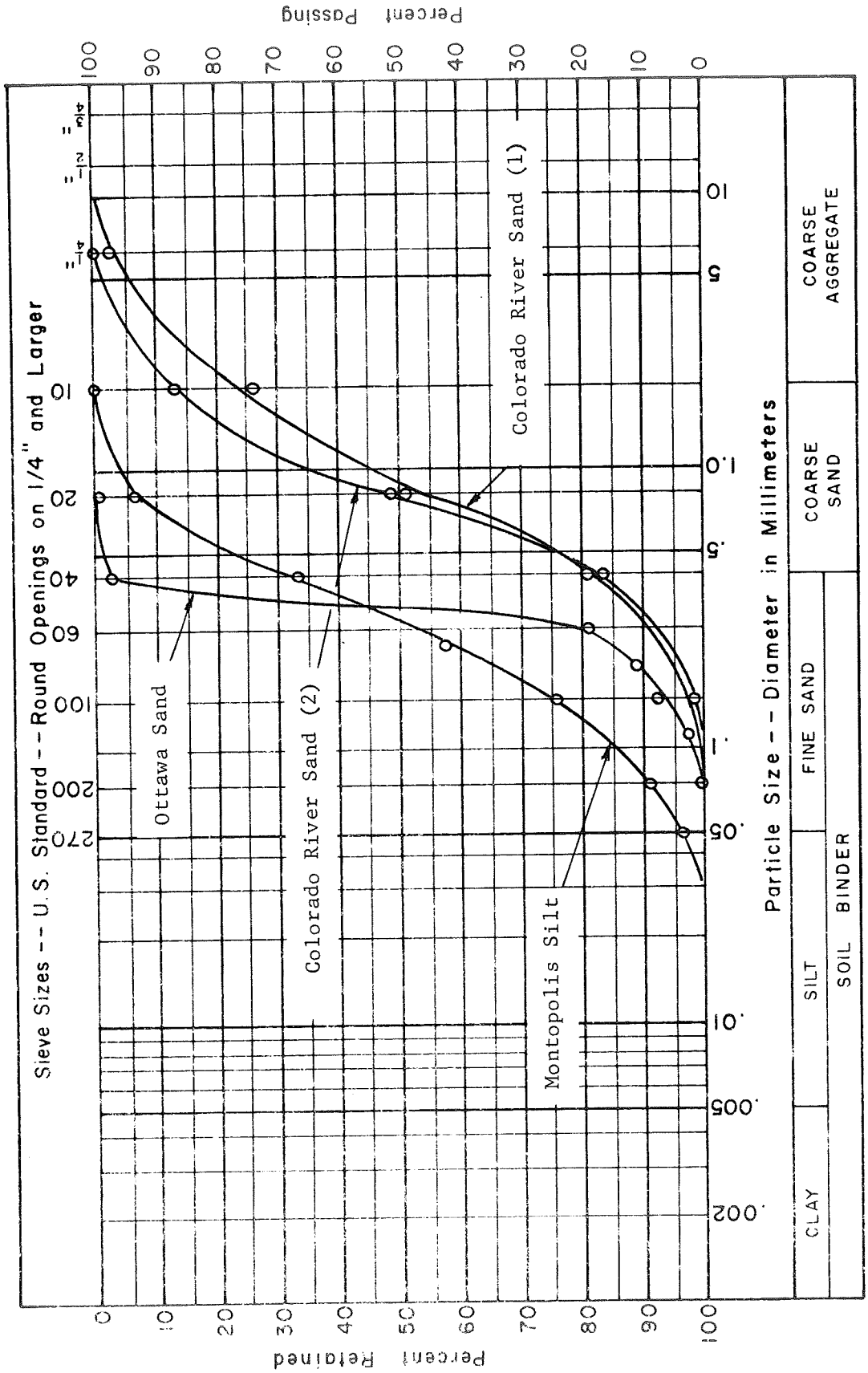


FIG. 56 MECHANICAL ANALYSES - GRAIN SIZE ACCUMULATION CURVES

TABLE NO. 22

ANGLE OF INTERNAL FRICTION VALUES FOR COLORADO RIVER SAND (1), OTTAWA SAND, AND COLORADO RIVER SAND (2)

| Soil Type | Angle of Internal Friction $\phi$ (degrees) | Dry Density $\gamma$ (pcf) | Maximum Void Ratio | Minimum Void Ratio | Maximum Density $\gamma$ (pcf) | Minimum Density $\gamma$ (pcf) | Specific Gravity |
|---|---|---|---|---|---|---|---|
| Colorado River Sand (1) | 25.5<br>35.0<br>43.5 | 105.2<br>110.0<br>115.3 | 0.57 | 0.41 | 116.6 | 105.0 | 2.64 |
| Ottawa Sand | 18.5<br>27.0<br>33.5 | 92.0<br>104.0<br>108.9 | 0.81 | 0.49 | 110.9 | 91.2 | 2.65 |
| Colorado River Sand (2) | 24.5<br>34.5<br>44.5 | 98.3<br>106.6<br>110.5 | 0.68 | 0.45 | 113.8 | 98.0 | 2.64 |

TABLE NO. 23

INDEX AND STRENGTH PROPERTIES FOR DEL RIO CLAY, SANDY CLAY, AND MONTOPOLIS SILT

| Soil Type | Liquid Limit LL (%) | Plastic Limit PL (%) | Plastic Index LL-PL (%) | Classification | Cohesion c (psi) | Angle of Internal Friction $\phi$ (degrees) |
|---|---|---|---|---|---|---|
| Del Rio Clay | 60 | 34 | 26 | CH | 5.0 | 4 |
| Sandy Clay | 29 | 19 | 10 | CL | 5.8 | 27 |
| Montopolis Silt | 19.4 | 14.3 | 5.1 | ML | 4.2 | 32 |

Colorado River Sand (2)

This sand was placed in a test pit at Balcones Research Center for use in the author's impact tests with cones. As can be seen from Fig. 56 this sand does not contain as large a coarse fraction as Colorado River Sand (1); however, there are no other basic differences in the Colorado River Sands.

Ottawa Sand

Ottawa Sand is a grayish white color and has rounded particles composed of silica. It is uniformly graded and classified as (SP).

## Clays

Impact tests were conducted on two clay soils in an in situ condition. The strength and index properties for each clay are listed in Table No. 23.

Del Rio Clay

This clay is located at Balcones Research Center. The top soil was removed for several inches to allow the tests to be conducted on a level, vegetation free surface. It has a color ranging from dark brown to black and has been highly preconsolidated by desiccation. The clay contains calcareous nodules up to 1/4 in. in size with traces of sand and tiny grass roots. The approximate in situ density ($\gamma$) and moisture content (w) were 115 pcf and 33 percent, respectively. The specific gravity is 2.68 and the percent saturation was approximately 97.

Sandy Clay Located in a Terrace of the Colorado River

This soil was utilized by Poor[16] in his impact tests at the Austin Country Club. It is light brown in color and has been highly preconsolidated by desiccation. The average in situ density and moisture content were 129.3 pcf and 16.7 percent, respectively. The percent saturation was assumed

to be 90 since no measurements were made at the time of testing. This assumption was based upon discussions with a technician who was present at the time of testing.

Silts

Reese[18] utilized Montopolis Silt in his impact studies. It is reddish brown in color and contains a substantial amount of sand. Figure 56 contains a grain size distribution curve for Montopolis Silt. It was compacted at a moisture content (w) of 10 percent to a density of 125 pcf. Strength and index properties are listed in Table No. 23.

## APPENDIX D

## PREDICTION OF SOIL PRESSURES AT LOW ANGLE IMPACT

This appendix contains listings of low angle impact data for wedges, cylinders, and spheres. The low angle ($\alpha < 30$ degrees) impact data were taken from the output of Program IMPACT. It should be noted that the data were taken only from the rising portions of the force-penetration curves since Reichmuth's[19] prediction equations were empirically derived from high angle ($\alpha \geq 30$ degrees) impact data which were taken from the rising force-penetration curves. The data were substituted into Eqs. 20, 21, 24, 25, 26, and 27 for a comparison between the soil pressures calculated from these equations and the measured values. Comparisons between measured and calculated values are given. All of the calculations were performed on a high speed digital computer.

## Wedge

The data listed on pp. 162 through 165 were taken from output of Program IMPACT. Reichmuth[19] thoroughly discussed Program IMPACT and presented a program listing along with a guide for input data. The data were then input into a program, developed by the author, which calculated soil pressures using the regression equations generated by Reichmuth[19]. The input data were defined in the following manner.

Example from p. 162, lines 1 and 2.

| DATE | TEST NO. |
|---|---|
| 3-9-67 | No. 7 |

WLA1-10-0-OS = Light Wedge (WL) having an included angle of 60 degrees (A) and a width of 5.5 inches (1). The launch angle was 10 degrees and the pitch angle was 0 degrees. The target material was Ottawa Sand (OS).

Vertical penetration of tip ($D_t$) = 0.49 in.

Resultant Tangential Force ($F_T$) = 5.72 lb

Resultant Normal Force ($F_N$) = 35.63 lb

Horizontal Velocity at Center of Gravity (VHG) = 15.45 fps

Vertical Velocity of Center of Gravity (VVG) = 5.47 fps

Rotational Velocity ($V_\theta$) = 0.34 rps

Angle between leading face of the wedge and the soil surface ($\beta$) = 59.95 degrees

Distance between tip and center of gravity (DCG) = 0.7117 ft

Soil density ($\gamma$) = 98.31 pcf

The input data were manipulated to provide input for Eqs. 20 and 21.

$$(F_P)_N = 3.54(-V_\theta)^{0.44}(-V_V)^{0.28}V_H{}^{0.43}\gamma^{0.70}(-D_t)^{-0.04}\beta^{-1.19} \tag{20}$$

$$(F_P)_T = 3.10\beta^{0.89}(F_P)_N{}^{0.04} - 100 \tag{21}$$

The variables appearing in the above equations are defined on p. 53.

The necessary input data manipulations are listed as follows:

$$V_H = VHG - (V_\theta)(DCG)COS(PITCH) \quad , \tag{33}$$

$$V_V = VVG - (V_\theta)(DCG)Sin(PITCH) \quad , \tag{34}$$

$$PITCH = 90 \text{ degrees} - [0.5(\text{Included Wedge Angle}) + \beta] \ . \tag{35}$$

Examination of Eq. 20 shows that $V_\theta$, $V_V$, and $D_t$ each contain negative signs. It was necessary for Reichmuth[19] to place negative signs on these variables since according to his sign convention (see p. 150) these variables were negative. Thus, when the negative variables were substituted into Eq. 20 they became positive. It should be noted that the input data listed on pp. 162 through 165 do not contain minus quantities. The minus signs were deleted from the $V_\theta$, $V_V$, and $D_t$ variables and it, therefore, is not necessary to keep the minus signs which appear in Eq. 20.

The resultant normal and tangential forces were reduced to plane strain pressures by the following equations.

$$(F_P)_N = \frac{F_N}{D_P\left(\frac{K_e}{D_P} + 1.00\right)} \tag{36}$$

$$(F_P)_T = \frac{F_T}{D_p \left( \frac{K_e}{D_P} + 1.00 \right)} \qquad (37)$$

$D_p$ was 5.5 in. and 11.0 in. for the single and double width projectiles, respectively. A value of -1.41 was used for $K_e$ since all of the low angle tests were performed on sands.

The values from Eqs. 36 and 37 are listed under the heading "MEASURED" and the values from Eqs. 20 and 21 are listed under the heading "CALCULATED" on pp. 166 through 169.

The percent deviations were calculated by Eq. 38.

$$\text{Percent Deviation} = \left( \frac{\text{Measured - Calculated}}{\text{Measured}} \right) 100 \qquad (38)$$

INPUT DATA

```
3-9-67   NO. 7  WLA1-10-0-0S
 .49      5.72    35.63    15.45     5.47      .34     59.95     .7117    98.31
3-9-67   NO. 7  WLA1-10-0-0S
1.41     17.35    66.15    14.90     4.98     2.14     58.95     .7117    98.31
3-9-67   NO. 7  WLA1-10-0-0S
2.30     24.55   104.70    13.82     3.91     5.02     55.52     .7117    98.31
3-9-67   NO. 11 WLA1-10-0-0S
 .43      7.92    54.52    32.14     6.97      .36     59.97     .7117    86.01
3-9-67   NO. 11 WLA1-10-0-0S
 .99     19.11   124.90    31.67     6.60     2.06     59.53     .7117    86.01
3-9-67   NO. 11 WLA1-10-0-0S
1.50     32.47   155.30    30.98     5.98     4.46     58.27     .7117    86.01
3-9-67   NO. 8  WLA1-10-0-0S
 .67      9.01    69.93    15.48     5.98      .72     59.88     .7117   100.74
3-9-67   NO. 8  WLA1-10-0-0S
1.15     19.38   117.10    15.01     5.59     2.18     59.33     .7117   100.74
3-9-67   NO. 8  WLA1-10-0-0S
1.71     32.71   157.60    14.08     4.77     4.79     57.52     .7117   100.74
3-9-67   NO. 12 WLA1-10-0-0S
 .44     39.72   113.20    33.08     7.22      .71     59.94     .7117   100.74
3-9-67   NO. 12 WLA1-10-0-0S
 .86     54.77   232.20    32.46     6.58     3.02     59.43     .7117   100.74
3-9-67   NO. 12 WLA1-10-0-0S
1.23     40.59   264.60    31.56     5.75     5.93     58.14     .7117   100.74
3-9-67   NO. 13  WLA1-10-0-0S
 .46     31.07   159.30    31.77     7.29      .95     59.91     .7117    98.88
3-9-67   NO. 13  WLA1-10-0-0S
 .88     61.68   272.40    30.96     6.55     3.62     59.27     .7117    98.88
3-9-67   NO. 13  WLA1-10-0-0S
1.25     57.10   293.00    29.92     5.57     6.96     57.72     .7117    98.88
3-14-67  NO. 3   WL01-10-0-0S
 .26      -.67   121.80    14.71     6.65      .16     29.99     .5240   102.75
3-14-67  NO. 3   WL01-10-0-0S
 .59      4.84   327.70    14.26     5.82     1.11     29.85     .5240   102.75
3-14-67  NO. 3   WL01-10-0-0S
 .80     15.26   364.90    13.76     4.88     1.99     29.56     .5240   102.75
3-14-67  NO. 2   WL01-10-0-0S
 .40    -12.27    59.63    15.15     6.05      .22     29.98     .5240    92.91
3-14-67  NO. 2   WL01-10-0-0S
 .97    -10.14   120.70    14.78     5.58      .96     29.70     .5240    92.91
```

| | | | | | | | | |
|---|---|---|---|---|---|---|---|---|
| -14-67 | NO. 2 | WL01-10-0-0S | | | | | | |
| .45 | -8.85 | 212.70 | 14.03 | 4.39 | 1.77 | 29.05 | .5240 | 92.91 |
| -2-67 | NO. 3 | WLA1-20-0-0S | | | | | | |
| .42 | 25.18 | 87.37 | 17.01 | 7.31 | .32 | 59.97 | .7117 | 96.00 |
| -2-67 | NO. 3 | WLA1-20-0-0S | | | | | | |
| .20 | 83.54 | 246.80 | 15.87 | 6.12 | 3.36 | 59.09 | .7117 | 96.00 |
| -2-67 | NO. 3 | WLA1-20-0-0S | | | | | | |
| .77 | 112.40 | 283.40 | 14.26 | 4.02 | 7.97 | 56.01 | .7117 | 96.00 |
| -2-67 | NO. 4 | WLA1-20-0-0S | | | | | | |
| .57 | 22.26 | 64.89 | 17.03 | 8.82 | .37 | 59.96 | .7117 | 92.40 |
| -2-67 | NO. 4 | WLA1-20-0-0S | | | | | | |
| .82 | 56.62 | 150.70 | 16.02 | 7.64 | 3.72 | 58.63 | .7117 | 92.40 |
| -2-67 | NO. 4 | WLA1-20-0-0S | | | | | | |
| .02 | 64.32 | 183.60 | 14.39 | 5.39 | 8.42 | 53.01 | .7117 | 92.40 |
| -2-67 | NO. 6 | WLA1-20-0-0S | | | | | | |
| .45 | 17.14 | 49.99 | 17.22 | 8.85 | .20 | 59.99 | .7117 | 98.35 |
| -2-67 | NO. 6 | WLA1-20-0-0S | | | | | | |
| .10 | 58.81 | 174.30 | 16.75 | 8.30 | 1.96 | 59.64 | .7117 | 98.35 |
| -2-67 | NO. 6 | WLA1-20-0-0S | | | | | | |
| .87 | 98.07 | 239.30 | 15.61 | 6.84 | 5.54 | 57.85 | .7117 | 98.35 |
| -2-67 | NO. 9 | WLA1-20-0-0S | | | | | | |
| .89 | 20.24 | 120.30 | 28.37 | 12.51 | .77 | 59.92 | .7117 | 92.44 |
| -2-67 | NO. 9 | WLA1-20-0-0S | | | | | | |
| .74 | 99.27 | 366.90 | 27.41 | 11.67 | 3.76 | 59.24 | .7117 | 92.44 |
| -2-67 | NO. 9 | WLA1-20-0-0S | | | | | | |
| .70 | 136.60 | 452.70 | 25.23 | 9.18 | 10.42 | 56.08 | .7117 | 92.44 |
| -9-67 | NO. 3 | WHA2-10-0-0S | | | | | | |
| .26 | 35.64 | 98.68 | 13.17 | 4.41 | .18 | 59.98 | .6758 | 98.50 |
| -9-67 | NO. 3 | WHA2-10-0-0S | | | | | | |
| .75 | 40.49 | 257.20 | 12.67 | 3.90 | 1.51 | 59.56 | .6758 | 98.50 |
| -9-67 | NO. 3 | WHA2-10-0-0S | | | | | | |
| .07 | 21.73 | 291.90 | 12.08 | 3.46 | 2.94 | 58.63 | .6758 | 98.50 |
| -9-67 | NO. 5 | WHA2-10-0-0S | | | | | | |
| .33 | -1.40 | 135.90 | 27.33 | 4.40 | .45 | 59.95 | .6758 | 87.75 |
| -9-67 | NO. 5 | WHA2-10-0-0S | | | | | | |
| .80 | 25.08 | 312.20 | 26.68 | 3.99 | 2.26 | 59.28 | .6758 | 87.75 |
| -9-67 | NO. 5 | WHA2-10-0-0S | | | | | | |
| .19 | 33.68 | 392.60 | 25.66 | 3.20 | 4.90 | 57.41 | .6758 | 87.75 |
| -9-67 | NO. 6 | WHA2-10-0-0S | | | | | | |
| .37 | 28.80 | 191.50 | 26.72 | 5.66 | .39 | 59.96 | .6758 | 99.20 |
| -9-67 | NO. 6 | WHA2-10-0-0S | | | | | | |

| | | | | | | | | |
|---|---|---|---|---|---|---|---|---|
| .73 | 72.63 | 413.00 | 26.24 | 5.25 | 1.81 | 59.64 | .6758 | 99.20 |
| 3-9-67 | NO. 6 | WHA2-10-0-0S | | | | | | |
| 1.15 | 77.11 | 486.60 | 25.28 | 4.42 | 4.35 | 58.38 | .6758 | 99.20 |
| 3-9-67 | NO. 4 | WHA2-10-0-0S | | | | | | |
| .68 | 6.72 | 43.83 | 13.12 | 4.60 | .22 | 59.96 | .6758 | 89.00 |
| 3-9-67 | NO. 4 | WHA2-10-0-0S | | | | | | |
| 1.70 | 17.52 | 114.00 | 12.59 | 4.18 | 1.42 | 59.08 | .6758 | 89.00 |
| 3-9-67 | NO. 4 | WHA2-10-0-0S | | | | | | |
| 2.58 | 38.41 | 194.80 | 11.72 | 3.42 | 2.70 | 56.81 | .6758 | 89.00 |
| 3-7-67 | NO. 2 | WHA2-20-0-0S | | | | | | |
| 1.18 | 73.29 | 185.60 | 19.02 | 7.93 | .91 | 59.79 | .6758 | 98.31 |
| 3-7-67 | NO. 2 | WHA2-20-0-0S | | | | | | |
| 2.27 | 77.65 | 337.00 | 18.15 | 7.01 | 3.31 | 58.35 | .6758 | 98.31 |
| 3-7-67 | NO. 2 | WHA2-20-0-0S | | | | | | |
| 3.52 | 70.61 | 490.00 | 16.06 | 4.83 | 7.50 | 52.71 | .6758 | 98.31 |
| 3-7-67 | NO. 6 | WHA2-20-0-0S | | | | | | |
| 1.22 | 25.19 | 146.50 | 18.80 | 9.16 | .50 | 59.90 | .6758 | 87.20 |
| 3-7-67 | NO. 6 | WHA2-20-0-0S | | | | | | |
| 2.40 | 61.35 | 321.00 | 18.06 | 8.54 | 2.25 | 59.10 | .6758 | 87.20 |
| 3-7-67 | NO. 6 | WHA2-20-0-0S | | | | | | |
| 3.75 | 78.89 | 401.10 | 16.53 | 7.09 | 5.25 | 55.93 | .6758 | 87.20 |
| 3-7-67 | NO. 7 | WHA2-20-0-0S | | | | | | |
| .69 | 124.20 | 298.10 | 19.40 | 7.68 | .63 | 59.92 | .6758 | 99.73 |
| 3-7-67 | NO. 7 | WHA2-20-0-0S | | | | | | |
| 1.02 | 133.20 | 416.80 | 19.05 | 7.27 | 1.73 | 59.69 | .6758 | 99.73 |
| 3-7-67 | NO. 7 | WHA2-20-0-0S | | | | | | |
| 1.62 | 102.40 | 474.90 | 18.16 | 6.35 | 4.23 | 58.41 | .6758 | 99.73 |
| 3-7-67 | NO. 8 | WHA2-20-0-0S | | | | | | |
| .63 | 84.61 | 140.30 | 25.75 | 10.78 | .41 | 59.94 | .6758 | 91.04 |
| 3-7-67 | NO. 8 | WHA2-20-0-0S | | | | | | |
| 1.26 | 163.90 | 407.10 | 25.47 | 10.35 | 1.65 | 59.69 | .6758 | 91.04 |
| 3-7-67 | NO. 8 | WHA2-20-0-0S | | | | | | |
| 2.36 | 288.30 | 760.50 | 23.98 | 8.48 | 5.95 | 57.62 | .6758 | 91.04 |
| 3-7-67 | NO. 9 | WHA2-20-0-0S | | | | | | |
| .51 | 86.84 | 256.20 | 25.68 | 8.60 | .64 | 59.94 | .6758 | 97.49 |
| 3-7-67 | NO. 9 | WHA2-20-0-0S | | | | | | |
| 1.22 | 139.00 | 617.40 | 24.76 | 7.69 | 4.11 | 59.02 | .6758 | 97.49 |
| 3-7-67 | NO. 9 | WHA2-20-0-0S | | | | | | |
| 2.12 | 259.60 | 736.20 | 22.59 | 5.21 | 11.57 | 53.48 | .6758 | 97.49 |
| 3-9-67 | NO. 2 | WHA2-10-0-0S | | | | | | |
| .25 | 34.87 | 116.70 | 13.23 | 4.26 | .24 | 59.97 | .6758 | 99.84 |

3-9-67 NO. 2 WHA2-10-0-0S
.73 47.13 270.80 12.64 3.70 1.96 59.42 .6758 99.84

3-9-67 NO. 2 WHA2-10-0-0S
.93 40.44 295.80 12.23 3.37 3.05 58.70 .6758 99.84

3-23-67 NO. 2 WH02-10-0-0S
.48 -18.61 75.18 11.69 4.84 .16 29.97 .4858 95.50

3-23-67 NO. 2 WH02-10-0-0S
1.08 -30.31 210.40 11.33 4.40 .69 29.72 .4858 95.50

3-23-67 NO. 2 WH02-10-0-0S
1.80 -23.64 380.40 10.28 2.89 1.14 28.79 .4858 95.50

3-23-67 NO. 3 WH02-10-0-0S
.37 4.75 347.80 12.61 5.49 .27 29.97 .4858 100.33

3-23-67 NO. 3 WH02-10-0-0S
.54 3.22 537.10 12.39 5.09 .66 29.90 .4858 100.33

3-23-67 NO. 3 WH02-10-0-0S
.84 2.84 702.60 11.78 3.95 1.52 29.56 .4858 100.33

3-23-67 NO. 4 WH02-10-0-0S
.55 -47.95 145.10 21.63 5.32 .25 29.96 .4858 87.50

3-23-67 NO. 4 WH02-10-0-0S
1.22 -86.95 374.50 20.80 4.46 1.28 29.49 .4858 87.50

3-23-67 NO. 4 WH02-10-0-0S
1.73 -94.30 495.90 19.57 3.07 1.94 28.40 .4858 87.50

3-23-67 NO. 5 WH02-10-0-0S
.39 -48.38 270.60 22.05 5.70 .24 29.98 .4858 102.62

3-23-67 NO. 5 WH02-10-0-0S
.75 -99.99 878.40 21.20 4.66 1.54 29.72 .4858 102.62

3-23-67 NO. 5 WH02-10-0-0S
.90 -83.79 921.20 20.64 3.87 2.27 29.41 .4858 102.62

3-23-67 NO. 6 WH02-10-0-0S
.64 -46.90 220.00 26.52 6.13 .49 29.92 .4858 89.14

3-23-67 NO. 6 WH02-10-0-0S
1.40 -71.21 524.90 25.59 4.90 1.58 29.26 .4858 89.14

3-23-67 NO. 6 WH02-10-0-0S
1.94 -75.36 583.40 24.27 3.19 2.18 28.00 .4858 89.14

3-23-67 NO. 7 WH02-10-0-0S
.20 7.06 256.40 26.97 4.75 .16 29.99 .4858 99.98

3-23-67 NO. 7 WH02-10-0-0S
.47 -16.78 575.00 26.56 4.09 .86 29.85 .4858 99.98

3-23-67 NO. 7 WH02-10-0-0S
.68 -47.46 686.70 25.90 3.05 1.66 29.48 .4858 99.98

| IDENTIFICATION | TANGENTIAL PRESSURE MEASURED $(F_P)_T$/IN. | TANGENTIAL PRESSURE CALCULATED $(F_P)_T$/IN. | PERCENT DEVIATION |
|---|---|---|---|
| 3-9/7-WLA1-10-0-0S | 1.39 | 29.14 | -2001.21 |
| 3-9/7-WLA1-10-0-0S | 4.21 | 30.41 | -622.90 |
| 3-9/7-WLA1-10-0-0S | 5.95 | 25.92 | -335.56 |
| 3-9/11-WLA1-10-0-0S | 1.92 | 31.39 | -1534.99 |
| 3-9/11-WLA1-10-0-0S | 4.63 | 34.93 | -654.08 |
| 3-9/11-WLA1-10-0-0S | 7.87 | 33.55 | -326.20 |
| 3-9/8-WLA1-10-0-0S | 2.18 | 32.53 | -1389.27 |
| 3-9/8-WLA1-10-0-0S | 4.70 | 34.18 | -627.60 |
| 3-9/8-WLA1-10-0-0S | 7.93 | 32.09 | -304.74 |
| 3-9/12-WLA1-10-0-0S | 9.63 | 35.23 | -265.85 |
| 3-9/12-WLA1-10-0-0S | 13.28 | 38.12 | -187.07 |
| 3-9/12-WLA1-10-0-0S | 9.84 | 36.15 | -267.42 |
| 3-9/13-WLA1-10-0-0S | 7.53 | 37.03 | -391.59 |
| 3-9/13-WLA1-10-0-0S | 14.95 | 38.67 | -158.60 |
| 3-9/13-WLA1-10-0-0S | 13.84 | 35.83 | -158.85 |
| 3-14/3-WLO1-10-0-0S | -.16 | -26.77 | -16382.50 |
| 3-14/3-WLO1-10-0-0S | 1.17 | -24.13 | 2156.62 |
| 3-14/3-WLO1-10-0-0S | 3.70 | -24.46 | 761.28 |
| 3-14/2-WLO1-10-0-0S | -2.97 | -28.86 | -870.07 |
| 3-14/2-WLO1-10-0-0S | -2.46 | -27.43 | -1015.80 |
| 3-14/2-WLO1-10-0-0S | -2.15 | -27.21 | -1168.39 |
| 3-2/3-WLA1-20-0-0S | 6.10 | 33.89 | -455.25 |
| 3-2/3-WLA1-20-0-0S | 20.25 | 37.75 | -86.39 |
| 3-2/3-WLA1-20-0-0S | 27.25 | 32.07 | -17.69 |
| 3-2/4-WLA1-20-0-0S | 5.40 | 32.29 | -498.38 |
| 3-2/4-WLA1-20-0-0S | 13.73 | 34.12 | -148.58 |
| 3-2/4-WLA1-20-0-0S | 15.59 | 23.59 | -51.28 |
| 3-2/6-WLA1-20-0-0S | 4.16 | 30.98 | -645.47 |
| 3-2/6-WLA1-20-0-0S | 14.26 | 36.97 | -159.31 |
| 3-2/6-WLA1-20-0-0S | 23.77 | 35.01 | -47.24 |
| 3-2/9-WLA1-20-0-0S | 4.91 | 35.52 | -623.86 |
| 3-2/9-WLA1-20-0-0S | 24.07 | 40.27 | -67.32 |
| 3-2/9-WLA1-20-0-0S | 33.12 | 34.72 | -4.83 |
| 3-2/3-WHA2-10-0-0S | 3.72 | 30.11 | -708.59 |
| 3-2/3-WHA2-10-0-0S | 4.23 | 34.35 | -711.94 |
| 3-9/3-WHA2-10-0-0S | 2.27 | 33.16 | -1360.21 |
| 3-9/5-WHA2-10-0-0S | -.15 | 31.73 | 21790.07 |
| 3-9/5-WHA2-10-0-0S | 2.62 | 34.83 | -1229.09 |
| 3-9/5-WHA2-10-0-0S | 3.52 | 32.25 | -816.25 |
| 3-9/6-WHA2-10-0-0S | 3.01 | 33.57 | -1015.50 |
| 3-9/6-WHA2-10-0-0S | 7.59 | 37.09 | -388.65 |
| 3-9/6-WHA2-10-0-0S | 8.06 | 35.39 | -339.22 |
| 3-9/4-WHA2-10-0-0S | .70 | 25.92 | -3591.21 |
| 3-9/4-WHA2-10-0-0S | 1.83 | 29.12 | -1490.47 |
| 3-9/4-WHA2-10-0-0S | 4.01 | 27.39 | -582.52 |
| 3-7/2-WHA2-20-0-0S | 7.66 | 33.07 | -331.77 |
| 3-7/2-WHA2-20-0-0S | 8.11 | 33.35 | -311.08 |
| 3-7/2-WHA2-20-0-0S | 7.38 | 23.66 | -220.63 |

| IDENTIFICATION | TANGENTIAL PRESSURE MEASURED $(F_P)_T$/IN. | TANGENTIAL PRESSURE CALCULATED $(F_P)_T$/IN. | PERCENT DEVIATION |
|---|---|---|---|
| 3-7/6-WHA2-20-0-OS | 2.63 | 32.03 | -1116.81 |
| 3-7/6-WHA2-20-0-OS | 6.41 | 34.62 | -439.98 |
| 3-7/6-WHA2-20-0-OS | 8.24 | 29.32 | -255.65 |
| 3-7/7-WHA2-20-0-OS | 12.98 | 35.87 | -176.43 |
| 3-7/7-WHA2-20-0-OS | 13.92 | 37.24 | -167.54 |
| 3-7/7-WHA2-20-0-OS | 10.70 | 35.32 | -230.09 |
| 3-7/8-WHA2-20-0-OS | 8.84 | 31.88 | -260.57 |
| 3-7/8-WHA2-20-0-OS | 17.13 | 37.11 | -116.68 |
| 3-7/8-WHA2-20-0-OS | 30.13 | 36.23 | -20.27 |
| 3-7/9-WHA2-20-0-OS | 9.07 | 35.09 | -286.75 |
| 3-7/9-WHA2-20-0-OS | 14.52 | 38.02 | -161.75 |
| 3-7/9-WHA2-20-0-OS | 27.13 | 27.32 | -.71 |
| 3-9/2-WHA2-10-0-OS | 3.64 | 30.97 | -749.94 |
| 3-9/2-WHA2-10-0-OS | 4.92 | 34.35 | -597.45 |
| 3-9/2-WHA2-10-0-OS | 4.23 | 33.37 | -689.65 |
| 3-23/2-WHO2-10-0-OS | -1.94 | -30.59 | -1473.07 |
| 3-23/2-WHO2-10-0-OS | -3.17 | -28.21 | -790.71 |
| 3-23/2-WHO2-10-0-OS | -2.47 | -28.54 | -1055.38 |
| 3-23/3-WHO2-10-0-OS | .50 | -26.20 | 5379.53 |
| 3-23/3-WHO2-10-0-OS | .34 | -25.07 | 7549.95 |
| 3-23/3-WHO2-10-0-OS | .30 | -25.02 | 8532.49 |
| 3-23/4-WHO2-10-0-OS | -5.01 | -28.76 | -474.03 |
| 3-23/4-WHO2-10-0-OS | -9.09 | -27.04 | -197.63 |
| 3-23/4-WHO2-10-0-OS | -9.85 | -28.65 | -190.75 |
| 3-23/5-WHO2-10-0-OS | -5.06 | -26.92 | -432.50 |
| 3-23/5-WHO2-10-0-OS | -10.45 | -23.99 | -129.58 |
| 3-23/5-WHO2-10-0-OS | -8.76 | -24.55 | -180.39 |
| 3-23/6-WHO2-10-0-OS | -4.90 | -27.65 | -464.24 |
| 3-23/6-WHO2-10-0-OS | -7.44 | -26.56 | -256.99 |
| 3-23/6-WHO2-10-0-OS | -7.87 | -29.09 | -269.36 |
| 3-23/7-WHO2-10-0-OS | .74 | -27.06 | 3767.47 |
| 3-23/7-WHO2-10-0-OS | -1.75 | -24.97 | -1324.32 |
| 3-23/7-WHO2-10-0-OS | -4.96 | -25.27 | -409.62 |

| IDENTIFICATION | NORMAL PRESSURE MEASURED $(F_P)_N$/IN. | NORMAL PRESSURE CALCULATED $(F_P)_N$/IN. | PERCENT DEVIATION |
|---|---|---|---|
| 3-9/7-WLA1-10-0-OS | 8.64 | 2.24 | 74.12 |
| 3-9/7-WLA1-10-0-OS | 16.04 | 4.52 | 71.81 |
| 3-9/7-WLA1-10-0-OS | 25.38 | 5.67 | 77.67 |
| 3-9/11-WLA1-10-0-OS | 13.22 | 3.09 | 76.64 |
| 3-9/11-WLA1-10-0-OS | 30.28 | 6.24 | 79.39 |
| 3-9/11-WLA1-10-0-OS | 37.65 | 8.27 | 78.04 |
| 3-9/8-WLA1-10-0-OS | 16.95 | 3.19 | 81.21 |
| 3-9/8-WLA1-10-0-OS | 28.39 | 4.81 | 83.07 |
| 3-9/8-WLA1-10-0-OS | 38.21 | 5.96 | 84.39 |
| 3-9/12-WLA1-10-0-OS | 27.44 | 4.74 | 82.74 |
| 3-9/12-WLA1-10-0-OS | 56.29 | 8.31 | 85.23 |
| 3-9/12-WLA1-10-0-OS | 64.15 | 10.37 | 83.84 |
| 3-9/13-WLA1-10-0-OS | 38.62 | 5.22 | 86.49 |
| 3-9/13-WLA1-10-0-OS | 66.04 | 8.64 | 86.91 |
| 3-9/13-WLA1-10-0-OS | 71.03 | 10.52 | 85.20 |
| 3-14/3-WLO1-10-0-OS | 29.53 | 4.02 | 86.38 |
| 3-14/3-WLO1-10-0-OS | 79.44 | 8.59 | 89.19 |
| 3-14/3-WLO1-10-0-OS | 88.46 | 10.23 | 88.43 |
| 3-14/2-WLO1-10-0-OS | 14.46 | 4.18 | 71.11 |
| 3-14/2-WLO1-10-0-OS | 29.26 | 7.45 | 74.53 |
| 3-14/2-WLO1-10-0-OS | 51.56 | 8.87 | 82.79 |
| 3-2/3-WLA1-20-0-OS | 21.18 | 2.44 | 88.50 |
| 3-2/3-WLA1-20-0-OS | 59.83 | 5.78 | 90.33 |
| 3-2/3-WLA1-20-0-OS | 68.70 | 6.33 | 90.79 |
| 3-2/4-WLA1-20-0-OS | 15.73 | 2.63 | 83.27 |
| 3-2/4-WLA1-20-0-OS | 36.53 | 6.20 | 83.04 |
| 3-2/4-WLA1-20-0-OS | 44.51 | 7.02 | 84.22 |
| 3-2/6-WLA1-20-0-OS | 12.12 | 2.14 | 82.38 |
| 3-2/6-WLA1-20-0-OS | 42.25 | 5.31 | 87.43 |
| 3-2/6-WLA1-20-0-OS | 58.01 | 7.13 | 87.71 |
| 3-2/9-WLA1-20-0-OS | 29.16 | 4.90 | 83.20 |
| 3-2/9-WLA1-20-0-OS | 88.95 | 9.05 | 89.82 |
| 3-2/9-WLA1-20-0-OS | 109.75 | 11.89 | 89.16 |
| 3-2/3-WHA2-10-0-OS | 10.31 | 1.53 | 85.17 |
| 3-2/3-WHA2-10-0-OS | 26.88 | 3.47 | 87.11 |
| 3-9/3-WHA2-10-0-OS | 30.50 | 4.23 | 86.13 |
| 3-9/5-WHA2-10-0-OS | 14.20 | 2.86 | 79.87 |
| 3-9/5-WHA2-10-0-OS | 32.62 | 5.36 | 83.57 |
| 3-9/5-WHA2-10-0-OS | 41.02 | 6.80 | 83.42 |
| 3-9/6-WHA2-10-0-OS | 20.01 | 3.10 | 84.53 |
| 3-9/6-WHA2-10-0-OS | 43.16 | 5.69 | 86.81 |
| 3-9/6-WHA2-10-0-OS | 50.85 | 7.62 | 85.02 |
| 3-9/4-WHA2-10-0-OS | 4.59 | 1.51 | 67.00 |
| 3-9/4-WHA2-10-0-OS | 11.91 | 3.13 | 73.76 |
| 3-9/4-WHA2-10-0-OS | 20.36 | 3.74 | 81.62 |
| 3-7/2-WHA2-20-0-OS | 19.39 | 4.02 | 79.26 |
| 3-7/2-WHA2-20-0-OS | 35.21 | 6.44 | 81.70 |

| IDENTIFICATION | NORMAL PRESSURE MEASURED $(F_P)_N$/IN. | NORMAL PRESSURE CALCULATED $(F_P)_N$/IN. | PERCENT DEVIATION |
|---|---|---|---|
| 3-7/2-WHA2-20-0-OS | 51.20 | 7.59 | 85.17 |
| 3-7/6-WHA2-20-0-OS | 15.31 | 2.95 | 80.72 |
| 3-7/6-WHA2-20-0-OS | 33.54 | 5.29 | 84.23 |
| 3-7/6-WHA2-20-0-OS | 41.91 | 6.83 | 83.71 |
| 3-7/7-WHA2-20-0-OS | 31.15 | 3.54 | 88.65 |
| 3-7/7-WHA2-20-0-OS | 43.55 | 5.23 | 87.98 |
| 3-7/7-WHA2-20-0-OS | 49.62 | 7.01 | 85.87 |
| 3-7/8-WHA2-20-0-OS | 14.66 | 3.44 | 76.55 |
| 3-7/8-WHA2-20-0-OS | 42.54 | 6.01 | 85.86 |
| 3-7/8-WHA2-20-0-OS | 79.47 | 9.29 | 88.31 |
| 3-7/9-WHA2-20-0-OS | 26.77 | 4.14 | 84.54 |
| 3-7/9-WHA2-20-0-OS | 64.51 | 8.41 | 86.96 |
| 3-7/9-WHA2-20-0-OS | 76.93 | 10.50 | 86.36 |
| 3-9/2-WHA2-10-0-OS | 12.19 | 1.74 | 85.74 |
| 3-9/2-WHA2-10-0-OS | 28.30 | 3.83 | 86.46 |
| 3-9/2-WHA2-10-0-OS | 30.91 | 4.34 | 85.96 |
| 3-23/2-WHO2-10-0-OS | 7.86 | 3.09 | 60.66 |
| 3-23/2-WHO2-10-0-OS | 21.99 | 5.47 | 75.14 |
| 3-23/2-WHO2-10-0-OS | 39.75 | 5.84 | 85.30 |
| 3-23/3-WHO2-10-0-OS | 36.34 | 4.35 | 88.04 |
| 3-23/3-WHO2-10-0-OS | 56.12 | 6.14 | 89.06 |
| 3-23/3-WHO2-10-0-OS | 73.42 | 7.91 | 89.22 |
| 3-23/4-WHO2-10-0-OS | 15.16 | 4.71 | 68.93 |
| 3-23/4-WHO2-10-0-OS | 39.13 | 8.83 | 77.43 |
| 3-23/4-WHO2-10-0-OS | 51.82 | 9.50 | 81.67 |
| 3-23/5-WHO2-10-0-OS | 28.28 | 5.39 | 80.95 |
| 3-23/5-WHO2-10-0-OS | 91.79 | 11.02 | 88.00 |
| 3-23/5-WHO2-10-0-OS | 96.26 | 12.22 | 87.30 |
| 3-23/6-WHO2-10-0-OS | 22.99 | 7.24 | 68.48 |
| 3-23/6-WHO2-10-0-OS | 54.85 | 11.05 | 79.85 |
| 3-23/6-WHO2-10-0-OS | 60.96 | 11.38 | 81.33 |
| 3-23/7-WHO2-10-0-OS | 26.79 | 4.71 | 82.41 |
| 3-23/7-WHO2-10-0-OS | 60.08 | 9.09 | 84.86 |
| 3-23/7-WHO2-10-0-OS | 71.76 | 10.99 | 84.69 |

## Cylinder

The presentation of the cylinder data is similar to that of the wedge. The input data are defined in the following manner.

Example from p. 172, lines 1 and 2.

Line 1 gives the test identification system, which is explained in Appendix A.

The variables appearing in line 2 are:

Horizontal velocity at center of gravity $(V_H)$ = 19.21 fps,

Vertical velocity at center of gravity $(V_V)$ = 5.16 fps,

Rotational velocity $(V_\theta)$ = 0.30 rps,

Vertical penetration of tip $(D_T)$ = 0.10 in.,

Resultant horizontal force at center of gravity $(F_H)$ = 38.20 lb,

Resultant vertical force at center of gravity (FV) = 116.20 lb,

Soil density $(\gamma)$ = 100.00 pcf.

Equations 24 and 25 were used to calculate resultant plane strain pressures at the center of gravity.

$$(F_P)_H = 0.0859(-D_t)^{0.36} V_H^{0.27} (-V_V)^{0.58} (-V_\theta)^{0.39} \gamma^{1.09} \qquad (24)$$

$$(F_P)_V = 0.131(-D_t)^{0.37} V_H^{-0.13} (-V_V)^{1.01} (-V_\theta)^{0.24} \gamma^{1.25} \qquad (25)$$

The variables appearing in Eqs. 24 and 25 are devined on p. 60. It should be noted that the minus signs on $D_t$, $V_V$, and $V_\theta$ are not necessary since the input data have all been listed as positive.

The resultant horizontal and vertical forces were reduced to plane strain pressures by Eqs. 39 and 40.

$$(F_P)_H = \frac{F_H}{D_P \left(\frac{K_e}{D_P} + 1.00\right)} \tag{39}$$

$$(F_P)_V = \frac{F_V}{D_P \left(\frac{K_e}{D_P} + 1.00\right)} \tag{40}$$

Equations 39 and 40 were used to calculate the values listed under the "MEASURED" column on pp. 175 and 176. Equations 24 and 25 were used to calculate the values listed under the "CALCULATED" column on pp. 175 and 176. The percent deviation values were calculated using Eq. 38.

INPUT DATA

| | | | | | | |
|---|---|---|---|---|---|---|
| 3-16-67 | NO. 5 | CYL1 -10-0-0S | | | | |
| 19.210 | 5.160 | .030 | .100 | 38.200 | 116.200 | 100.000 |
| 3-16-67 | NO. 5 | CYL1 -10-0-0S | | | | |
| 19.110 | 4.940 | .160 | .200 | 176.400 | 319.300 | 100.000 |
| 3-16-67 | NO. 5 | CYL1 -10-0-0S | | | | |
| 18.870 | 4.490 | .450 | .300 | 261.800 | 520.400 | 100.000 |
| 3-16-67 | NO. 5 | CYL1 -10-0-0S | | | | |
| 18.540 | 3.880 | .770 | .380 | 326.300 | 561.600 | 100.000 |
| 3-16-67 | NO. 3 | CYL1 -10-0-0S | | | | |
| 29.020 | 7.310 | .050 | .240 | 30.600 | 79.400 | 84.500 |
| 3-16-67 | NO. 3 | CYL1 -10-0-0S | | | | |
| 28.940 | 7.120 | .190 | .470 | 62.900 | 133.300 | 84.500 |
| 3-16-67 | NO. 3 | CYL1 -10-0-0S | | | | |
| 28.600 | 6.530 | .430 | 1.130 | 69.800 | 116.000 | 84.500 |
| 3-16-67 | NO. 3 | CYL1 -10-0-0S | | | | |
| 28.230 | 5.920 | .410 | 1.730 | 66.700 | 114.700 | 84.500 |
| 3-16-67 | NO. 3 | CYL1 -10-0-0S | | | | |
| 27.520 | 4.830 | .300 | 2.430 | 128.200 | 195.600 | 84.500 |
| 3-16-67 | NO. 6 | CYL1 -10-0-0S | | | | |
| 12.810 | 5.370 | .040 | .110 | 48.000 | 173.900 | 102.600 |
| 3-16-67 | NO. 6 | CYL1 -10-0-0S | | | | |
| 12.700 | 5.030 | .210 | .210 | 203.300 | 533.100 | 102.600 |
| 3-16-67 | NO. 6 | CYL1 -10-0-0S | | | | |
| 12.420 | 4.380 | .580 | .310 | 296.900 | 571.600 | 102.600 |
| 3-23-67 | NO. 10 | CYL2-10-0-0S | | | | |
| 21.050 | 5.650 | .180 | .460 | 145.400 | 271.100 | 92.900 |
| 3-23-67 | NO. 10 | CYL2-10-0-0S | | | | |
| 20.800 | 5.230 | .400 | .740 | 184.000 | 299.800 | 92.900 |
| 3-23-67 | NO. 8 | CYL2-10-0-0S | | | | |
| 26.580 | 6.080 | .260 | .340 | 391.100 | 1027.000 | 101.000 |
| 3-23-67 | NO. 8 | CYL2-10-0-0S | | | | |
| 26.240 | 5.170 | .870 | .490 | 453.800 | 1354.000 | 101.000 |
| 3-23-67 | NO. 8 | CYL2-10-0-0S | | | | |
| 25.860 | 4.120 | 1.630 | .610 | 545.800 | 1358.000 | 101.000 |
| 3-23-67 | NO. 9 | CYL2-10-0-0S | | | | |
| 26.060 | 7.200 | .110 | .250 | 157.300 | 294.600 | 89.300 |
| 3-23-67 | NO. 9 | CYL2-10-0-0S | | | | |
| 25.660 | 6.520 | .560 | .710 | 216.300 | 349.400 | 89.300 |
| 3-23-67 | NO. 9 | CYL2-10-0-0S | | | | |
| 25.200 | 5.840 | .730 | 1.130 | 315.400 | 443.300 | 89.300 |

| | | | | | | |
|---|---|---|---|---|---|---|
| 3-23-67 | NO. 9 | CYL2-10-0-0S | | | | |
| 24.550 | 5.000 | .780 | 1.490 | 347.900 | 470.600 | 89.300 |
| 3-23-67 | NO. 14 | CYL2-10-0-0S | | | | |
| 12.570 | 5.760 | .070 | .190 | 79.100 | 167.600 | 87.800 |
| 3-23-67 | NO. 14 | CYL2-10-0-0S | | | | |
| 12.380 | 5.390 | .390 | .540 | 102.800 | 214.400 | 87.800 |
| 3-23-67 | NO. 13 | CYL2-10-0-0S | | | | |
| 12.750 | 6.400 | .150 | .170 | 223.700 | 607.500 | 99.800 |
| 3-23-67 | NO. 13 | CYL2-10-0-0S | | | | |
| 12.500 | 5.800 | .560 | .330 | 478.100 | 1046.000 | 99.800 |
| 3-23-67 | NO. 13 | CYL2-10-0-0S | | | | |
| 12.140 | 4.990 | 1.080 | .470 | 481.900 | 1165.000 | 99.800 |
| 3-23-67 | NO. 12 | CYL2-10-0-0S | | | | |
| 20.740 | 4.040 | .340 | .170 | 513.300 | 963.500 | 100.000 |
| 3-23-67 | NO. 12 | CYL2-10-0-0S | | | | |
| 20.430 | 3.480 | .760 | .250 | 552.300 | 1030.000 | 100.000 |
| 3-23-67 | NO. 12 | CYL2-10-0-0S | | | | |
| 20.120 | 2.920 | 1.120 | .310 | 548.500 | 1064.000 | 100.000 |
| 3-23-67 | NO. 12 | CYL2-10-0-0S | | | | |
| 19.860 | 2.380 | 1.360 | .360 | 582.100 | 1065.000 | 100.000 |
| 3-30-67 | NO. 4 | CYL2-5-0-0S | | | | |
| 19.080 | 9.540 | .090 | .260 | 160.400 | 149.400 | 101.300 |
| 3-30-67 | NO. 4 | CYL2-5-0-0S | | | | |
| 18.860 | 9.180 | .400 | .520 | 507.100 | 1085.000 | 101.300 |
| 3-30-67 | NO. 4 | CYL2-5-0-0S | | | | |
| 18.400 | 8.190 | .990 | .750 | 704.400 | 1414.000 | 101.300 |
| 3-30-67 | NO. 2 | CYL2-5-0-0S | | | | |
| 20.810 | 8.740 | .100 | .540 | 100.200 | 117.700 | 90.000 |
| 3-30-67 | NO. 2 | CYL2-5-0-0S | | | | |
| 20.560 | 8.360 | .340 | 1.060 | 201.800 | 387.200 | 90.000 |
| 3-30-67 | NO. 5 | CYL2-5-0-0S | | | | |
| 19.170 | 9.920 | .100 | .270 | 152.600 | 1077.000 | 99.700 |
| 3-30-67 | NO. 5 | CYL2-5-0-0S | | | | |
| 18.930 | 8.910 | .440 | .530 | 612.300 | 1413.000 | 99.700 |
| 3-30-67 | NO. 6 | CYL2-5-0-0S | | | | |
| 19.110 | 9.240 | .060 | .250 | 96.700 | 212.500 | 98.900 |
| 3-30-67 | NO. 6 | CYL2-5-0-0S | | | | |
| 18.890 | 8.780 | .360 | .500 | 663.400 | 1328.000 | 98.900 |
| 3-30-67 | NO. 6 | CYL2-5-0-0S | | | | |
| 18.310 | 7.620 | 1.060 | .720 | 749.700 | 1525.000 | 98.900 |
| 3-31-67 | NO. 3 | CYL2-5-0-CA | | | | |

| | | | | | | |
|---|---|---|---|---|---|---|
| 21.010 | 6.940 | .130 | .440 | 125.500 | 125.200 | 99.000 |
| 3-31-67 | NO. 3 | CYL2-5-0-CA | | | | |
| 20.710 | 6.570 | .500 | .870 | 220.200 | 336.100 | 99.000 |
| 3-31-67 | NO. 3 | CYL2-5-0-CA | | | | |
| 20.290 | 5.920 | .780 | 1.260 | 261.100 | 379.200 | 99.000 |
| 3-31-67 | NO. 3 | CYL2-5-0-CA | | | | |
| 19.930 | 5.240 | .700 | 1.610 | 132.500 | 382.300 | 99.000 |

| IDENTIFICATION | MEASURED $(F_P)_H$/IN. | CALCULATED $(F_P)_H$/IN. | PERCENT DEVIATION |
|---|---|---|---|
| 3-16/5-CYL1-10-0-OS | 9.26 | 8.32 | 10.19 |
| 3-16/5-CYL1-10-0-OS | 42.76 | 19.97 | 53.31 |
| 3-16/5-CYL1-10-0-OS | 63.47 | 32.60 | 48.63 |
| 3-16/5-CYL1-10-0-OS | 79.10 | 40.03 | 49.40 |
| 3-16/3-CYL1-10-0-OS | 7.42 | 15.84 | -113.52 |
| 3-16/3-CYL1-10-0-OS | 15.25 | 33.42 | -119.16 |
| 3-16/3-CYL1-10-0-OS | 16.92 | 59.74 | -253.07 |
| 3-16/3-CYL1-10-0-OS | 16.17 | 64.36 | -298.00 |
| 3-16/3-CYL1-10-0-OS | 31.08 | 56.83 | -82.85 |
| 3-16/6-CYL1-10-0-OS | 11.64 | 9.08 | 21.94 |
| 3-16/6-CYL1-10-0-OS | 49.28 | 21.03 | 57.34 |
| 3-16/6-CYL1-10-0-OS | 71.98 | 32.98 | 54.18 |
| 3-23/10-CYL2-10-0-OS | 15.19 | 28.89 | -90.15 |
| 3-23/10-CYL2-10-0-OS | 19.23 | 44.61 | -132.04 |
| 3-23/8-CYL2-10-0-OS | 40.87 | 36.41 | 10.92 |
| 3-23/8-CYL2-10-0-OS | 47.42 | 60.33 | -27.23 |
| 3-23/8-CYL2-10-0-OS | 57.03 | 72.82 | -27.67 |
| 3-23/9-CYL2-10-0-OS | 16.44 | 22.36 | -36.01 |
| 3-23/9-CYL2-10-0-OS | 22.60 | 57.73 | -155.44 |
| 3-23/9-CYL2-10-0-OS | 32.96 | 70.65 | -114.37 |
| 3-23/9-CYL2-10-0-OS | 36.35 | 72.68 | -99.92 |
| 3-23/14-CYL2-10-0-OS | 8.27 | 12.03 | -45.53 |
| 3-23/14-CYL2-10-0-OS | 10.74 | 32.80 | -205.39 |
| 3-23/13-CYL2-10-0-OS | 23.38 | 19.09 | 18.34 |
| 3-23/13-CYL2-10-0-OS | 49.96 | 38.06 | 23.82 |
| 3-23/13-CYL2-10-0-OS | 50.36 | 50.78 | -.84 |
| 3-23/12-CYL2-10-0-OS | 53.64 | 22.99 | 57.14 |
| 3-23/12-CYL2-10-0-OS | 57.71 | 33.01 | 42.80 |
| 3-23/12-CYL2-10-0-OS | 57.31 | 37.32 | 34.88 |
| 3-23/12-CYL2-10-0-OS | 60.83 | 37.60 | 38.18 |
| 3-30/4-CYL2-5-0-OS | 16.76 | 26.03 | -55.33 |
| 3-30/4-CYL2-5-0-OS | 52.99 | 58.28 | -9.99 |
| 3-30/4-CYL2-5-0-OS | 73.61 | 88.03 | -19.60 |
| 3-30/2-CYL2-5-0-OS | 10.47 | 30.18 | -188.29 |
| 3-30/2-CYL2-5-0-OS | 21.09 | 60.24 | -185.69 |
| 3-30/5-CYL2-5-0-OS | 15.95 | 27.68 | -73.58 |
| 3-30/5-CYL2-5-0-OS | 63.98 | 58.89 | 7.96 |
| 3-30/6-CYL2-5-0-OS | 10.10 | 20.97 | -107.50 |
| 3-30/6-CYL2-5-0-OS | 69.32 | 52.38 | 24.44 |
| 3-30/6-CYL2-5-0-OS | 78.34 | 83.12 | -6.11 |
| 3-31/3-CYL2-5-0-CA | 13.11 | 30.22 | -130.48 |
| 3-31/3-CYL2-5-0-CA | 23.01 | 63.04 | -173.98 |
| 3-31/3-CYL2-5-0-CA | 27.28 | 80.20 | -193.97 |
| 3-31/3-CYL2-5-0-CA | 13.85 | 77.87 | -462.41 |

| IDENTIFICATION | MEASURED $(F_P)_V$/IN. | CALCULATED $(F_P)_V$/IN. | PERCENT DEVIATION |
|---|---|---|---|
| 3-16/5-CYL1-10-0-OS | 28.17 | 27.21 | 3.41 |
| 3-16/5-CYL1-10-0-OS | 77.41 | 50.32 | 34.99 |
| 3-16/5-CYL1-10-0-OS | 126.16 | 68.15 | 45.98 |
| 3-16/5-CYL1-10-0-OS | 136.15 | 73.18 | 46.25 |
| 3-16/3-CYL1-10-0-OS | 19.25 | 46.42 | -141.15 |
| 3-16/3-CYL1-10-0-OS | 32.32 | 79.88 | -147.19 |
| 3-16/3-CYL1-10-0-OS | 28.12 | 123.38 | -338.75 |
| 3-16/3-CYL1-10-0-OS | 27.81 | 129.55 | -365.91 |
| 3-16/3-CYL1-10-0-OS | 47.42 | 111.34 | -134.81 |
| 3-16/6-CYL1-10-0-OS | 42.16 | 34.22 | 18.82 |
| 3-16/6-CYL1-10-0-OS | 129.24 | 60.65 | 53.07 |
| 3-16/6-CYL1-10-0-OS | 138.57 | 77.96 | 43.74 |
| 3-23/10-CYL2-10-0-OS | 28.33 | 72.66 | -156.51 |
| 3-23/10-CYL2-10-0-OS | 31.33 | 97.22 | -210.33 |
| 3-23/8-CYL2-10-0-OS | 107.31 | 82.31 | 23.30 |
| 3-23/8-CYL2-10-0-OS | 141.48 | 107.08 | 24.32 |
| 3-23/8-CYL2-10-0-OS | 141.90 | 107.54 | 24.21 |
| 3-23/9-CYL2-10-0-OS | 30.78 | 60.93 | -97.93 |
| 3-23/9-CYL2-10-0-OS | 36.51 | 120.10 | -228.96 |
| 3-23/9-CYL2-10-0-OS | 46.32 | 136.32 | -194.29 |
| 3-23/9-CYL2-10-0-OS | 49.17 | 131.60 | -167.63 |
| 3-23/14-CYL2-10-0-OS | 17.51 | 42.43 | -142.30 |
| 3-23/14-CYL2-10-0-OS | 22.40 | 88.38 | -294.47 |
| 3-23/13-CYL2-10-0-OS | 63.48 | 63.71 | -.37 |
| 3-23/13-CYL2-10-0-OS | 109.30 | 01.41 | 7.22 |
| 3-23/13-CYL2-10-0-OS | 121.73 | 16.69 | 4.15 |
| 3-23/12-CYL2-10-0-OS | 100.68 | 45.85 | 54.46 |
| 3-23/12-CYL2-10-0-OS | 107.63 | 55.28 | 48.64 |
| 3-23/12-CYL2-10-0-OS | 111.18 | 55.14 | 50.41 |
| 3-23/12-CYL2-10-0-OS | 111.29 | 49.75 | 55.30 |
| 3-30/4-CYL2-5-0-OS | 15.61 | 95.44 | -511.32 |
| 3-30/4-CYL2-5-0-OS | 113.38 | 169.96 | -49.91 |
| 3-30/4-CYL2-5-0-OS | 147.75 | 216.27 | -46.37 |
| 3-30/2-CYL2-5-0-OS | 12.30 | 100.14 | -714.23 |
| 3-30/2-CYL2-5-0-OS | 40.46 | 165.09 | -308.04 |
| 3-30/5-CYL2-5-0-OS | 112.54 | 101.15 | 10.12 |
| 3-30/5-CYL2-5-0-OS | 147.65 | 166.49 | -12.76 |
| 3-30/6-CYL2-5-0-OS | 22.20 | 80.17 | -261.06 |
| 3-30/6-CYL2-5-0-OS | 138.77 | 151.50 | -9.18 |
| 3-30/6-CYL2-5-0-OS | 159.35 | 195.51 | -22.69 |
| 3-31/3-CYL2-5-0-CA | 13.08 | 88.12 | -573.60 |
| 3-31/3-CYL2-5-0-CA | 35.12 | 148.53 | -322.93 |
| 3-31/3-CYL2-5-0-CA | 39.62 | 171.06 | -331.71 |
| 3-31/3-CYL2-5-0-CA | 39.95 | 161.72 | -304.82 |

## Sphere

The sphere data and comparison of measured and calculated soil forces are presented on the following pages. Lines 1 and 2 on p. 179 are discussed as an example of the data input to the computer.

Line 1 contains the test identification, which is explained in Appendix A.

Line 2 contains the following variables which were taken from the output of program IMPACT.

Horizontal velocity at center of gravity $(V_H)$ = 24.80 fps

Vertical velocity at center of gravity $(V_V)$ = 6.60 fps

Rotational velocity $(V_\theta)$ = 1.09 rps

Vertical penetration of tip $(D_t)$ = 0.13 in.

Resultant horizontal force at center of gravity $(F_H)$ = 90.50 lb

Resultant vertical force at center of gravity $(F_V)$ = 168.30 lb

Soil density $(\gamma)$ = 107.10 lb

The resultant horizontal and vertical forces at the projectile center of gravity were calculated using Eqs. 26 and 27.

$$F_H = 0.683\ (-D_t)^{0.70} V_H^{0.52} (-V_V)^{-0.21} (-V_\theta)^{0.28} \gamma^{1.23} \qquad (26)$$

$$V_V = 1.89\ (-D_t)^{0.87} V_H^{-0.11} (-V_V)^{0.26} (-V_\theta)^{0.21} \gamma^{1.38} \qquad (27)$$

The variables appearing in the above equations are defined on p. 61. It should be noted once again that the minus signs on $D_t$, $V_V$, and $V_\theta$ are not necessary since the input data have all been listed as positive.

The values listed under the "MEASURED" column on pp. 181 and 182 were obtained directly from the input data since edge effects were not accounted for in tests with spherical projectiles. The values listed under the "CALCULATED" column were obtained from Eqs. 26 and 27.

INPUT DATA

3-16-67 NO.14 SL-10-0-0S
24.800 6.600 1.090 .130 90.500 168.300 107.100

3-16-67 NO.14 SL-10-0-0S
24.620 6.260 1.370 .250 219.900 407.000 107.100

3-16-67 NO.14 SL-10-0-0S
24.280 5.660 1.840 .360 330.200 542.200 107.100

3-16-67 NO.14 SL-10-0-0S
23.820 4.940 2.340 .460 392.800 583.900 107.100

3-16-67 NO.12 SL-10-0-0S
30.620 7.040 1.090 .230 31.800 107.800 88.810

3-16-67 NO.12 SL-10-0-0S
30.510 6.720 1.320 .350 77.700 193.300 88.810

3-16-67 NO.12 SL-10-0-0S
30.310 6.260 1.570 .650 114.300 246.100 88.810

3-16-67 NO.12 SL-10-0-0S
30.030 5.690 1.790 .840 158.700 309.700 88.810

3-16-67 NO.12 SL-10-0-0S
29.660 4.990 2.030 1.020 200.900 358.700 88.810

3-16-67 NO.12 SL-10-0-0S
29.200 4.210 2.190 1.160 232.600 389.100 88.810

3-16-67 NO.8 SL-10-0-0S
13.370 5.430 1.030 .180 22.100 51.700 89.490

3-16-67 NO.8 SL-10-0-0S
13.300 5.280 1.120 .350 39.200 90.900 89.490

3-16-67 NO.8 SL-10-0-0S
13.190 5.060 1.260 .520 63.000 120.300 89.490

3-16-67 NO.8 SL-10-0-0S
13.040 4.780 1.420 .670 85.600 149.300 89.490

3-16-67 NO.8 SL-10-0-0S
12.840 4.450 1.590 .820 100.200 154.400 89.490

3-16-67 NO.8 SL-10-0-0S
12.620 4.120 1.730 .960 107.300 168.600 89.490

3-16-67 NO.8 SL-10-0-0S
12.390 3.750 1.840 1.090 116.300 191.300 89.490

3-16-67 NO.8 SL-10-0-0S
12.130 3.320 1.950 1.200 128.200 204.500 89.490

3-16-67 NO.13 SL-10-0-0S
24.450 4.120 1.490 .510 49.460 151.400 87.880

3-16-67 NO.13 SL-10-0-0S
24.380 3.900 1.680 .580 64.600 194.400 87.880

| | | | | | | |
|---|---|---|---|---|---|---|
| 3-16-67 | NO.13 | SL-10-0-0S | | | | |
| 24.290 | 3.640 | 1.900 | .660 | 78.440 | 226.100 | 87.880 |
| 3-16-67 | NO.13 | SL-10-0-0S | | | | |
| 24.190 | 3.350 | 2.120 | .720 | 86.380 | 240.200 | 87.880 |
| 3-16-67 | NO. 9 | SL-10-0-0S | | | | |
| 19.030 | 4.170 | 1.050 | .140 | 26.280 | 52.010 | 90.600 |
| 3-16-67 | NO. 9 | SL-10-0-0S | | | | |
| 18.950 | 4.020 | 1.170 | .270 | 43.470 | 80.680 | 90.600 |
| 3-16-67 | NO. 9 | SL-10-0-0S | | | | |
| 18.850 | 3.830 | 1.330 | .400 | 56.040 | 99.990 | 90.600 |
| 3-16-67 | NO. 9 | SL-10-0-0S | | | | |
| 18.720 | 3.610 | 1.480 | .520 | 69.330 | 121.000 | 90.600 |
| 3-16-67 | NO. 9 | SL-10-0-0S | | | | |
| 18.560 | 3.330 | 1.630 | .630 | 76.990 | 138.300 | 90.600 |
| 3-16-67 | NO. 9 | SL-10-0-0S | | | | |
| 18.390 | 3.030 | 1.770 | .730 | 83.210 | 140.700 | 90.600 |
| 3-16-67 | NO. 9 | SL-10-0-0S | | | | |
| 18.210 | 2.740 | 1.880 | .830 | 87.940 | 146.600 | 90.600 |
| 3-16-67 | NO. 9 | SL-10-0-0S | | | | |
| 18.020 | 2.420 | 1.970 | .910 | 93.570 | 155.400 | 90.600 |
| 3-16-67 | NO. 9 | SL-10-0-0S | | | | |
| 17.820 | 2.070 | 2.050 | .980 | 97.090 | 167.600 | 90.600 |
| 3-16-67 | NO. 10 | SL-10-0-0S | | | | |
| 13.430 | 5.750 | 1.060 | .110 | 47.190 | 84.230 | 99.000 |
| 3-16-67 | NO. 10 | SL-10-0-0S | | | | |
| 13.310 | 5.510 | 1.290 | .220 | 158.800 | 366.700 | 99.000 |
| 3-16-67 | NO. 10 | SL-10-0-0S | | | | |
| 13.070 | 4.950 | 1.770 | .310 | 217.700 | 485.500 | 99.000 |
| 3-16-67 | NO. 10 | SL-10-0-0S | | | | |
| 12.780 | 4.310 | 2.300 | .400 | 228.900 | 499.800 | 99.000 |
| 3-16-67 | NO. 10 | SL-10-0-0S | | | | |
| 12.520 | 3.760 | 2.710 | .480 | 231.100 | 503.400 | 99.000 |
| 3-16-67 | NO.11 | SL-10-0-0S | | | | |
| 30.400 | 7.230 | 1.540 | .240 | 252.200 | 548.700 | 100.100 |
| 3-16-67 | NO.11 | SL-10-0-0S | | | | |
| 29.640 | 5.660 | 2.920 | .450 | 477.800 | 916.000 | 100.100 |
| 3-16-67 | NO.11 | SL-10-0-0S | | | | |
| 28.590 | 3.770 | 4.240 | .590 | 495.800 | 839.100 | 100.100 |

| IDENTIFICATION | MEASURED $F_H$/IN. | CALCULATED $F_H$/IN. | PERCENT DEVIATION |
|---|---|---|---|
| 3-16/14-SL-10-0-0S | 90.50 | 188.07 | -107.81 |
| 3-16/14-SL-10-0-0S | 219.90 | 319.22 | -45.17 |
| 3-16/14-SL-10-0-0S | 330.20 | 453.80 | -37.43 |
| 3-16/14-SL-10-0-0S | 392.80 | 587.08 | -49.46 |
| 3-16/12-SL-10-0-0S | 31.80 | 245.16 | -670.94 |
| 3-16/12-SL-10-0-0S | 77.70 | 349.78 | -350.17 |
| 3-16/12-SL-10-0-0S | 114.30 | 572.88 | -401.21 |
| 3-16/12-SL-10-0-0S | 158.70 | 722.07 | -354.99 |
| 3-16/12-SL-10-0-0S | 200.90 | 875.14 | -335.61 |
| 3-16/12-SL-10-0-0S | 232.60 | 1005.48 | -332.28 |
| 3-16/8-SL-10-0-0S | 22.10 | 140.82 | -537.20 |
| 3-16/8-SL-10-0-0S | 39.20 | 230.35 | -487.62 |
| 3-16/8-SL-10-0-0S | 63.00 | 315.55 | -400.87 |
| 3-16/8-SL-10-0-0S | 85.60 | 391.98 | -357.92 |
| 3-16/8-SL-10-0-0S | 100.20 | 469.31 | -368.38 |
| 3-16/8-SL-10-0-0S | 107.30 | 540.47 | -403.70 |
| 3-16/8-SL-10-0-0S | 116.30 | 607.16 | -422.06 |
| 3-16/8-SL-10-0-0S | 128.20 | 669.74 | -422.42 |
| 3-16/13-SL-10-0-0S | 49.46 | 459.17 | -828.37 |
| 3-16/13-SL-10-0-0S | 64.60 | 524.84 | -712.44 |
| 3-16/13-SL-10-0-0S | 78.44 | 602.18 | -667.70 |
| 3-16/13-SL-10-0-0S | 86.38 | 670.11 | -675.77 |
| 3-16/9-SL-10-0-0S | 26.28 | 153.11 | -482.59 |
| 3-16/9-SL-10-0-0S | 43.47 | 251.31 | -478.12 |
| 3-16/9-SL-10-0-0S | 56.04 | 345.54 | -516.60 |
| 3-16/9-SL-10-0-0S | 69.33 | 431.61 | -522.54 |
| 3-16/9-SL-10-0-0S | 76.99 | 513.55 | -567.04 |
| 3-16/9-SL-10-0-0S | 83.21 | 591.46 | -610.81 |
| 3-16/9-SL-10-0-0S | 87.94 | 668.71 | -660.42 |
| 3-16/9-SL-10-0-0S | 93.57 | 737.66 | -688.36 |
| 3-16/9-SL-10-0-0S | 97.09 | 807.15 | -731.35 |
| 3-16/10-SL-10-0-0S | 47.19 | 112.77 | -138.96 |
| 3-16/10-SL-10-0-0S | 158.80 | 194.38 | -22.40 |
| 3-16/10-SL-10-0-0S | 217.70 | 273.55 | -25.65 |
| 3-16/10-SL-10-0-0S | 228.90 | 358.04 | -56.42 |
| 3-16/10-SL-10-0-0S | 231.10 | 433.63 | -87.64 |
| 3-16/11-SL-10-0-0S | 252.20 | 319.36 | -26.63 |
| 3-16/11-SL-10-0-0S | 477.80 | 616.31 | -28.99 |
| 3-16/11-SL-10-0-0S | 495.80 | 883.92 | -78.28 |

| IDENTIFICATION | MEASURED $F_V$/IN. | CALCULATED $F_V$/IN. | PERCENT DEVIATION |
|---|---|---|---|
| 3-16/14-SL-10-0-OS | 168.30 | 236.73 | -40.66 |
| 3-16/14-SL-10-0-OS | 407.00 | 433.07 | -6.41 |
| 3-16/14-SL-10-0-OS | 542.20 | 617.34 | -13.86 |
| 3-16/14-SL-10-0-OS | 583.90 | 777.34 | -33.13 |
| 3-16/12-SL-10-0-OS | 107.80 | 298.41 | -176.82 |
| 3-16/12-SL-10-0-OS | 193.30 | 442.41 | -128.87 |
| 3-16/12-SL-10-0-OS | 246.10 | 772.41 | -213.86 |
| 3-16/12-SL-10-0-OS | 309.70 | 969.08 | -212.91 |
| 3-16/12-SL-10-0-OS | 358.70 | 1140.15 | -217.86 |
| 3-16/12-SL-10-0-OS | 389.10 | 1241.74 | -219.13 |
| 3-16/8-SL-10-0-OS | 51.70 | 246.53 | -376.84 |
| 3-16/8-SL-10-0-OS | 90.90 | 444.47 | -388.97 |
| 3-16/8-SL-10-0-OS | 120.30 | 636.45 | -429.05 |
| 3-16/8-SL-10-0-OS | 149.30 | 802.69 | -437.63 |
| 3-16/8-SL-10-0-OS | 154.40 | 963.50 | -524.03 |
| 3-16/8-SL-10-0-OS | 168.60 | 1104.67 | -555.20 |
| 3-16/8-SL-10-0-OS | 191.30 | 1222.06 | -538.82 |
| 3-16/8-SL-10-0-OS | 204.50 | 1306.10 | -538.68 |
| 3-16/13-SL-10-0-OS | 151.40 | 559.95 | -269.85 |
| 3-16/13-SL-10-0-OS | 194.40 | 633.33 | -225.79 |
| 3-16/13-SL-10-0-OS | 226.10 | 714.60 | -216.05 |
| 3-16/13-SL-10-0-OS | 240.20 | 772.24 | -221.50 |
| 3-16/9-SL-10-0-OS | 52.01 | 181.71 | -249.37 |
| 3-16/9-SL-10-0-OS | 80.68 | 326.19 | -304.30 |
| 3-16/9-SL-10-0-OS | 99.99 | 466.07 | -366.11 |
| 3-16/9-SL-10-0-OS | 121.00 | 590.17 | -387.74 |
| 3-16/9-SL-10-0-OS | 138.30 | 697.55 | -404.38 |
| 3-16/9-SL-10-0-OS | 140.70 | 788.02 | -460.07 |
| 3-16/9-SL-10-0-OS | 146.60 | 870.26 | -493.63 |
| 3-16/9-SL-10-0-OS | 155.40 | 922.91 | -493.90 |
| 3-16/9-SL-10-0-OS | 167.60 | 954.30 | -469.39 |
| 3-16/10-SL-10-0-OS | 84.23 | 188.45 | -123.73 |
| 3-16/10-SL-10-0-OS | 366.70 | 355.31 | 3.11 |
| 3-16/10-SL-10-0-OS | 485.50 | 498.66 | -2.71 |
| 3-16/10-SL-10-0-OS | 499.80 | 635.97 | -27.25 |
| 3-16/10-SL-10-0-OS | 503.40 | 746.20 | -48.23 |
| 3-16/11-SL-10-0-OS | 548.70 | 395.81 | 27.86 |
| 3-16/11-SL-10-0-OS | 916.00 | 736.06 | 19.64 |
| 3-16/11-SL-10-0-OS | 839.10 | 910.15 | -8.47 |

# APPENDIX E

## CONE IMPACT DATA

This appendix contains the cone data which were obtained by the author from the impact tests on Ottawa and Colorado River Sand. Table Nos. 24 through 29 contain the Ottawa Sand data and Table Nos. 30 through 35 contain the Colorado River Sand data.

For clarity, several of the columns appearing in the tables are explained. The test identification column refers to the month, day, and number of the test on that particular date (7-14-3). The column also specifies the type of cone (light cone = LC and heavy cone = HC) and the impact angle and projectile pitch (90 - 0). A complete explanation of the test numbering and coding system is given in Appendix A.

The two soil columns list the soil density ($\gamma$) and the moisture content (w).

The rise time is the elapsed time from the instant of impact to the development of the peak acceleration.

The calculated penetration was obtained by double numerical integration of the acceleration-time curve.

The correction factor (CORFA) was a multiplier that was used to correct the acceleration ordinates so that the final projectile velocity was approximately zero. Appendix F contains a discussion on the application of correction factors (CORFA) to acceleration-time curves.

TABLE NO. 24

TABULATION OF PEAK ACCELERATIONS FOR VERTICAL IMPACT OF LIGHT CONE ON LOOSE, DRY OTTAWA SAND

| Test Identification | Soil $\gamma$ (pcf) | Soil w (%) | Vertical Impact Velocity (fps) | Peak Acceleration (g's) | Rise Time (msec) | Measured Penetration (in.) | Calculated Penetration (in.) | Correction Factor (CORFA) |
|---|---|---|---|---|---|---|---|---|
| 7-14-3-LC-90-0 | 93.2 | 1.45 | 10.2 | 6.9 | 60.5 | 10.0 | 6.7 | 1.76 |
| 7-14-4-LC-90-0 | 92.0 | 1.57 | 10.0 | 5.6 | 54.9 | 9.9 | 6.2 | 1.55 |
| 7-24-8-LC-90-0 | 90.5 | 0.83 | 14.6 | 9.6 | 64.0 | 12.0 | 8.9 | 2.13 |
| 7-11-7-LC-90-0 | 91.0 | 2.95 | 16.9 | 14.1 | 52.4 | 11.6 | 7.7 | 2.08 |
| 7-14-1-LC-90-0 | 90.5 | 1.56 | 17.2 | 11.8 | 48.4 | 11.2 | 10.2 | 2.22 |
| 7-14-2-LC-90-0 | 92.7 | 1.65 | 17.3 | 14.1 | 57.9 | 12.5 | 10.2 | 2.00 |
| 7-11-5-LC-90-0 | 91.7 | 0.95 | 19.6 | 14.6 | 48.3 | 12.7 | 12.2 | 2.25 |
| 7-11-6-LC-90-0 | 91.7 | 0.87 | 19.9 | 14.1 | 43.7 | 12.0 | 11.5 | 2.29 |
| 7-10-3-LC-90-0 | 91.5 | 1.86 | 23.2 | 15.2 | 58.2 | 13.8 | 13.6 | 1.62 |
| 7-10-4-LC-90-0 | 89.4 | 1.64 | 23.1 | 16.1 | 54.4 | 13.9 | 13.6 | 1.85 |
| 7-10-5-LC-90-0 | 90.2 | 1.56 | 30.4 | 22.6 | 41.5 | 15.6 | 16.2 | 1.84 |

TABLE NO. 25

TABULATION OF PEAK ACCELERATIONS FOR VERTICAL IMPACT OF LIGHT CONE ON DENSE, DRY OTTAWA SAND

| Test Identification | Soil $\gamma$ (pcf) | Soil w (%) | Vertical Impact Velocity (fps) | Peak Acceleration (g's) | Rise Time (msec) | Measured Penetration (in.) | Calculated Penetration (in.) | Correction Factor (CORFA) |
|---|---|---|---|---|---|---|---|---|
| 7-14-5-LC-90-0 | 105.2 | 1.33 | 10.1 | 14.8 | 25.4 | 4.8 | 3.4 | 1.37 |
| 7-14-6-LC-90-0 | 103.6 | 1.14 | 10.1 | 14.5 | 27.9 | 5.1 | 2.6 | 1.48 |
| 7-24-5-LC-90-0 | 104.7 | 0.72 | 14.4 | 20.0 | 22.4 | 5.1 | 4.1 | 1.30 |
| 7-24-6-LC-90-0 | 106.2 | 0.81 | 14.3 | 17.6 | 25.2 | 5.9 | 4.3 | 1.35 |
| 7-14-7-LC-90-0 | 101.8 | 1.38 | 17.3 | 26.8 | 23.2 | 5.6 | 4.5 | 1.29 |
| 7-14-8-LC-90-0 | 100.6 | 1.07 | 18.0 | 29.0 | 19.0 | 5.5 | 4.2 | 1.39 |
| 7-11-3-LC-90-0 | 104.7 | 1.34 | 19.6 | 28.2 | 25.7 | 5.4 | 5.2 | 1.32 |
| 7-11-4-LC-90-0 | 101.9 | 0.95 | 19.6 | 30.8 | 22.6 | 5.6 | 5.3 | 1.45 |
| 7-10-1-LC-90-0 | 107.5 | 2.29 | 23.8 | 40.4 | 16.5 | 5.7 | 5.4 | 1.42 |
| 7-10-2-LC-90-0 | 106.6 | 1.79 | 23.6 | 38.8 | 16.3 | 6.3 | 5.4 | 1.44 |
| 7-11-1-LC-90-0 | 106.8 | 1.73 | 30.8 | 45.3 | 16.9 | 7.2 | 7.5 | 1.30 |
| 7-11-2-LC-90-0 | 101.3 | 1.61 | 30.5 | 47.5 | 16.1 | 7.4 | 6.7 | 1.42 |

TABLE NO. 26

TABULATION OF PEAK ACCELERATIONS FOR VERTICAL IMPACT OF LIGHT CONE ON SATURATED OTTAWA SAND

| Test Identification | Soil $\gamma$ (pcf) | Soil w (%) | Vertical Impact Velocity (fps) | Peak Acceleration (g's) | Rise Time (msec) | Measured Penetration (in.) | Calculated Penetration (in.) | Correction Factor (CORFA) |
|---|---|---|---|---|---|---|---|---|
| 7-25-3-LC-90-0 | 134.4 | 16.4 | 10.3 | 27.5 | 23.7 | 3.4 | 1.7 | 1.25 |
| 7-25-4-LC-90-0 | 133.3 | 17.1 | 10.2 | 24.9 | 23.7 | 3.3 | 2.2 | 1.25 |
| 7-25-1-LC-90-0 | 134.6 | 16.0 | 14.4 | 26.4 | 23.0 | -- | 3.1 | 1.42 |
| 7-25-2-LC-90-0 | 133.7 | 16.8 | 14.3 | 30.0 | 21.4 | 3.7 | 3.1 | 1.35 |
| 7-25-5-LC-90-0 | 132.2 | 17.7 | 17.3 | 37.7 | 21.7 | 4.6 | 4.5 | 1.14 |
| 7-25-6-LC-90-0 | 133.0 | 17.3 | 17.5 | 38.3 | 20.1 | 3.9 | 4.0 | 1.34 |
| 7-25-7-LC-90-0 | 132.2 | 18.1 | 20.0 | 43.7 | 15.7 | 4.0 | 3.7 | 1.10 |
| 7-25-8-LC-90-0 | 135.4 | 15.3 | 19.9 | 44.5 | 18.7 | 4.3 | 4.1 | 1.13 |
| 7-25-9-LC-90-0 | 132.8 | 17.3 | 23.6 | 51.4 | 15.8 | 4.6 | 4.6 | 1.26 |
| 7-25-10-LC-90-0 | 131.4 | 18.4 | 22.9 | 49.1 | 15.8 | 4.5 | 4.3 | 1.25 |

TABLE NO. 27

TABULATION OF PEAK ACCELERATIONS FOR VERTICAL IMPACT OF HEAVY CONE ON LOOSE, DRY OTTAWA SAND

| Test Identification | Soil | | Vertical Impact Velocity | Peak Acceleration | Rise Time | Measured Penetration | Calculated Penetration | Correction Factor |
|---|---|---|---|---|---|---|---|---|
| | $\gamma$ (pcf) | w (%) | (fps) | (g's) | (msec) | (in.) | (in.) | (CORFA) |
| 7-20-7-HC-90-0 | 91.6 | 0.94 | 10.5 | 8.3 | 96.7 | 14.4 | 7.9 | 2.35 |
| 7-20-8-HC-90-0 | 88.8 | 1.01 | 10.3 | 7.0 | 96.7 | 14.5 | 10.5 | 2.00 |
| 7-21-1-HC-90-0 | 89.3 | 1.03 | 14.3 | 11.9 | 85.2 | 16.3 | 9.8 | 2.00 |
| 7-24-1-HC-90-0 | 92.4 | 0.83 | 14.5 | 12.6 | 71.3 | 14.9 | 8.2 | 2.25 |
| 7-20-5-HC-90-0 | 86.0 | 1.10 | 17.9 | 17.3 | 77.4 | 15.8 | 14.9 | 2.20 |
| 7-20-1-HC-90-0 | 88.7 | 1.09 | 20.4 | 19.3 | 66.5 | 16.4 | 16.0 | 1.60 |
| 7-20-2-HC-90-0 | 90.1 | 1.05 | 19.5 | 24.4 | 75.1 | 15.6 | 14.3 | 1.82 |
| 7-20-9-HC-90-0 | 89.3 | 1.10 | 23.1 | 21.3 | 57.5 | 16.0 | 15.0 | 1.50 |
| 7-20-10-HC-90-0 | 90.4 | 1.00 | 23.8 | 29.7 | 66.2 | 16.1 | 15.0 | 2.00 |
| 7-20-11-HC-90-0 | 93.1 | 1.13 | 27.1 | 31.4 | 67.0 | 18.9 | 17.9 | 1.68 |
| 7-20-12-HC-90-0 | 88.3 | 1.17 | 27.1 | 28.4 | 62.5 | 17.2 | 16.8 | 1.75 |
| 7-20-13-HC-90-0 | 86.2 | 1.05 | 27.1 | 34.8 | 57.4 | 16.7 | 16.7 | 1.54 |

TABLE NO. 28

TABULATION OF PEAK ACCELERATIONS FOR VERTICAL IMPACT OF HEAVY CONE ON DENSE, DRY OTTAWA SAND

| Test Identification | Soil | | Vertical Impact Velocity | Peak Acceleration | Rise Time | Measured Penetration | Calculated Penetration | Correction Factor |
|---|---|---|---|---|---|---|---|---|
| | $\gamma$ (pcf) | w (%) | (fps) | (g's) | (msec) | (in.) | (in.) | (CORFA) |
| 7-17-2-HC-90-0 | 101.6 | 0.85 | 10.3 | 14.3 | 37.6 | 6.6 | 3.5 | 1.63 |
| 7-17-3-HC-90-0 | 103.2 | 1.00 | 10.4 | 14.8 | 35.9 | 7.1 | 3.2 | 1.70 |
| 7-14-9-HC-90-0 | 108.3 | 1.99 | 15.8 | 17.3 | 25.5 | 8.1 | 5.4 | 1.14 |
| 7-17-1-HC-90-0 | 102.6 | 0.69 | 16.6 | 19.7 | 36.4 | 7.7 | 6.6 | 1.37 |
| 7-17-4-HC-90-0 | 102.0 | 0.77 | 19.5 | 23.8 | 30.4 | 8.3 | 7.2 | 1.44 |
| 7-18-1-HC-90-0 | 103.8 | 0.54 | 20.0 | 25.3 | 40.2 | 7.8 | 8.2 | 1.54 |
| 7-18-2-HC-90-0 | 105.2 | 0.52 | 22.5 | 26.9 | 36.1 | 8.3 | 10.5 | 1.47 |
| 7-18-3-HC-90-0 | 103.9 | 0.45 | 23.1 | 29.4 | 33.9 | 8.6 | 10.2 | 1.51 |
| 7-18-4-HC-90-0 | 105.7 | 0.47 | 23.1 | 27.5 | 31.5 | 9.1 | 10.0 | 1.42 |

TABLE NO. 29

TABULATION OF PEAK ACCELERATIONS FOR VERTICAL IMPACT OF HEAVY CONE ON SATURATED OTTAWA SAND

| Test Identification | Soil $\gamma$ (pcf) | Soil w (%) | Vertical Impact Velocity (fps) | Peak Acceleration (g's) | Rise Time (msec) | Measured Penetration (in.) | Calculated Penetration (in.) | Correction Factor (CORFA) |
|---|---|---|---|---|---|---|---|---|
| 7-26-10-HC-90-0 | 136.0 | 15.2 | 10.3 | 17.1 | 33.3 | 5.3 | 3.6 | 1.28 |
| 7-26-11-HC-90-0 | 135.7 | 15.2 | 10.3 | 19.5 | 30.8 | 5.0 | 2.5 | 1.50 |
| 7-26-8-HC-90-0 | 136.0 | 15.2 | 14.3 | 21.7 | 30.0 | 5.5 | 4.5 | 1.10 |
| 7-26-9-HC-90-0 | 131.1 | 18.7 | 14.6 | 23.0 | 29.2 | 5.6 | 4.5 | 1.25 |
| 7-26-6-HC-90-0 | 133.1 | 17.2 | 17.6 | 32.8 | 29.4 | 6.3 | 3.8 | 1.45 |
| 7-26-7-HC-90-0 | 133.1 | 17.2 | 17.7 | 26.2 | 27.3 | 5.6 | 5.4 | 1.28 |
| 7-26-4-HC-90-0 | 133.1 | 17.2 | 19.8 | 30.9 | 27.3 | 6.8 | 5.8 | 1.32 |
| 7-26-5-HC-90-0 | 134.4 | 16.4 | 19.8 | 31.2 | 27.3 | 6.5 | 5.8 | 1.36 |
| 7-25-11-HC-90-0 | 132.2 | 17.7 | 24.8 | 38.6 | 23.6 | 6.7 | 6.7 | 1.34 |
| 7-26-1-HC-90-0 | 134.7 | 16.3 | 24.8 | 38.0 | 25.0 | 7.5 | 6.8 | 1.32 |
| 7-26-2-HC-90-0 | 133.4 | 17.0 | 24.3 | 34.3 | 25.0 | 7.3 | 6.8 | 1.32 |
| 7-26-3-HC-90-0 | 131.1 | 19.0 | 23.6 | 36.3 | 33.3 | 7.6 | 8.6 | 1.40 |

TABLE NO. 30

TABULATION OF PEAK ACCELERATIONS FOR VERTICAL IMPACT
OF LIGHT CONE ON LOOSE, DRY COLORADO RIVER SAND

| Test Identification | Soil | | Vertical Impact Velocity | Peak Acceleration | Rise Time | Measured Penetration | Calculated Penetration | Correction Factor |
|---|---|---|---|---|---|---|---|---|
| | $\gamma$ (pcf) | w (%) | (fps) | (g's) | (msec) | (in.) | (in.) | (CORFA) |
| 8-1-1-LC-90-0 | 95.8 | 1.99 | 9.9 | 7.6 | 39.1 | 8.2 | 5.2 | 1.25 |
| 8-1-2-LC-90-0 | 94.3 | 1.91 | 10.0 | 7.7 | 64.5 | 9.3 | 7.1 | 1.45 |
| 8-1-4-LC-90-0 | 96.3 | 2.11 | 14.1 | 11.3 | 52.3 | 10.4 | 8.2 | 1.39 |
| 8-1-5-LC-90-0 | 94.4 | 2.07 | 13.8 | 13.1 | 54.7 | 10.2 | 6.0 | 2.00 |
| 8-1-6-LC-90-0 | 91.7 | 2.70 | 14.0 | 10.4 | 70.2 | 10.0 | 9.8 | 1.80 |
| 8-1-7-LC-90-0 | 94.5 | 2.10 | 17.1 | 18.9 | 42.8 | 10.2 | 6.7 | 2.25 |
| 8-1-8-LC-90-0 | 95.1 | 1.86 | 17.7 | 18.1 | 61.5 | 10.0 | 11.1 | 2.10 |
| 8-1-9-LC-90-0 | 91.7 | 1.80 | 19.9 | 19.4 | 48.7 | 10.8 | 10.0 | 1.94 |
| 8-1-10-LC-90-0 | 94.0 | 2.93 | 19.6 | 21.1 | 50.5 | 10.9 | 10.3 | 2.14 |
| 8-1-11-LC-90-0 | 95.9 | 2.00 | 20.1 | 18.8 | 48.1 | 11.3 | 9.6 | 2.35 |
| 8-1-12-LC-90-0 | 92.2 | 1.80 | 24.2 | 21.4 | 51.5 | 11.4 | 14.0 | 1.80 |
| 8-1-13-LC-90-0 | 97.1 | 1.78 | 23.6 | 21.9 | 46.0 | 12.0 | 11.8 | 1.90 |

TABLE NO. 31

TABULATION OF PEAK ACCELERATIONS FOR VERTICAL IMPACT OF LIGHT CONE ON DENSE, DRY COLORADO RIVER SAND

| Time Identification | Soil $\gamma$ (pcf) | Soil w (%) | Vertical Impact Velocity (fps) | Peak Acceleration (g's) | Rise Time (msec) | Measured Penetration (in.) | Calculated Penetration (in.) | Correction Factor (CORFA) |
|---|---|---|---|---|---|---|---|---|
| 8-2-12-LC-90-0 | 104.5 | 0.90 | 10.1 | 17.4 | 27.1 | 5.0 | 3.0 | 1.40 |
| 8-2-13-LC-90-0 | 105.9 | 1.03 | 10.1 | 16.8 | 22.9 | 4.9 | 2.5 | 1.40 |
| 8-2-10-LC-90-0 | 105.6 | 1.14 | 14.1 | 27.8 | 21.9 | 5.4 | 2.8 | 1.54 |
| 8-2-11-LC-90-0 | 103.4 | 0.84 | 14.2 | 21.8 | 22.4 | 5.2 | 3.8 | 1.40 |
| 8-2-6-LC-90-0 | 108.0 | 1.10 | 17.1 | 24.4 | 21.9 | 5.4 | 4.5 | 1.36 |
| 8-2-7-LC-90-0 | 106.7 | 0.99 | 17.4 | 24.5 | 21.9 | 5.5 | 4.8 | 1.47 |
| 8-2-3-LC-90-0 | 101.3 | 2.22 | 19.9 | 27.5 | 24.7 | 5.9 | 6.5 | 1.50 |
| 8-2-4-LC-90-0 | 105.1 | 1.34 | 19.9 | 30.8 | 20.6 | 5.9 | 5.2 | 1.50 |
| 8-2-1-LC-90-0 | 105.3 | 1.51 | 23.7 | 32.6 | 18.5 | 6.7 | 6.2 | 1.50 |
| 8-2-2-LC-90-0 | 104.1 | 1.31 | 23.2 | 37.0 | 19.1 | 6.7 | 5.9 | 1.50 |

TABLE NO. 32

TABULATION OF PEAK ACCELERATIONS FOR VERTICAL IMPACT
OF LIGHT CONE ON SATURATED COLORADO RIVER SAND

| Test Identification | Soil $\gamma$ (pcf) | Soil w (%) | Vertical Impact Velocity (fps) | Peak Acceleration (g's) | Rise Time (msec) | Measured Penetration (in.) | Calculated Penetration (in.) | Correction Factor (CORFA) |
|---|---|---|---|---|---|---|---|---|
| 8-10-9-LC-90-0 | 131.9 | 18.3 | 9.9 | 16.1 | 34.3 | 3.9 | 3.4 | 1.26 |
| 8-10-10-LC-90-0 | 132.3 | 17.1 | 10.0 | 16.8 | 32.1 | 4.5 | 3.5 | 1.10 |
| 8-10-7-LC-90-0 | 135.6 | 15.2 | 14.2 | 26.7 | 25.7 | 4.3 | 3.5 | 1.18 |
| 8-10-8-LC-90-0 | 130.3 | 19.3 | 14.3 | 23.7 | 30.0 | 4.2 | 4.5 | 1.30 |
| 8-10-5-LC-90-0 | 135.6 | 15.2 | 17.3 | 28.6 | 25.9 | 4.4 | 4.7 | 1.27 |
| 8-10-6-LC-90-0 | 135.6 | 15.2 | 17.2 | 30.6 | 24.3 | 4.5 | 4.3 | 1.10 |
| 8-10-3-LC-90-0 | 130.6 | 19.2 | 20.0 | 38.1 | 21.4 | 4.5 | 4.2 | 1.19 |
| 8-10-4-LC-90-0 | 132.5 | 17.8 | 19.9 | 35.5 | 24.3 | 4.6 | 5.1 | 1.34 |
| 8-10-1-LC-90-0 | 132.2 | 18.2 | 23.9 | 45.2 | 23.6 | -- | 6.2 | 1.42 |
| 8-10-2-LC-90-0 | 136.1 | 15.0 | 23.7 | 45.2 | 18.6 | 5.5 | 5.1 | 1.38 |

TABLE NO. 33

TABULATION OF PEAK ACCELERATIONS FOR VERTICAL IMPACT
OF HEAVY CONE ON LOOSE, DRY COLORADO RIVER SAND

| Test Identification | Soil | | Vertical Impact Velocity | Peak Acceleration | Rise Time | Measured Penetration | Calculated Penetration | Correction Factor |
|---|---|---|---|---|---|---|---|---|
| | $\gamma$ (pcf) | w (%) | (fps) | (g's) | (msec) | (in.) | (in.) | (CORFA) |
| 8-3-1-HC-90-0 | 97.6 | 1.44 | 10.5 | 7.0 | 75.7 | 12.7 | 9.2 | 1.35 |
| 8-3-2-HC-90-0 | 99.2 | 1.31 | 10.6 | 8.8 | 81.7 | 12.6 | 9.0 | 1.78 |
| 8-3-3-HC-90-0 | 96.5 | 1.45 | 14.6 | 14.4 | 61.2 | 13.4 | 6.7 | 2.20 |
| 8-3-5-HC-90-0 | 95.3 | 1.24 | 17.8 | 16.3 | 73.4 | 13.3 | 14.2 | 1.85 |
| 8-3-6-HC-90-0 | 95.9 | 1.41 | 17.8 | 19.6 | 72.5 | 13.4 | 10.9 | 2.36 |
| 8-3-7-HC-90-0 | 96.1 | 1.24 | 20.4 | 20.8 | 64.8 | 13.7 | 13.0 | 1.82 |
| 8-3-8-HC-90-0 | 96.7 | 1.28 | 19.6 | 17.9 | 53.1 | 13.3 | 11.5 | 1.72 |
| 8-3-9-HC-90-0 | 95.8 | 1.23 | 20.4 | 19.7 | 56.0 | 14.1 | 13.1 | 1.75 |
| 8-3-10-HC-90-0 | 99.1 | 1.19 | 19.6 | 19.0 | 63.0 | 13.3 | 14.5 | 1.82 |
| 8-3-11-HC-90-0 | 98.6 | 1.20 | 23.5 | 25.4 | 67.5 | 13.2 | 19.1 | 1.54 |
| 8-3-12-HC-90-0 | 100.8 | 1.17 | 23.5 | 28.8 | 59.2 | 13.4 | 12.6 | 1.85 |
| 8-3-13-HC-90-0 | 100.0 | 1.77 | 24.2 | 25.5 | 55.3 | 14.0 | 14.9 | 1.55 |

TABLE NO. 34

TABULATION OF PEAK ACCELERATIONS FOR VERTICAL IMPACT
OF HEAVY CONE ON DENSE, DRY COLORADO RIVER SAND

| Test Identification | Soil $\gamma$ (pcf) | Soil w (%) | Vertical Impact Velocity (fps) | Peak Acceleration (g's) | Rise Time (msec) | Measured Penetration (in.) | Calculated Penetration (in.) | Correction Factor (CORFA) |
|---|---|---|---|---|---|---|---|---|
| 8-9-5-HC-90-0 | 108.2 | 1.37 | 10.5 | 11.3 | 36.1 | 7.1 | 4.2 | 1.53 |
| 8-9-6-HC-90-0 | 109.6 | 1.19 | 9.8 | 11.3 | 45.5 | 7.2 | 4.9 | 1.54 |
| 8-9-3-HC-90-0 | 106.6 | 1.49 | 14.3 | 15.1 | 40.1 | 7.2 | 7.0 | 1.75 |
| 8-9-4-HC-90-0 | 106.9 | 1.28 | 14.4 | 18.4 | 41.5 | 7.6 | 6.4 | 1.73 |
| 8-9-1-HC-90-0 | 108.4 | 1.41 | 17.8 | 18.8 | 37.3 | 8.4 | 8.4 | 1.60 |
| 8-9-2-HC-90-0 | 109.0 | 1.60 | 17.8 | 23.8 | 35.0 | 7.8 | 7.8 | 1.82 |
| 8-8-4-HC-90-0 | 102.3 | 1.95 | 20.5 | 23.2 | 38.5 | 8.9 | 9.7 | 1.45 |
| 8-8-5-HC-90-0 | 106.5 | 2.57 | 20.0 | 23.2 | 38.7 | 8.4 | 9.1 | 1.63 |
| 8-8-6-HC-90-0 | 102.5 | 2.88 | 19.8 | 25.4 | 33.2 | 8.4 | 8.2 | 1.52 |
| 8-8-2-HC-90-0 | 105.3 | 2.56 | 24.4 | 31.0 | 31.1 | 8.9 | 9.2 | 1.54 |
| 8-8-3-HC-90-0 | 104.3 | 2.16 | 24.4 | 34.1 | 31.8 | 9.9 | 9.5 | 1.59 |

TABLE NO. 35

TABULATION OF PEAK ACCELERATIONS FOR VERTICAL IMPACT
OF HEAVY CONE ON SATURATED COLORADO RIVER SAND

| Test Identification | Soil | | Vertical Impact Velocity | Peak Acceleration | Rise Time | Measured Penetration | Calculated Penetration | Correction Factor |
|---|---|---|---|---|---|---|---|---|
| | $\gamma$ (pcf) | w (%) | (fps) | (g's) | (msec) | (in.) | (in.) | (CORFA) |
| 8-9-7-HC-90-0 | 131.4 | 18.4 | 10.2 | 10.9 | 41.4 | 6.7 | 4.3 | 1.11 |
| 8-9-8-HC-90-0 | 133.9 | 16.7 | 10.4 | 13.3 | 39.6 | 5.5 | 4.1 | 1.18 |
| 8-9-9-HC-90-0 | 129.7 | 19.8 | 14.0 | 18.8 | 33.3 | 5.5 | 4.5 | 1.24 |
| 8-9-10-HC-90-0 | 134.6 | 16.2 | 14.2 | 19.3 | 30.4 | 6.1 | 4.6 | 1.08 |
| 8-9-11-HC-90-0 | 132.1 | 17.7 | 17.4 | 26.4 | 29.0 | 5.6 | 4.9 | 1.87 |
| 8-9-12-HC-90-0 | 135.3 | 15.8 | 17.4 | 24.3 | 31.2 | 6.1 | 5.2 | 1.24 |
| 8-9-13-HC-90-0 | 133.4 | 17.0 | 19.8 | 29.6 | 25.0 | 6.3 | 5.3 | 1.30 |
| 8-9-14-HC-90-0 | 132.1 | 18.2 | 19.9 | 29.6 | 35.0 | 6.6 | 7.0 | 1.28 |
| 8-9-15-HC-90-0 | 132.2 | 17.8 | 23.8 | 36.2 | 23.6 | 7.0 | 6.2 | 1.35 |
| 8-9-16-HC-90-0 | 131.4 | 18.7 | 23.7 | 35.9 | 25.0 | 7.0 | 6.3 | 1.32 |

# APPENDIX F

## CORRECTION OF ACCELEROMETER DATA

It was noticed during the course of the author's cone testing that the complete numerical integration of the acceleration-time curve did not reduce the calculated cone velocity to zero. A thorough investigation of the causes of this apparent discrepancy in the data was performed and it is the purpose of this appendix to present the findings of this investigation.

### Impact Velocity Measurement

When it was first noticed that the area under the acceleration-time curve was not large enough to reduce the projectile velocity to zero each possible source of error was critically reviewed. The first step consisted of checking the method for determining the initial impact velocity. As previously discussed in Chapter IV the initial impact velocity was determined by two independent methods. The first method involved the use of a velocity detector system and the latter method utilized the travel time which was calculated from oscilloscope settings.

In reviewing the high angle ($\alpha \geq 30$ degrees) test data it was found that generally the impact velocities as determined by the above methods agreed within ± 5 percent for tests with spheres and cylinders. The agreement for low angle tests ($\alpha < 30$ degrees) was not nearly as good since the effect of gravity was significant in these cases. Some of the cone tests (vertical impact) also exhibited a lack of agreement. These cases required special methods for calculating the initial impact velocity and the methods are discussed in Chapter IV.

In conclusion, it is felt that the initial impact velocity is known within ± 5 percent of the true impact velocity for all conditions of testing.

This magnitude of error was not sufficient to cause the apparent discrepancy in the data.

Integration Method

The method of numerical integration was checked for errors. A half sine wave pulse was input into Program IMPACT. The pulse approximated typical accelerometer output from the impact tests. Care was taken to divide the pulse into approximately the same number of increments as were used in the actual impact data.

Exact values of velocity and displacement were calculated by hand using integral calculus. These values were compared with the values obtained from Program IMPACT. The values from the program calculation method were within ±0.3 percent of the hand calculated values.

Thus, it was concluded that the numerical integration techniques were sufficiently accurate.

Accelerometer Calibration

After finding that the impact velocity measurement method and the numerical integration method involved a combined total of less than 6 percent error, each section of the electrical circuitry was examined in detail.

The voltages to each portion of the accelerometer circuits were checked and found to be at the correct values. The 565 dual beam Tektronix oscilloscope, upon which the accelerometer outputs were recorded, was recalibrated. The recalibration showed that the oscilloscope was functioning properly.

A check on accelerometer calibration was obtained through a series of vertical drop tests in the laboratory. Two accelerometers were mounted on a spherical segment. One of the accelerometers had been utilized by Poor[16] and the other by the author. The accelerometer utilized by Poor had a ±500 g maximum range and was known to be approximately in calibration.

The drop test conditions were controlled so the acceleration-time curves resembled the field curves in shape and magnitude. It was also thought that possibly the balancing unit or the filter networks were not functioning properly. To check these portions of the circuitry tests were conducted with the following types of hookups:

(1) Accelerometer connected directly to the oscilloscope,

(2) Accelerometer connected to the filter networks,

(3) Accelerometer connected to both the filter and balancing network.

The ±500 g accelerometer was always connected directly to the oscilloscope while the ±250 g accelerometer that was used by the author was connected in one of the three ways listed above. It should be noted that the initial impact velocity was attained by allowing the projectile to fall through a measured height. The initial impact velocity was calculated by

$$V = \sqrt{2\,g\,h} \quad , \tag{41}$$

where $g$ is the acceleration of gravity and $h$ is the height of drop. High speed movies from a previous investigation[18] have shown this method to yield velocities within 3 percent of the true values.

The results from the laboratory drop tests are listed in Table No. 36. The A and B test designations represent the ±250 g and ±500 g accelerometer outputs, respectively, for the same drop test. Column 7 in Table No. 36 represents the ratio of the final calculated velocity of the projectile to the initial impact velocity. Complete integration of the acceleration-time curve should yield a final velocity of zero. Table No. 36 shows that approximately 10 to 15 percent of the initial velocity is still present upon complete integration of the acceleration curves for both the ±250 g and ±500 g

accelerometers. It should be noted that a velocity in the downward direction was considered positive.

Table No. 37 lists average ratios of final velocity to initial velocity for each type of electrical hookup and accelerometer. As illustrated by the table, the most favorable situation was when both the balancing unit and filter networks were connected between the accelerometer and the oscilloscope. This type hookup was similar to that used in the field tests. There was not any noticeable difference in the response of the two accelerometers. The tables also show that the type of electrical hookup made very little difference in the recorded accelerometer outputs.

It was concluded from these tests that approximately a 10 to 15 percent error was involved in using the accelerometer calibration constant listed by the manufacturer. Both of the accelerometers were manufactured by Consolidated Electrodynamics Corporation.

Accelerometer Trace Drift

The previously discussed sources of error account for only a portion of the error present in many of the cone tests. To locate the remaining source or sources of error the acceleration-time records and computer program (IMPACT) outputs were examined in detail.

Examination of the final calculated velocities for each of the field tests showed that the tests on sand in a saturated state exhibited smaller final velocities than tests on dense, dry sands and loose, dry sands. In many of the cone tests on loose, dry sand the final calculated velocity was nearly 50 percent of the initial impact velocity.

Acceleration-time records were examined and it was found that the records for tests on loose, dry sand exhibited large rebound portions. Previous testing experience had shown that sands exhibit small amounts of

TABLE NO. 36

COMPARISON OF ACCELEROMETER OUTPUT

| Test No. | Accelerometer Range (g's) | Type of Hookup | Peak Acceleration (g's) | Initial Velocity (fps) | Final Velocity (fps) | Ratio of Final Velocity to Initial Velocity (%) |
|---|---|---|---|---|---|---|
| 1A | 250 | | 46.5 | 17.21 | 4.25 | 24.6 |
| 1B | 500 | | 48.0 | 17.21 | 2.63 | 15.3 |
| 2A | 250 | Oscilloscope | 44.0 | 18.52 | 1.89 | 10.2 |
| 2B | 500 | | 41.2 | 18.52 | 2.54 | 13.7 |
| 3A | 250 | | 29.5 | 12.19 | 1.50 | 12.3 |
| 3B | 500 | | 31.0 | 12.19 | 1.36 | 11.2 |
| 4A | 250 | Filters | 43.4 | 18.62 | 1.32 | 7.1 |
| 4B | 500 | Oscilloscope | 53.0 | 18.62 | 4.11 | 22.1 |
| 5A | 250 | Filters | 36.9 | 18.52 | 4.32 | 23.4 |
| 5B | 500 | Oscilloscope | 45.0 | 18.52 | 3.81 | 20.6 |
| 6A | 250 | Filters | 49.0 | 18.52 | 3.85 | 20.8 |
| 6B | 500 | Oscilloscope | 58.0 | 18.52 | 1.70 | 9.2 |
| 7A | 250 | Bal & Filter Circuit | 49.5 | 18.59 | 2.28 | 12.3 |
| 7B | 500 | Oscilloscope | 58.0 | 18.59 | 1.44 | 7.8 |
| 8A | 250 | Bal & Filter Circuit | 43.5 | 16.21 | 2.53 | 15.6 |
| 8B | 500 | Oscilloscope | 47.1 | 16.21 | 2.00 | 12.3 |
| 9A | 250 | Bal & Filter Circuit | 27.0 | 12.92 | 0.82 | 6.3 |
| 9B | 500 | Oscilloscope | 32.0 | 12.92 | -0.40 | -3.1 |

TABLE NO. 37

AVERAGE RATIOS OF FINAL VELOCITY TO INITIAL VELOCITY

| No. of Values | Accelerometer Range (g's) | Type of Hookup | Average of Ratio of Final Velocity to Initial Velocity (%) |
|---|---|---|---|
| 9 | 500 | Oscilloscope | 12.1 |
| 3 | 250 | Oscilloscope | 15.7 |
| 3 | 250 | Filter | 17.1 |
| 3 | 250 | Bal & Filter Circuit | 11.4 |

elastic rebound. Thus, it was concluded that the accelerometer base lines were drifting during the impact event.

Figures 57 and 58 illustrate acceleration-time records for cone tests on saturated Ottawa Sand and loose, dry Ottawa Sand, respectively. Two accelerometer traces were recorded for each vertical drop test. The accelerometers both recorded the vertical acceleration of the cone. The vertical cone acceleration was obtained by averaging the acceleration indicated by the accelerometers. The horizontal portions of the traces on the left side of the photo represent the base lines from which the trace deviations were measured. Upon impact the traces deviate downward indicating that the cone is undergoing deceleration. Trace deviations above the base line indicate that the projectile experiences rebound. It should be noted that the projectiles were essentially rigid, thus, the rebound was produced by energy stored in the sand. After the projectile comes to rest the traces should return to the base lines from which they originated. The photo in Fig. 57 shows no indication of base line drift.

Figure 58 indicates that the projectile experiences a large amount of rebound and it can also be seen that the traces did not return to the base lines from which they originated. The large rebound portions of the traces are much larger than those observed by Reichmuth[19]. It also does not seem probable that rebound would be greater in loose sand than in dense sand, which is indicated by the author's cone test data. It appears as though the base lines drifted upward during the impact event, thus, causing the trace deviations below the original base lines to be too small and those above the original base lines to be too large.

The duration of the impact events for tests on saturated sand and dense, dry sand were much shorter than the test durations for tests on loose,

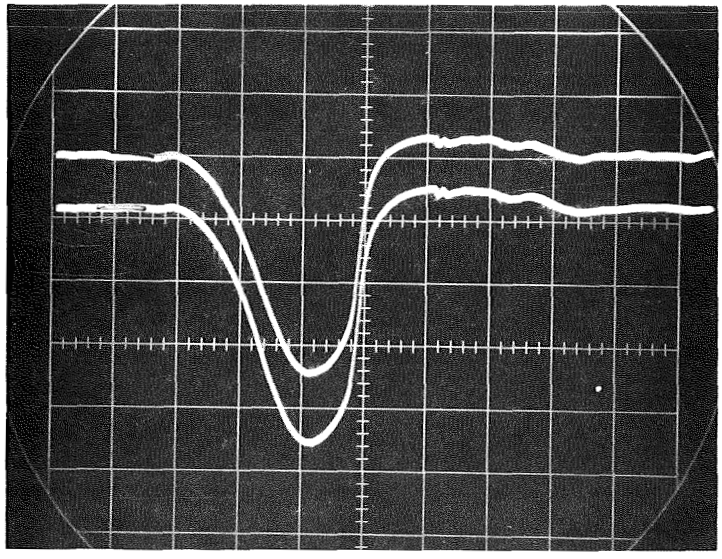

Fig. 57 Acceleration-Time Trace for Impact of Light Cone on Saturated Ottawa Sand - Test 7-25-2-LC-90-0

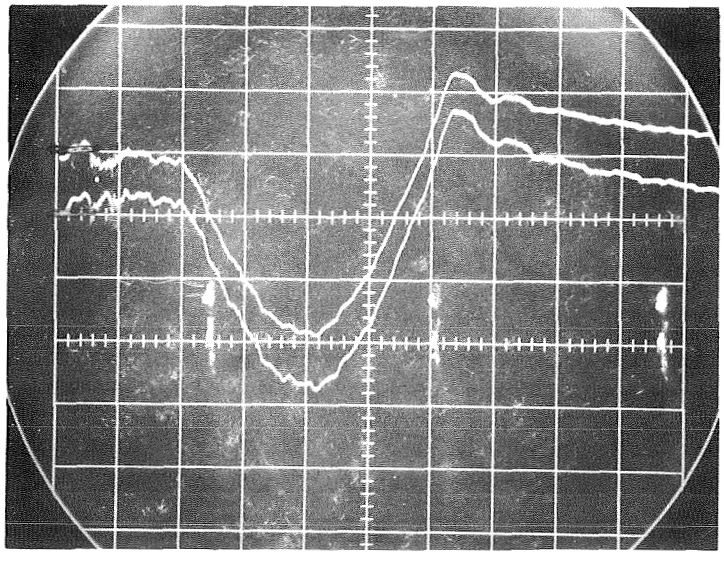

Fig. 58 Acceleration-Time Trace for Impact of Light Cone on Loose, Dry Ottawa Sand - Test 7-11-7-LC-90-0

dry sand. Therefore, for tests on loose sand the longer test duration allowed more time for drift to occur. The sweep times for the tests shown in Figs. 57 and 58 were 10 and 20 msec per centimeter, respectively. The accelerations for tests on loose, dry sand were also significantly lower than accelerations for tests on saturated sand and dense, dry sand. Therefore, any drift during the tests on loose, dry sand would cause a greater error. The peak accelerations for the tests shown in Figs. 57 and 58 were approximately 30 and 14 g's, respectively.

Summary of Errors Associated with Cone Impact Data

The previous discussions have shown that the major portion of the error involved in obtaining the cone impact data developed from two sources.

The first source of error developed from the use of calibration constants recommended by the manufacturer. Nearly all of the cone accelerations were within the 0 to 50 g range. This range of accelerations was far below the maximum rated range of 250 g's. The laboratory drop tests showed that both the ±250 g accelerometers used by the author and the ±500 g accelerometer used by Poor[16] tended to register accelerations approximately 15 percent below the true values for accelerations within the 0 to 50 g range. It is believed that if higher accelerations had developed during the impact tests the calibration constant would have yielded more nearly correct acceleration values. Poor's test data tends to substantiate this statement since in many of his tests with the ±500 g accelerometer, the accelerations were above 100 g's and integration of the accelerometer record yielded a final computed velocity of approximately zero. However, it was noted that in approximately 30 percent of the tests conducted by Poor the area under the acceleration curve was not sufficient to reduce the calculated final velocity to zero even though the

accelerations were above the 100 g level. These tests indicated that the measured accelerations were 10 to 25 percent below the true values.

It should be emphasized that it is not known whether the total acceleration curve is in error or if just portions of the curves are erroneous. The values of error calculated by the author are based upon the assumption that the total acceleration curve is in error.

Reese[18] has noted that the acceleration data he took with a crystal accelerometer (Endevco) were approximately 5 percent below the true acceleration values. He also stated that an undershoot of the acceleration-time trace is typical of crystal accelerometers.

The second major source of error in the author's cone tests was attributed to drift of the accelerometer base line during the impact event. For tests of short duration (20 msec) the error introduced by drift of the base line was not nearly as significant as in tests of longer duration (100 msec). For cone tests on loose, dry sand the error attributed to drift was approximately 60 percent. The cone tests on dense, dry sand and saturated sand exhibited errors due to drift of approximately 30 and 10 percent, respectively.

It should be emphasized once again that the error calculations are based on the assumption that each point on the acceleration-time curve is in error by the same amount. Examination of the acceleration-time curves showed that the error due to drift became progressively worse as the time after impact increased, therefore, the assumption did involve error which may have been significant in some cases.

Correction of Acceleration-Time Traces

After thoroughly examining the sources of error involved in the cone impact data it was decided to adjust the measured acceleration values so that

the calculated final velocities were zero. Equation 42 states Newton's second law of particle motion.

$$F = M\ a \tag{42}$$

Since bodies are made up of particles this law may be extended to apply to bodies. The variables appearing in Eq. 42 are defined as follows:

$F$ = Resultant force (lb),

$M$ = Mass of the body (lb-sec$^2$/ft),

$a$ = Acceleration of the body (fps$^2$).

Equation 42 was applied to the cone-soil system and the following equation resulted.

$$W_{cone} - F_s(t) = M\ a(t) \tag{43}$$

The variables appearing in Eq. 43 are defined as follows:

$W_{cone}$ = Weight of cone (lb),

$F_s(t)$ = Resultant soil force on cone (lb),

$M$ = Mass of the cone (lb-sec$^2$/ft),

$a(t)$ = Acceleration of the cone (fps$^2$).

Equation 44 is obtained by dividing Eq. 43 by the mass of the cone.

$$g - a_s(t) = a(t) \tag{44}$$

The variables $a_s(t)$ was the acceleration indicated by the accelerometer.

The change in projectile velocity is expressed by Eq. 45.

$$\int_0^T a(t)dt = \int_V^0 dv(t) \tag{45}$$

Where,

T = Duration of the impact event (sec),

V = Initial impact velocity (fps).

Integration of the right side of Eq. 45 and transposing the resulting term yielded Eq. 46.

$$\int_0^T a(t)dt + V = 0 \tag{46}$$

Substitution of Eq. 44 into Eq. 46 yielded Eq. 47.

$$\int_0^T g dt - \int_0^T a_s(t)dt + V = 0 \tag{47}$$

Due to errors in the recorded acceleration-time trace $(a_s(t))$, Eq. 47 was not satisfied. The left side of Eq. 47 was forced to zero by applying a correction factor (CORFA) to the accelerometer data. Equation 48 illustrates how the recorded accelerometer data were corrected so that Eq. 47 was satisfied.

$$\int_0^T g dt - CORFA \int_0^T a_s(t)dt + V = 0 \tag{48}$$

It should be noted that a downward velocity was considered as positive. Accelerometer trace deflections $(a_s(t))$ below the base line were also considered as positive. It should also be noted that the accelerometer data were integrated numerically.

Appendix E contains listings (Table Nos. 24 through 35) of the values of CORFA which were necessary to satisfy Eq. 48 for each of the cone tests. Table No. 5 on p. 70 contains average values of CORFA for each weight of cone and soil condition.

REFERENCES


1. Awoshika, K., and Cox, W. R., "An Application of Similitude to Model Design of a Soil-Projectile System," a report from Department of Civil Engineering, The University of Texas at Austin, to National Aeronautics and Space Administration, Langley Research Center, Hampton, Virginia, NASA Contractor Report CR-1210, November 1968.

2. Casagrande, A., and Shannon, W. L., "Stress-Deformation and Strength Characteristics of Soils Under Dynamic Loads," Proceedings of the Second International Conference on Soil Mechanics and Foundation Engineering, Vol. 5, 1948, pp. 29-34.

3. Cunny, R. W., and Sloan, R. C., Discussion of "Static and Dynamic Behavior of Small Footings," Journal of the Soil Mechanics and Foundations Division, ASCE, Vol. 88, No. SM4, Part 1, August 1962, pp. 200-206.

4. Ghazzaly, O. I., and Cox, W. R., "Load-Settlement Behavior of Geometric Shapes on Silty Clay," a report from Department of Civil Engineering, The University of Texas, to National Aeronautics and Space Administration, Langley Research Center, Hampton, Virginia, August 1967.

5. Ghazzaly, O. I., and Dawson, R. F., "Laboratory Stress-Deformation Characteristics of Soils Under Static Loading," a report from Department of Civil Engineering, The University of Texas, to National Aeronautics and Space Administration, Langley Research Center, Hampton, Virginia, NASA Contractor Report CR-571, October 1966.

6. Heller, L. W., "Failure Modes of Impact-Loaded Footings on Dense Sand," U. S. Naval Civil Engineering Laboratory, Port Hueneme, California, Technical Report R 281, January 1964.

7. Hustad, P. A., and Cox, W. R., "Force-Penetration Characteristics of a Sand Horizontally Penetrated by Plates, Cones, and Spherical Segments," a report from Department of Civil Engineering, The University of Texas, to National Aeronautics and Space Administration, Langley Research Center, Hampton, Virginia, NASA Contractor Report CR-1252, January 1969.

8. Iliya, R. A., and Reese, L. C., "Static Load Versus Settlement for Geometric Shapes on Cohesionless Soil," a report from Department of Civil Engineering, The University of Texas, to National Aeronautics and Space Administration, Langley Research Center, Hampton, Virginia, May 1965.

9. Jackson, J. G., Jr., and Hadala, P. F., "Dynamic Bearing Capacity of Soils. Report 3: The Application of Similitude to Small-Scale Footing Tests," U. S. Army Engineer Waterways Experiment Station, Vicksburg, Miss., Technical Report No. 3-599, Report 3, December 1964.

10. Korvin-Kroubovsky, B. V., Savitsky, D., and Lehman, W. F., "Wetted Area and Center of Pressure of Planing Surfaces," Institute of the Aeronautical Sciences, Preprint No. 244, 1949.

11. McDonnell Aircraft Corporation, "Ground and Water Impact Tests of a Full Scale Boiler Plate Capsule," 1961.

12. NASA, Manned Spacecraft Center, "Operational Evaluation of the Corner Landing Concept," Preliminary Copy of a NASA General Working Paper, Houston, Texas, 1965.

13. North American Aviation Inc., Space and Information Systems Division, Water Impact Test Nos. 75-79, ATO-D-TD-64-20-118, December 19, 1964.

14. Olson, R. E., and Parola, J. F., "An Experimental Investigation of the Dynamic Response of Model Silo-Type Structures in Cohesive Soils Phase I, Soil Properties," Air Force Weapons Laboratory, Kirtland Air Force Base, New Mexico, Technical Report No. AFWL-TR-67-16, October 1967.

15. Oweis, I. S., and Cox, W. R., "A Solution of Nonlinear Plane Strain Problems in Dynamic Soil Mechanics," a report from Department of Civil Engineering, The University of Texas at Austin, to National Aeronautics and Space Administration, Langley Research Center, Hampton, Virginia, October 1968.

16. Poor, A. R., Cox, W. R., and Reese, L. C., "Behavior of a Sandy Clay Under Vertical Impact of Geometric Shapes," a report from Department of Civil Engineering, The University of Texas, to National Aeronautics and Space Administration, Langley Research Center, Hampton, Virginia, May 1965.

17. Proctor, R. R., "Soil Compaction," Four-Article Series in Engineering News-Record, Vol. III, Nos. 9, 10, 12, 13, 1933.

18. Reese, L. C., Dawson, R. F., Coyle, H. M., Baker, W. E., Ghazzaly, O. L., and Smith, R. E., "Investigation of the Effects of Soil Conditions on the Landing of a Manned Spacecraft," a report from The University of Texas Structural Mechanics Research Laboratory, to NASA Manned Spacecraft Center, Houston, Texas, Contract NAS 9-1386, March 1964.

19. Reichmuth, D. R., Stagg, R. P., Womack, D. P., and Cox, W. R., "A Study of Soil-Spacecraft Interaction During Impact," a report from Department of Civil Engineering, The University of Texas, to National Aeronautics and Space Administration, Manned Spacecraft Center, Houston, Texas, December 1966.

20. Richart, F. E., Jr., Dynamically Loaded Foundations," Proceedings of a Symposium on Bearing Capacity and Settlement of Foundations, Department of Civil Engineering, Duke University, 1967, pp. 69-81.

21. Schimming, R. B., and Saxe, H. C., "Inertial Effects and Soil Strength Criteria," Proceedings of The Symposium on Soil-Structure Interaction, University of Arizona, September 1964, pp. 118-128.

22. Selig, E. T., and McKee, K. E., "Static and Dynamic Behavior of Small Footings," Journal of the Soil Mechanics and Foundations Division, ASCE, Vol. 87, No. SM6, Part I, December 1961, pp. 29-47.

23. Shenkman, S., and McKee, K. E., "Bearing Capacities of Dynamically Loaded Footings," Symposium on Soil Dynamics, 64th Annual Meeting of the American Society for Testing and Materials, Special Technical Publication No. 305, June 1961.

24. Skempton, A. W., "The Bearing Capacity of Clays," Proceedings of the Building Research Congress, Div. I, Part III, London, 1951, pp. 180-189.

25. Taylor, D. W., Fundamentals of Soil Mechanics, John Wiley and Sons, Inc., New York, 1948, pp. 613-617.

26. Terzaghi, K., Theoretical Soil Mechanics, John Wiley and Sons, Inc., New York, 1943.

27. Terzaghi, K., "Evaluation of Coefficients of Subgrade Reaction," Geotechnique, Vol. 5, No. 4, London, Dec. 1955, pp. 297-326.

28. Terzaghi, K., and Peck, R. B., Soil Mechanics in Engineering Practice, Wiley, New York, 1948, p. 100.

29. Vallabhan, C. V. G., and Reese, L. C., "Finite Element Method Applied to Problems in Stresses and Deformations of Soil," a report from Department of Civil Engineering, The University of Texas, to National Aeronautics and Space Administration, Langley Research Center, Hampton, Virginia, January 1967.

30. Wagner, H., "Landing of Seaplanes," NACA T.M. No. 672, May 1931.

31. Whitman, R. V., "The Behavior of Soils Under Transient Loading," Proceedings of the Fourth International Conference on Soil Mechanics and Foundation Engineering, Vol. 1, 1957, pp. 207-210.

32. Whitman, R. V., Discussion of "Impact Waves on Sand: Theory Compared With Experiment on Sand Columns," Journal of the Soil Mechanics and Foundations Division, ASCE, Vol. 88, No. SM1, Part 1, February 1962, pp. 49-58.

33. Womack, D. P., and Cox, W. R., "Penetrometer Measurement of Soil Impact Response," a report from Department of Civil Engineering, The University of Texas, to National Aeronautics and Space Administration, Langley Research Center, Hampton, Virginia, NASA Contractor Report CR-849, August 1967.

34. Young, C. W., "Depth Prediction for Earth-Penetrating Projectiles," Journal of the Soil Mechanics and Foundations Division, ASCE, Vol. 95, No. SM3, May 1969, pp. 803-817.